

TOC

1	Synthesis and analytical data	3
1.1	Compound 1a	3
1.2	Compound 1b	4
1.3	Compound 1c	4
1.4	Compound 1d	4
1.5	Compound 2c	5
1.6	Compound 2d	5
1.7	Compound 3a	6
1.8	Compound 3b	6
1.9	Compound 3c	6
1.10	Compound 3d	7
1.11	Compound 4a	7
1.12	Compound 4b	8
1.13	Compound 4c	8
1.14	Compound 4d	9
1.15	Compound 5a	9
1.16	Compound 5b	9
1.17	Compound 5c	10
1.18	Compound 5d	10
1.19	Compound 6a	11
1.20	Compound 6b	11
1.21	Compound 6c	11
1.22	Compound 6d	12
1.23	Compound 9	12
1.24	Compound 17	13
1.25	Compound 10	13
1.26	Compound 11	14
1.27	Compound 20	14
1.28	Compound 12	14
2	Cyclic voltammetry.....	16
3	Solubility and chemical stability.....	29
4	Electrochemical characterization on glassy carbon rotating disc electrode (RDE).....	31
5	Evaluation of electrochemical stability in flow battery cell	45
6	NMR of electrolytes before and after cycling in flow battery cell	56

7	NMR spectra of target compounds	75
8	References	97

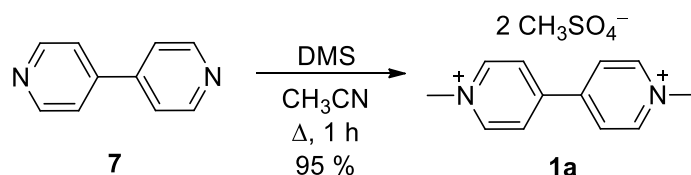
1 Synthesis and analytical data

All reagents and solvents were reagent grade and were purchased from TCI, Aldrich, Fluka or Penta and used as received. The solvents used were evaporated on Heidolph Laborota 4001 rotavap. The starting materials were purchased from Sigma or TCI and used without further purification. Thin layer chromatography (TLC) was conducted on aluminium sheets coated with silica gel 60 F254 (Merck) with visualization by a UV lamp (254 or 360 nm). ^1H - and ^{13}C -NMR spectra were recorded on a Bruker AVANCE III 400/500 spectrometer (400/500 MHz or 100/125 MHz, respectively). Some signals in ^{13}C -NMR spectra are missing. Chemical shifts are reported in ppm relative to the signal of Me_4Si . The residual solvent signal was used as an internal reference (CDCl_3 – 7.25 and 77.23; $\text{DMSO-}d_6$ – 2.55 and 39.51; D_2O – 4.80 ppm for ^1H - or ^{13}C -NMR respectively). For ^{13}C -NMR spectra measured in D_2O as a solvent, 1,4-dioxane with a chemical shift 66.66 ppm was used as an internal standard. Apparent resonance multiplicities are described as s (singlet), bs (broad singlet), d (doublet), dd (doublet of doublet), t (triplet), q (quartet), quint (quintet) and m (multiplet). The coupling constants J , are reported in Hertz (Hz). Post mortem ^1H -NMR spectra were obtained directly from the electrolyte solutions using external $\text{DMSO-}d_6$ standard and a PRESAT sequence to suppress the signal of water. The observed chemical shifts were referenced to the external standard and not corrected. Mass spectra were measured by GC/EI-MS configuration consisting of gas chromatograph Agilent Technologies 6890N equipped with mass detector Network MS detector 5973. High-resolution MALDI mass spectrometry data were collected on an LTQ Orbitrap XL (thermo Fisher Scientific). Elemental analyzes were performed on an EA 1108 Fisons. Büchi B-540 instrument was used for measuring of melting points.

General procedure A: Dimethyl sulfate (DMS) alkylation was conducted according to a modified literature procedure.^[1] The appropriate pyridine derivative (1 mmol) was dissolved in acetonitrile (10 ml) and DMS (1 or 2 mmol) was added into the reaction mixture for mono- or two-fold *N*-alkylation. The resulting reaction mixture was heated to reflux for 18 hours. After cooling to room temperature, the precipitated solid was filtered off and air-dried.

General procedure B: 1,3-Propanesultone (PS) alkylation was conducted according to a modified literature procedure.^[2] The appropriate pyridine derivative (1 mmol) was dissolved in acetonitrile (10 ml) and PS (1.5 or 5 mmol) was added into the reaction mixture for mono- or two-fold *N*-alkylation. The resulting reaction mixture was heated to reflux for 18 hours. After cooling to room temperature, the precipitated solid was filtered off and air-dried.

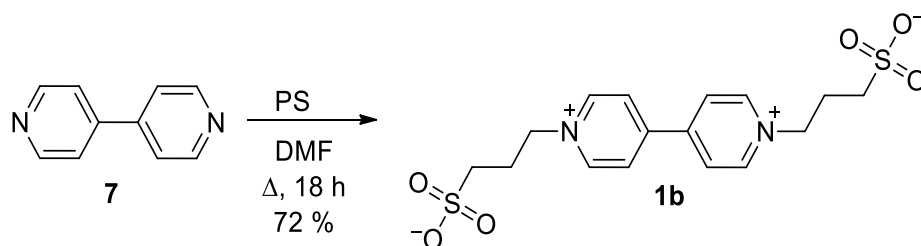
1.1 Compound 1a



The title compound was synthesized from bipyrindine **7** (468 mg, 3 mmol) and DMS (756 mg, 6 mmol) following the general procedure A, whereas reaction time was reduced to 1 hour. White solid; yield 1.16 g (95 %); mp = 160–163 °C. ^1H -NMR (500 MHz, D_2O , 25 °C): δ = 9.03 (d, 4H, J = 6.8 Hz, CH_{Py}), 8.51 (d, 4H, J = 6.8 Hz, CH_{Py}), 4.49 (s, 6H, $\text{CH}_3(\text{Py})$), 3.67 ppm (s, 6H, $\text{CH}_3(\text{DMS})$). ^{13}C -NMR (125 MHz, D_2O /1,4-dioxane, 25 °C): δ = 149.9; 146.4; 126.8; 55.4; 48.4 ppm. HR-FT-MALDI-MS (DHB) m/z : calculated for $\text{C}_{12}\text{H}_{14}\text{N}_2^{2+}$ ($[\text{M}]^+$): 186.11515;

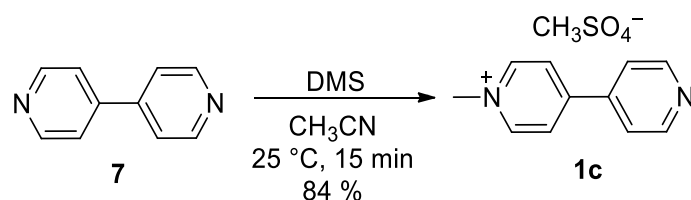
found 186.11489. Elemental analysis: calculated for $C_{14}H_{20}N_2O_8S_2$: C (41.17 %), H (4.94 %), N (6.86 %), S (15.70 %); found C (41.44 %), H (4.80 %), N (6.73 %), S (15.74 %).

1.2 Compound 1b



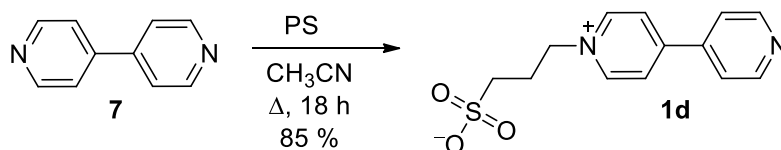
The title compound was synthesized from bipyridine **7** (468 mg, 3 mmol) and PS (2200 mg, 18 mmol) following the general procedure B, whereas DMF was used as solvent. The crude product was purified by crystallization from CH_3OH/H_2O (5:1). White solid; yield 864 mg (72 %; lit.^[21] 77 %); mp = 382–387 °C. 1H -NMR (400 MHz, D_2O , 25 °C): δ = 9.19 (d, 4H, J = 6.8 Hz, CH_{Py}), 8.60 (d, 4H, J = 6.8 Hz, CH_{Py}), 4.92 (t, 4H, J = 7.4 Hz, CH_2), 3.05 (t, 4H, J = 7.2 Hz, CH_2), 2.56 ppm (quint, 4H, J = 7.2 Hz, CH_2). ^{13}C -NMR (100 MHz, $D_2O/1,4$ -dioxane, 25 °C): δ = 150.4; 145.8; 127.3; 60.3; 47.1; 26.3 ppm. HR-FT-MALDI-MS (DHB) m/z : calculated for $C_{16}H_{22}N_2O_6S_2$ $[M+2H]^+$: 402.09138; found 402.09203. Elemental analysis: calculated for $C_{16}H_{20}N_2O_6S_2$: C (47.99 %), H (5.03 %), N (7.00 %), S (16.01 %); found C (47.67 %), H (5.03 %), N (6.81 %), S (16.04 %).

1.3 Compound 1c



The title compound was synthesized from bipyridine **7** (780 mg, 5 mmol) and DMS (315 mg, 2.5 mmol) following the general procedure A, whereas the reaction was performed at room temperature for 15 min. White solid; yield 420 mg (84 %); mp = 184–187 °C. 1H -NMR (500 MHz, D_2O , 25 °C): δ = 8.86 (d, 2H, J = 6.7 Hz, CH_{Py}), 8.67 (dd, 2H, J_1 = 4.7 Hz, J_2 = 1.6 Hz, CH_{Py}), 8.31 (d, 2H, J = 6.7 Hz, CH_{Py}), 7.83 (dd, 2H, J_1 = 4.7 Hz, J_2 = 1.6 Hz, CH_{Py}), 4.42 (s, 3H, $CH_3(Py)$), 3.67 ppm (s, 3H, $CH_3(DMS)$). ^{13}C -NMR (125 MHz, $D_2O/1,4$ -dioxane, 25 °C): δ = 154.1; 150.6; 146.2; 143.2; 126.3; 123.1; 56.0; 48.4 ppm. HR-FT-MALDI-MS (DHB) m/z : calculated for $C_{11}H_{11}N_2^+$ $[M]^+$: 171.09167; found 171.09173. Elemental analysis: calculated for $C_{12}H_{14}N_2O_4S$: C (51.05 %), H (5.00 %), N (9.92 %), S (11.36 %); found C (51.30 %), H (4.97 %), N (9.64 %), S (10.97 %).

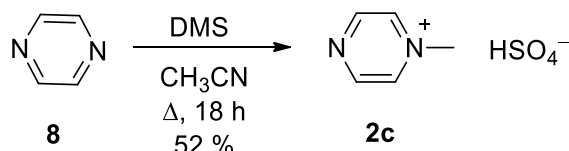
1.4 Compound 1d



The title compound was synthesized from bipyridine **7** (468 mg, 3 mmol) and PS (366 mg, 3 mmol) following the general procedure B. White solid; yield 712 mg (85 %) mp = 248–250 °C.

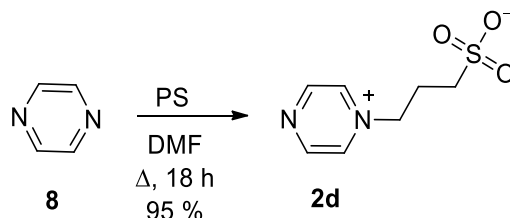
¹H-NMR (500 MHz, D₂O, 25 °C): δ = 8.98 (d, 2H, J = 6.9 Hz, CH_{Py}), 8.69 (dd, 2H, J_1 = 4.7 Hz, J_2 = 1.7 Hz, CH_{Py}), 8.37 (d, 2H, J = 6.9 Hz, CH_{Py}), 7.84 (dd, 2H, J_1 = 4.7 Hz, J_2 = 1.7 Hz, CH_{Py}), 4.80 (t, 2H, J = 7.8 Hz, CH₂), 2.99 (t, 2H, J = 7.4 Hz, CH₂), 2.48 ppm (quint, 2H, J = 7.4 Hz, CH₂). ¹³C-NMR (125 MHz, D₂O/1,4-dioxane, 25 °C): δ = 154.6; 150.6; 145.6; 143.1; 126.8; 123.1; 60.2; 47.7; 26.8 ppm. HR-FT-MALDI-MS (DHB) m/z : calculated for C₁₃H₁₅N₂O₃S ([M+H]⁺): 279.07979; found 279.08009. Elemental analysis: calculated for C₁₃H₁₄N₂O₃S: C (56.10 %), H (5.07 %), N (10.06 %), S (11.52 %); found C (55.48 %), H (4.94 %), N (9.70 %), S (11.22 %).

1.5 Compound 2c



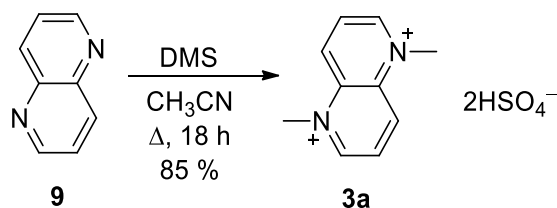
The title compound was synthesized from pyrazine **8** (480 mg, 6 mmol) and DMS (378 mg, 3 mmol) following the general procedure A. The solid formed was washed with acetone and dichloromethane. Green-brown solid; yield 601 mg (52 %); mp = 134–137 °C. ¹H-NMR (400 MHz, D₂O, 25 °C): δ = 9.40 (bs, 2H, CH_{Py}), 8.96–8.97 (m, 2H, CH_{Py}), 4.49 ppm (s, 3H, CH_{3(Py)}). ¹³C-NMR (100 MHz, D₂O/1,4-dioxane, 25 °C): δ = 151.2; 138.83; 138.74; 138.65; 49.7 ppm. HR-FT-MALDI-MS (DHB) m/z : calculated for C₁₀H₁₅N₄²⁺ ([2M+H]⁺): 191.12912; found 191.12935. Elemental analysis: calculated for C₅H₈N₂O₄S: C (31.25 %), H (4.20 %), N (14.58 %), S (16.68 %); found C (31.71 %), H (4.11 %), N (14.34 %), S (16.68 %).

1.6 Compound 2d



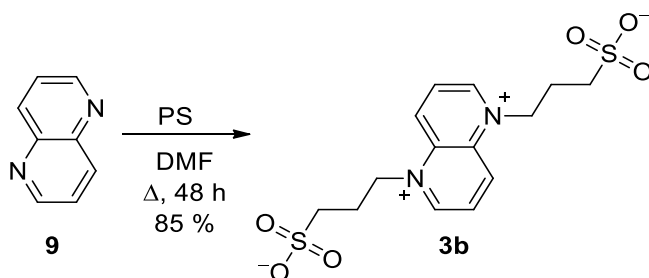
The title compound was synthesized from pyrazine **8** (320 mg, 4 mmol) and 1,3-propanesultone (2 g, 16.4 mmol) following the general procedure B, whereas DMF (10 ml) was used as solvent and reaction mixture was heated to 120 °C for 18 hours. Brown solid; yield 768 mg (95 %); mp = 194–196 °C. ¹H-NMR (400 MHz, D₂O, 25 °C): δ = 9.50 (bs, 2H, CH_{Py}), 9.13–9.14 (m, 2H, CH_{Py}), 4.94 (t, 2H, J = 7.5 Hz, CH₂), 3.07 (t, 2H, J = 7.2 Hz, CH₂), 2.55 ppm (quint, 2H, J = 7.2 Hz, CH₂). ¹³C-NMR (125 MHz, D₂O/1,4-dioxane, 25 °C): δ = 151.7; 138.10; 138.03; 137.96; 61.7; 47.5; 26.6 ppm. HR-FT-MALDI-MS (DHB) m/z : calculated for C₇H₁₁N₂O₃S ([M+H]⁺): 203.04849; found 203.04863. Elemental analysis: calculated for C₇H₁₀N₂O₃S: C (41.57 %), H (4.98 %), N (13.85 %), S (15.86 %); found C (39.74 %), H (5.17 %), N (13.07 %), S (15.18 %).

1.7 Compound 3a



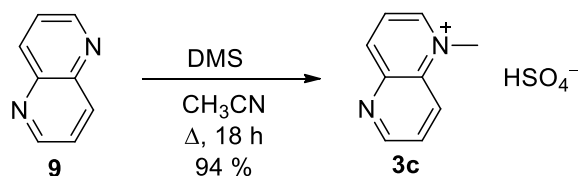
The title compound was synthesized from 1,5-naphthyridine **9** (260 mg, 2 mmol) and DMS (504 mg, 4 mmol) following the general procedure A. The crude product was purified by crystallization from CH₃OH/H₂O (10:1). Brown solid; yield 602 mg (85 %); mp = 167–171 °C. ¹H-NMR (400 MHz, D₂O, 25 °C): δ = 9.85 (d, 2H, *J* = 5.7 Hz, CH_{Py}), 9.73 (d, 2H, *J* = 9.3 Hz, CH_{Py}), 8.74 (dd, 2H, *J*₁ = 9.3 Hz, *J*₂ = 5.7 Hz, CH_{Py}), 4.91 ppm (s, 6H, CH_{3(Py)}). ¹³C-NMR (100 MHz, D₂O/1,4-dioxane, 25 °C): δ = 154.4; 138.3; 136.9; 130.1; 47.2 ppm. HR-FT-MALDI-MS (DHB) *m/z*: calculated for C₁₀H₁₂N₂²⁺ ([M]⁺): 160.09950; found 160.09967. Elemental analysis: calculated for C₁₀H₁₄N₂O₈S₂: C (33.89 %), H (3.98 %), N (7.91 %), S (18.10 %); found C (33.97 %), H (3.86 %), N (7.85 %), S (18.49 %).

1.8 Compound 3b



The title compound was synthesized from 1,5-naphthyridine **9** (260 mg, 2 mmol) and PS (2 g, 16.4 mmol) following the general procedure B, whereas DMF (10 ml) was used as solvent and reaction mixture was heated to 120 °C for 48 hours. The crude product was purified by crystallization from CH₃OH/H₂O (10:1). White solid; yield 635 mg (85 %); mp = 305–307 °C. ¹H-NMR (400 MHz, D₂O, 25 °C): δ = 10.01 (bs, 2H, CH_{Py}), 9.88 (d, 2H, *J* = 8 Hz, CH_{Py}), 8.85 (bs, 2H, CH_{Py}), 5.51 (bs, 4H, CH₂), 3.17 (t, 4H, *J* = 6.7 Hz, CH₂), 2.60 ppm (bs, 4H, CH₂). ¹³C-NMR (125 MHz, D₂O/1,4-dioxane, 25 °C): δ = 154.8; 138.8; 137.4; 131.3; 59.1; 47.7; 26.1 ppm. HR-FT-MALDI-MS (DHB) *m/z*: calculated for C₁₄H₂₀N₂O₆S₂ ([M+2H]⁺): 376.07573; found 376.07628. Elemental analysis: calculated for C₁₆H₂₀N₂O₆S₂: C (44.91 %), H (4.85 %), N (7.48 %), S (17.13 %); found C (44.78 %), H (4.84 %), N (7.36 %), S (17.15 %).

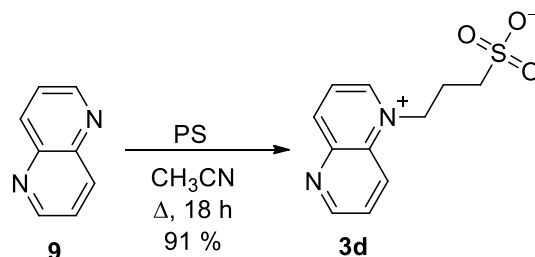
1.9 Compound 3c



The title compound was synthesized from 1,5-naphthyridine **9** (260 mg, 2 mmol) and DMS (252 mg, 2 mmol) following the general procedure A. The crude product was purified by crystallization from CH₃OH/H₂O (10:1). Brown solid; yield 457 mg (94 %); mp = 168–171 °C. ¹H-NMR (400 MHz, D₂O, 25 °C): δ = 9.39 (d, 1H, *J* = 5.7 Hz, CH_{Py}), 9.32 (d, 1H, *J* = 4.3 Hz,

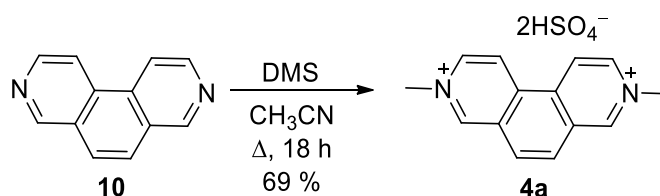
CH_{Py}), 9.21 (d, 1H, *J* = 8.7 Hz, CH_{Py}), 8.93 (d, 1H, *J* = 9.1 Hz, CH_{Py}), 8.32 (dd, 1H, *J*₁ = 8.8 Hz, *J*₂ = 6 Hz, CH_{Py}), 8.24 (dd, 1H, *J*₁ = 9.2 Hz, *J*₂ = 4.3 Hz, CH_{Py}), 4.73 ppm (s, 3H, CH_{3(Py)}). ¹³C-NMR (100 MHz, D₂O/1,4-dioxane, 25 °C): δ = 155.2; 151.0; 147.9; 143.6; 137.3; 130.1; 128.8; 126.2; 45.8 ppm. HR-FT-MALDI-MS (DHB) *m/z*: calculated for C₉H₉N₂⁺ ([M]⁺): 145.07602; found 145.07593. Elemental analysis: calculated for C₉H₁₀N₂O₄S: C (44.62 %), H (4.16 %), N (11.56 %), S (13.24 %); found C (44.11 %), H (4.05 %), N (11.27 %), S (13.60 %).

1.10 Compound 3d



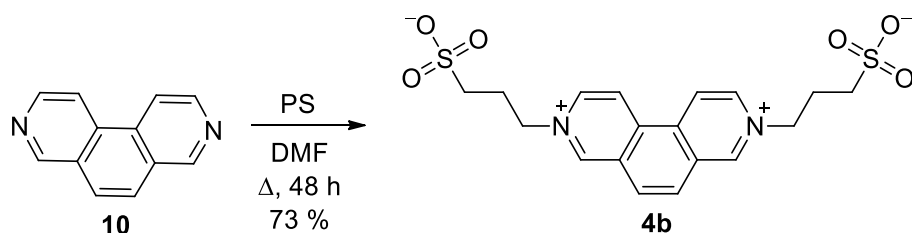
The title compound was synthesized from 1,5-naphthyridine **9** (260 mg, 2 mmol) and PS (500 mg, 4.1 mmol) following the general procedure B. The crude product was purified by crystallization from CH₃OH/H₂O (10:1). Brownish solid; yield 457 mg (91 %); mp = 259–266 °C. ¹H-NMR (500 MHz, D₂O, 25 °C): δ = 9.54 (d, 1H, *J* = 5.8 Hz, CH_{Py}), 9.39 (d, 1H, *J* = 4.1 Hz, CH_{Py}), 9.29 (d, 1H, *J* = 8.7 Hz, CH_{Py}), 9.08 (d, 1H, *J* = 9.2 Hz, CH_{Py}), 8.43 (dd, 1H, *J*₁ = 7.9 Hz, *J*₂ = 6.2 Hz, CH_{Py}), 8.32 (dd, 1H, *J*₁ = 9.1 Hz, *J*₂ = 4.1 Hz, CH_{Py}), 5.35 (t, 2H, *J* = 7.9 Hz, CH₂), 3.17 (t, 2H, *J* = 7.1 Hz, CH₂), 2.61 ppm (quint, 2H, *J* = 7.2 Hz, CH₂). ¹³C-NMR (100 MHz, D₂O/1,4-dioxane, 25 °C): δ = 155.3; 150.5; 148.5; 144.2; 136.7; 130.4; 128.5; 126.4; 56.9; 47.9; 25.8 ppm. HR-FT-MALDI-MS (DHB) *m/z*: calculated for C₁₁H₁₃N₂O₃S ([M+H]⁺): 253.06414; found 253.06423. Elemental analysis: calculated for C₁₁H₁₂N₂O₃S: C (52.37 %), H (4.79 %), N (11.10 %), S (12.71 %); found C (48.77 %), H (4.80 %), N (9.77 %), S (13.18 %).

1.11 Compound 4a



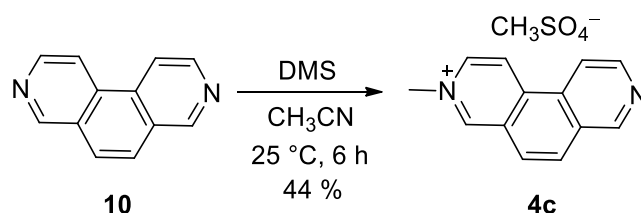
The title compound was synthesized from 3,8-phenanthroline **10** (360 mg, 2 mmol) and DMS (504 mg, 4 mmol) following the general procedure A. The crude product was purified by crystallization from CH₃OH/H₂O (10:1). Beige solid; yield 556 mg (69 %); mp = 247–250 °C. ¹H-NMR (400 MHz, D₂O, 25 °C): δ = 9.94 (s, 2H, CH_{Py}), 9.41 (d, 2H, *J* = 6.8 Hz, CH_{Py}), 9.04 (d, 2H, *J* = 6.8 Hz, CH_{Py}), 8.58 (s, 2H, CH_{Ar}), 4.69 ppm (s, 6H, CH_{3(Py)}). ¹³C-NMR (125 MHz, D₂O/1,4-dioxane, 25 °C): δ = 150.0; 140.5; 136.3; 131.5; 130.5; 124.5; 49.5 ppm. HR-FT-MALDI-MS (DHB) *m/z*: calculated for C₁₄H₁₄N₂²⁺ ([M-2H]⁺): 210.11515; found 210.11534. Elemental analysis: calculated for C₁₄H₁₆N₂O₈S₂: C (41.58 %), H (3.99 %), N (6.93 %), S (15.86 %); found C (41.32 %), H (3.98 %), N (6.61 %), S (15.71 %).

1.12 Compound 4b



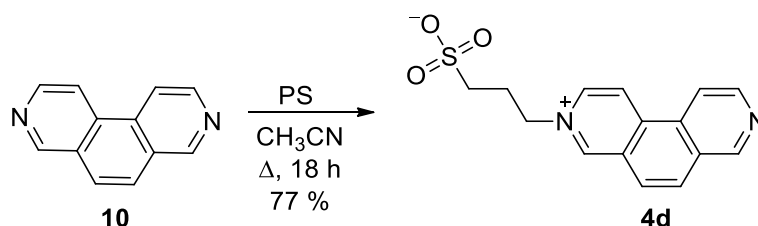
The title compound was synthesized from 3,8-phenanthroline **10** (360 mg, 2 mmol) and PS (1.5 g, 12.3 mmol) following the general procedure B, whereas DMS was used as solvent and reaction time was prolonged to 48 h. The crude product was purified by crystallization from CH₃OH/H₂O (5:1). Yellowish solid; yield 620 mg (73 %); mp = 378–382 °C. ¹H-NMR (400 MHz, D₂O, 25 °C): δ = 10.09 (s, 2H, CH_{Py}), 9.50 (d, 2H, J = 6.8 Hz, CH_{Py}), 9.20 (d, 2H, J = 6.6 Hz, CH_{Py}), 8.63 (s, 2H, CH_{Ar}), 5.12 (t, 4H, J = 9.2 Hz, CH₂), 3.09 (t, 4H, J = 8.9 Hz, CH₂), 2.65 ppm (t, 4H, J = 9.2 Hz, CH₂). ¹³C-NMR (500 MHz, D₂O/1,4-dioxane, 25 °C): δ = 149.6; 139.8; 136.7; 131.8; 130.7; 125.1; 61.4; 47.7; 27.0 ppm. HR-FT-MALDI-MS (DHB) m/z : calculated for C₁₈H₂₂N₂O₆S₂ ([M+2H]⁺): 426.09138; found 426.09202. Elemental analysis: calculated for C₁₈H₂₀N₂O₆S₂: C (50.93 %), H (4.75 %), N (6.60 %), S (15.11 %); found C (49.61 %), H (4.75 %), N (6.36 %), S (14.37 %).

1.13 Compound 4c



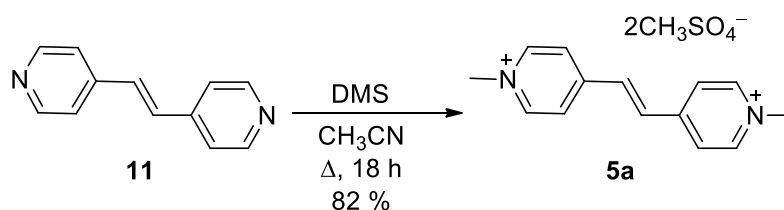
The title compound was synthesized from 3,8-phenanthroline **10** (720 mg, 4 mmol) and DMS (252 mg, 2 mmol) following the general procedure A, whereas reaction time was reduced to 6 h. The crude product was purified by crystallization from acetone/CH₃OH (5:1). Green-brown solid; yield 268 mg (44 %); mp= 133–139 °C. ¹H-NMR (400 MHz, D₂O, 25 °C): δ = 9.66 (s, 1H, CH_{Py}), 9.29 (s, 1H, CH_{Py}), 9.10 (d, 1H, J = 6.8 Hz, CH_{Py}), 8.83 (d, 1H, J = 6.8 Hz, CH_{Py}), 8.78 (d, 1H, J = 5.8 Hz, CH_{Py}), 8.58 (d, 1H, J = 5.8 Hz, CH_{Py}), 8.24 (d, 1H, J = 9 Hz, CH_{Ar}), 8.16 (d, 1H, J = 9 Hz, CH_{Ar}), 4.63 (s, 3H, CH_{3(Py)}), 3.73 (s, 3H, CH_{3(DMS)}). ¹³C-NMR (125 MHz, D₂O/1,4-dioxane, 25 °C): δ = 152.4; 148.7; 146.3; 138.9; 137.6; 132.2; 131.2; 129.8; 129.6; 126.5; 123.1; 118.6; 56.0; 48.9 ppm. HR-FT-MALDI-MS (DHB) m/z : calculated for C₁₃H₁₁N₂⁺ ([M]⁺): 195.09167; found 195.09170. Elemental analysis: calculated for C₁₄H₁₄N₂O₄S: C (54.89 %), H (4.61 %), N (9.14 %), S (10.47 %); found C (54.71 %), H (4.80 %), N (8.85 %), S (9.88 %).

1.14 Compound 4d



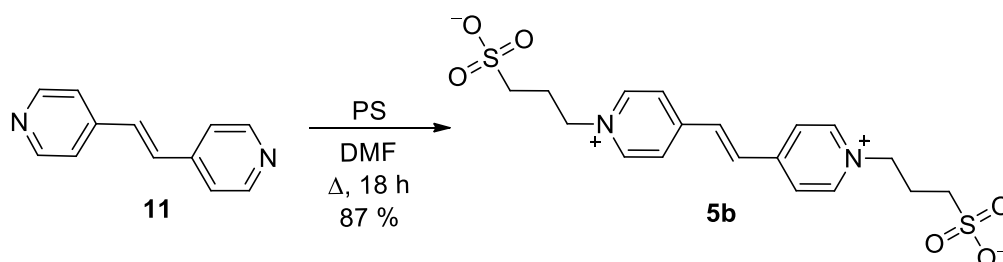
The title compound was synthesized from 3,8-phenanthroline **10** (360 mg, 2 mmol) and PS (244 mg, 2 mmol) following the general procedure B. The crude product was purified by crystallization from CH₃OH/H₂O (10:1). Beige solid; yield 465 mg (77 %); mp = 293–297 °C. ¹H-NMR (500 MHz, D₂O, 25 °C): δ = 9.63 (s, 1H, CH_{Py}), 8.84 (d, 1H, *J* = 6.8 Hz, CH_{Py}), 8.78 (d, 2H, *J* = 6 Hz, CH_{Py}), 8.36 (d, 1H, *J* = 5.8 Hz, CH_{Py}), 8.06 (d, 1H, *J* = 5.8 Hz, CH_{Py}), 7.88 (d, 1H, *J* = 9 Hz, CH_{Ar}), 7.80 (d, 1H, *J* = 9 Hz, CH_{Ar}), 4.96 (t, 2H, *J* = 7.4 Hz, CH₂), 3.07 (t, 2H, *J* = 7.1 Hz, CH₂), 2.58 ppm (quint, 2H, *J* = 7.4 Hz). ¹³C-NMR (500 MHz, D₂O/1,4-dioxane, 25 °C): δ = 152.0; 148.1; 146.1; 138.3; 137.4; 131.4; 130.9; 129.6; 129.0; 126.5; 123.3; 118.2; 60.9; 47.9; 27.1 ppm. HR-FT-MALDI-MS (DHB) *m/z*: calculated for C₁₅H₁₅N₂O₃S ([M+H]⁺: 303.07979; found 303.08024. Elemental analysis: calculated for C₁₅H₁₄N₂O₃S: C (59.59 %), H (4.67 %), N (9.27 %), S (10.61 %); found C (57.07 %), H (4.77 %), N (8.73 %), S (10.03 %).

1.15 Compound 5a



The title compound was synthesized from diazastilbene **11** (364 mg, 2 mmol) and DMS (504 mg, 4 mmol) following the general procedure A. The crude product was purified by crystallization from acetone/CH₃OH (10:1). Orange solid; yield 710 mg (82 %); mp = 228–233 °C. ¹H-NMR (500 MHz, D₂O, 25 °C): δ = 8.74 (d, 4H, *J* = 6.5 Hz, CH_{Py}), 8.18 (d, 4H, *J* = 6.5 Hz, CH_{Py}), 7.83 (s, 2H, CH), 4.34 (s, 6H, CH_{3(Py)}), 3.68 ppm (s, 6H, CH_{3(DMS)}). ¹³C-NMR (125 MHz, D₂O/1,4-dioxane, 25 °C): δ = 151.0; 145.4; 133.7; 125.7; 55.5; 47.8 ppm. HR-FT-MALDI-MS (DHB) *m/z*: calculated for C₁₄H₁₆N₂²⁺ ([M]⁺): 212.13080; found 212.13066. Elemental analysis: calculated for C₁₆H₂₂N₂O₈S₂: C (44.23 %), H (5.10 %), N (6.45 %), S (14.76 %); found C (44.28 %), H (4.94 %), N (6.21 %), S (14.97 %).

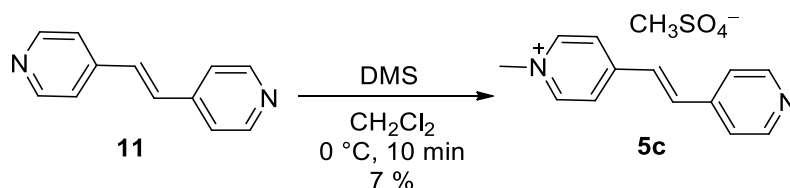
1.16 Compound 5b



The title compound was synthesized from diazastilbene **11** (364 mg, 2 mmol) and PS (1 g, 8.2 mmol) following the general procedure B, whereas DMF was used as solvent. The crude

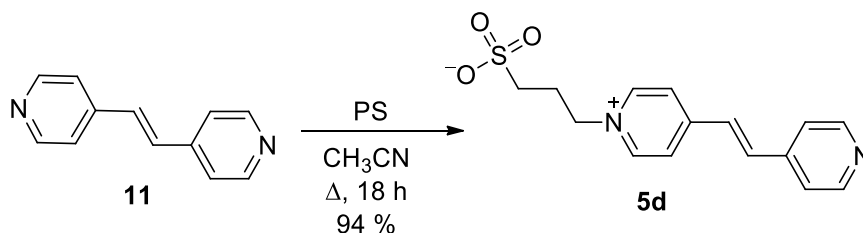
product was purified by crystallization from CH₃OH/H₂O (10:1). Beige solid; yield 743 mg (87 %); mp = 275–280 °C. ¹H-NMR (400 MHz, D₂O, 25 °C): δ = 8.90 (d, 4H, *J* = 6.8 Hz, CH_{Py}), 8.29 (d, 4H, *J* = 6.8 Hz, CH_{Py}), 7.91 (s, 2H, CH), 3.02 (quint, 4H, *J* = 7.2 Hz, CH₂), 2.50 ppm (t, 2H, *J* = 7.2 Hz, CH₂). Signal of CH₂ is missing due to its overlap with H₂O signal in D₂O at 4.80 ppm. ¹³C-NMR (100 MHz, D₂O/1,4-dioxane, 25 °C): 152.1; 145.3; 134.5; 126.7; 60.1; 47.7; 26.7 ppm. HR-FT-MALDI-MS (DHB) *m/z*: calculated for C₁₈H₂₄N₂O₆S₂ ([M+2H]⁺: 428.10703; found 428.10769. Elemental analysis: calculated for C₁₈H₂₂N₂O₆S₂: C (50.69 %), H (5.20 %), N (6.57 %), S (15.04 %); found C (47.41 %), H (5.41 %), N (6.02 %), S (13.92 %).

1.17 Compound 5c



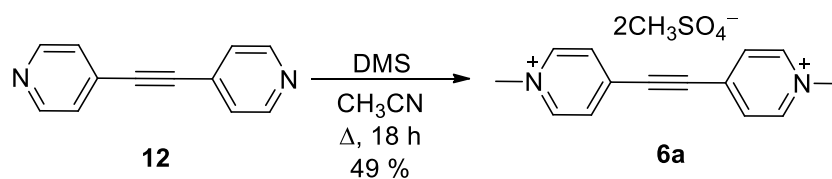
The title compound was synthesized from diazastilbene **11** (546 mg, 3 mmol) and DMS (252 mg, 2 mmol) following the general procedure A, whereas CH₂Cl₂ was used as solvent, temperature of the reaction was suppressed to the 0 °C and reaction time was reduced to 10 min. The crude product was purified by crystallization from acetone/CH₃OH (10:1). Light pink solid; yield 61 mg (7 %); mp = 162–165 °C. ¹H-NMR (400 MHz, D₂O, 25 °C): δ = 8.63 (d, 2H, *J* = 6.6 Hz, CH_{Py}), 8.50 (d, 2H, *J* = 7.4 Hz, CH_{Py}), 8.03 (d, 2H, *J* = 6.7 Hz, CH_{Py}), 7.59–7.64 (m, 3H, CH_{Py}+CH), 7.46 (d, 1H, *J* = 16.4 Hz, CH), 4.31 (s, 3H, CH_{3(Py)}), 3.73 ppm (s, 3H, CH_{3(DMS)}). ¹³C-NMR (125 MHz, D₂O/1,4-dioxane, 25 °C): δ = 152.7; 149.7; 145.4; 144.2; 137.7; 128.4; 125.3; 123.1; 56.0; 47.9 ppm. HR-FT-MALDI-MS (DHB) *m/z*: calculated for C₁₃H₁₃N₂⁺ ([M]⁺): 197.10732; found 197.10718. Elemental analysis: calculated for C₁₄H₁₆N₂O₄S: C (54.53 %), H (5.23 %), N (9.08 %), S (10.40 %); found C (53.32 %), H (5.03 %), N (8.54 %), S (10.49 %).

1.18 Compound 5d



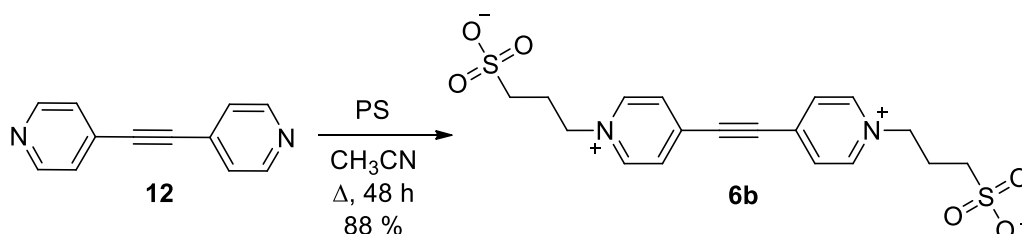
The title compound was synthesized from diazastilbene **11** (400 mg, 2.2 mmol) and PS (244 mg, 2 mmol) following the general procedure B. Light brown solid; yield 572 mg (94 %); mp = 266–269 °C. ¹H-NMR (400 MHz, D₂O, 25 °C): δ = 8.78 (d, 2H, *J* = 6.7 Hz, CH_{Py}), 8.56 (d, 2H, *J* = 6 Hz, CH_{Py}), 8.13 (d, 2H, *J* = 6.6 Hz, CH_{Py}), 7.71 (d, 1H, *J* = 16.4 Hz, CH), 7.65 (d, 2H, *J* = 6 Hz, CH_{Py}), 7.54 (d, 1H, *J* = 16.4 Hz, CH), 4.72 (t, 2H, *J* = 7.4 Hz, CH₂), 3.02 (t, 2H, *J* = 7.2 Hz, CH₂), 2.50 ppm (quint, 2H, *J* = 7.4 Hz, CH₂). ¹³C-NMR (125 MHz, D₂O/1,4-dioxane, 25 °C): δ = 153.5; 150.0; 144.8; 144.0; 138.3; 128.4; 125.7; 123.0; 59.7; 47.7; 26.7 ppm. HR-FT-MALDI-MS (DHB) *m/z*: calculated for C₁₅H₁₇N₂O₃S ([M+H]⁺: 305.09544; found 305.09612. Elemental analysis: calculated for C₁₅H₁₆N₂O₃S: C (59.19 %), H (5.30 %), N (9.20 %), S (10.54 %); found C (59.31 %), H (5.21 %), N (9.27 %), S (9.73 %).

1.19 Compound 6a



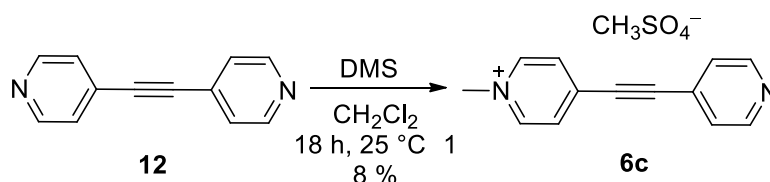
The title compound was synthesized from 1,2-bis(4-pyridyl)acetylene **12** (360 mg, 2 mmol) and DMS (504 mg, 4 mmol) following the general procedure A. Black solid; yield 421 mg (49 %); mp = 170 °C (decomp). ¹H-NMR (500 MHz, D₂O, 25 °C): 8.87 (d, 4H, *J* = 6.2 Hz, CH_{Py}), 8.22 (d, 4H, *J* = 6 Hz, CH_{Py}), 4.41 (s, 6H, CH_{3(Py)}), 3.68 ppm (s, 6H, CH_{3(DMS)}). ¹³C-NMR (500 MHz, D₂O/1,4-dioxane, 25 °C): 146.1; 138.1; 130.8; 94.8; 56.0; 49.0 ppm. HR-FT-MALDI-MS (DHB) *m/z*: calculated for C₁₄H₁₄N₂²⁺ ([M]⁺): 210.11515; found 210.11529. Elemental analysis: calculated for C₁₆H₂₀N₂O₈S₂: C (44.44 %), H (4.66 %), N (6.48 %), S (14.83 %); found C (44.01 %), H (4.66 %), N (6.22 %), S (14.39 %).

1.20 Compound 6b



The title compound was synthesized from 1,2-bis(4-pyridyl)acetylene **12** (360 mg, 2 mmol) and PS (1.2 g, 9.84 mmol) following the general procedure B, whereas reaction time was prolonged to 48 h. The crude product was purified by crystallization from CH₃OH/H₂O (5:1). Brown solid; yield 750 mg (88 %); mp = 230 °C (decomp). ¹H-NMR (400 MHz, D₂O, 25 °C): 9.01 (d, 4H, *J* = 6.8 Hz, CH_{Py}), 8.27 (d, 4H, *J* = 6.8 Hz, CH_{Py}), 4.82 (t, 4H, *J* = 7.2 Hz, CH₂), 3.02 (t, 4H, *J* = 7.2 Hz, CH₂), 2.51 ppm (quint, 4H, *J* = 7.2 Hz, CH₂). ¹³C-NMR (125 MHz, D₂O/1,4-dioxane, 25 °C): 145.0; 138.0; 130.7; 94.5; 60.3; 47.1; 26.2 ppm. HR-FT-MALDI-MS (DHB) *m/z*: calculated for C₁₈H₂₂N₂O₆S₂ ([M+2H]⁺): 426.09138; found 426.09216. Elemental analysis: calculated for C₁₈H₂₀N₂O₆S₂: C (50.93 %), H (4.75 %), N (6.60 %), S (15.11 %); found C (46.99 %), H (5.15 %), N (5.94 %), S (14.15 %).

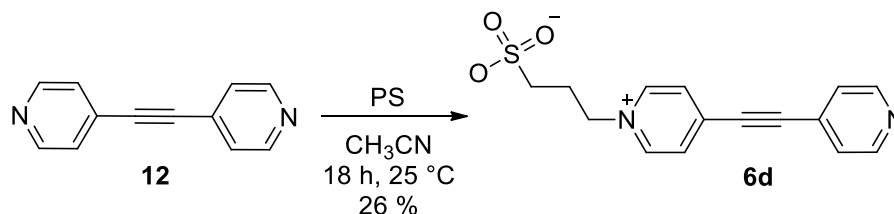
1.21 Compound 6c



The title compound was synthesized from 1,2-bis(4-pyridyl)acetylene **12** (720 mg, 4 mmol) and DMS (300 mg, 2.38 mmol) following the general procedure A, whereas CH₂Cl₂ was used as solvent. Product of dialkylation as by-product was separated by filtration. Hexane (10 ml) was subsequently added into filtrate and precipitation of desired product **6c** occurred. Final product was filtered off and dried. Brown solid; yield 133 mg (18 %); mp = 90 °C (decomp). ¹H-NMR (400 MHz, D₂O, 25 °C): 8.80 (d, 2H, *J* = 6.4 Hz, CH_{Py}), 8.61 (d, 2H, *J* = 5.2 Hz, CH_{Py}), 8.1 (d,

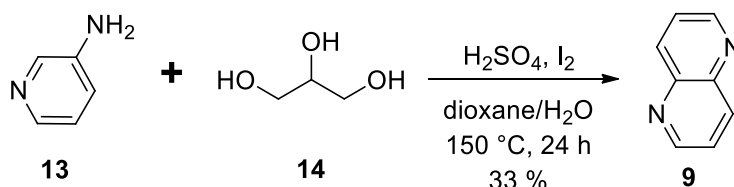
2H, $J = 6.4$ Hz, CH_{Py}), 7.64 (d, 2H, $J = 5.6$ Hz, CH_{Py}), 4.38 (s, 3H, CH_{3(Py)}), 3.72 ppm (s, 3H, CH_{3(DMS)}). ¹³C-NMR (400 MHz, D₂O/1,4-dioxane, 25 °C): 149.7; 145.2; 139.0; 129.9; 129.7; 125.5; 98.3; 88.2; 55.4; 48.2 ppm. (HR-FT-MALDI-MS (DHB) m/z : calculated for C₁₃H₁₁N₂⁺ ([M]⁺): 195.09167; found 195.09192. Elemental analysis: calculated for C₁₄H₁₄N₂O₄S: C (54.89 %), H (4.61 %), N (9.14 %), S (10.47 %); found C (52.82 %), H (4.71 %), N (8.44 %), S (10.28 %).

1.22 Compound 6d



The title compound was synthesized from 1,2-bis(4-pyridyl)acetylene **12** (540 mg, 3 mmol) and PS (500 mg, 4.1 mmol) following the general procedure B, whereas reaction was performed at room temperature. The crude product was purified by crystallization from CH₃OH. Brown solid; yield 234 mg (26 %); mp = 90 °C (decomp). ¹H-NMR (400 MHz, D₂O, 25 °C): 8.91 (d, 2H, $J = 6.8$ Hz, CH_{Py}), 8.61 (dd, 2H, $J_1 = 4.4$ Hz, $J_2 = 1.2$ Hz, CH_{Py}), 8.16 (d, 2H, $J = 6.4$ Hz, CH_{Py}), 7.65 (dd, 2H, $J_1 = 4.8$ Hz, $J_2 = 1.6$ Hz, CH_{Py}), 4.77 (t, 2H, $J = 7.6$ Hz, CH₂), 3.01 (t, 2H, $J = 7.6$ Hz, CH₂), 2.49 ppm (quint, 2H, $J = 7.6$ Hz, CH₂). ¹³C-NMR (125 MHz, D₂O/1,4-dioxane, 25 °C): 149.2; 144.6; 139.7; 130.3; 129.7; 126.5; 98.8; 88.2; 60.0; 47.1; 26.2 ppm. HR-FT-MALDI-MS (DHB) m/z : calculated for C₁₅H₁₅N₂O₃S ([M+H]⁺): 303.07979; found 303.08021. Elemental analysis: calculated for C₁₅H₁₄N₂O₃S: C (59.59 %), H (4.67 %), N (9.27 %), S (10.61 %); found C (56.96 %), H (4.88 %), N (8.65 %), S (10.01 %).

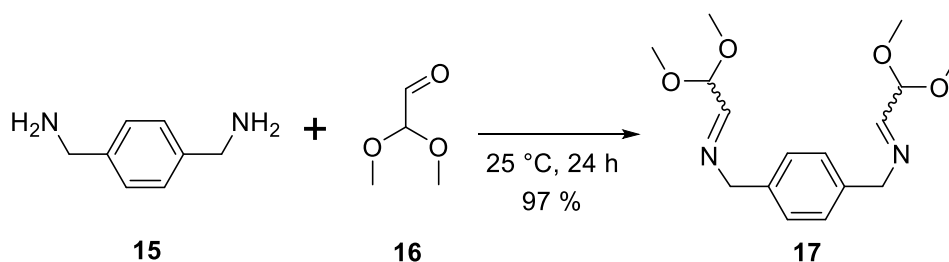
1.23 Compound 9



The title compound was synthesized according to the literature procedure.^[3] 3-Aminopyridine **13** (5 g, 53 mmol) was dissolved in the mixture 1,4-dioxane/H₂O 1:1 (30:30 ml). Subsequently, glycerol **14** (15.5 ml, 212 mmol), 96% H₂SO₄ (55 ml) and I₂ (4.04 g, 15.9 mmol) was added. Resulting reaction mixture was stirred at 150 °C for 24 h. After cooling to room temperature, solution was neutralized with NaOH (50% aq. sol.) to pH ≈ 7. Then, sodium thiosulfate (sat. aq. sol.; 50 ml) was added and resulting solution was filtered through the pad of Celite. The filtrate was diluted with water (500 ml) and extracted with Et₂O (3×250 ml). The combined organic layers were dried over anhydrous Na₂SO₄ and the solvents were evaporated *in vacuo*. The crude product was purified by crystallization from hexane/toluene (1:1). Brown solid; yield 2.3 g (33 %); mp = 68–72 °C (lit.^[4] 74–75 °C). EI-MS (70 eV) m/z (rel. int.): 130 ([M]⁺, 100), 104 (14), 76 (11). ¹H-NMR (400 MHz, CDCl₃, 25 °C): $\delta = 8.94$ (dd, 2H, $J_1 = 4.1$ Hz; $J_2 = 1.6$ Hz, CH_{Py}), 8.37 (dd, 2H, $J_1 = 8.1$ Hz; $J_2 = 1.4$ Hz, CH_{Py}), 7.60 ppm (dd, 2H, $J_1 = 8.4$ Hz; $J_2 = 4.1$ Hz, CH_{Py}). ¹³C-NMR (100 MHz, CDCl₃, 25 °C): $\delta = 151.3$; 144.1; 137.6; 124.5 ppm.

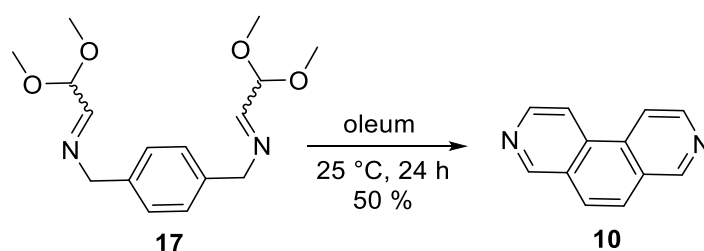
Elemental analysis: calculated for C₈H₆N₂: C (73.83 %), H (4.65 %), N (21.52 %); found: C (73.70 %), H (4.69 %), N (21.61 %).

1.24 Compound 17



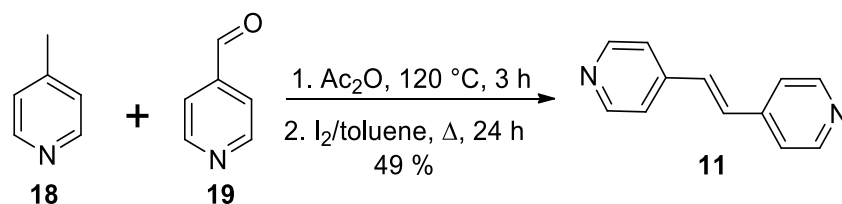
The title compound was synthesized according to the literature procedure.^[4] Diamine **15** (1 g, 7.35 mmol) and acetal **16** (3.4 ml, 22.05 mmol, 60% aq. sol.) were stirred at room temperature for 24 h. Water was evaporated *in vacuo* and resulting product was dried. Yellow oil; yield 2.19 g (97 %). EI-MS (70 eV) *m/z* (rel. int.): 308 ([M]⁺, 0), 278 (14), 221 (12), 174 (18), 104 (10), 75 (100). ¹H-NMR (400 MHz, CDCl₃, 25 °C): δ = 7.55 (s, 2H, CH=N), 7.19 (s, 4H, CH_{Ar}), 4.68 (s, 2H, CH), 4.59 (s, 4H, CH₂), 3.37 ppm (s, 12H, CH₃). ¹³C-NMR (100 MHz, CDCl₃, 25 °C): δ = 161.4; 137.2; 128.4; 103.1; 64.3; 54.1 ppm.

1.25 Compound 10



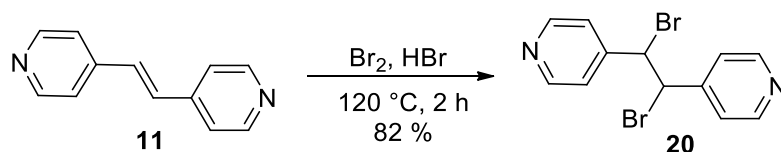
The title compound was synthesized according to the literature procedure.^[4] Bisimine **17** (13.21 g, 43 mmol) was added into ice water cooled oleum (25 %, 75 ml) dropwise in 5 minutes. Resulting reaction mixture was stirred at room temperature for 24 h and then poured into the ice (500 g). Solution was neutralized with Na₂CO₃ (sat. aq. sol.) to pH ≈ 7 and subsequently alkalinized with 2 M NaOH (50 ml). Precipitated impurities were filtered off and filtrate was extracted with CH₂Cl₂ (3×150 ml). Combined organic layers were dried over anhydrous Na₂SO₄ and solvents were evaporated *in vacuo*. The crude product was purified by flash chromatography (SiO₂, CH₃OH). Ocher solid; yield 6.63 g (50 %); mp = 143–145 °C (lit.^[4] 140–141 °C), *R_f* = 0.15 (SiO₂, EtOAc). EI-MS (70 eV) *m/z* (rel. int.): 180 ([M]⁺, 100), 153 (18), 126 (10). ¹H-NMR (400 MHz, CDCl₃, 25 °C): δ = 9.29 (s, 2H, CH_{Py}), 8.81 (d, 2H, *J* = 5.7 Hz, CH_{Py}), 8.34 (d, 2H, *J* = 5.7 Hz, CH_{Py}), 7.89 ppm (s, 2H, CH_{Ar}). ¹³C-NMR (100 MHz, CDCl₃, 25 °C): δ = 152.2; 146.0; 133.2; 128.2; 126.4; 116.5 ppm. Elemental analysis: calculated for C₁₂H₈N₂: C (79.98 %), H (4.47 %), N (15.55 %); found C (79.22 %), H (4.44 %), N (15.27 %).

1.26 Compound 11



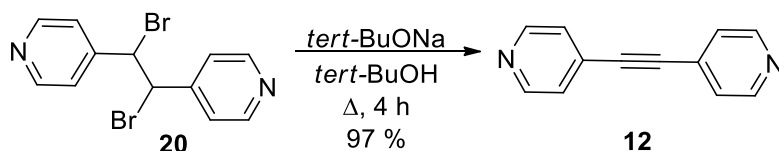
The title compound was synthesized according to the literature procedure.^[5] 4-Methylpyridine **18** (468 mg, 5 mmol), pyridine-4-carbaldehyde **19** (540 mg, 5 mmol) and acetic anhydride (556 μl , 5.88 mmol) were heated to $120\text{ }^\circ\text{C}$ for 3 h. After cooling reaction mixture to room temperature, 10% NaOH (4 ml) was added. Resulting precipitate was filtered off and crystallized from EtOH/H₂O (4:1). Product was dissolved in toluene (50 ml) and catalytic amount of I₂ was added. Solution was heated to reflux for 24 h. To the cooled solution was added sodium thiosulfate (sat. aq. sol.). Separated organic layer was dried over anhydrous Na₂SO₄ and the solvent was evaporated *in vacuo*. Brown solid; yield 446 mg (49 %); mp = $145\text{--}150\text{ }^\circ\text{C}$ (lit.^[6] $148\text{--}152\text{ }^\circ\text{C}$). EI-MS (70 eV) m/z (rel. int.): 181 ($[\text{M}]^+$, 100), 154 (27), 127 (12), 51 (10). ¹H-NMR (400 MHz, CDCl₃, 25 °C): δ = 8.57 (dd, 4H, $J_1 = 4.6\text{ Hz}$, $J_2 = 1.4\text{ Hz}$, CH_{Py}), 7.33 (dd, 4H, $J_1 = 4.6\text{ Hz}$, $J_2 = 1.6\text{ Hz}$, CH_{Py}), 7.15 ppm (s, 2H, CH). ¹³C-NMR (100 MHz, CDCl₃, 25 °C): δ = 150.5; 143.4; 130.6; 121.2 ppm. Elemental analysis: calculated for C₁₂H₁₀N₂: C (79.10 %), H (5.53 %), N (15.37 %); found C (79.01 %), H (5.51 %), N (15.23 %).

1.27 Compound 20



The title compound was synthesized according to the literature procedure.^[5] Diazastilbene **11** (14.46 g, 79.5 mmol), was dissolved in 48% sol. HBr (200 ml) with stirring. After cooling of the mixture to $0\text{ }^\circ\text{C}$, bromine (14.4 ml, 280 mmol) was added dropwise. Resulting reaction mixture was heated to $120\text{ }^\circ\text{C}$ for 2 h. After cooling to room temperature, formed precipitate was filtered off and wash with water (250 ml). Then, precipitate was suspended in NaOH (2 M aq. sol., 500 ml) and stirred for 30 min. Suspension was filtered and solid was dried. White solid; yield 22.2 g (82 %); mp = $232\text{--}236\text{ }^\circ\text{C}$. ¹H-NMR (400 MHz, CDCl₃, 25 °C): δ = 8.68 (d, 4H, $J = 4.4\text{ Hz}$, CH_{Py}), 7.38 (d, 4H, $J = 5.2\text{ Hz}$, CH_{Py}), 5.26 ppm (s, 2H, CH). ¹³C-NMR (100 MHz, CDCl₃, 25 °C): δ = 150.7; 147.8; 122.7; 52.0 ppm. HR-FT-MALDI-MS (DHB) m/z : calculated for C₁₂H₁₁N₂Br₂ ($[\text{M}+\text{H}]^+$): 342.92630; found 342.92687.

1.28 Compound 12



The title compound was synthesized according to the literature procedure.^[5] Sodium (70 mg, 3 mmol) was added into *tert*-BuOH (7 ml) and this reaction mixture was heated to $80\text{ }^\circ\text{C}$ under argon atmosphere until sodium was completely dissolved. Then, dibromoderivative **20** (220 mg, 0.64 mmol) was added and resulting solution was heated to reflux for 4 h. *Tert*-BuOH was

evaporated *in vacuo*. Water (20 ml) was added into crude product resulting suspension was extracted with CH₂Cl₂ (3×15 ml). Combined organic phases were dried (Na₂SO₄) and solvent was evaporated *in vacuo*. Brown solid; yield 112 mg (97 %); mp = 112–117 °C (lit.^[7] 117 °C). EI-MS (70 eV) *m/z* (rel. int.): 180 ([M]⁺, 100). ¹H-NMR (400 MHz, CDCl₃, 25 °C): δ = 8.64 (d, 4H, *J* = 5.9 Hz, CH_{Py}), 7.39 ppm (d, 4H, *J* = 5.9 Hz, CH_{Py}). ¹³C-NMR (100 MHz, CDCl₃, 25 °C): δ = 150.2; 130.4; 125.8; 90.8 ppm. Elemental analysis: calculated for C₁₂H₈N₂: C (79.98 %), H (4.47 %), N (15.55 %); found C (80.30 %), H (4.56 %), N (15.43 %).

2 Cyclic voltammetry

Preliminary electrochemical characterization of all target compounds **1–6** has been carried out by cyclic voltammetry (CV) in aqueous solutions of different pH. 1 mol·dm⁻³ solutions of H₂SO₄, Na₂SO₄, and NaOH in deionized water were used as working electrolytes. Based on our recent experience with similar structures,^[8] these target molecules showed a chemical instability in the alkaline electrolyte (1 mol·dm⁻³ NaOH) as well, therefore this electrolyte has not further been used for electrochemical measurements. Target compounds were electrochemically determined at 1 mmol·dm⁻³ concentrations in corresponding acidic and neutral electrolytes. Cyclic voltammetry was performed in a three electrode cell with a volume of 2.5 ml under argon atmosphere. The working electrode was glassy carbon disk (1 mm in diameter). The surface of GC electrode has been cleaned mechanically (polishing by alumina suspension and sonication in deionized water) and electrochemically (activation of the surface in 14 mol·dm⁻³ NaOH) before each electrochemical analysis. Leakless Ag/AgCl electrode (SSCE) containing filling electrode (3.4 mol·dm⁻³ KCl) and titanium rod with a thick coating of platinum were used as the reference and auxiliary electrodes. The target molecules were subjected to voltammetric characterizations within the available potential window (pH dependent), which was -0.9 to +1.8 V in 1 mol·dm⁻³ H₂SO₄ and -1.6 to +1.7 V vs. SHE in 1 mol·dm⁻³ Na₂SO₄ at scan rate 100 mV·s⁻¹. The cathodic and anodic peak potentials E_p^c/E_p^a were determined from the obtained cyclic voltammograms. All potentials were assigned from the first cycle at scan rate 100 mV·s⁻¹ and were related to the SHE. Voltammetric measurements were performed by using an integrated potentiostat system ER466 (eDAQ) operated with EChem Electrochemistry software.

Table S1 – Electrochemical properties of target compounds measured in 1 mol·dm⁻³ H₂SO₄.

Reduction	Reversibility	Potential	Bipyridines				Pyrazines				Naphthyridines						
			1a	1b	1c	1d	2c		2d		3a	3b	3c	3d			
1.	(quasi)rev.	E_p^c [mV] ^a		-450				-20	+20		-30	+30	-100	-70			
		E_p^a [mV] ^a		-390				+60	+90		+40	+100	-40	-10			
		$E_{1/2}$ [mV] ^b		-420				+20	+55		+5	+65	-70	-40			
		ΔE_p [mV] ^c		60				80	70		70	70	60	60			
	irr.	E_p^c [mV] ^a		-530		-550	-480										
2.	(quasi)rev.	E_p^c [mV] ^a															
		E_p^a [mV] ^a															
		$E_{1/2}$ [mV] ^b															
		ΔE_p [mV] ^c															
	irr.	E_p^c [mV] ^a		-600		-630	-620				-230	-220	-300	-300	-480	-440	
Reduction	Reversibility	Potential	Phenanthrolines				Diazastilbenes				Bis(pyridyl)acetylenes						
			4a	4b	4c	4d	5a	5b	5c	5d	6a	6b	6c	6d			
1.	(quasi)rev.	E_p^c [mV] ^a															
		E_p^a [mV] ^a															
		$E_{1/2}$ [mV] ^b															
		ΔE_p [mV] ^c															
	irr.	E_p^c [mV] ^a		-480		-430	-440	-430			-420	-410	-410	-410	-500	-480	-510
2.	(quasi)rev.	E_p^c [mV] ^a															
		E_p^a [mV] ^a															
		$E_{1/2}$ [mV] ^b															
		ΔE_p [mV] ^c															
	irr.	E_p^c [mV] ^a															

^a E_p^a and E_p^c represent peak potentials of anodic and cathodic maxima of the given reduction process; ^b Half-wave potential $E_{1/2} = (E_p^a + E_p^c)/2$; ^c Peak-to-peak separation $\Delta E_p = |E_p^c - E_p^a|$. Stated potentials were taken from first cycle at 100 mV·s⁻¹ related to SHE.

Table S2 – Electrochemical properties of target compounds measured in $1 \text{ mol dm}^{-3} \text{ Na}_2\text{SO}_4$.

Reduction	Reversibility	Potential	Bipyridines				Pyrazines				Naphthyridines			
			1a	1b	1c	1d	2c		2d		3a	3b	3c	3d
1.	<i>(quasi)rev.</i>	E_p^c [mV] ^a	-490	-420	-790	-760			-290	-270	-30	+40	-300	-360
		E_p^a [mV] ^a	-430	-360	-710 ^d	-670 ^d			-130	-140	+40	+100	-220	-240
		$E_{1/2}$ [mV] ^b	-460	-390					-210	-205	+5	+70	-260	-300
		ΔE_p [mV] ^c	60	60					160	130	70	60	80	120
2.	<i>irr.</i>	E_p^c [mV] ^a												
		E_p^a [mV] ^a	-780	-780					-420	-530				
		$E_{1/2}$ [mV] ^b	-730 ^d	-720					-340	-440				
		ΔE_p [mV] ^c		-750					-380	-485				
1.	<i>(quasi)rev.</i>	E_p^c [mV] ^a												
		E_p^a [mV] ^a												
		$E_{1/2}$ [mV] ^b												
		ΔE_p [mV] ^c		60					80	90				
2.	<i>irr.</i>	E_p^c [mV] ^a												
		E_p^a [mV] ^a												
		$E_{1/2}$ [mV] ^b												
		ΔE_p [mV] ^c												
1.	<i>(quasi)rev.</i>	E_p^c [mV] ^a												
		E_p^a [mV] ^a		-410										
		$E_{1/2}$ [mV] ^b		-350										
		ΔE_p [mV] ^c		-380										
2.	<i>irr.</i>	E_p^c [mV] ^a												
		E_p^a [mV] ^a	-470		-630	-630	-550	-480	-660	-630	-480	-440	-720	-510
		$E_{1/2}$ [mV] ^b												
		ΔE_p [mV] ^c												
1.	<i>(quasi)rev.</i>	E_p^c [mV] ^a												
		E_p^a [mV] ^a												
		$E_{1/2}$ [mV] ^b												
		ΔE_p [mV] ^c												
2.	<i>irr.</i>	E_p^c [mV] ^a												
		E_p^a [mV] ^a	-930	-800			-1280	-1270	-1290	-1300	-640	-730		-770
		$E_{1/2}$ [mV] ^b												
		ΔE_p [mV] ^c												

^a E_p^a and E_p^c represent peak potentials of anodic and cathodic maxima of the given reduction process; ^b Half-wave potential $E_{1/2} = (E_p^a + E_p^c)/2$; ^c Peak-to-peak separation $\Delta E_p = |E_p^c - E_p^a|$. ^d Quasi-reversible process of adsorbed particles on the electrode surface, typical sharp anodic peak of re-oxidation. Stated potentials were taken from first cycle at $100 \text{ mV} \cdot \text{s}^{-1}$ related to SHE.

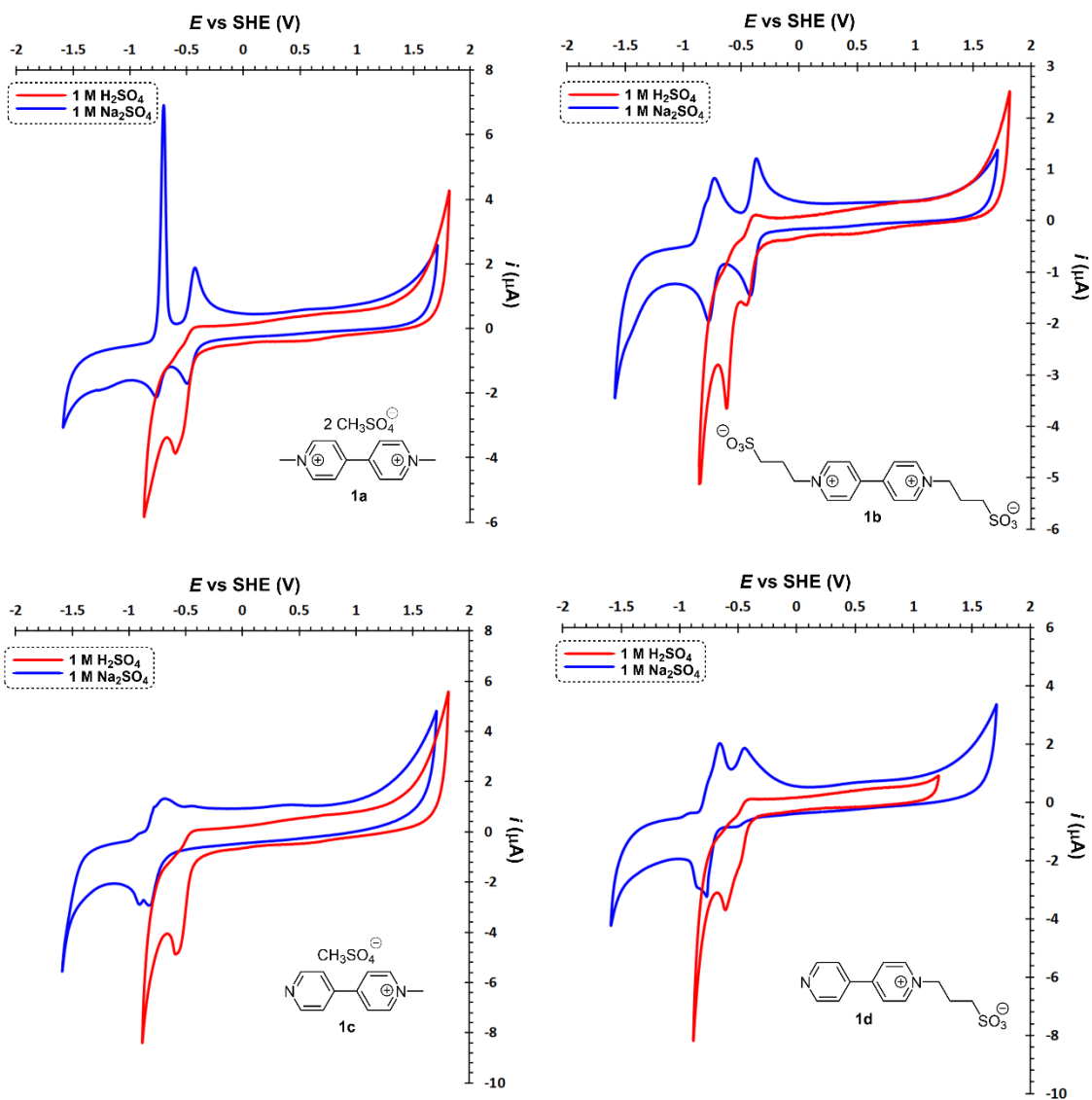


Figure S1 – Complete cyclic voltammograms of bipyridine salts **1a–d** in neutral and acid media; $v = 100 \text{ mV}\cdot\text{s}^{-1}$.

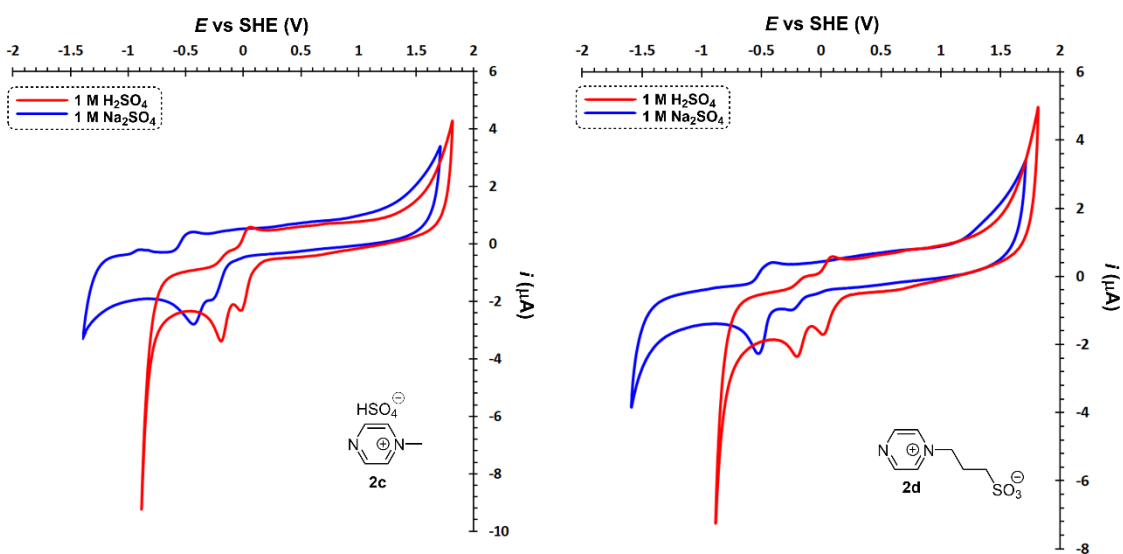


Figure S2 – Complete cyclic voltammograms of pyrazine salts **2c–d** in neutral and acid media; $v = 100 \text{ mV}\cdot\text{s}^{-1}$.

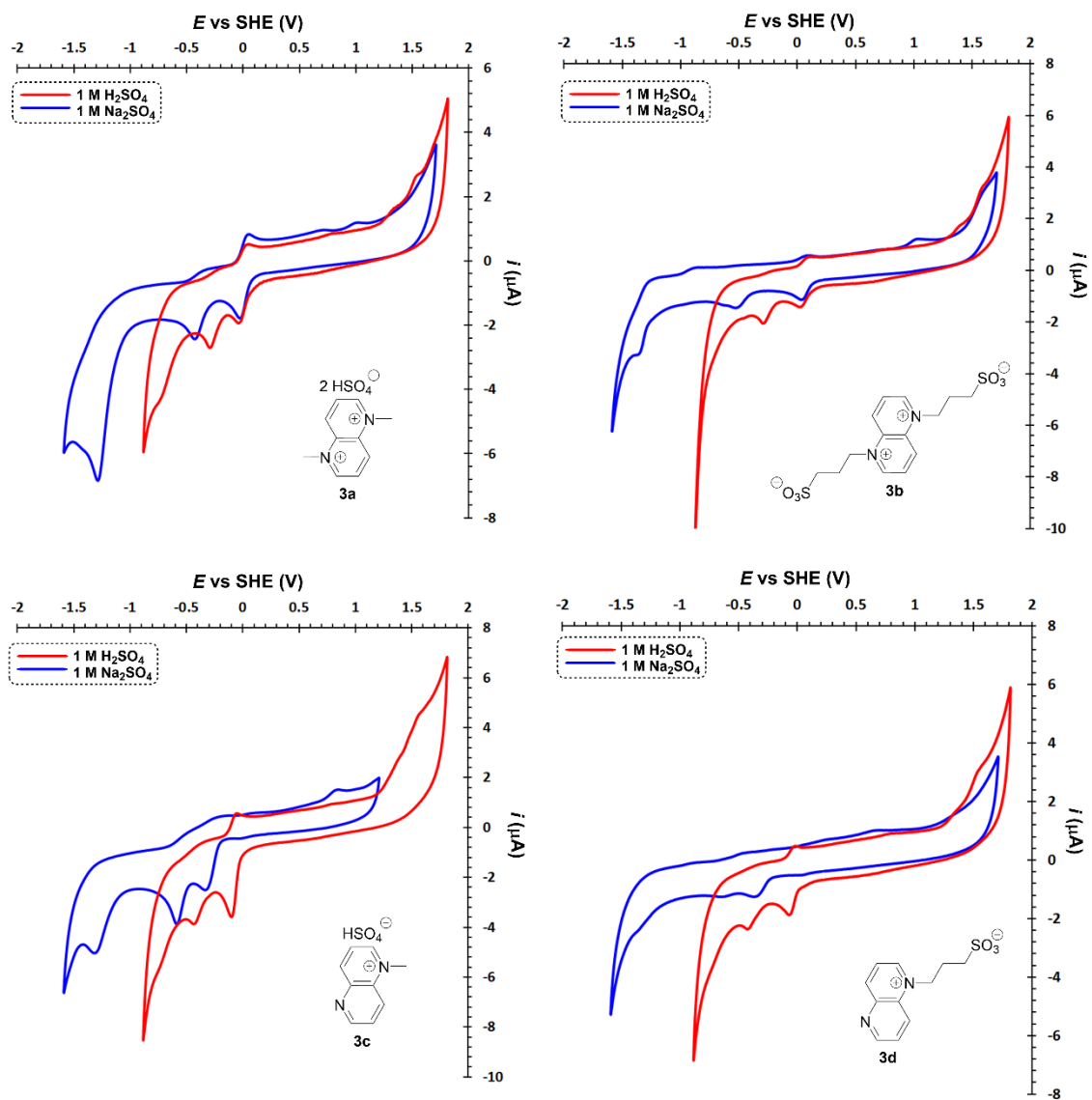


Figure S3 – Complete cyclic voltammograms of naftiridine salts **3a–d** in neutral and acid media; $v = 100 \text{ mV}\cdot\text{s}^{-1}$.

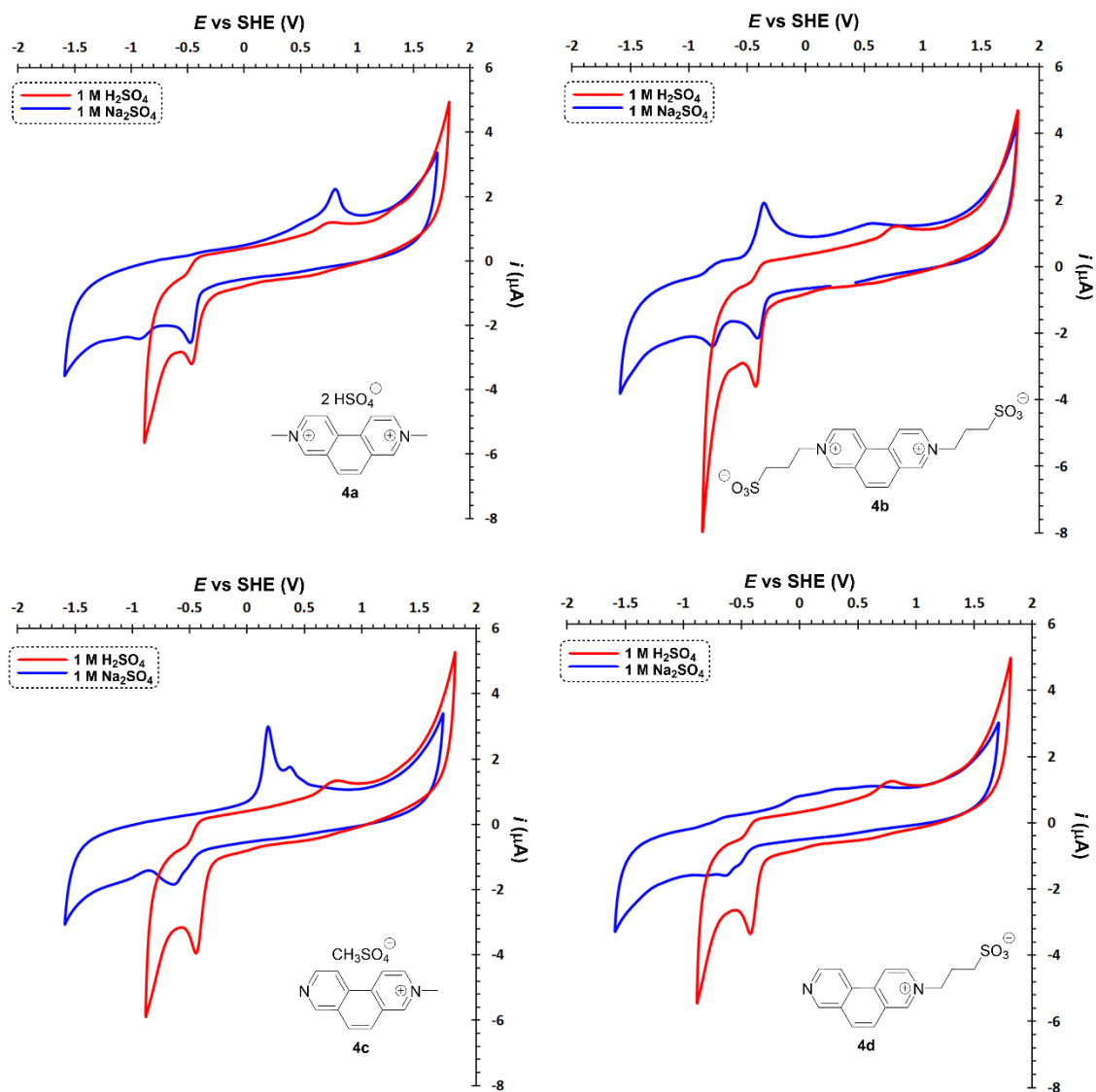


Figure S4 – Complete cyclic voltammograms of phenanthroline salts **4a–d** in neutral and acid media; $v = 100 \text{ mV}\cdot\text{s}^{-1}$.

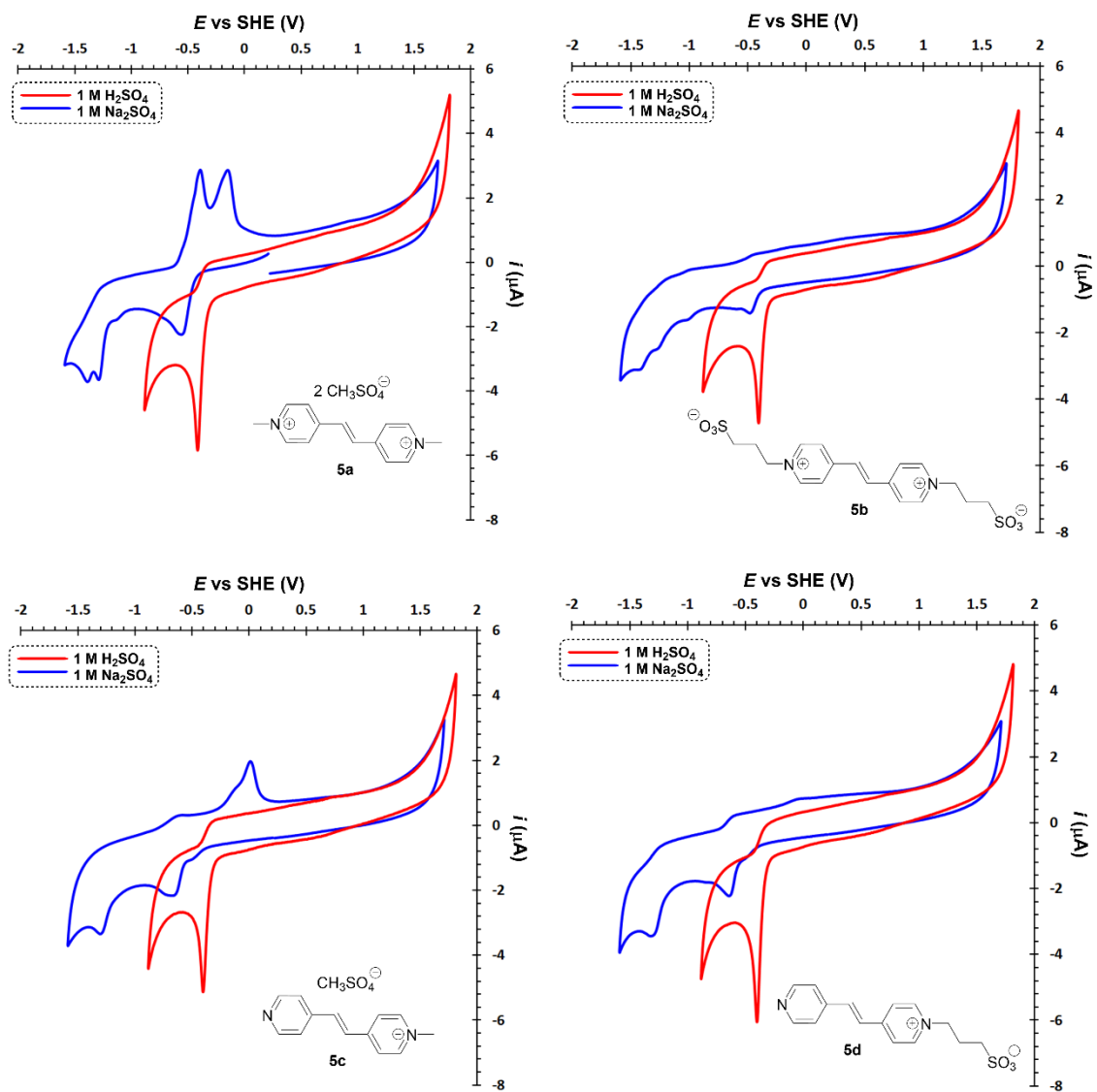


Figure S5 – Complete cyclic voltammograms of diazastilbene salts **5a–d** in neutral and acid media; $\nu = 100 \text{ mV}\cdot\text{s}^{-1}$.

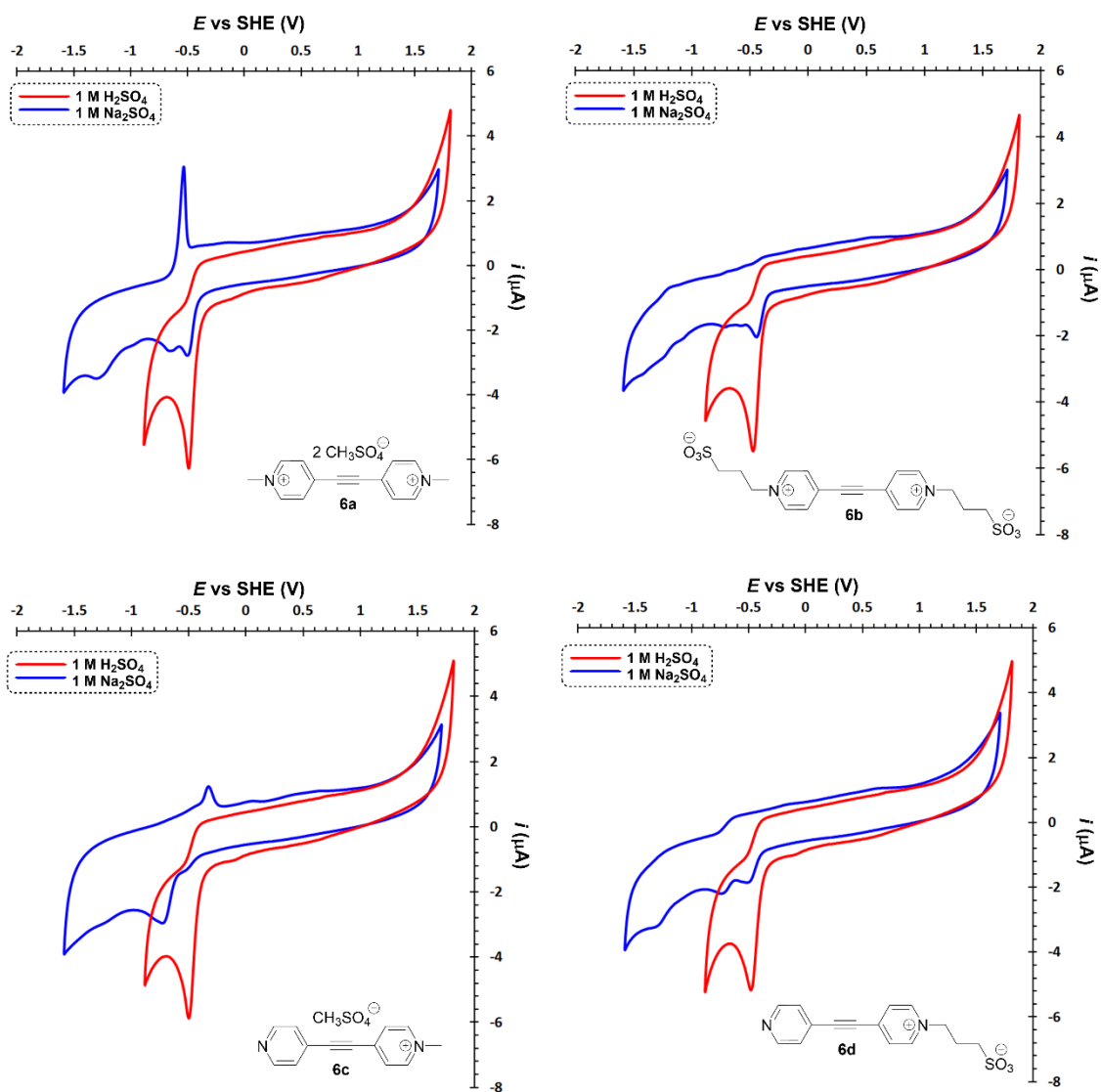


Figure S6 – Complete cyclic voltammograms of bis(4-pyridyl)acetylene salts **6a–d** in neutral and acid media; $v = 100 \text{ mV}\cdot\text{s}^{-1}$.

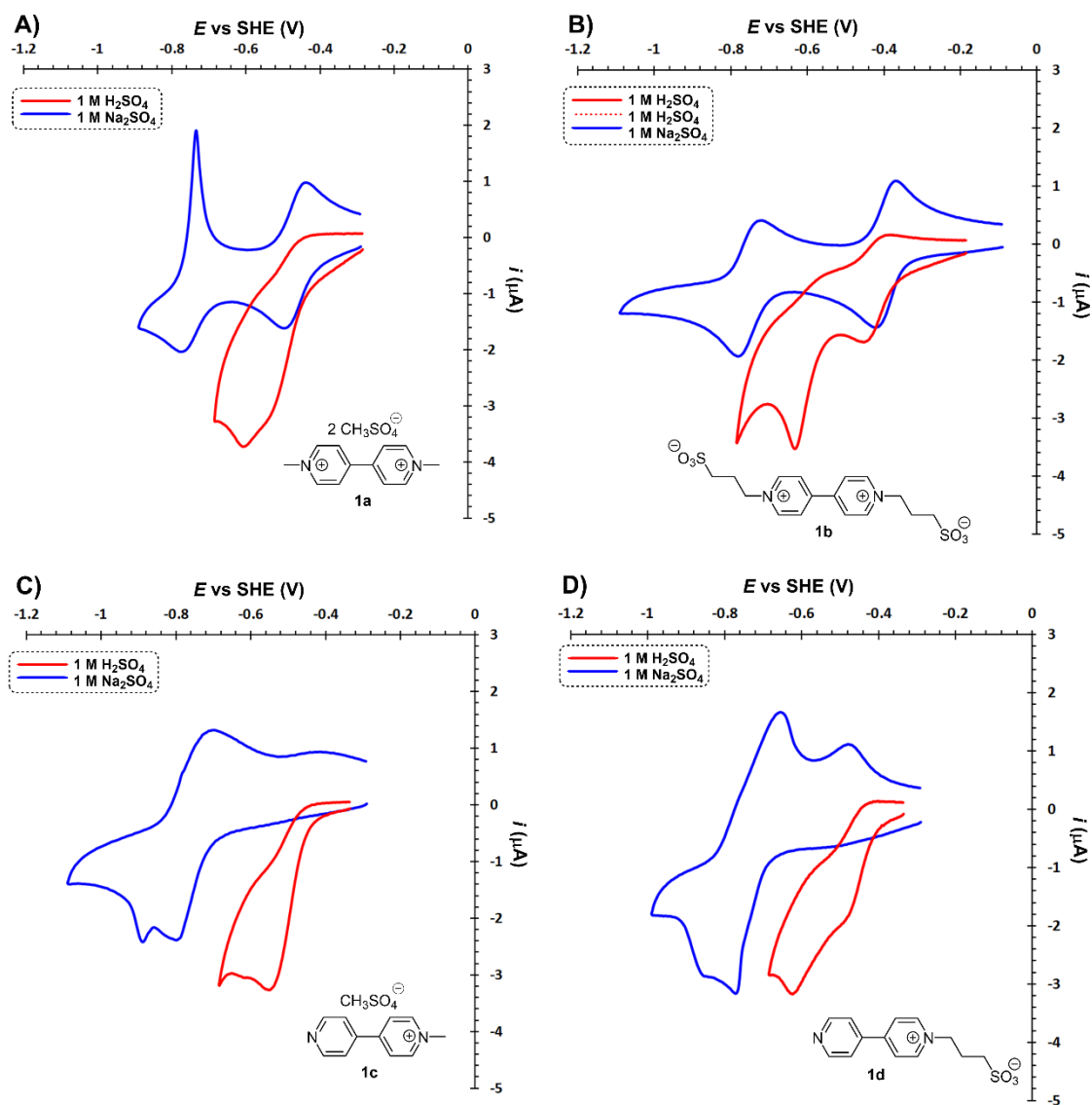


Figure S7 – Electrochemical reductions of bipyridinium salts **1a–d** on glassy carbon electrode in neutral and acid media; $\nu = 100 \text{ mV}\cdot\text{s}^{-1}$.

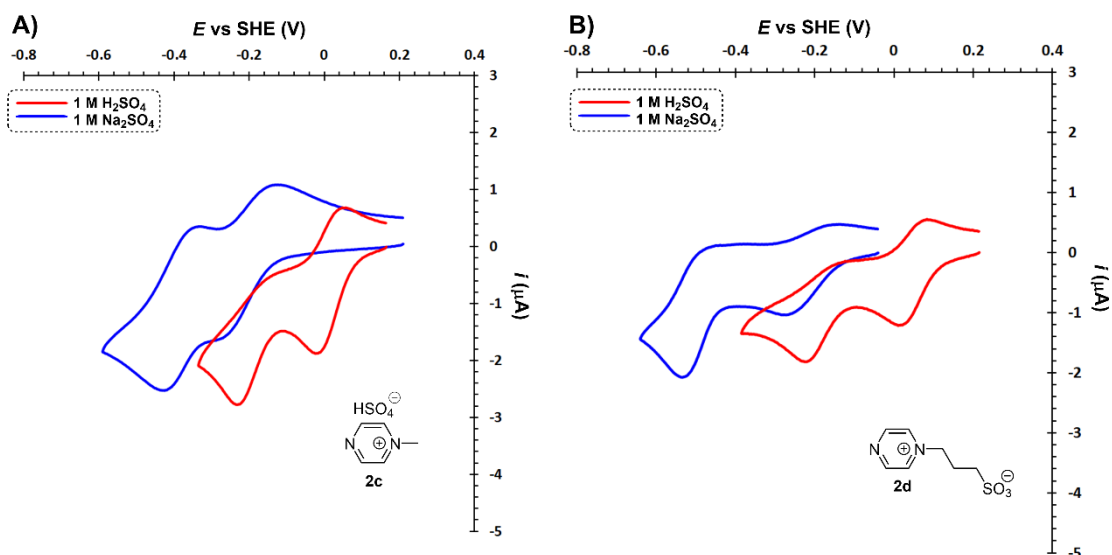


Figure S8 – Electrochemical reductions of pyrazine salts **2c–d** on glassy carbon electrode in neutral and acid media; $\nu = 100 \text{ mV}\cdot\text{s}^{-1}$.

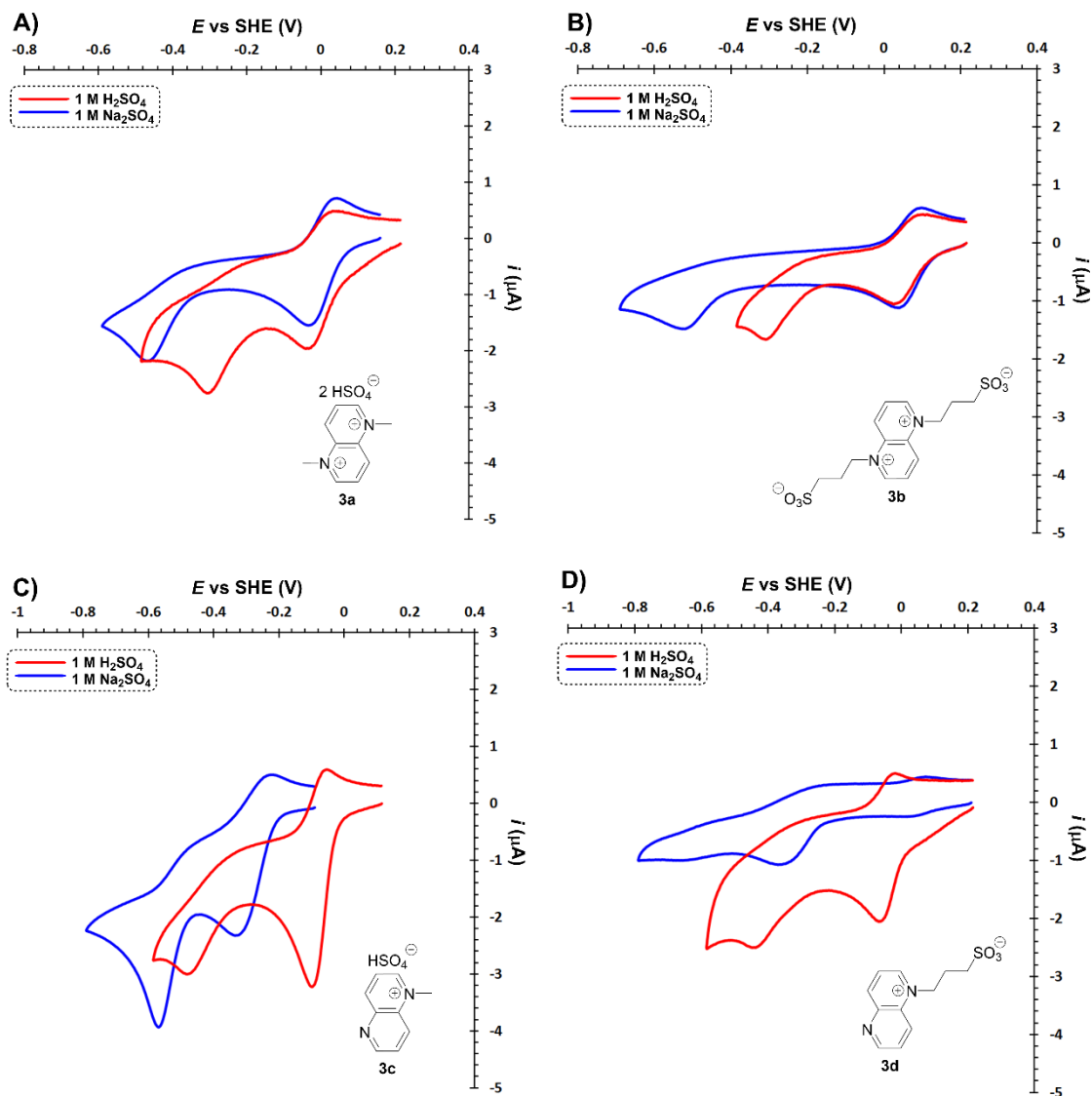


Figure S9 – Electrochemical reductions of naphthyridine salts **3a–d** on glassy carbon electrode in neutral and acid media; $\nu = 100 \text{ mV}\cdot\text{s}^{-1}$.

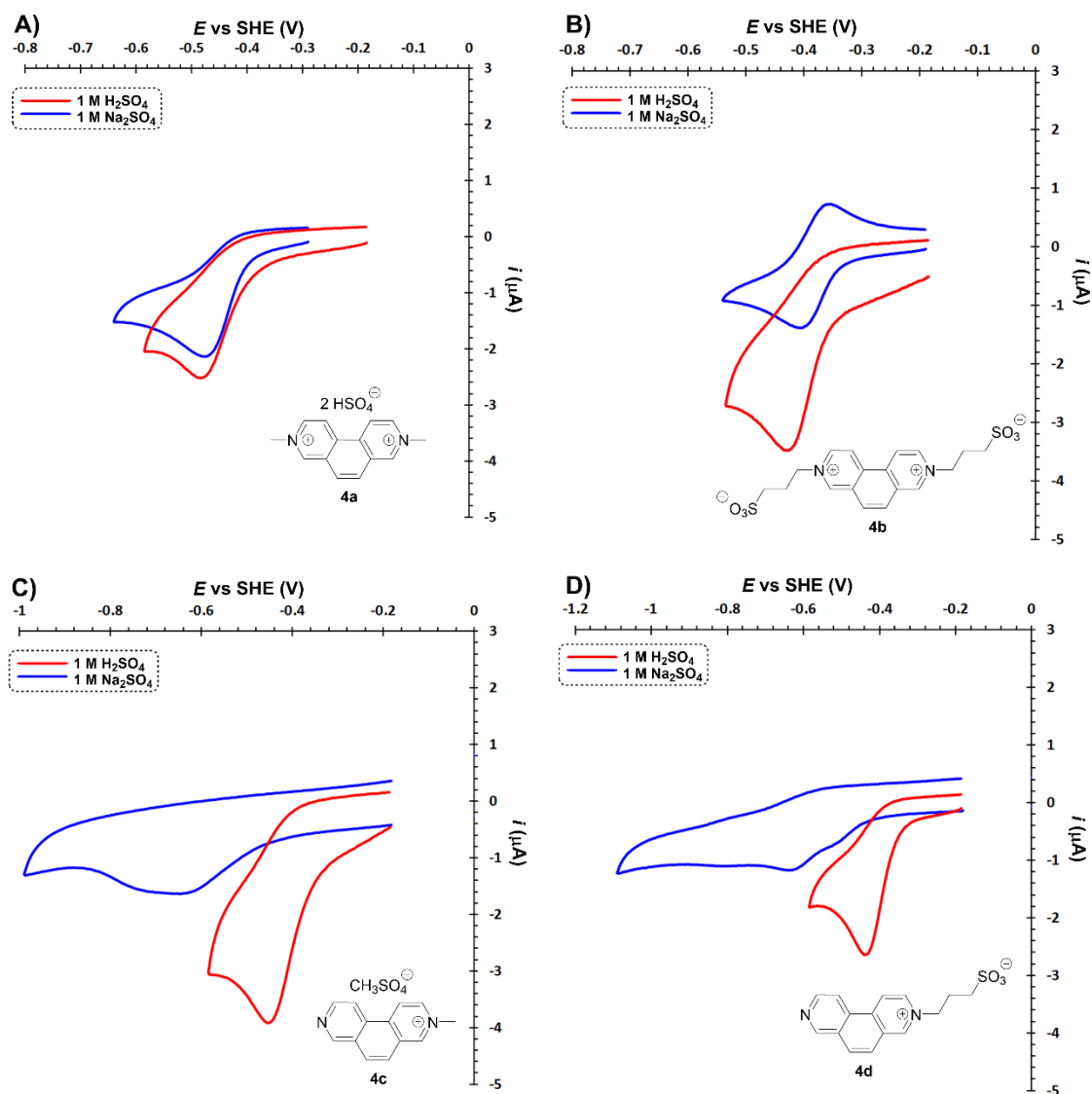


Figure S10 – Electrochemical reductions of phenanthroline salts **4a–d** on glassy carbon electrode in neutral and acid media; $v = 100 \text{ mV}\cdot\text{s}^{-1}$.

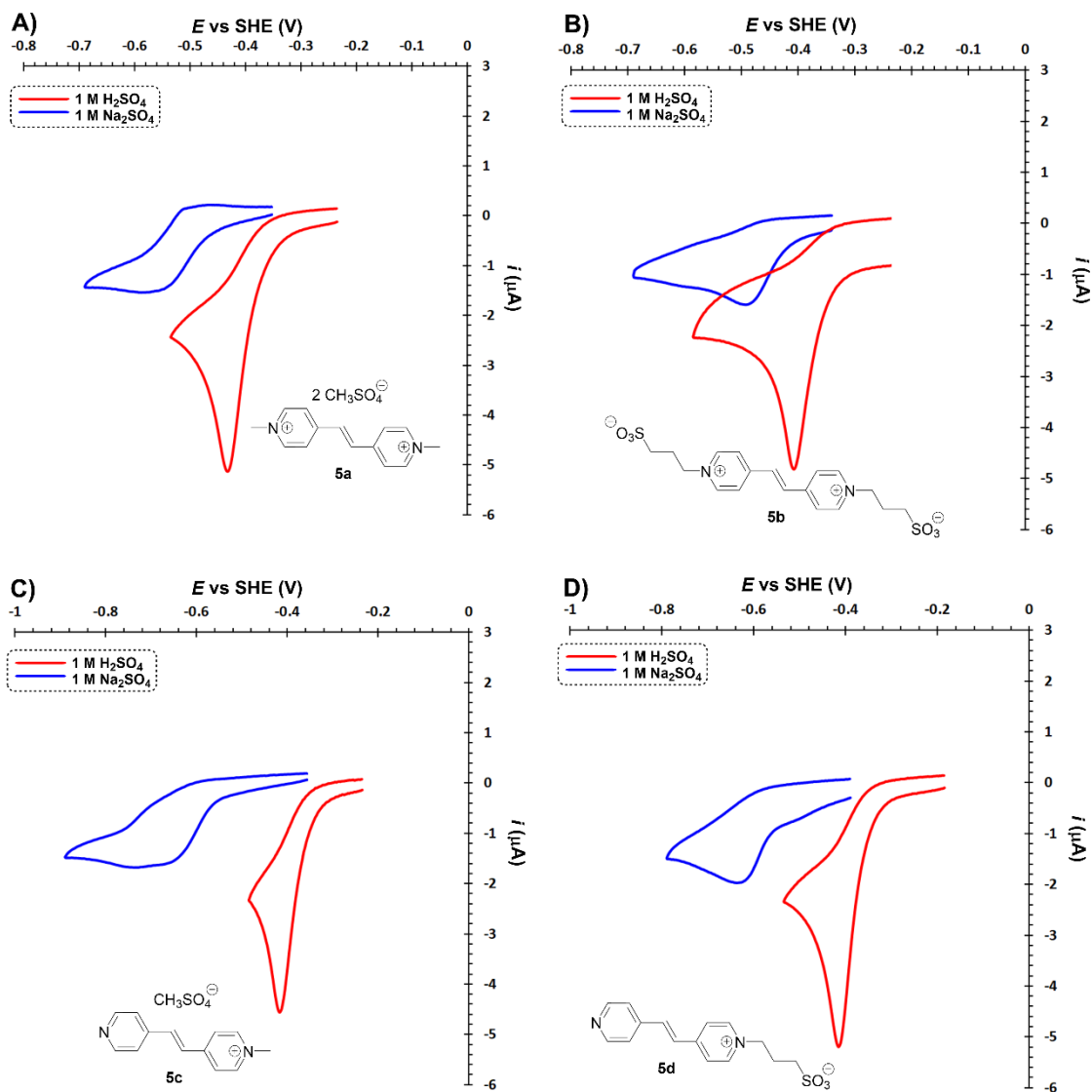


Figure S11 – Electrochemical reductions of diazastilbene salts **5a–d** on glassy carbon electrode in neutral and acid media; $v = 100 \text{ mV}\cdot\text{s}^{-1}$.

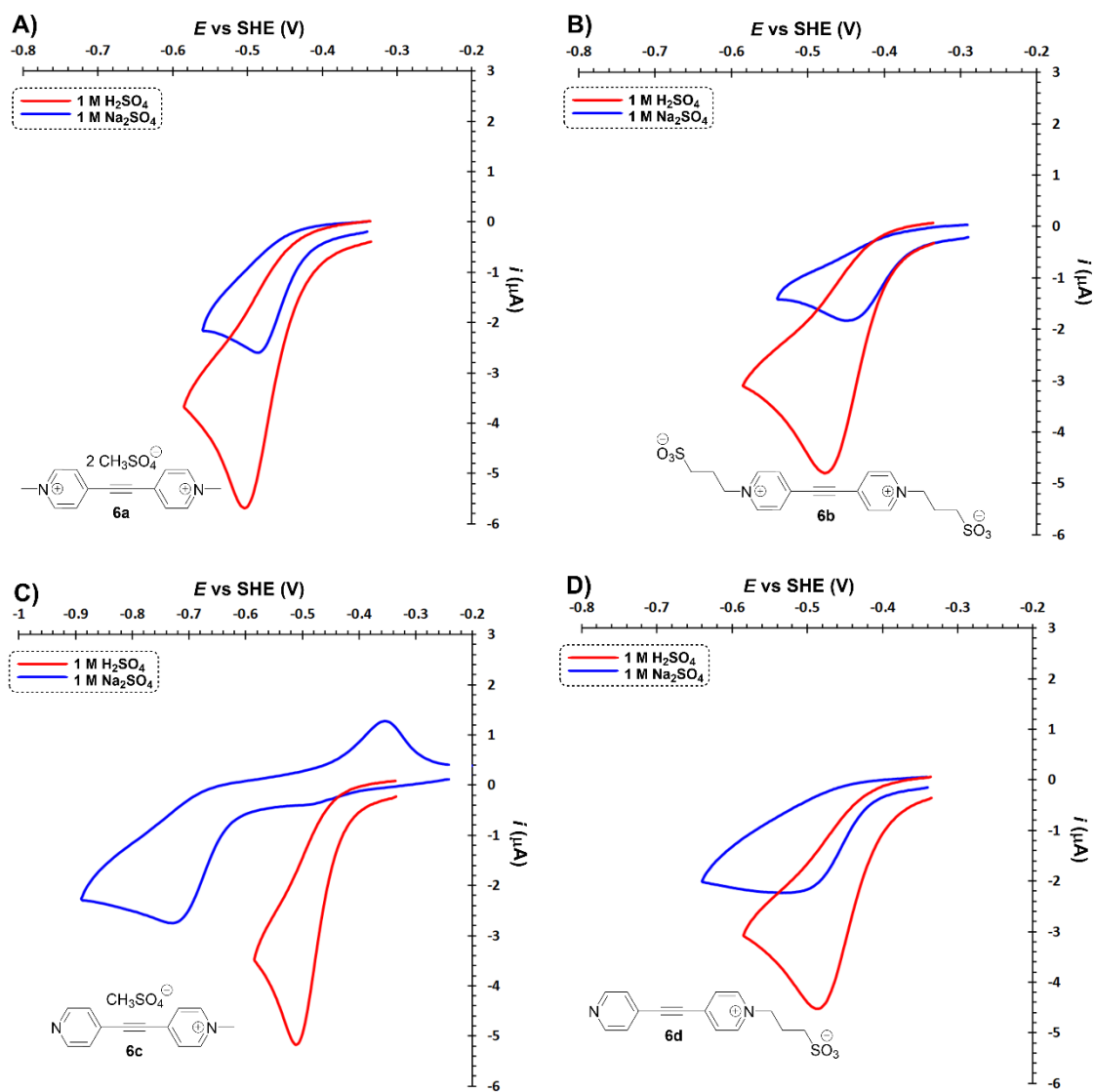


Figure S12 – Electrochemical reductions of bis(4-pyridyl)acetylene salts **6a–d** on glassy carbon electrode in neutral and acid media; $v = 100 \text{ mV}\cdot\text{s}^{-1}$.

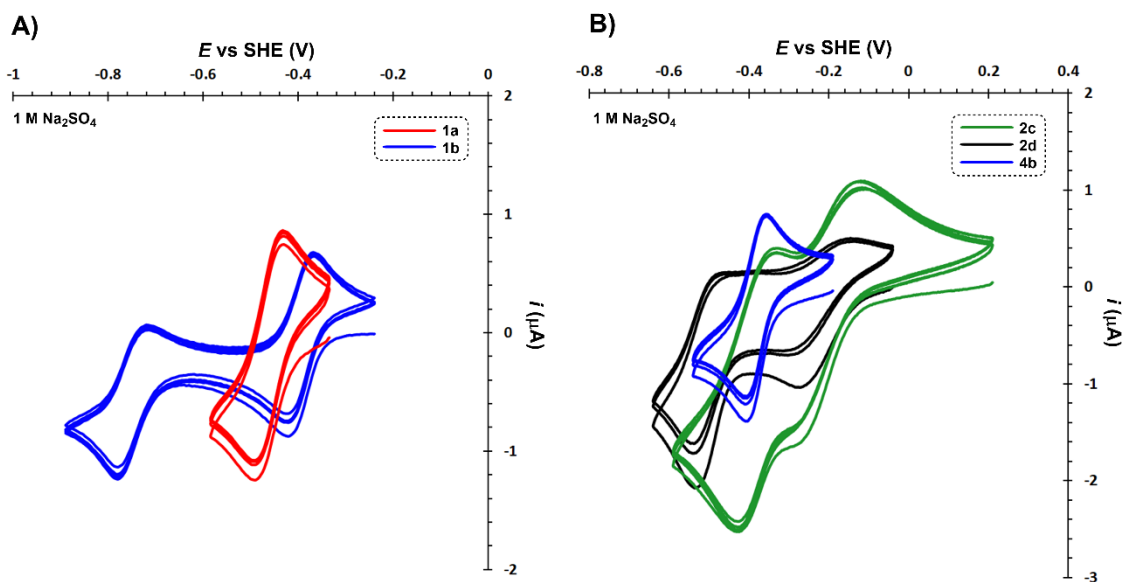


Figure S13 – Cyclic voltammograms of (quasi)reversible reductions of the bipyridine salts **1a–b** (A) and pyridazine/phenanthroline salts **2c–d/4b** (B) on glassy carbon electrode in neutral media; $\nu = 100 \text{ mV}\cdot\text{s}^{-1}$.

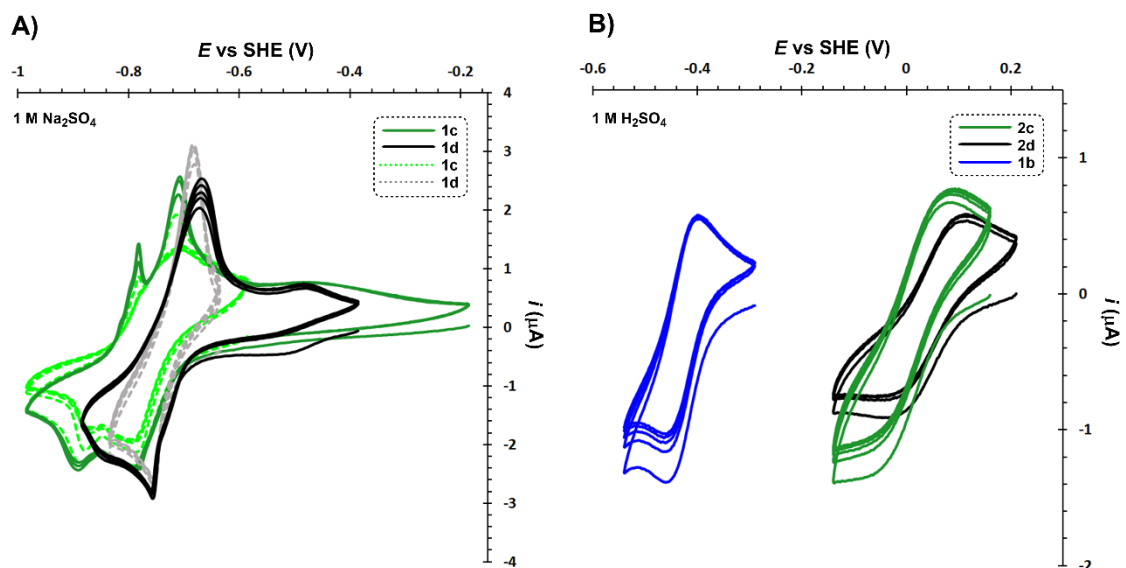


Figure S14 – Cyclic voltammograms of (quasi)reversible reductions of the bipyridine salts **1c–d** in neutral media (A) and pyridazine/bipyridine salts **2c–d/1b** on glassy carbon electrode in acidic media (B); $\nu = 100 \text{ mV}\cdot\text{s}^{-1}$.

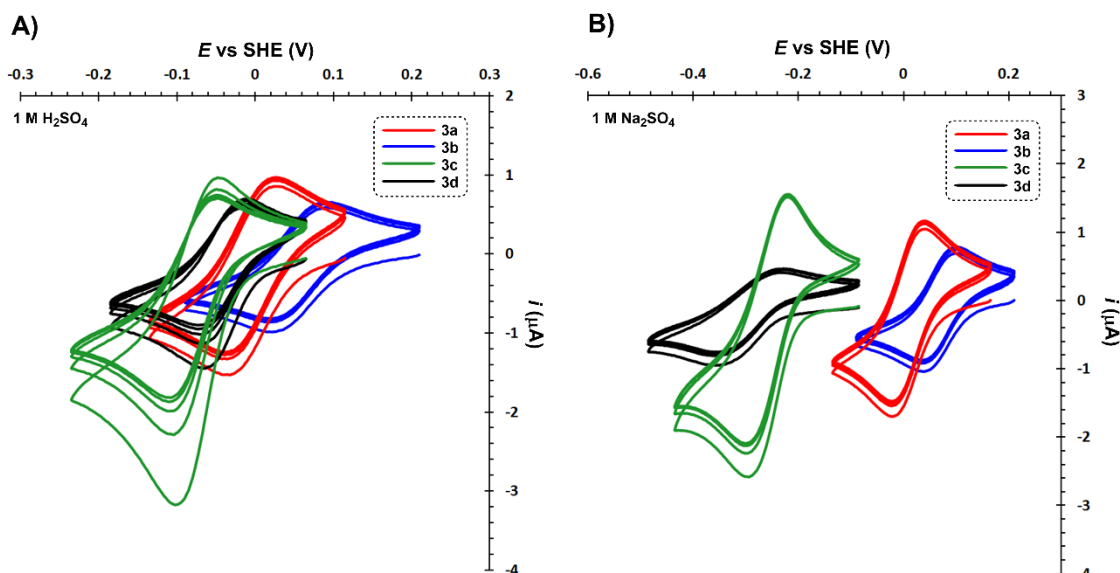


Figure S15 – Cyclic voltammograms of (quasi)reversible reductions of the naphthyridine salts **3a–d** on glassy carbon electrode in acidic (A) and neutral media (B); $v = 100 \text{ mV}\cdot\text{s}^{-1}$.

3 Solubility and chemical stability

The solubility measurement was performed in a glass apparatus, loaded with exact volume of aqueous electrolyte (0.5 ml), placed in ultrasonic bath tempered at 30 °C. The measured azinium salts (in its initial, i.e., oxidized form) was gradually added to the aqueous electrolyte with simultaneous sonication. The addition was continued until the first excess of measured salt was no longer dissolved and the saturated solution was formed (after 15 minutes of sonication). The corresponding solubility was calculated from the known volume of electrolyte and the amount of dissolved salt. The measurement was repeated three times.

Table S3 – Solubility of **1a–d** in aqueous electrolytes at 30 °C.

Comp.	Solubility in 1M Na ₂ SO ₄	Solubility in 1M H ₂ SO ₄
	[g·l ⁻¹ /mol·l ⁻¹]	[g·l ⁻¹ /mol·l ⁻¹]
1a	4656/11.4	4848/11.9
1b	519/1.3	870/2.2
1c	2962/10.5	2846/10.1
1d	102/0.4	768/2.8

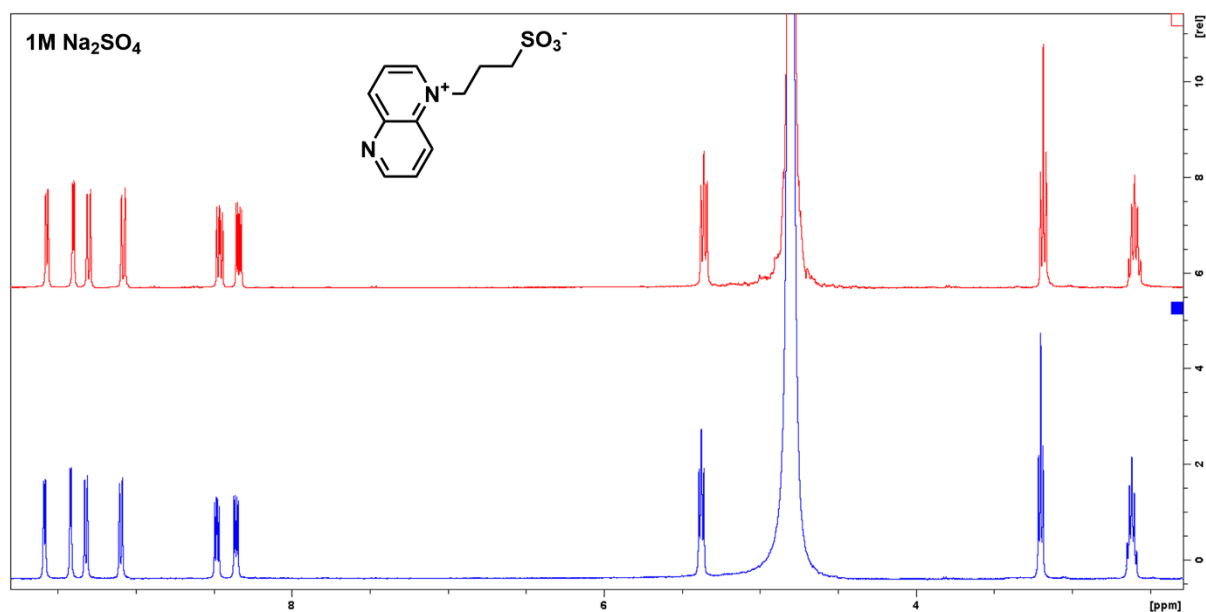


Figure S16 – ¹H-NMR spectra of 1,5-naphthyridine **3d** measured fresh (blue line) and after 50 days (red line) in 1 mol dm⁻³ Na₂SO₄.

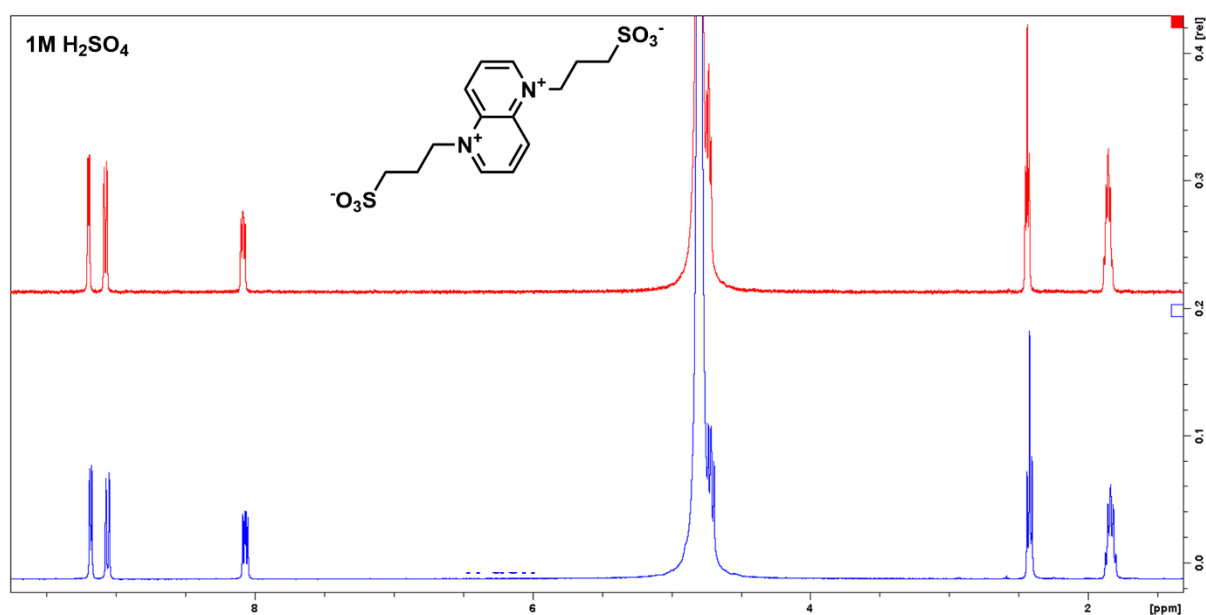


Figure S17 – ¹H-NMR spectra of 1,5-naphthyridine **3b** measured fresh (blue line) and after 50 days (red line) in 1 mol dm⁻³ H₂SO₄.

4 Electrochemical characterization on glassy carbon rotating disc electrode (RDE)

The selected promising compounds **1a**, **1b**, **1d**, **2d**, **3a**, **3b**, **3c** and **3d** providing chemically reversible redox processes on pyridine cycle were electrochemically characterized using rotating disc electrode (RDE) using ALS RRDE-3A by ALS Co., Ltd. Measurements were performed in three-electrode set-up using: glassy carbon working electrode (3.0 mm diameter), mercury sulfate reference electrode (MSE filled with sat. K₂SO₄ inner electrolyte with potential of 0.650 V vs. SHE) and platinum foil counter electrode. Before every experiment glassy carbon was pre-treated by mechanical polishing using grit papers (P1000 and P4000 by Wirtz-Buehler) followed by ultrasonication in isopropanol and water (5 min each) and subsequent electrochemical pretreatment in 14 mol·dm⁻³ NaOH according to Bystron *et al.*,^[9] which is in detail described in our previous publication.^[8] The electrolytes contained 1 mmol·dm⁻³ of electroactive compound in 1 mol·dm⁻³ aqueous solution of Na₂SO₄ (for neutral environment) or H₂SO₄ (for acidic environment).

The diffusion coefficient was evaluated from limiting currents at various rotation rates of RDE (500, 1000, 1500, 2000, 2500 and 3000 rpm) according to Levich equation (1):

$$i_{lim} = 0.62 z F A D^{2/3} \omega^{1/2} \nu^{-1/6} c_0 \quad (1)$$

where z represent the stoichiometric number of electrons involved in an electrode reaction, F the Faraday constant (C·mol⁻¹), A is geometric electrode area (cm²) D diffusion coefficient (cm²·s⁻¹), ω angular frequency of rotation ($2\pi f$), ν kinematic viscosity (cm²·s⁻¹), c_0 bulk concentration of species (mol·cm⁻³)

Kinetic parameters were evaluated from the same experimental data using Koutecky-Levich equation (2):

$$\frac{1}{i} = \frac{1}{i_k} + \frac{1}{i_{lim}} = \frac{1}{i_k} + 1/(0.62 z F A D^{2/3} \omega^{1/2} \nu^{-1/6} c_0) \quad (2)$$

Kinetic currents i_k at various potentials in the Tafel region were extrapolated from $1/i$ vs. $\omega^{-1/2}$ dependency for infinite rotation rate ($\omega^{-1/2} \rightarrow 0$). Subsequently, $\log i_k$ vs. E dependence was constructed and the exchange current i_0 and i_k were evaluated for $E_{1/2}$ and the slope, respectively, according to (3–4):

$$\alpha = 2.3 \text{ slope } \frac{RT}{F} \quad (3)$$

$$i_0 = 10^{(\text{slope } E_{1/2} + \text{offset})} \quad (4)$$

The heterogeneous rate constant k° was evaluated from i_0 according to (5):

$$k^\circ = \frac{i_0}{zFAc_0} \quad (5)$$

Half-wave potential $E_{1/2}$ was estimated from cyclic voltammetry curves measured at various scan rates (in the range of 5000 – 10 mV·s⁻¹) according to (6):

$$E_{1/2} = (E_{pa} + E_{pc})/2 \quad (6)$$

where E_{pa} and E_{pc} are potentials of anodic and cathodic peaks, respectively. These measurements were also used for estimation of k° from peak separation $\Delta E_p = E_{pa} - E_{pc}$ using Nicholson's method (7):

$$k^\circ = \Psi\left(\frac{\pi D z F v}{RT}\right)^{1/2} \quad (7)$$

The measured CV and LSV curves together with the following figure used for evaluation of kinetics parameters are for neutral and acid environment shown in Figures S18-S42. The evaluated parameters are summarized in Tab. S4.

Table S4 – Electrochemical parameters of the selected compounds in acidic and neutral environment evaluated from experiments on glassy carbon rotating disc electrode.

Compound	Supporting electrolyte	$E_{1/2}$ ^a [V vs. SHE]	D ^b [10 ⁻⁶ cm ² s ⁻¹]	α ^c [-]	k_{LK}° ^c [cm s ⁻¹]	k_{Nic}° ^a [cm s ⁻¹]
1a	1M Na ₂ SO ₄	-0.448	2.0±0.5	0.48±0.02	0.003±0.000	0.066±0.000
1b	1M Na ₂ SO ₄	-0.398	6.2±2.6	0.71±0.12	0.013±0.002	0.044±0.014
1d	1M Na ₂ SO ₄	-0.776	-	-	-	-
2d	1M H ₂ SO ₄	0.010	4.3±0.5	0.47±0.03	0.024±0.007	0.032±0.012
2d	1M Na ₂ SO ₄	-0.042	3.7±0.1	0.49±0.01	0.025±0.001	0.051±0.012
3a	1M H ₂ SO ₄	-0.041	1.8±0.2	0.61±0.09	0.180±0.017	0.048±0.004
3a	1M Na ₂ SO ₄	-0.002	4.3±0.1	0.37±0.00	0.023±0.000	0.029±0.007
3b	1M H ₂ SO ₄	0.050	4.0±0.1	0.50±0.08	0.017±0.003	0.010±0.000
3b	1M Na ₂ SO ₄	0.073	2.2±0.4	0.64±0.11	0.031±0.016	0.010±0.000
3c	1M H ₂ SO ₄	-0.121	2.9±0.1	0.48±0.05	0.017±0.004	0.094±0.015
3c	1M Na ₂ SO ₄	-0.330	2.0±0.1	0.47±0.06	0.021±0.012	0.011±0.003
3d	1M H ₂ SO ₄	-0.072	5.6±0.1	0.44±0.01	0.014±0.001	0.014±0.001

^aEvaluated from CV measurements using Nicholson's method; ^bEvaluated from RDE measurements using Levich equation; ^cEvaluated from RDE measurements using Levich-Koutecky equation.

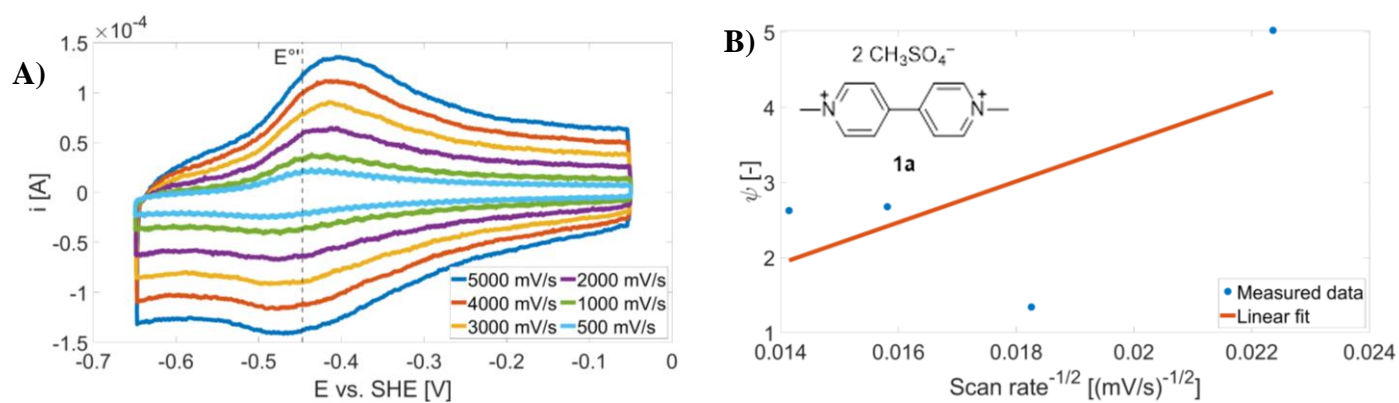


Figure S18 – CV of 1 mM solutions of **1a** in 1M Na₂SO₄ supporting electrolyte on glassy carbon electrode at various scan rates (A); Dependence of Ψ on $v^{-1/2}$ used for estimation of $E_{1/2}$ and k° using Nicholson method (B).

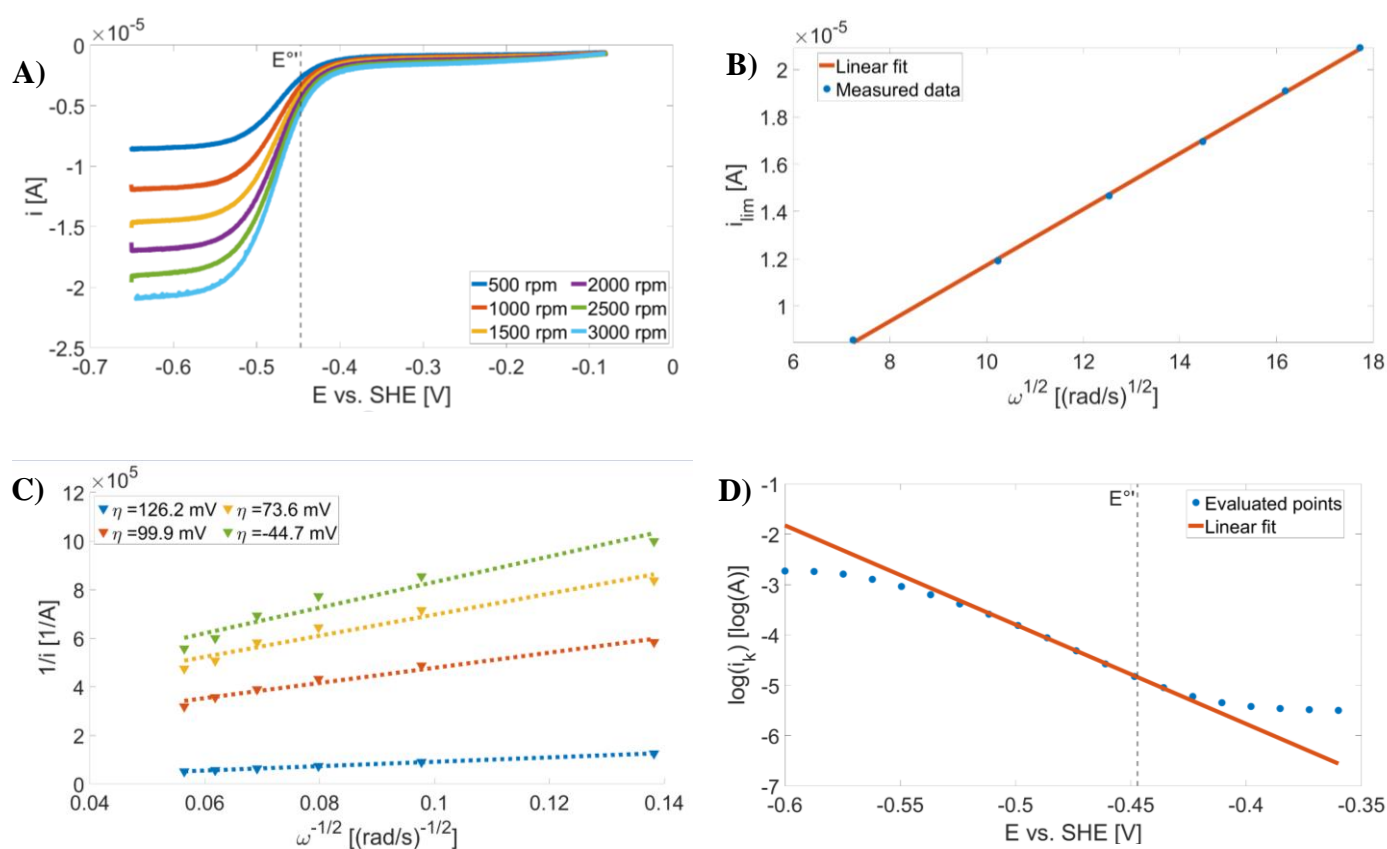


Figure S19 – LSV of 1 mM solutions of **1a** in 1M Na₂SO₄ supporting electrolyte on glassy carbon RDE at various rotations (A); Linear dependence of i_{lim} on $\omega^{1/2}$ used for evaluation of D using Levich equation (B); Linear dependence of $1/i$ on $\omega^{-1/2}$ at various overpotentials used for evaluation of i_k using Levich–Koutecky equation (C); Dependence of $\log i_k$ on E for evaluation k° and α using Tafel equation (D).

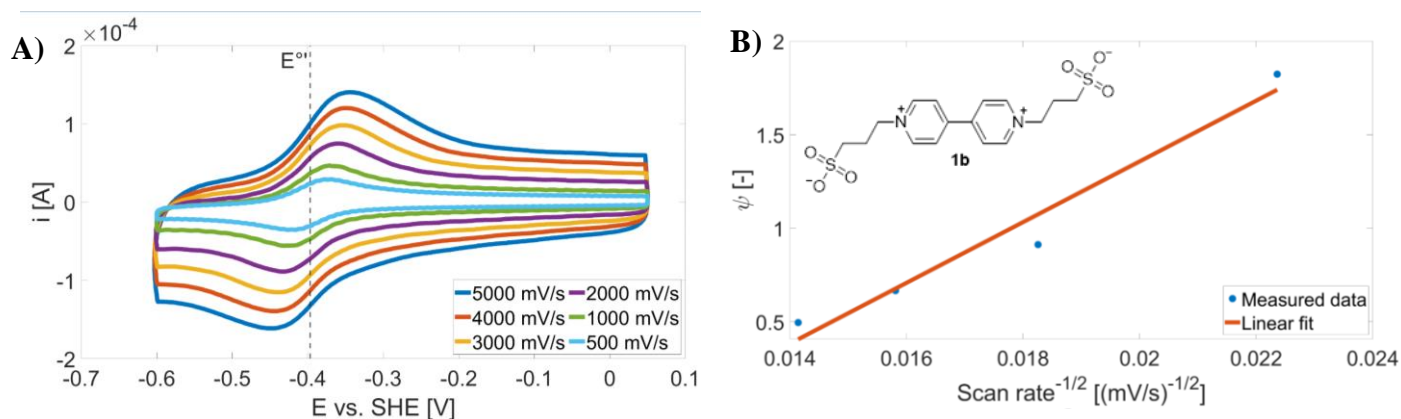


Figure S20 – CV of 1 mM solutions of **1b** in 1M Na₂SO₄ supporting electrolyte on glassy carbon electrode at various scan rates (A); Dependence of Ψ on $v^{-1/2}$ used for estimation of $E_{1/2}$ and k° using Nicholson method (B).

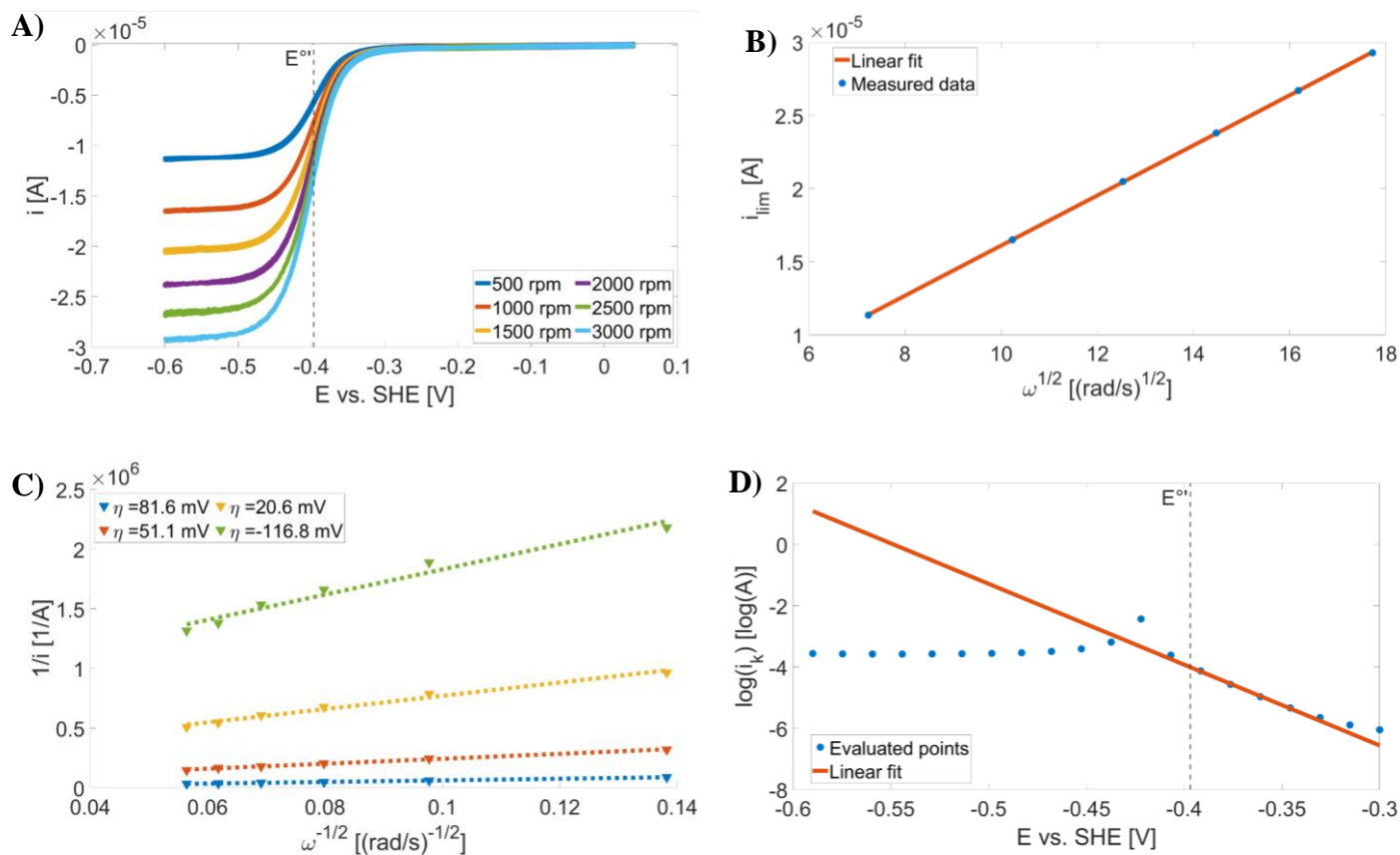


Figure S21 – LSV of 1 mM solutions of **1b** in 1M Na₂SO₄ supporting electrolyte on glassy carbon RDE at various rotations (A); Linear dependence of i_{lim} on $\omega^{1/2}$ used for evaluation of D using Levich equation (B); Linear dependence of $1/i$ on $\omega^{-1/2}$ at various overpotentials used for evaluation of i_k using Levich–Koutecky equation (C); Dependence of $\log i_k$ on E for evaluation k° and α using Tafel equation (D).

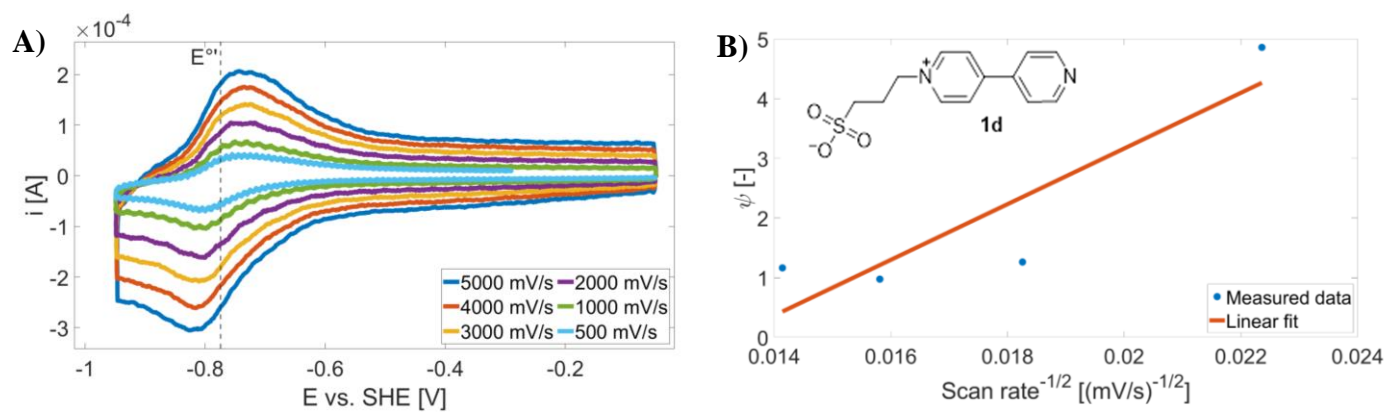


Figure S22 – CV of 1 mM solutions of **1d** in 1M Na₂SO₄ supporting electrolyte on glassy carbon electrode at various scan rates (A); Dependence of Ψ on $v^{1/2}$ used for estimation of $E_{1/2}$ and k^0 using Nicholson method (B).

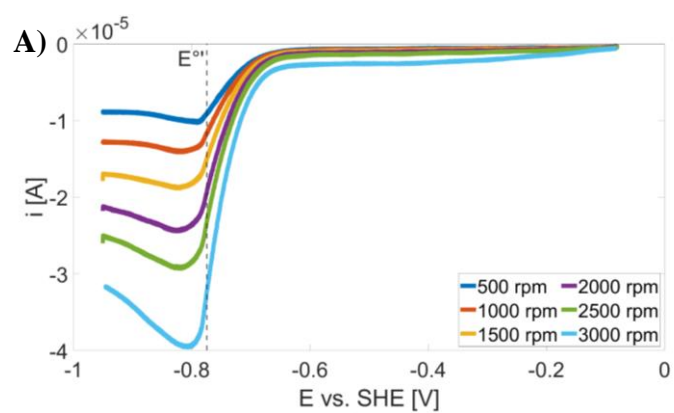


Figure S23 – LSV of 1 mM solutions of **1d** in 1M Na₂SO₄ supporting electrolyte on glassy carbon RDE at various rotations (A).

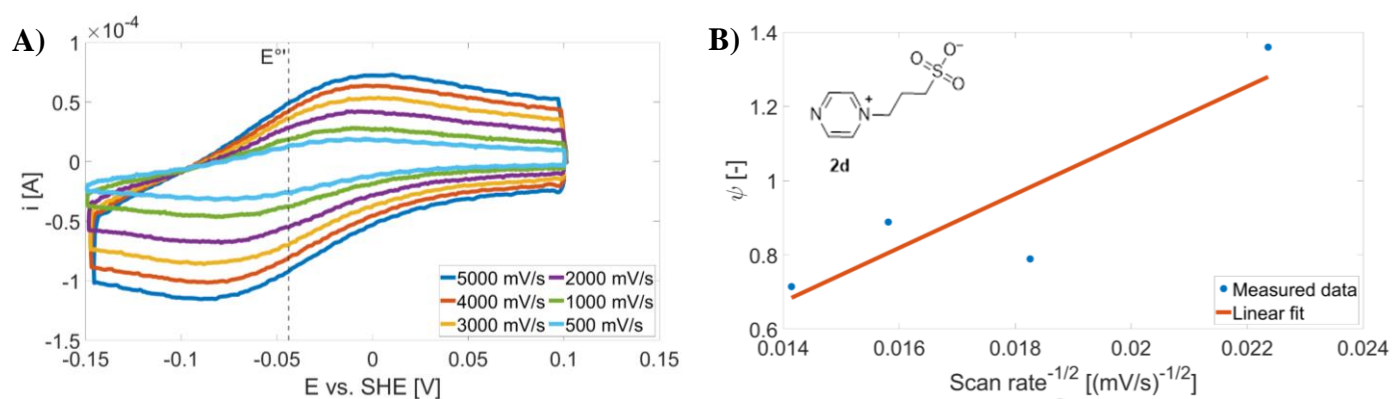


Figure S24 – CV of 1 mM solutions of **2d** in 1M Na₂SO₄ supporting electrolyte on glassy carbon electrode at various scan rates (A); Dependence of Ψ on $v^{-1/2}$ used for estimation of $E_{1/2}$ and k° using Nicholson method (B).

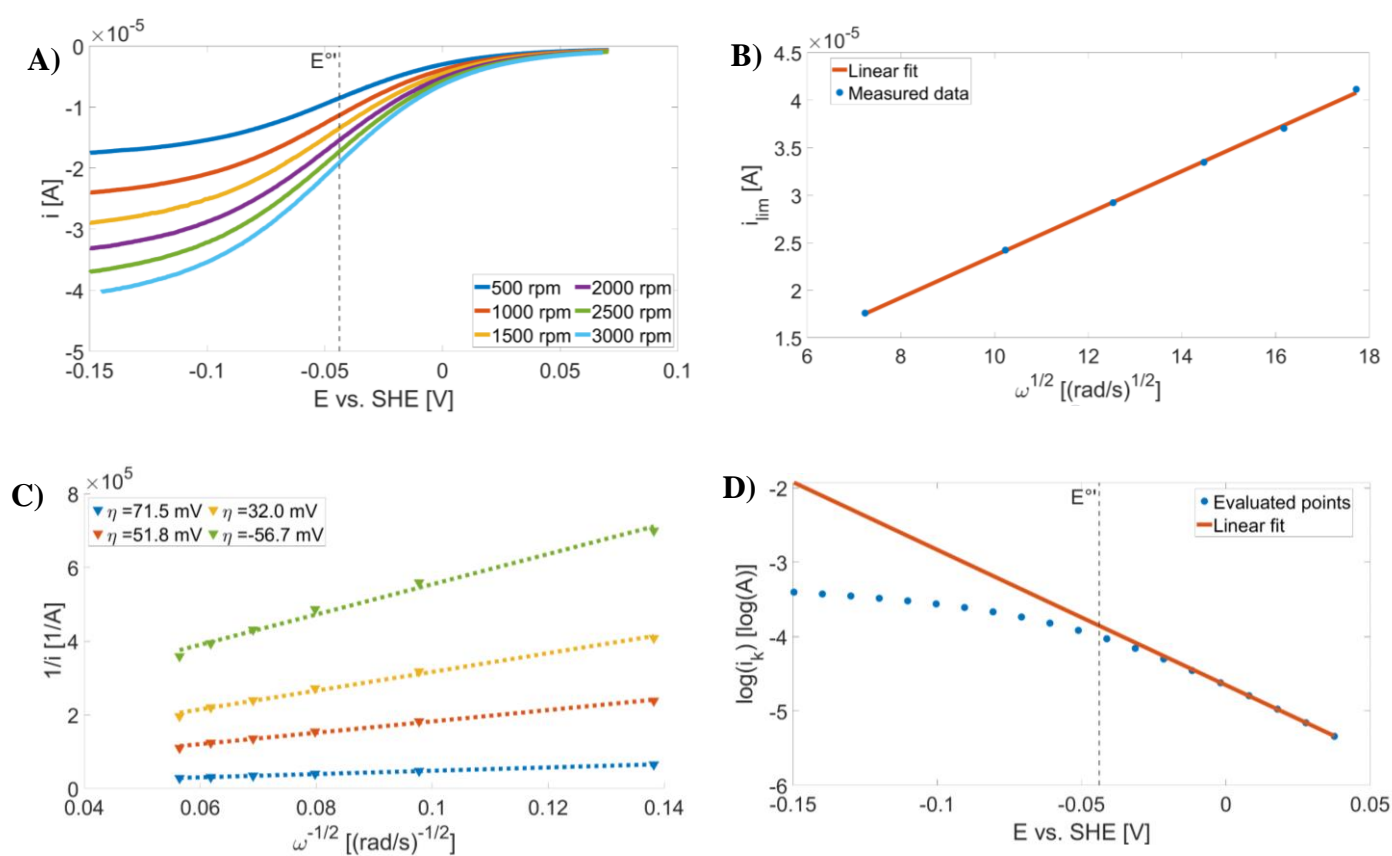


Figure S25 – LSV of 1 mM solutions of **2d** in 1M Na₂SO₄ supporting electrolyte on glassy carbon RDE at various rotations (A); Linear dependence of i_{lim} on $\omega^{1/2}$ used for evaluation of D using Levich equation (B); Linear dependence of $1/i$ on $\omega^{-1/2}$ at various overpotentials used for evaluation of i_k using Levich–Koutecky equation (C); Dependence of $\log i_k$ on E for evaluation k° and α using Tafel equation (D).

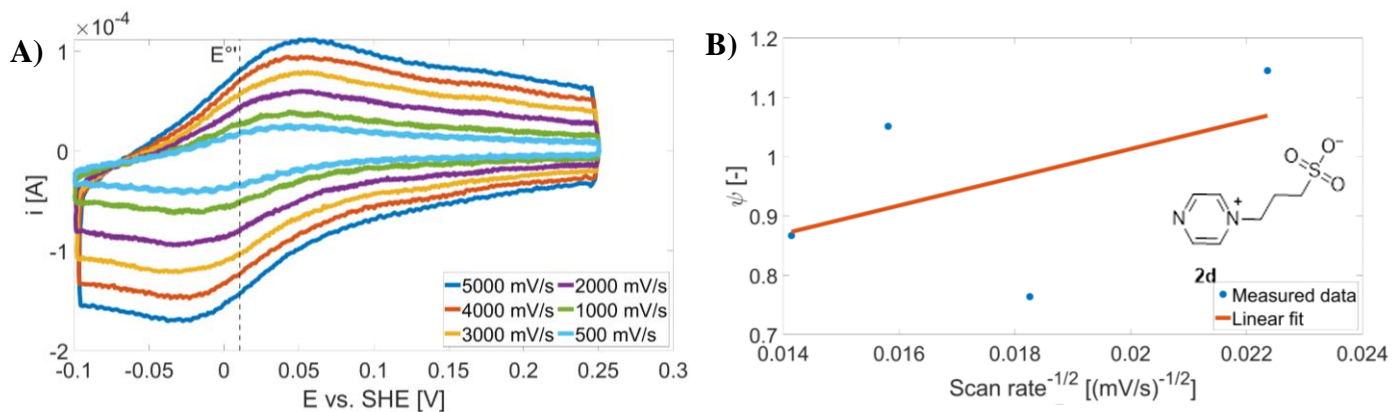


Figure S26 – CV of 1 mM solutions of **2d** in 1M H_2SO_4 supporting electrolyte on glassy carbon electrode at various scan rates (A); Dependence of Ψ on $v^{-1/2}$ used for estimation of $E_{1/2}$ and k° using Nicholson method (B).

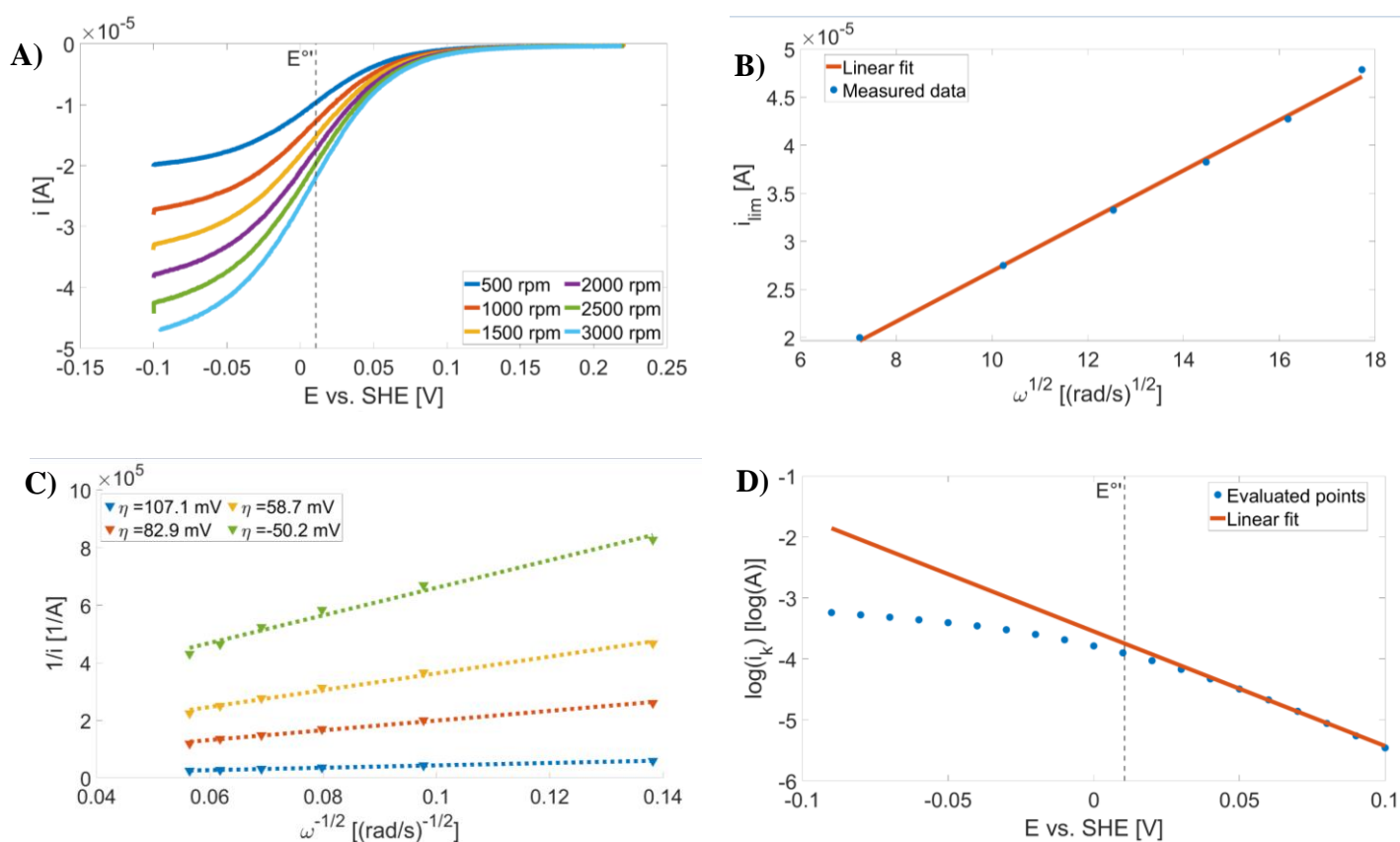


Figure S27 – LSV of 1 mM solutions of **2d** in 1M H_2SO_4 supporting electrolyte on glassy carbon RDE at various rotations (A); Linear dependence of i_{lim} on $\omega^{1/2}$ used for evaluation of D using Levich equation (B); Linear dependence of $1/i$ on $\omega^{-1/2}$ at various overpotentials used for evaluation of i_k using Levich –Koutecky equation (C); Dependence of $\log i_k$ on E for evaluation k° and α using Tafel equation (D).

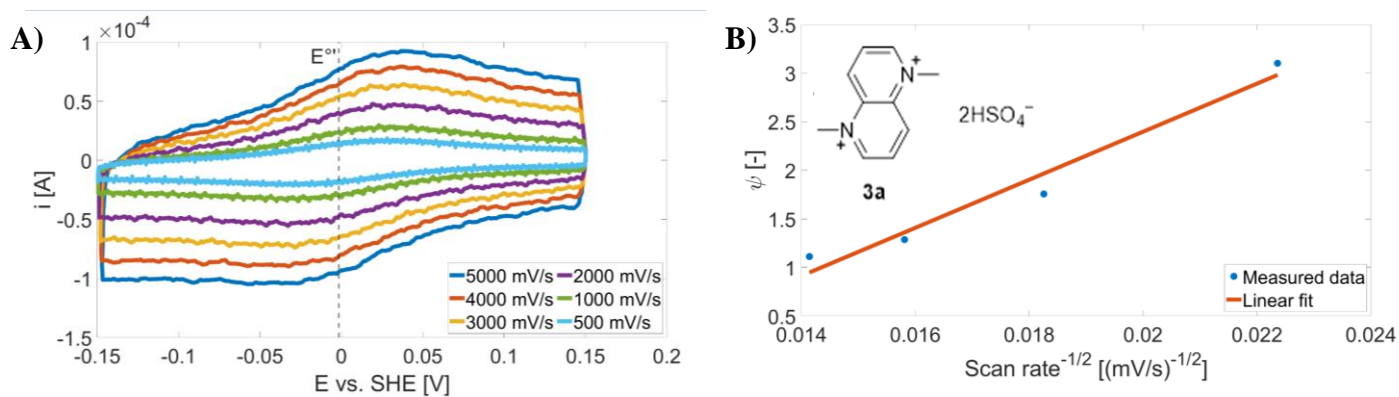


Figure S28: CV of 1 mM solutions of **3a** in 1M Na₂SO₄ supporting electrolyte on glassy carbon electrode at various scan rates (A); Dependence of ψ on $v^{-1/2}$ used for estimation of $E_{1/2}$ and k° using Nicholson method (B).

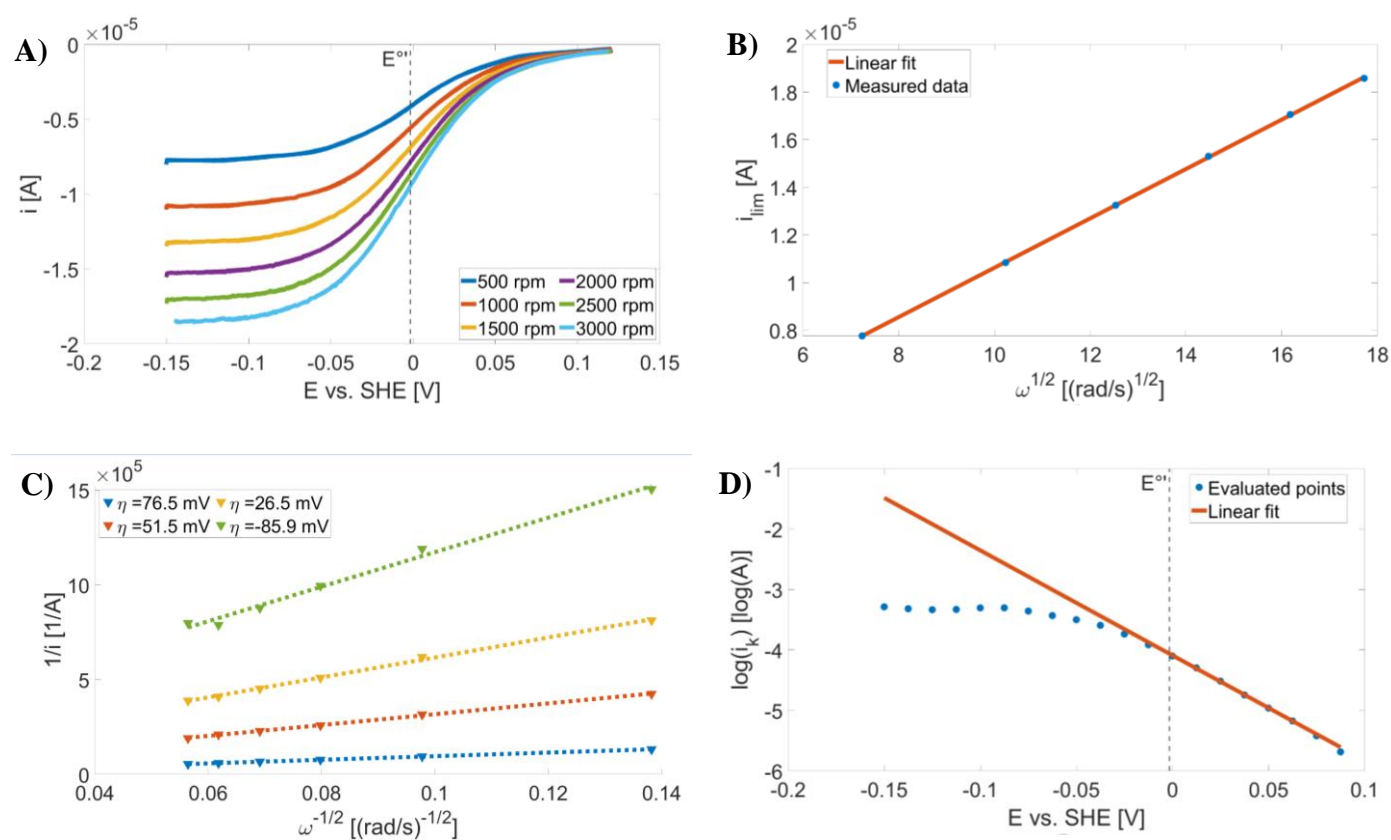


Figure S29 – LSV of 1 mM solutions of **3a** in 1M Na₂SO₄ supporting electrolyte on glassy carbon RDE at various rotations (A); Linear dependence of i_{lim} on $\omega^{1/2}$ used for evaluation of D using Levich equation (B); Linear dependence of $1/i$ on $\omega^{-1/2}$ at various overpotentials used for evaluation of i_k using Levich –Koutecky equation (C); Dependence of $\log i_k$ on E for evaluation k° and α using Tafel equation (D).

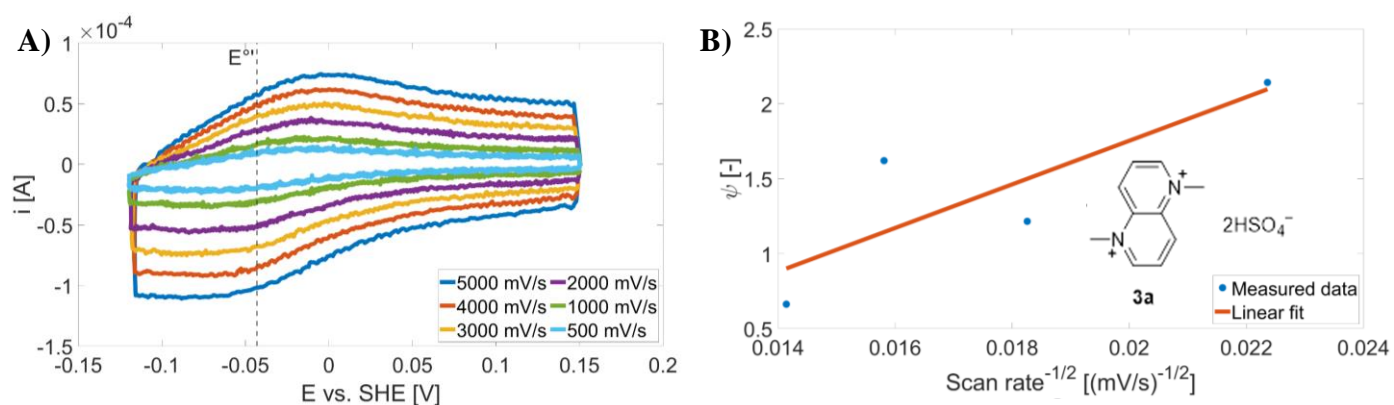


Figure S30 – CV of 1 mM solutions of **3a** in 1M H_2SO_4 supporting electrolyte on glassy carbon electrode at various scan rates (A); Dependence of Ψ on $v^{-1/2}$ used for estimation of $E_{1/2}$ and k^o using Nicholson method (B).

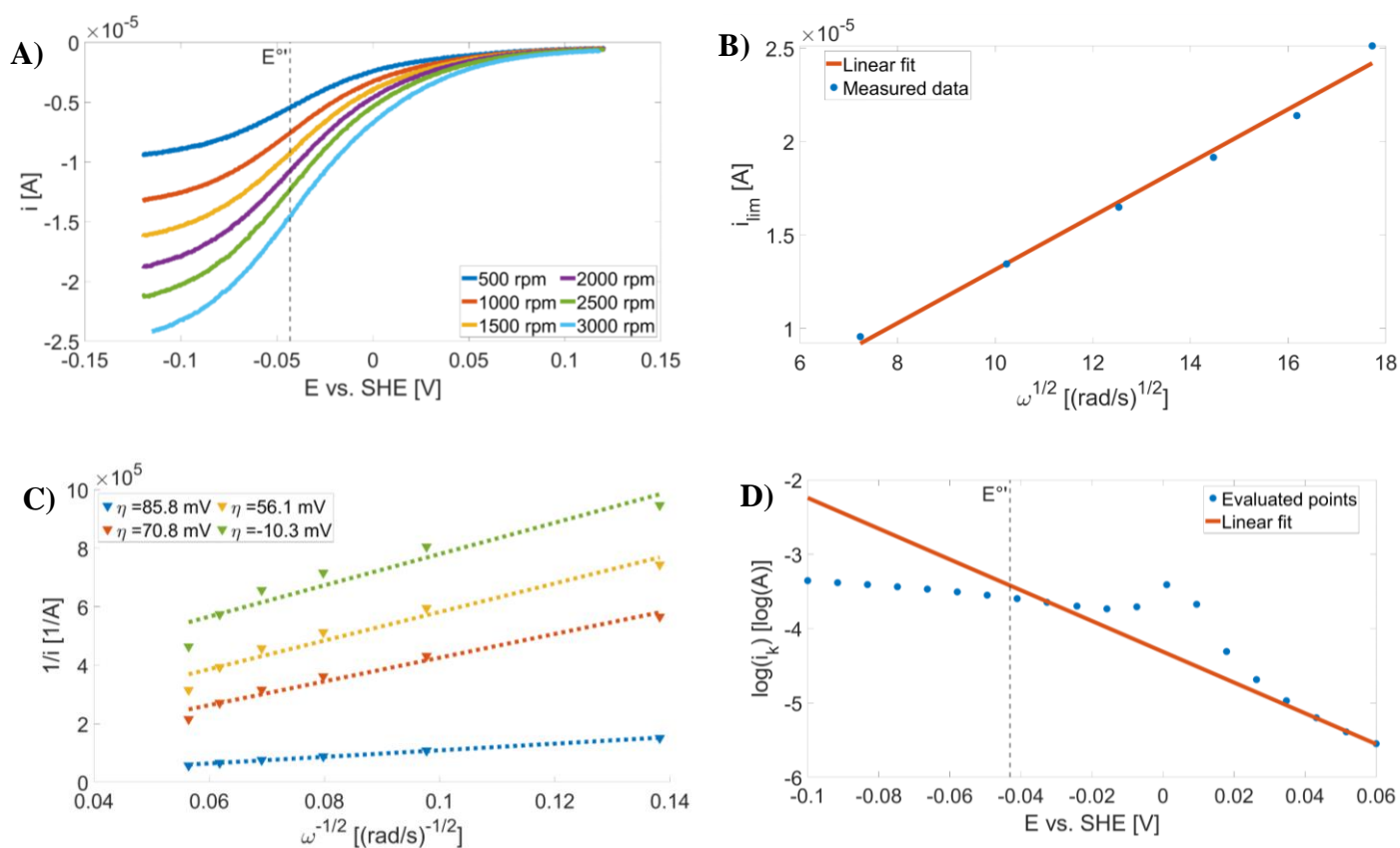


Figure S31 – LSV of 1 mM solutions of **3a** in 1M H_2SO_4 supporting electrolyte on glassy carbon RDE at various rotations (A); Linear dependence of i_{lim} on $\omega^{1/2}$ used for evaluation of D using Levich equation (B); Linear dependence of $1/i$ on $\omega^{-1/2}$ at various overpotentials used for evaluation of i_k using Levich –Koutecky equation (C); Dependence of $\log i_k$ on E for evaluation k^o and α using Tafel equation (D).

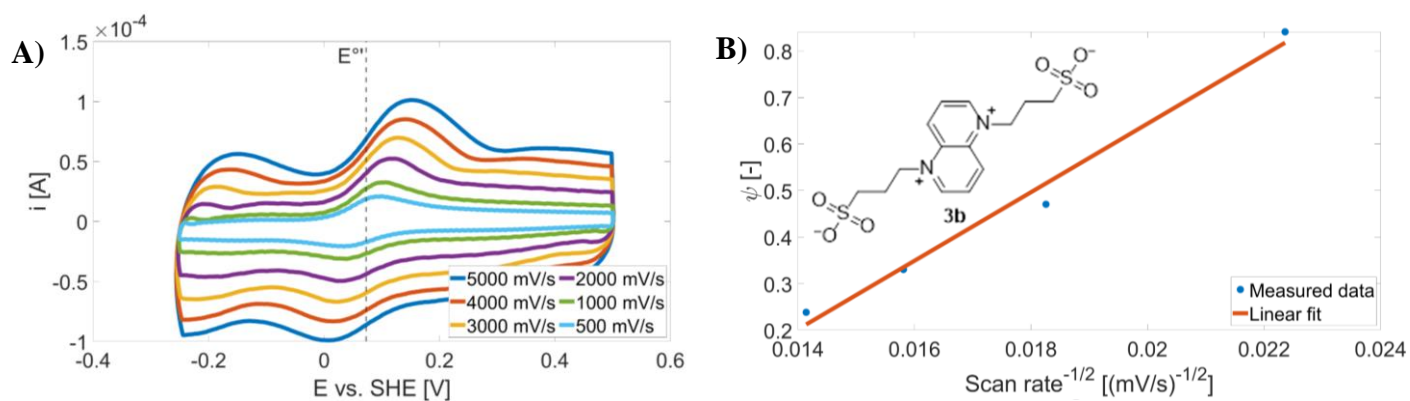


Figure S32 – CV of 1 mM solutions of **3b** in 1M Na₂SO₄ supporting electrolyte on glassy carbon electrode at various scan rates (A); Dependence of Ψ on $v^{-1/2}$ used for estimation of $E_{1/2}$ and k° using Nicholson method (B).

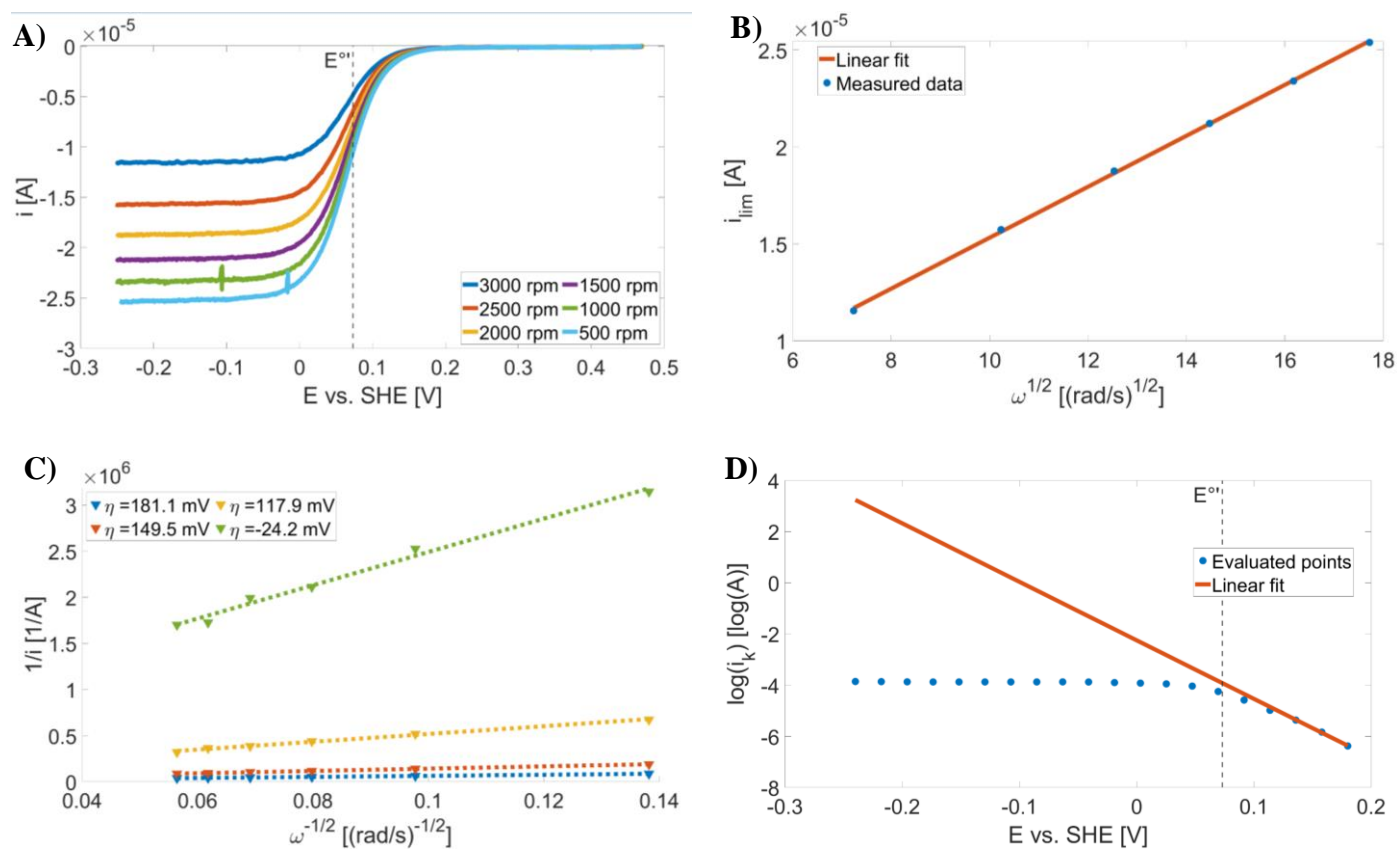


Figure S33 – LSV of 1 mM solutions of **3b** in 1M Na₂SO₄ supporting electrolyte on glassy carbon RDE at various rotations (A); Linear dependence of i_{lim} on $\omega^{1/2}$ used for evaluation of D using Levich equation (B); Linear dependence of $1/i$ on $\omega^{-1/2}$ at various overpotentials used for evaluation of i_k using Levich–Koutecky equation (C); Dependence of $\log i_k$ on E for evaluation k° and a using Tafel equation (D).

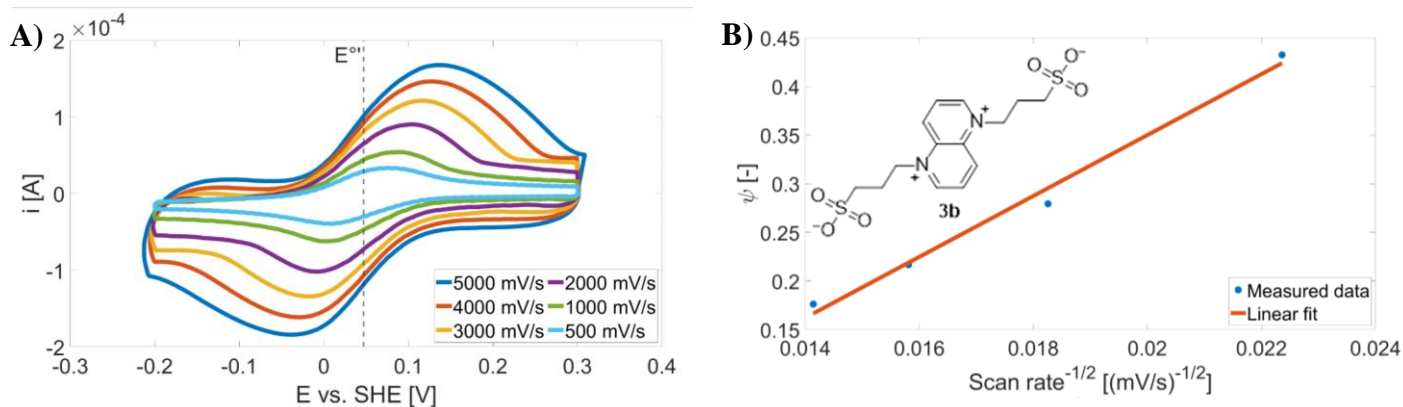


Figure S34 – CV of 1 mM solutions of **3b** in 1M H_2SO_4 supporting electrolyte on glassy carbon electrode at various scan rates (A); Dependence of Ψ on $v^{-1/2}$ used for estimation of $E_{1/2}$ and k° using Nicholson method (B).

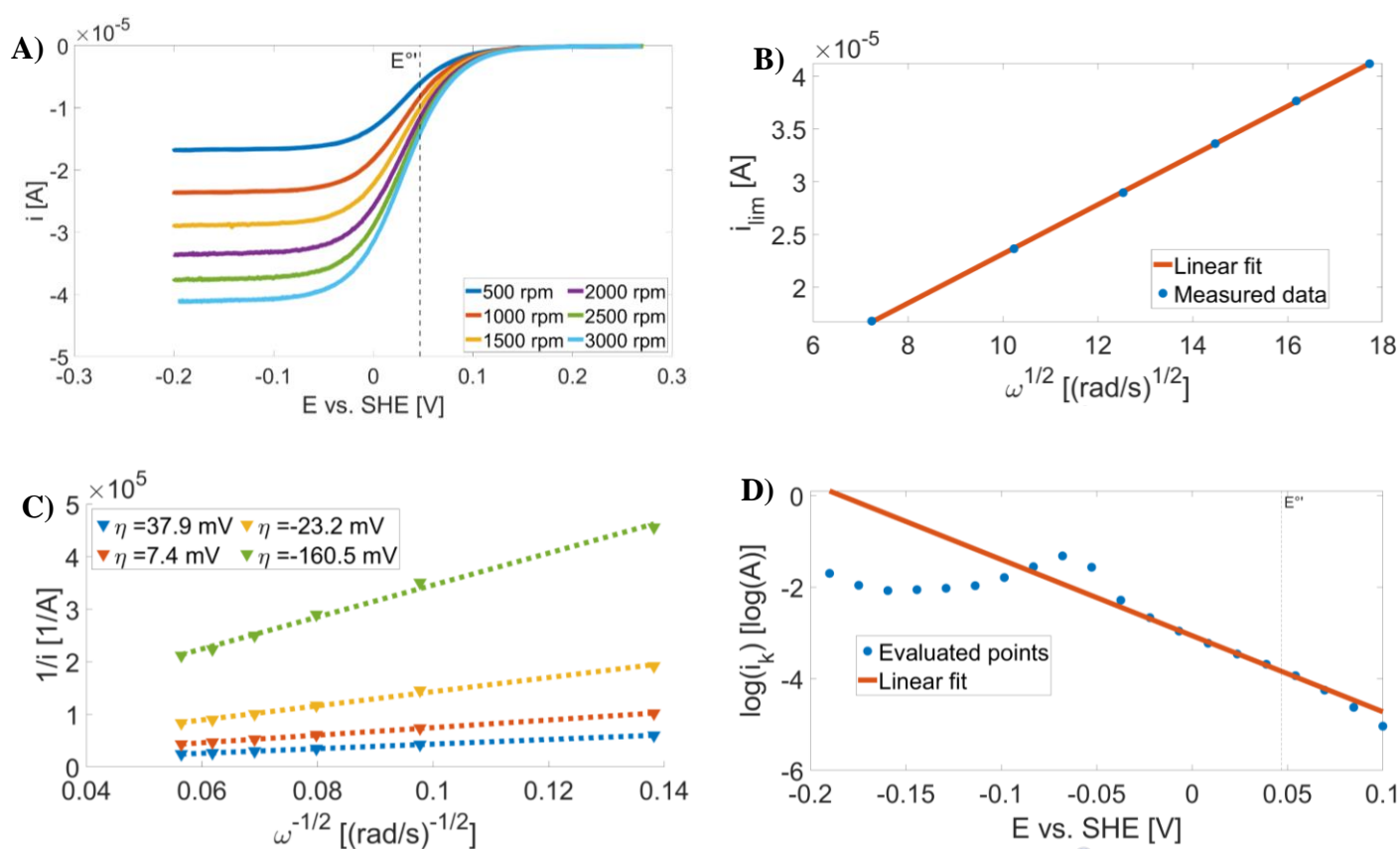


Figure S35 – LSV of 1 mM solutions of **3b** in 1M H_2SO_4 supporting electrolyte on glassy carbon RDE at various rotations (A); Linear dependence of i_{lim} on $\omega^{1/2}$ used for evaluation of D using Levich equation (B); Linear dependence of $1/i$ on $\omega^{-1/2}$ at various overpotentials used for evaluation of i_k using Levich–Koutecky equation (C); Dependence of $\log i_k$ on E for evaluation k° and α using Tafel equation (D).

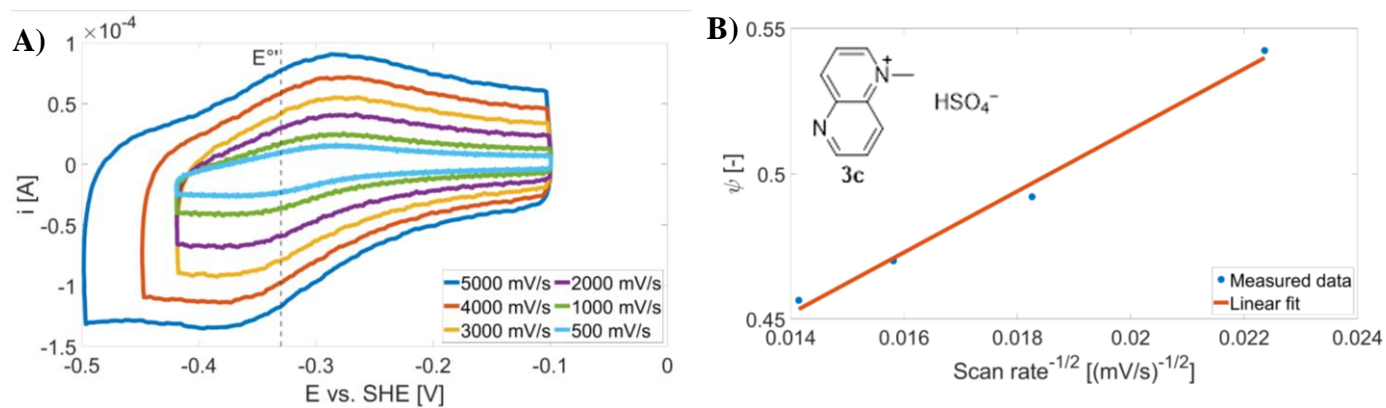


Figure S36 – CV of 1 mM solutions of **3c** in 1M Na₂SO₄ supporting electrolyte on glassy carbon electrode at various scan rates (A); Dependence of Ψ on $v^{1/2}$ used for estimation of $E_{1/2}$ and k° using Nicholson method (B).

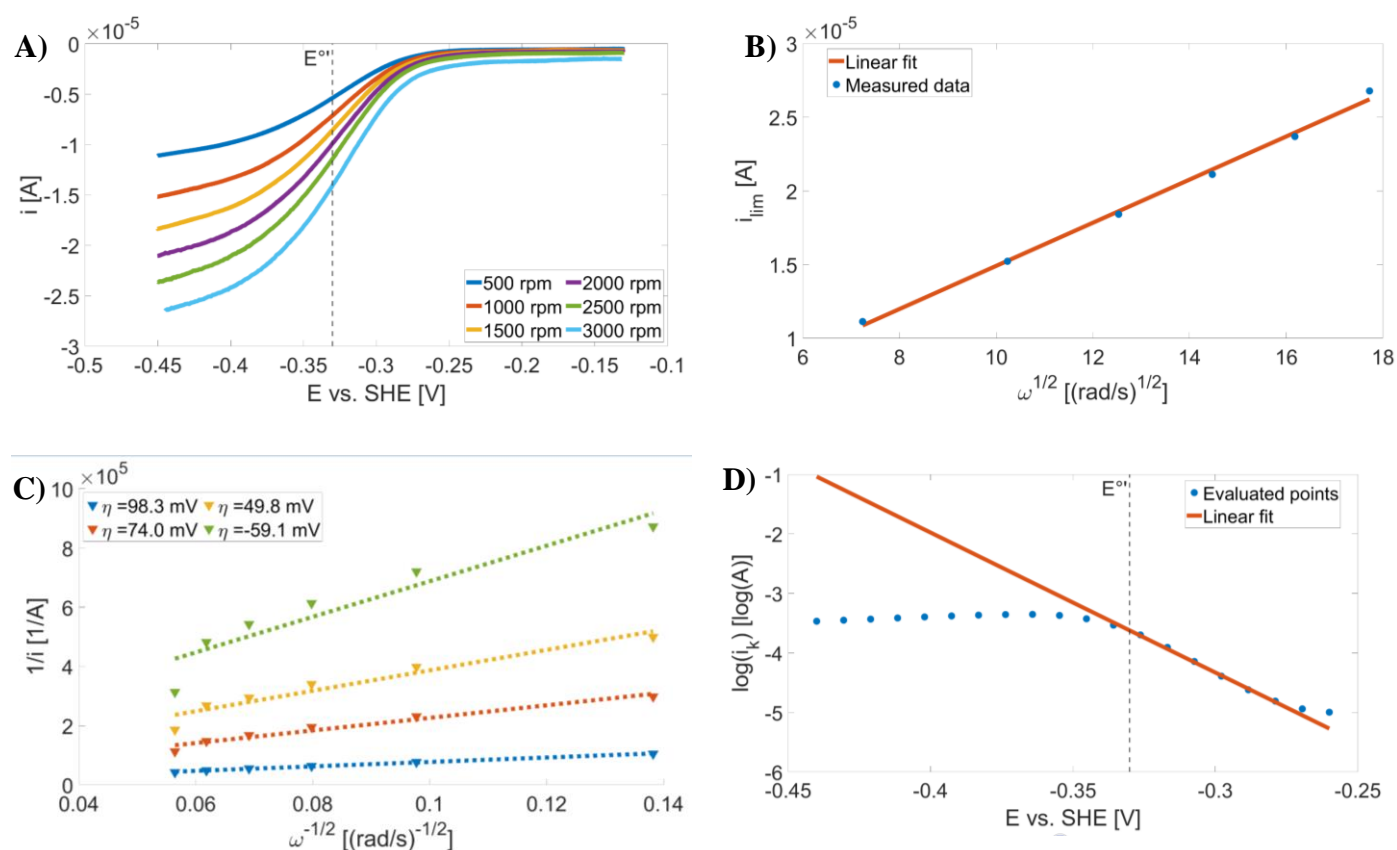


Figure S37 – LSV of 1 mM solutions of **3c** in 1M Na₂SO₄ supporting electrolyte on glassy carbon RDE at various rotations (A); Linear dependence of i_{lim} on $\omega^{1/2}$ used for evaluation of D using Levich equation (B); Linear dependence of $1/i$ on $\omega^{-1/2}$ at various overpotentials used for evaluation of i_k using Levich –Koutecky equation (C); Dependence of $\log i_k$ on E for evaluation k° and α using Tafel equation (D).

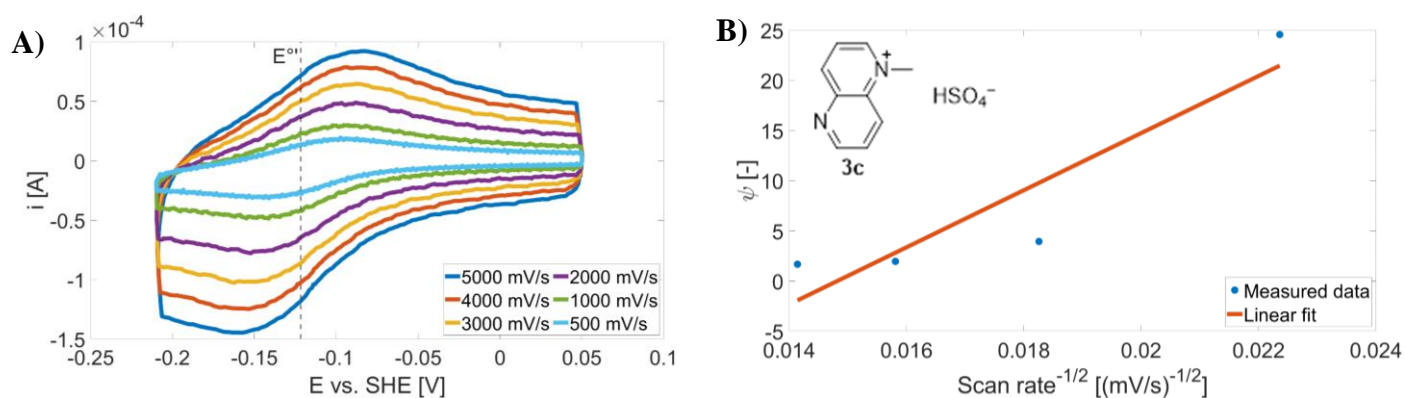


Figure S38 – CV of 1 mM solutions of **3c** in 1M H_2SO_4 supporting electrolyte on glassy carbon electrode at various scan rates (A); Dependence of Ψ on $v^{1/2}$ used for estimation of $E_{1/2}$ and k° using Nicholson method (B).

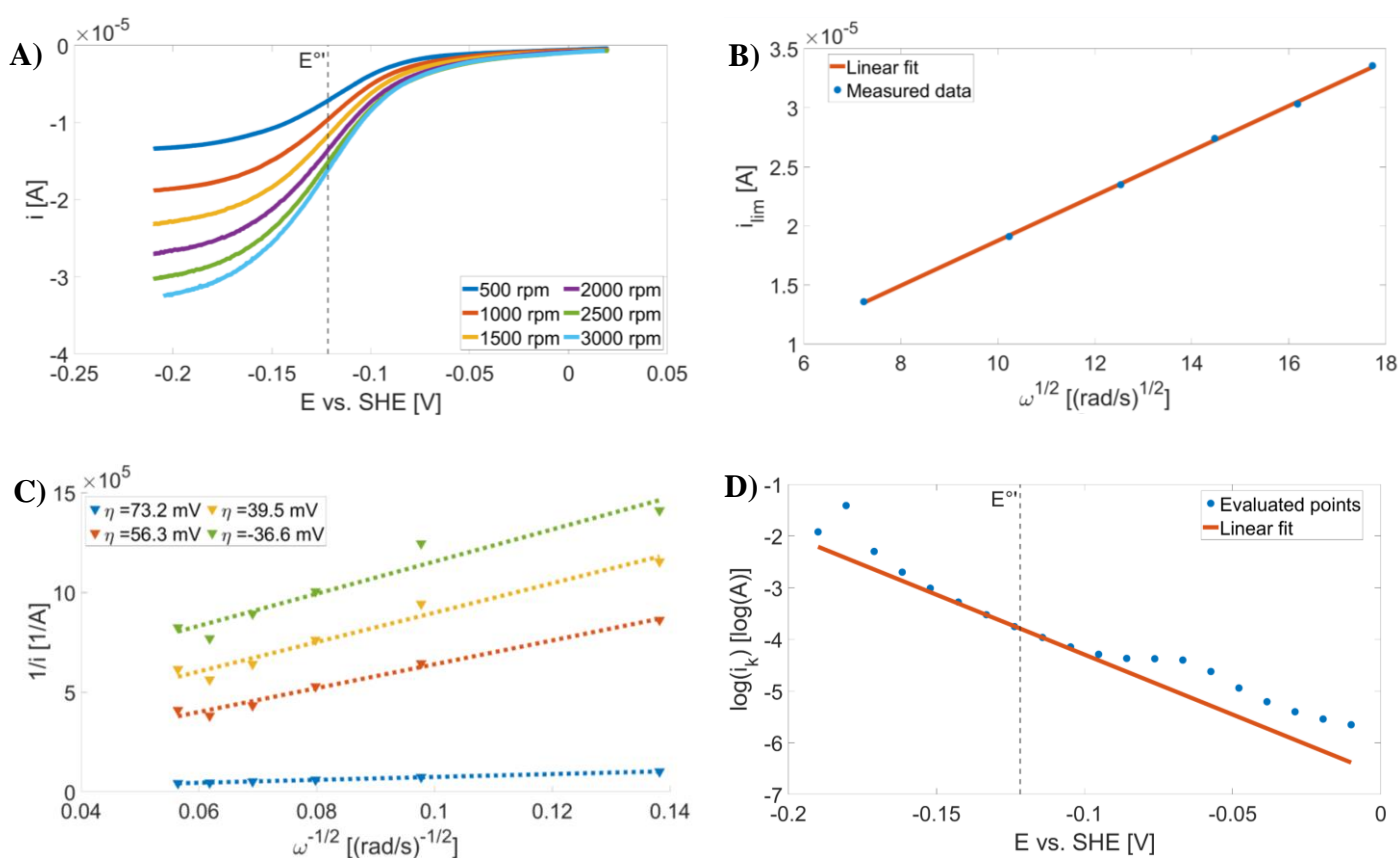


Figure S39 – LSV of 1 mM solutions of **3c** in 1M H_2SO_4 supporting electrolyte on glassy carbon RDE at various rotations (A); Linear dependence of i_{lim} on $\omega^{1/2}$ used for evaluation of D using Levich equation (B); Linear dependence of $1/i$ on $\omega^{-1/2}$ at various overpotentials used for evaluation of i_k using Levich–Koutecky equation (C); Dependence of $\log i_k$ on E for evaluation k° and α using Tafel equation (D).

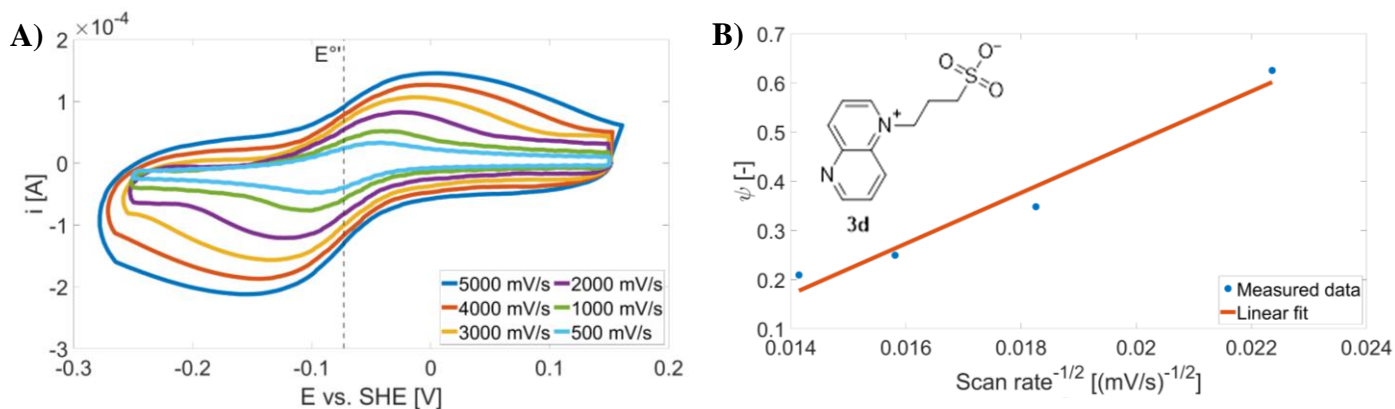


Figure S40: CV of 1 mM solutions of **3d** in 1M H_2SO_4 supporting electrolyte on glassy carbon electrode at various scan rates (A); Dependence of Ψ on $v^{-1/2}$ used for estimation of $E_{1/2}$ and k° using Nicholson method (B).

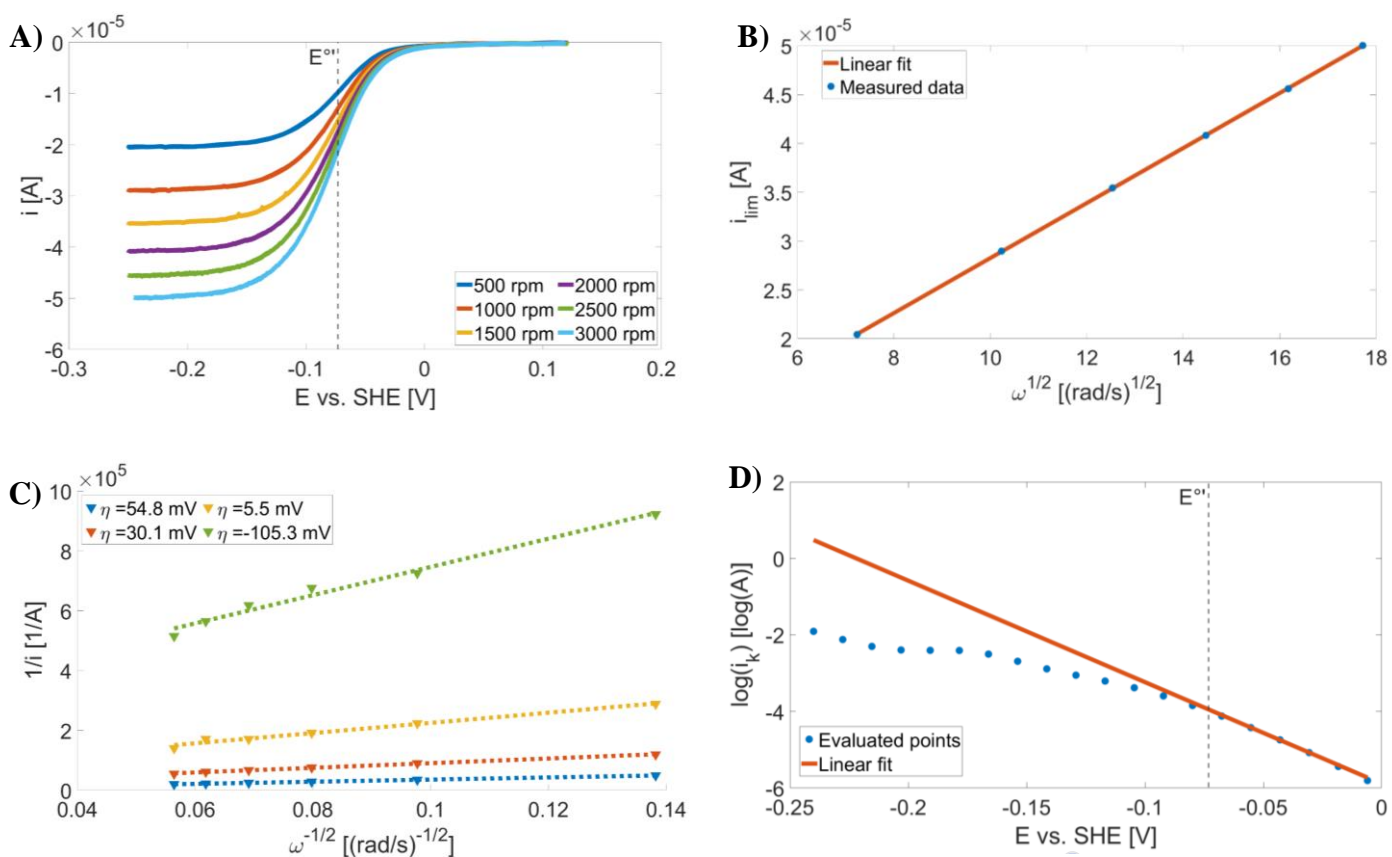


Figure S41 – LSV of 1 mM solutions of **3d** in 1M H_2SO_4 supporting electrolyte on glassy carbon RDE at various rotations (A); Linear dependence of i_{lim} on $\omega^{1/2}$ used for evaluation of D using Levich equation (B); Linear dependence of $1/i$ on $\omega^{-1/2}$ at various overpotentials used for evaluation of i_k using Levich –Koutecky equation (C); Dependence of $\log(i_k)$ on E for evaluation k° and α using Tafel equation (D).

5 Evaluation of electrochemical stability in flow battery cell

The selected compounds were tested in a flow electrolysis cell (Pinflow energy storage, s.r.o.) using thermally activated PAN-based carbon felt working electrode (4 cm² active geometric area, 5.0 mm initial thickness, compressed to approx. 75% of its initial thickness) and platinised titanium plate and mesh counter electrode. Both half-cells were mutually separated by suitable ion-exchange membrane (FAA-3-PK-130 for cationic compounds and cation-exchange membrane F1850 for zwitterionic compounds, both provided by Fumatech). The working electrolyte contained 25 mmol·dm⁻³ of active compound in 1 mol·dm⁻³ Na₂SO₄ or H₂SO₄ aqueous supporting electrolyte and it was circulated through the felt at 40 ml·min⁻¹ flow rate using peristaltic pump (Watson Marlow), corresponding to linear velocity of 54 cm·s⁻¹. The pristine supporting electrolyte was circulated through counter electrode half-cell at same flow rate where water splitting reactions proceeded. The galvanostatic charging (reduction) – discharging (oxidation) cycles were performed in the suitable potential window (selected based on previous CV measurements). The capacity utilization CU, coulombic efficiency CE and capacity decay CD were calculated from the obtained curves using equations (7-9):

$$CU = \frac{Q_{\text{dis}}}{Q_{\text{theor.}}} = \frac{Q_{\text{dis}}}{cVzF} \quad (7)$$

$$CE = \frac{Q_{\text{dis}}}{Q_{\text{char}}} \quad (8)$$

$$CD = \frac{dQ_{\text{dis}}}{d(\text{cycle})} / Q_{\text{theor.}} \quad (9)$$

where Q_{char} and Q_{dis} represent capacity of charge and discharge half-cycle, respectively; $Q_{\text{theor.}}$ is theoretical capacity of the electrolyte calculated from concentration of electroactive compound c in working electrolyte of volume V , z is number of exchanged electrons and F is Faraday constant. Relative CD was evaluated from the slope linear part of Q_{dis} -cycle number dependency divided by $Q_{\text{theor.}}$

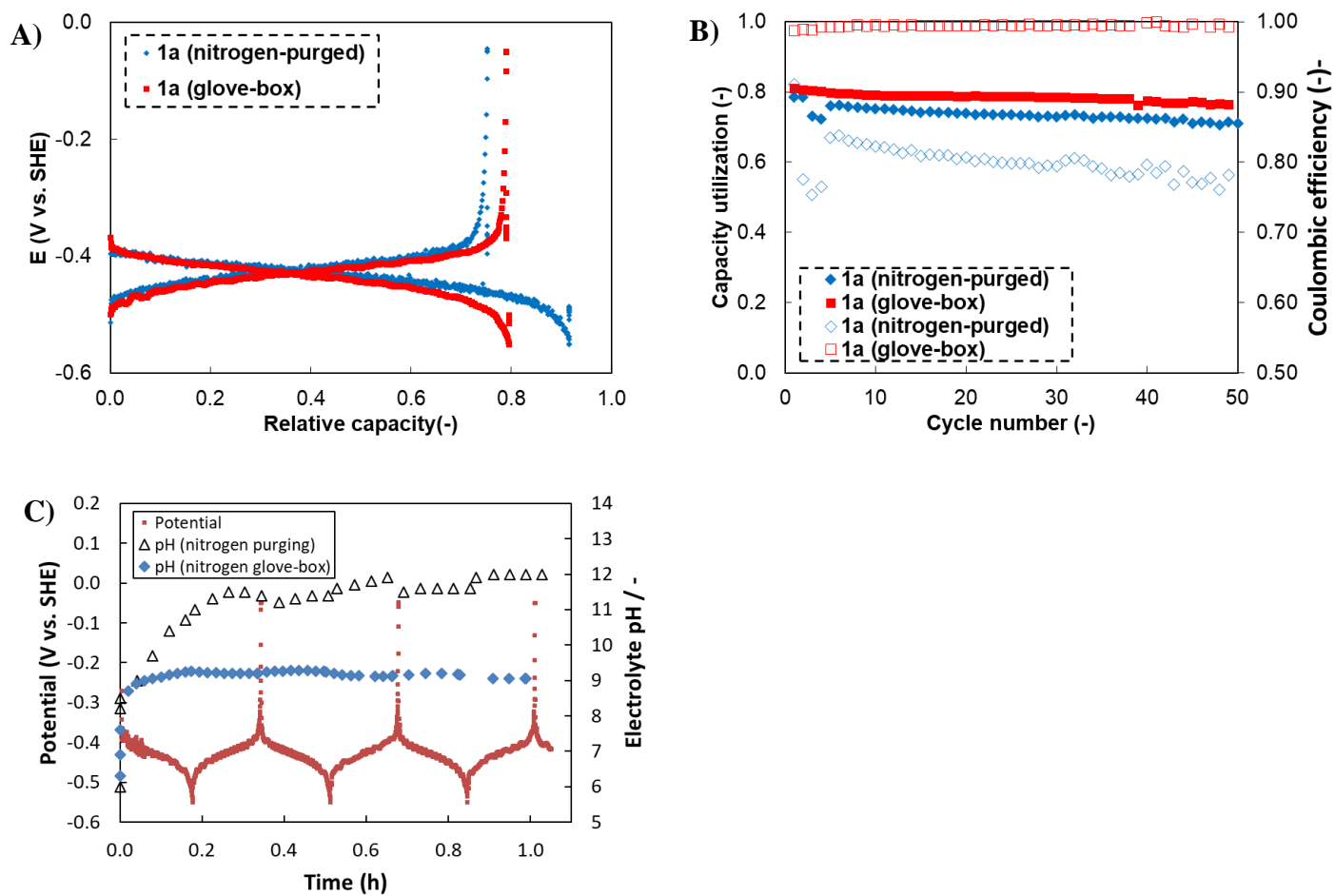


Figure S42 – Development of working electrode potential during galvanostatic cycling (2nd cycle) of **1a** in 1 M Na₂SO₄ (A); Development of capacity utilization (filled symbols) and coulombic efficiency (empty symbols) during cycling (B); Development of working electrode potential and pH during first 3 cycles when measured in nitrogen glovebox and when electrolyte was purged by nitrogen 5.0 purity (C).

Table S5 – Parameters of charge discharge cycling of electrolytes in a flow battery cell

	<i>CE</i> ^a	<i>CU</i> ^b	<i>CD</i> ^c	<i>CD</i> ^d	<i>pH</i>	
	%	%	% <i>Q</i> _{theor./cycle}	% <i>Q</i> _{theor.}	before	after
1M Na₂SO₄						
1a (1 st step)	99.2	82	−0.1	−6	4.4	9.6
1a (both steps)	99.6	65	−0.3	−34	4.4	8.7
1b (1 st step)	99.5	91	0.0	0	4.4	10.6
1b (both steps)	99.5	85	−0.6	−4	4.4	11.4
1d (1 st step)	96.3	93	−1.6	−83	7.0	9.8
2d (1 st step)	Irreversible reduction				5.9	8.2
3a (1 st step)	98.5	74	−0.6	−63	2.8	3.5
3b (1 st step)	100.0	78	−0.1	−23	3.9	4.7
3c (1 st step)	Irreversible reduction				2.6	4.2
3d (1 st step)	Irreversible reduction				6.3	7.5
1M H₂SO₄						
1a (1 st step)	Irreversible reduction.					
1b (1 st step)	Irreversible reduction.					
1d (1 st step)	Irreversible reduction.					
2d (1 st step)	Irreversible reduction.					
3a (1 st step)	92.9	14	−0.0	−99		
3b (1 st step)	97.3	80	−0.7	−63		
3c (1 st step)	Irreversible reduction.					
3d (1 st step)	Irreversible reduction.					

^a averaged from 11th-50th cycle; ^b calculated from maximal discharge capacity; ^c evaluated from slope of linear region of *Q*_{dis} – cycle number dependency (11th-50th cycle); ^d total decrease in capacity within 50 cycles related to *Q*_{theor.}

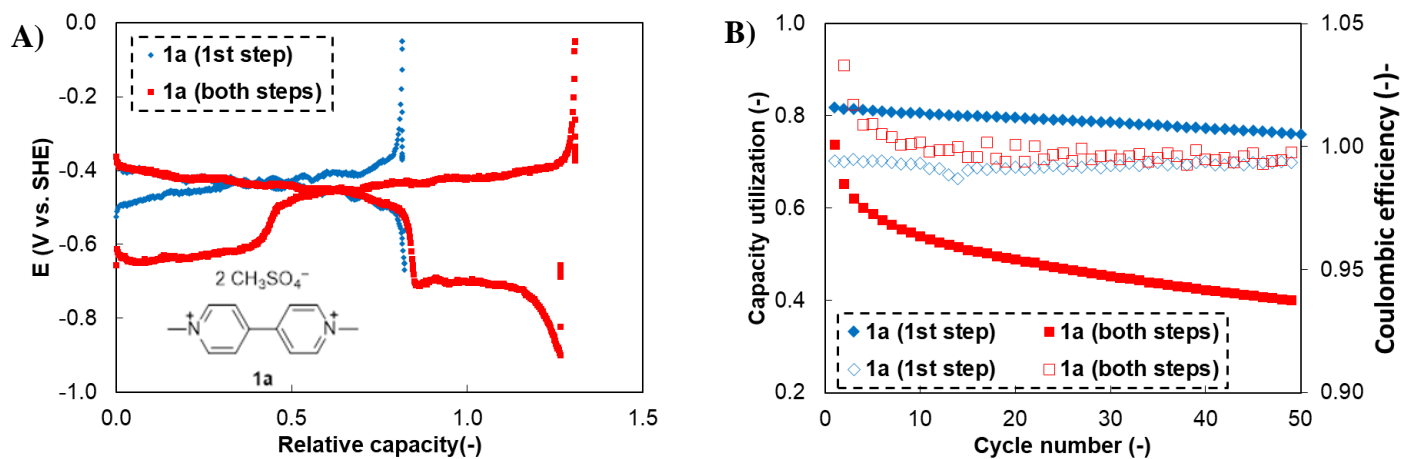


Figure S43 – Development of working electrode potential during galvanostatic cycling (2nd cycle) of **1a** in 1 M Na₂SO₄ (A); Development of capacity utilization (filled symbols) and coulombic efficiency (empty symbols) during cycling (B).

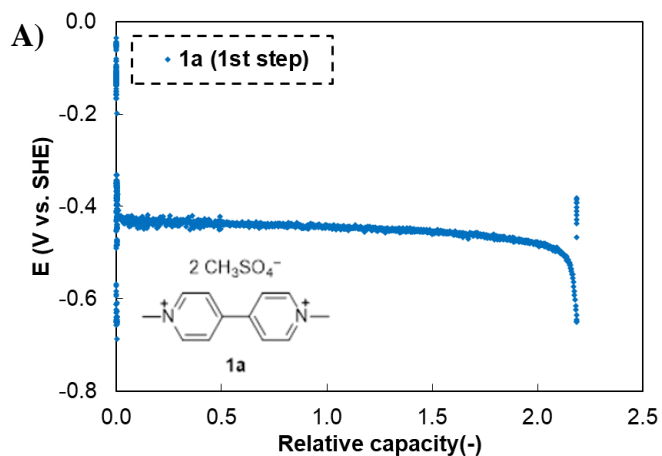


Figure S44 – Development of working electrode potential during galvanostatic cycling (2nd cycle) of **1a** in 1 M H₂SO₄ (A). Irreversible reduction observed.

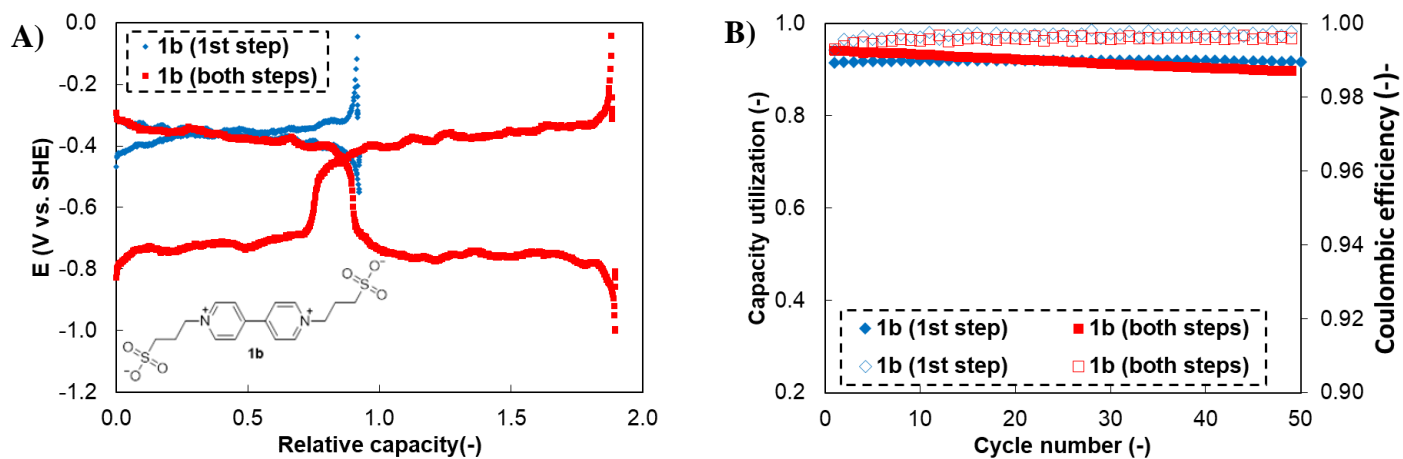


Figure S45 – Development of working electrode potential during galvanostatic cycling (2nd cycle) of **1b** in 1 M Na₂SO₄ (A); Development of capacity utilization (filled symbols) and coulombic efficiency (empty symbols) during cycling (B).

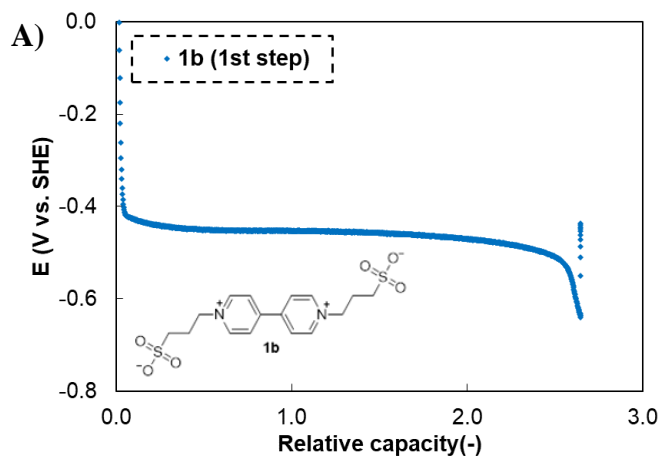


Figure S46 – Development of working electrode potential during galvanostatic cycling (2nd cycle) of **1b** in 1 M H₂SO₄ (A). Irreversible reduction observed.

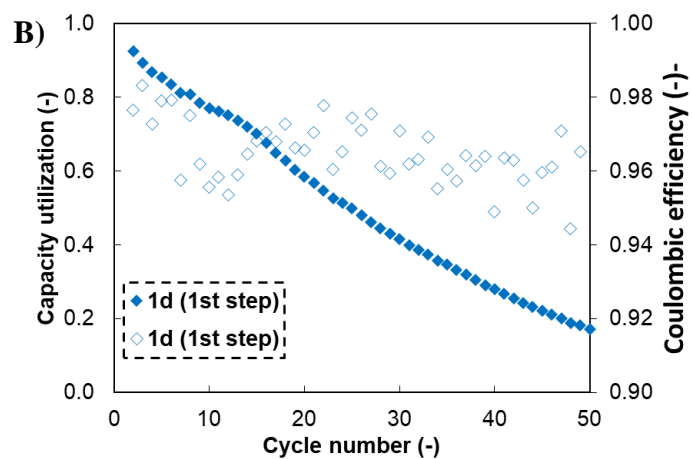
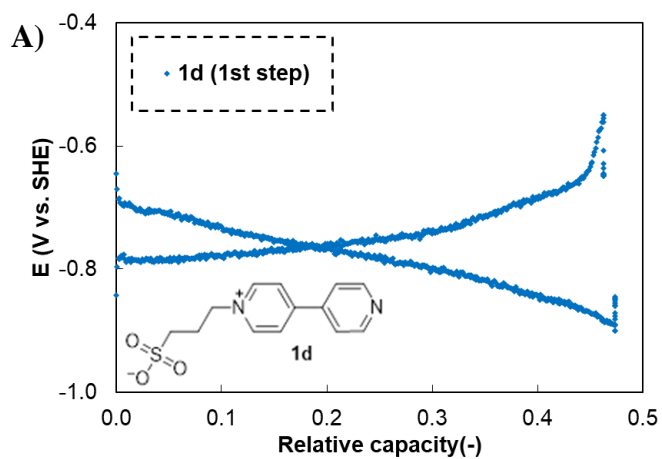


Figure S47 – Development of working electrode potential during galvanostatic cycling (2nd cycle) of **1d** in 1 M Na₂SO₄ (A); Development of capacity utilization (filled symbols) and coulombic efficiency (empty symbols) during cycling (B).

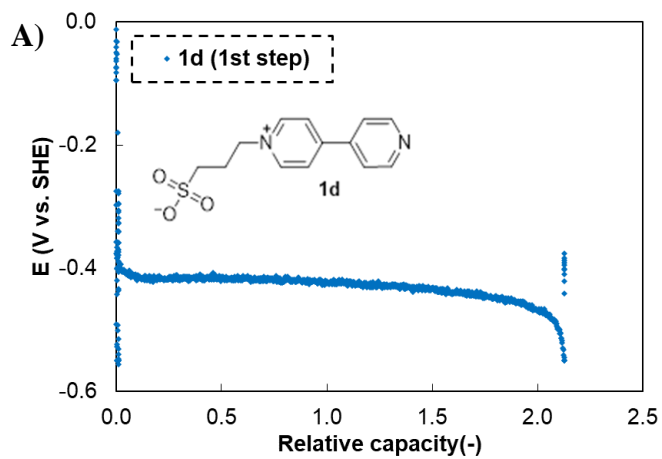


Figure S48 – Development of working electrode potential during galvanostatic cycling (all cycles) of **1d** in 1 M H₂SO₄ (A). Irreversible reduction observed.

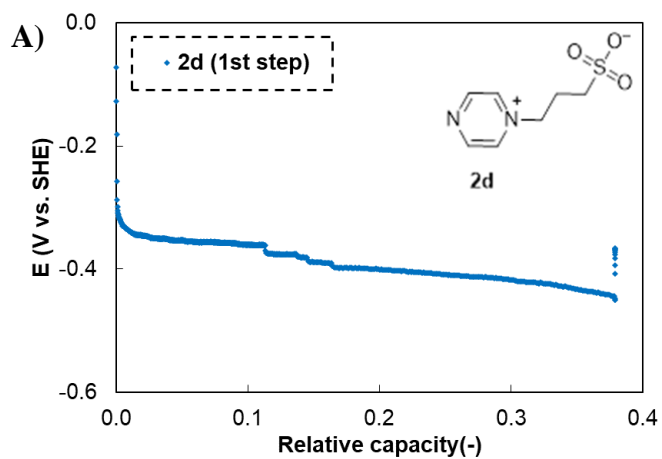


Figure S49 – Development of working electrode potential during galvanostatic cycling (1st cycle) of **2d** in 1 M Na₂SO₄ (A). Irreversible reduction observed.

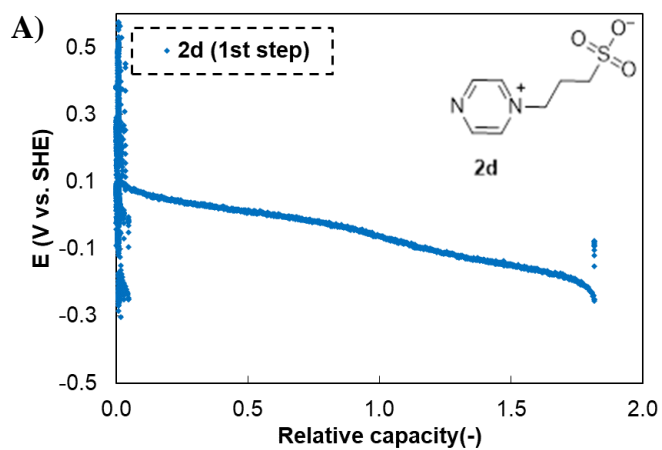


Figure S50 – Development of working electrode potential during galvanostatic cycling (all cycles) of **2d** in 1 M H₂SO₄ (A). Irreversible reduction observed.

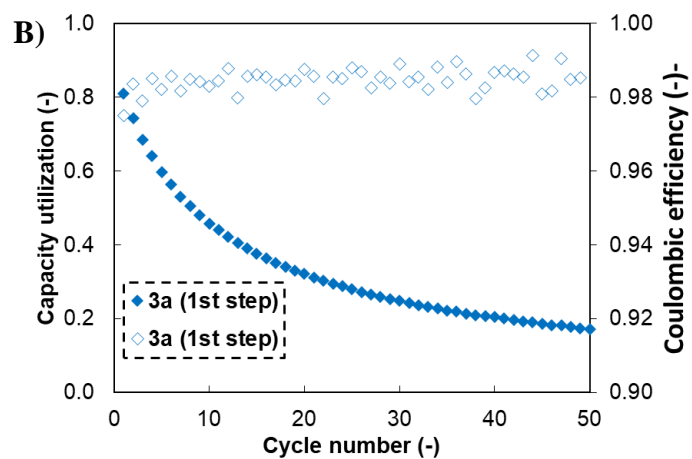
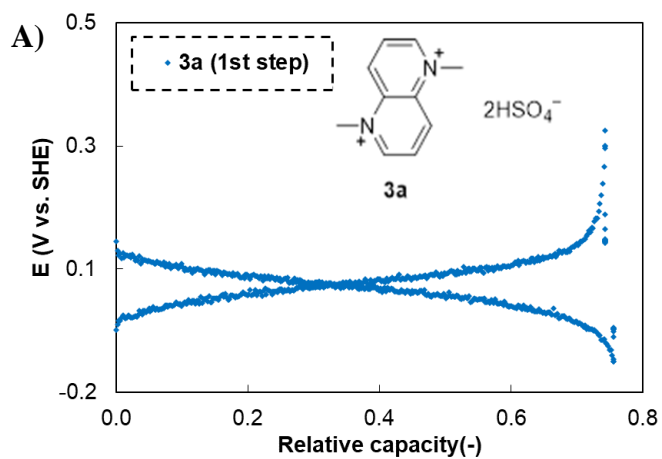


Figure S51 – Development of working electrode potential during galvanostatic cycling (2nd cycle) of **3a** in 1 M Na₂SO₄ (A); Development of capacity utilization (filled symbols) and coulombic efficiency (empty symbols) during cycling (B).

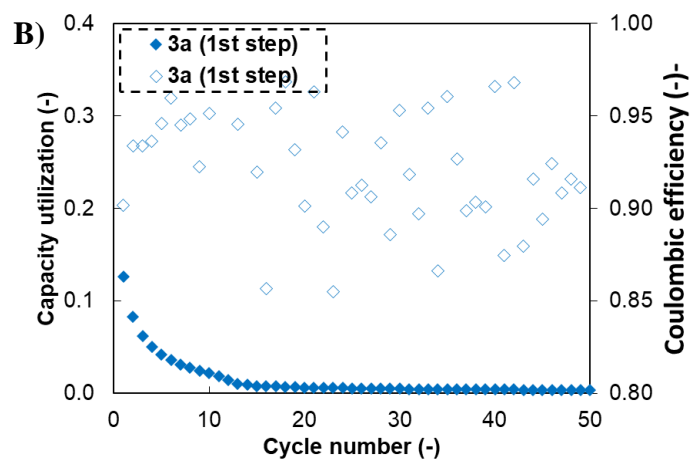
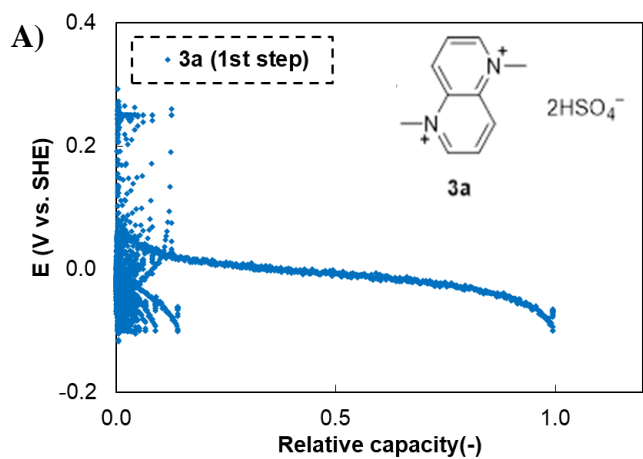


Figure S52 – Development of working electrode potential during galvanostatic cycling (all cycles) of **3a** in 1 M H₂SO₄ (A); Development of capacity utilization (filled symbols) and coulombic efficiency (empty symbols) during cycling (B).

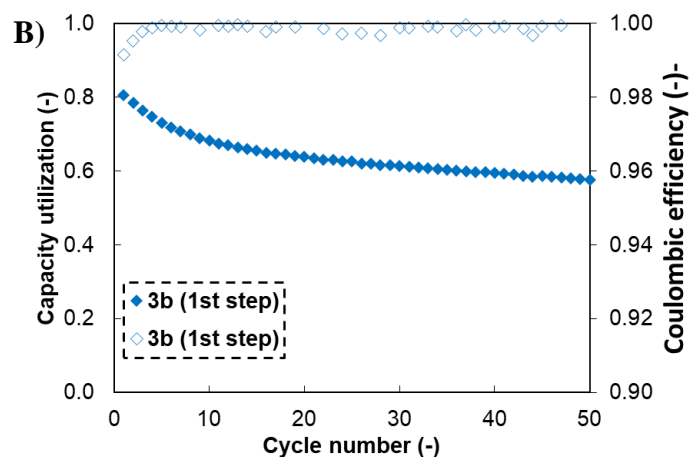
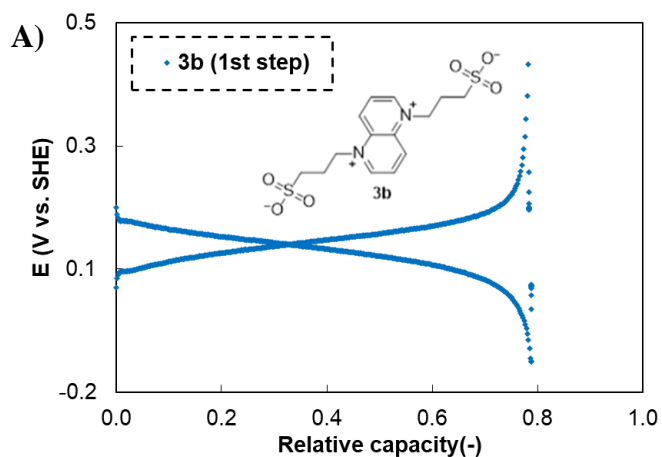


Figure S53 – Development of working electrode potential during galvanostatic cycling (2nd cycle) of **3b** in 1 M Na₂SO₄ (A); Development of capacity utilization (filled symbols) and coulombic efficiency (empty symbols) during cycling (B).

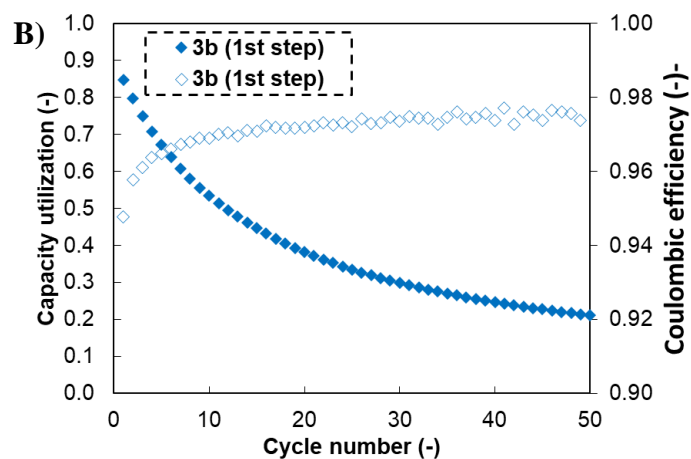
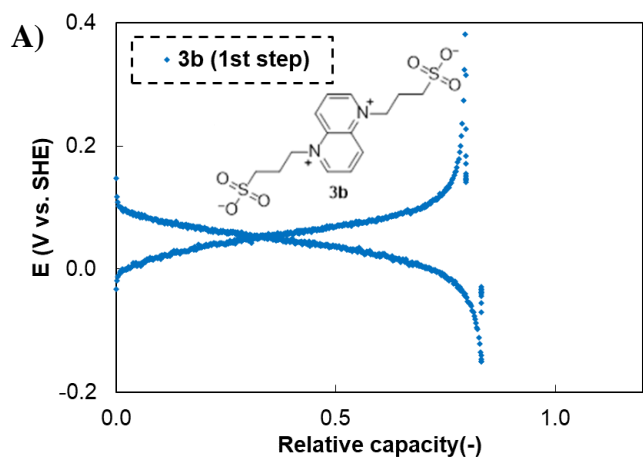


Figure S54 – Development of working electrode potential during galvanostatic cycling (all cycles) of **3b** in 1 M H₂SO₄ (A); Development of capacity utilization (filled symbols) and coulombic efficiency (empty symbols) during cycling (B).

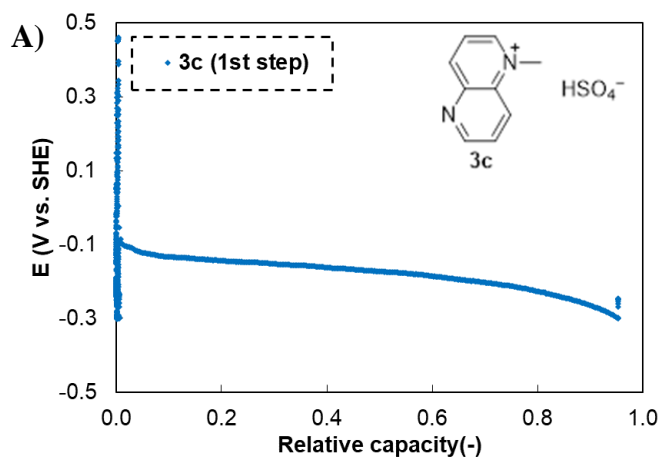


Figure S55 – Development of working electrode potential during galvanostatic cycling (all cycles) of **3c** in 1 M Na_2SO_4 (A). Irreversible reduction observed.

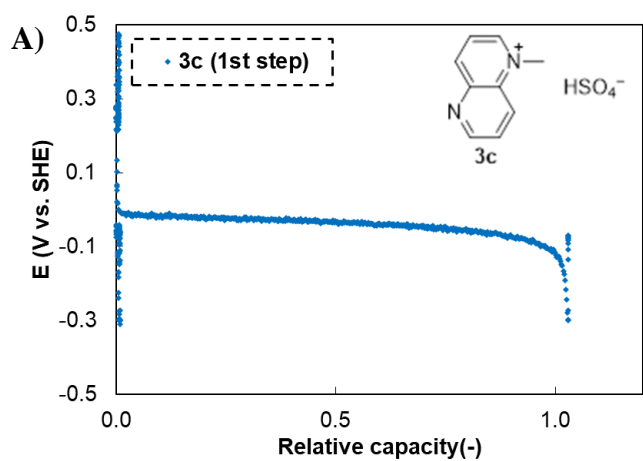


Figure S56 – Development of working electrode potential during galvanostatic cycling (all cycles) of **3c** in 1 M H_2SO_4 (A); Irreversible reduction observed.

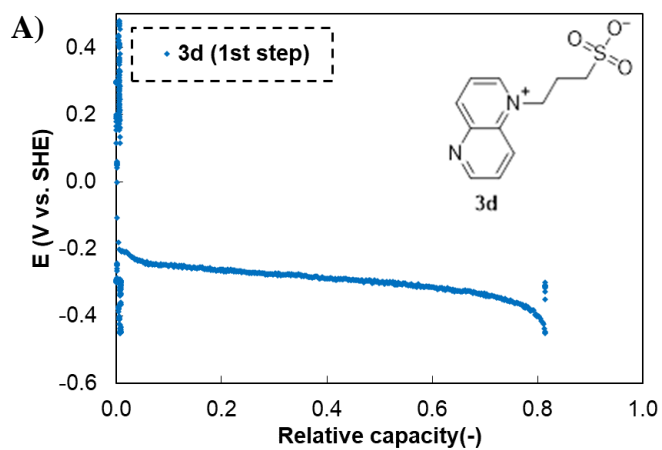


Figure S57 – Development of working electrode potential during galvanostatic cycling (all cycles) of **3d** in 1 M Na_2SO_4 (A). Irreversible reduction observed.

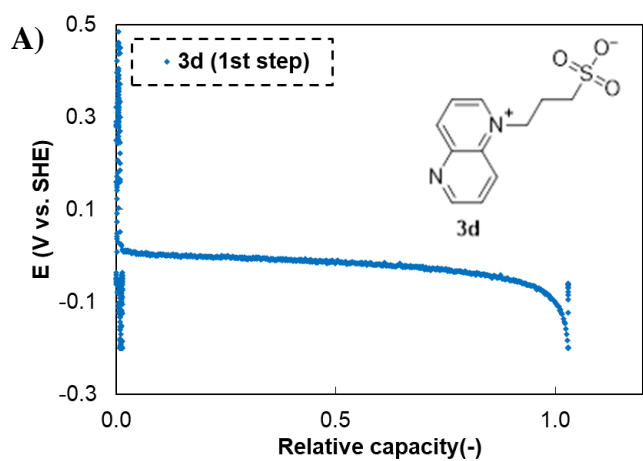


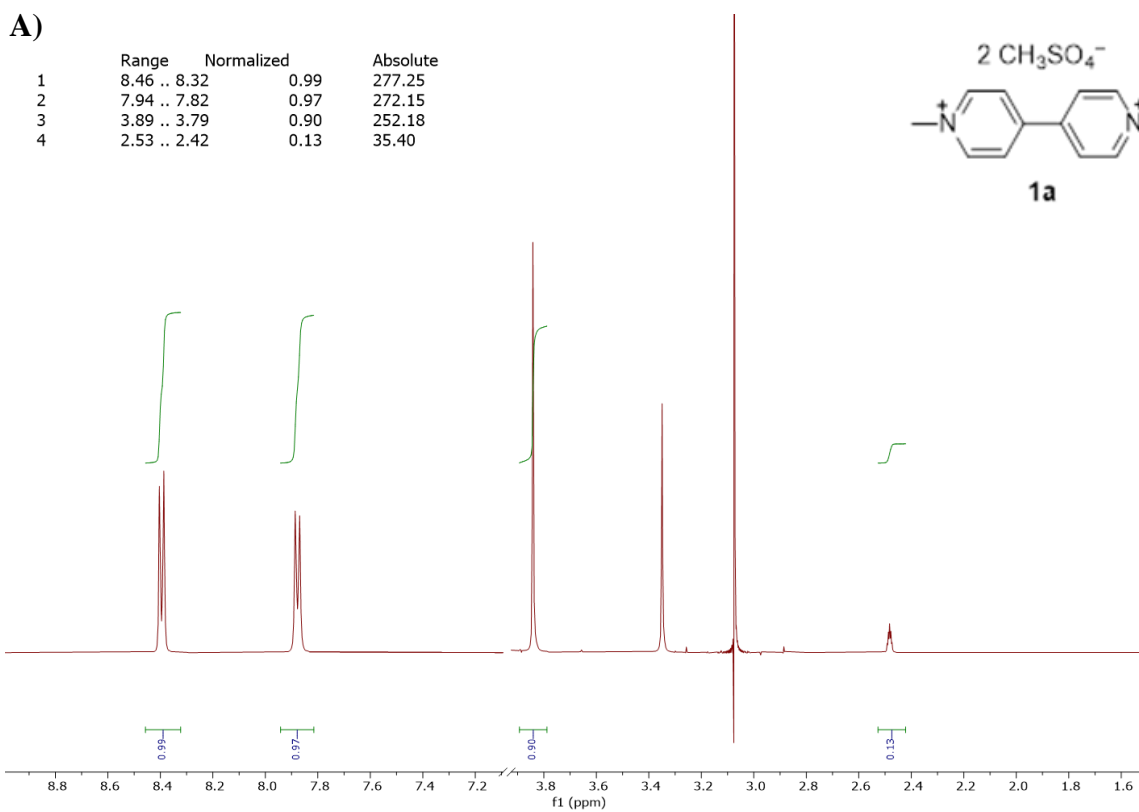
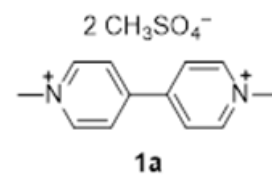
Figure S58 – Development of working electrode potential during galvanostatic cycling (all cycles) of **3d** in 1 M H_2SO_4 (A). Irreversible reduction observed.

6 NMR of electrolytes before and after cycling in flow battery cell

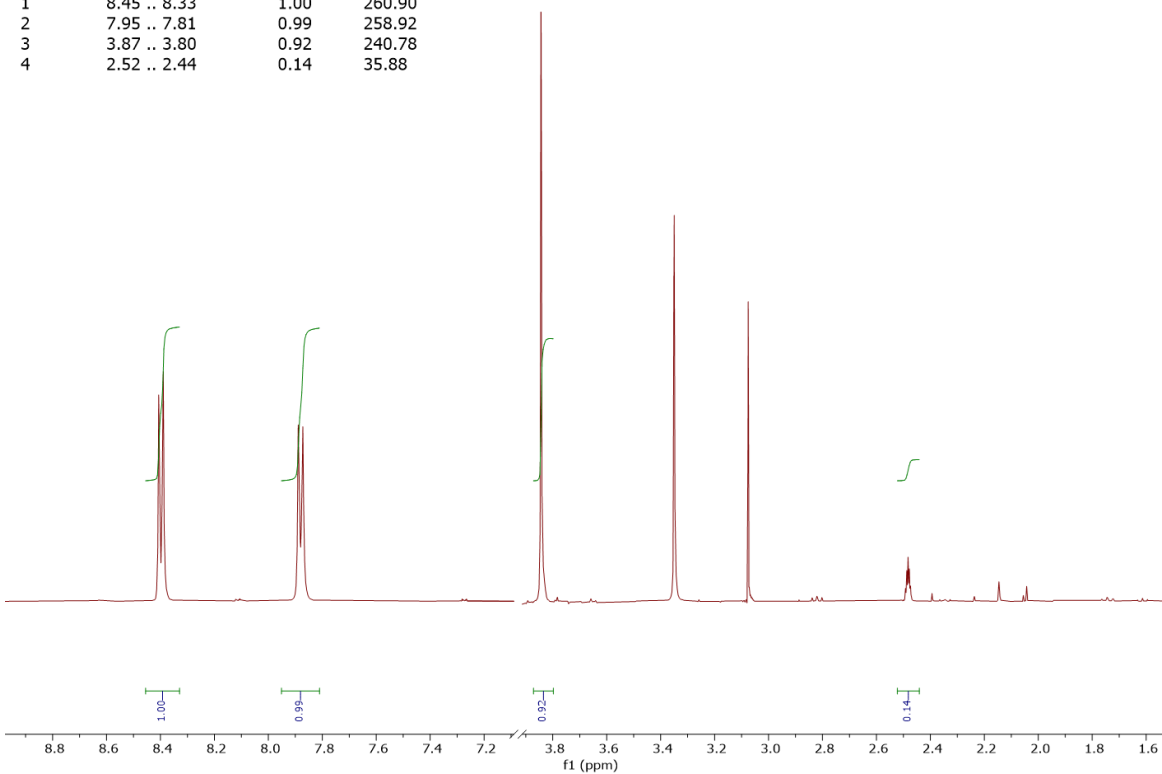
Post mortem ^1H NMR spectra of the mixtures after electrochemical experiments were recorded with an Agilent 400-MR DDR2 spectrometer at 400 MHz using external $\text{DMSO-}d_6$ standard and PRESAT sequence. The analyses were performed with neat electrolytes using external $\text{DMSO-}d_6$ insert both for locking and integration. To avoid ADC overloading while keeping pulse width sufficiently high, PRESAT pulse sequence using long weak irradiation centered at the solvent peak was employed. In selected cases, the signals of compounds overlaid by solvent were detected using the PRESAT-COSY pulse sequence as the corresponding cross-peaks.

A)

	Range	Normalized	Absolute
1	8.46 .. 8.32	0.99	277.25
2	7.94 .. 7.82	0.97	272.15
3	3.89 .. 3.79	0.90	252.18
4	2.53 .. 2.42	0.13	35.40

**B)**

	Range	Normalized	Absolute
1	8.45 .. 8.33	1.00	260.90
2	7.95 .. 7.81	0.99	258.92
3	3.87 .. 3.80	0.92	240.78
4	2.52 .. 2.44	0.14	35.88



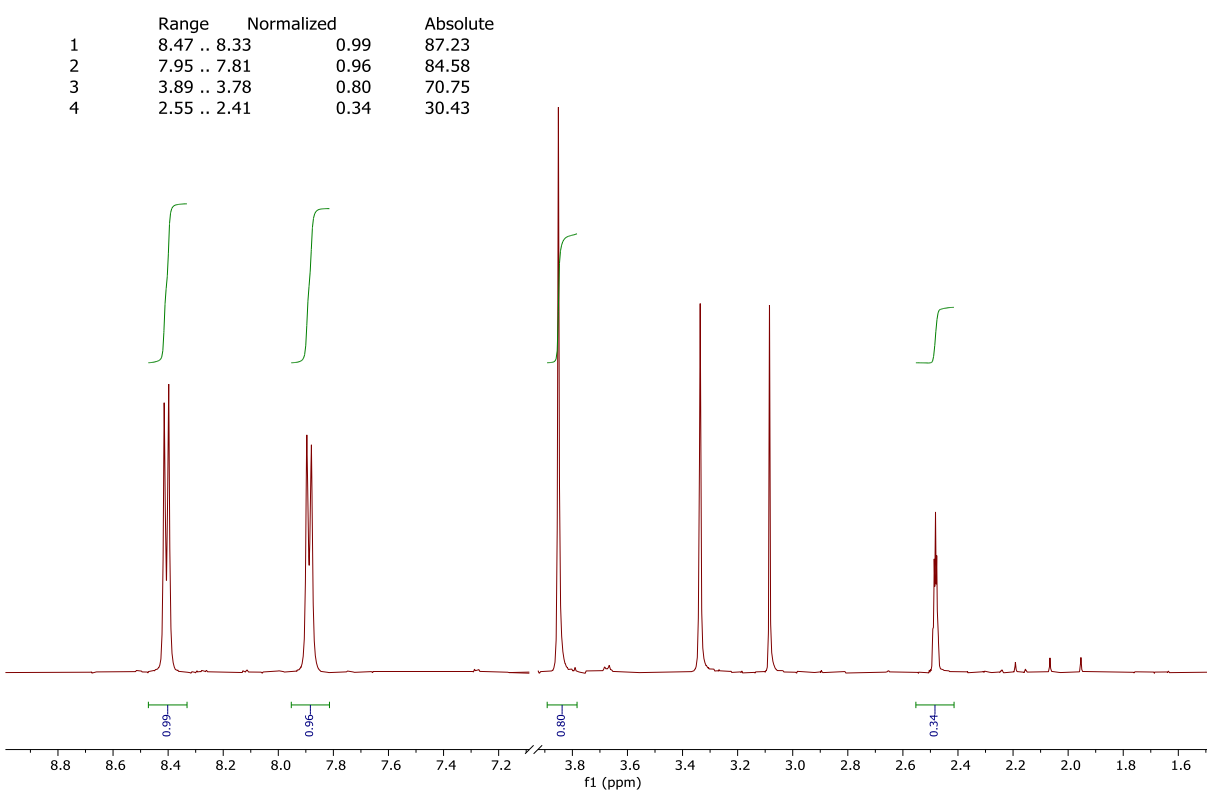
C

Figure S59 – $^1\text{H-NMR}$ post mortem analysis of the electrolyte containing **1a** in $1\text{M Na}_2\text{SO}_4$ before (A), after galvanostatic cycling for 1st redox step (B), after galvanostatic cycling for both redox steps (C).

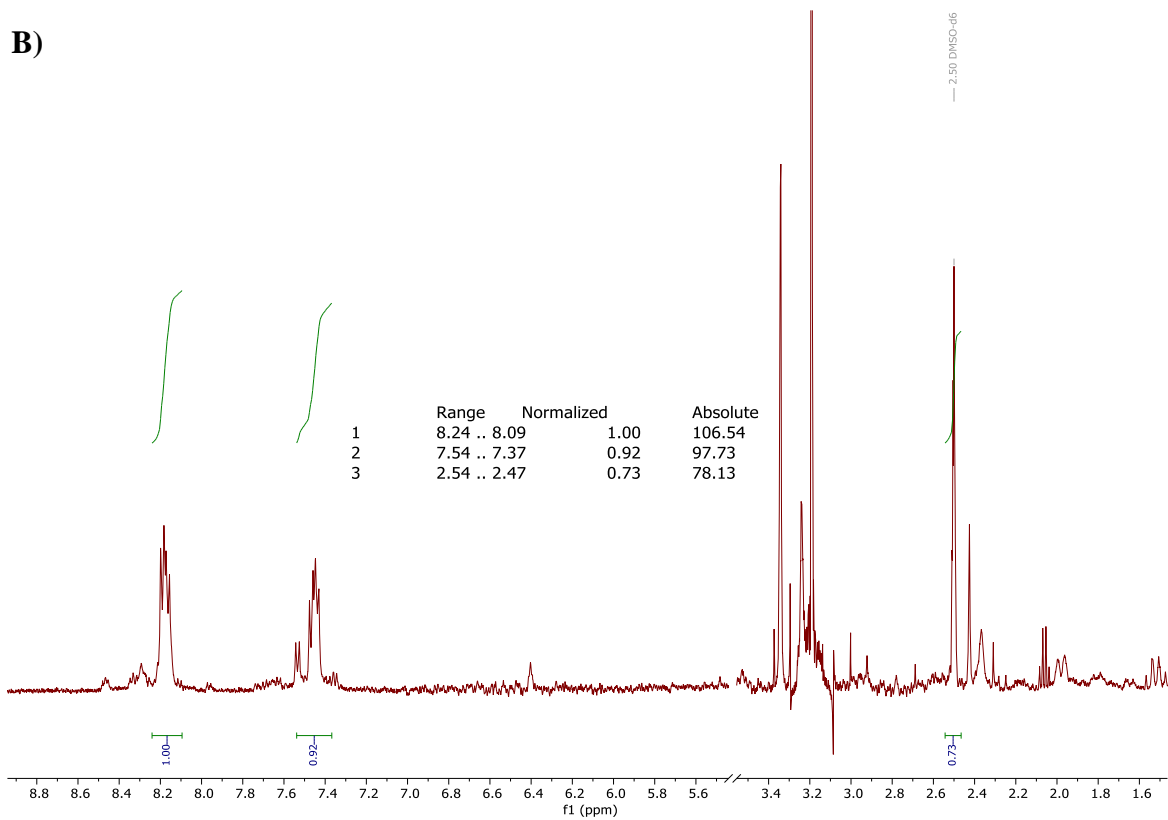
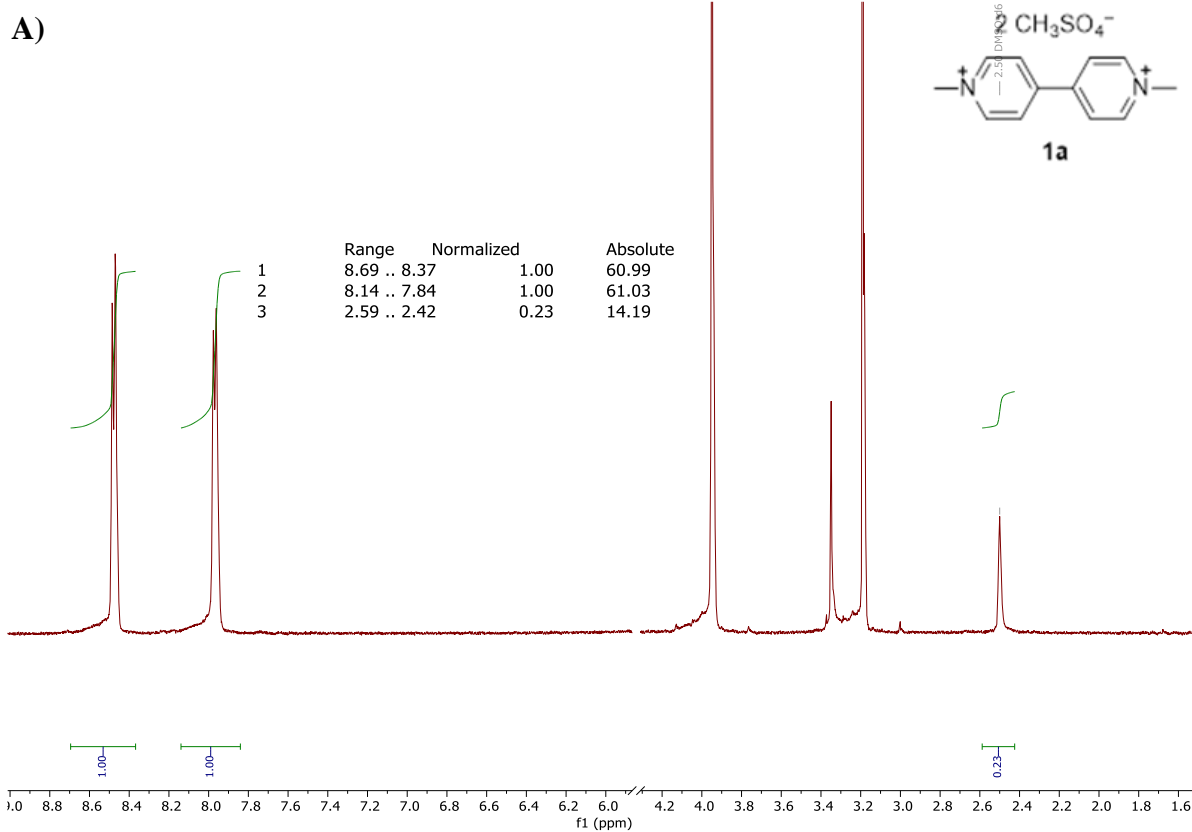
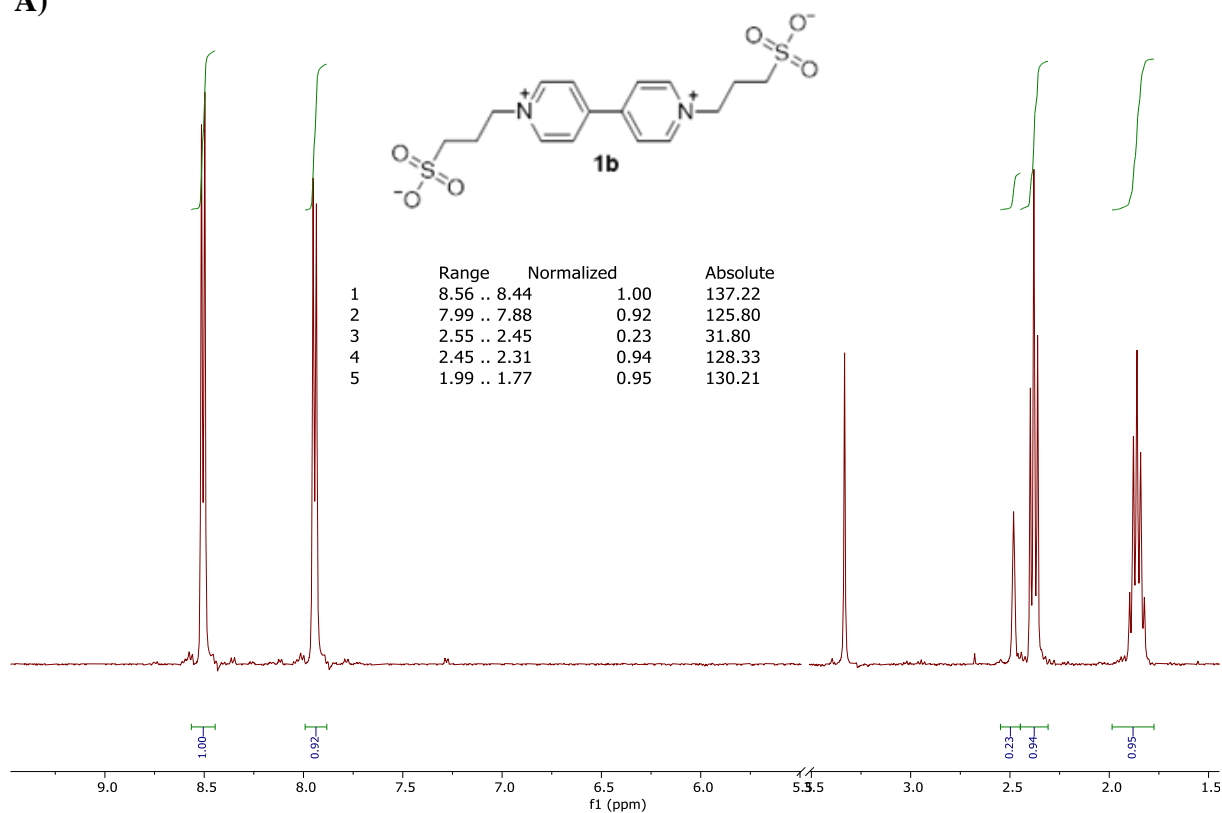
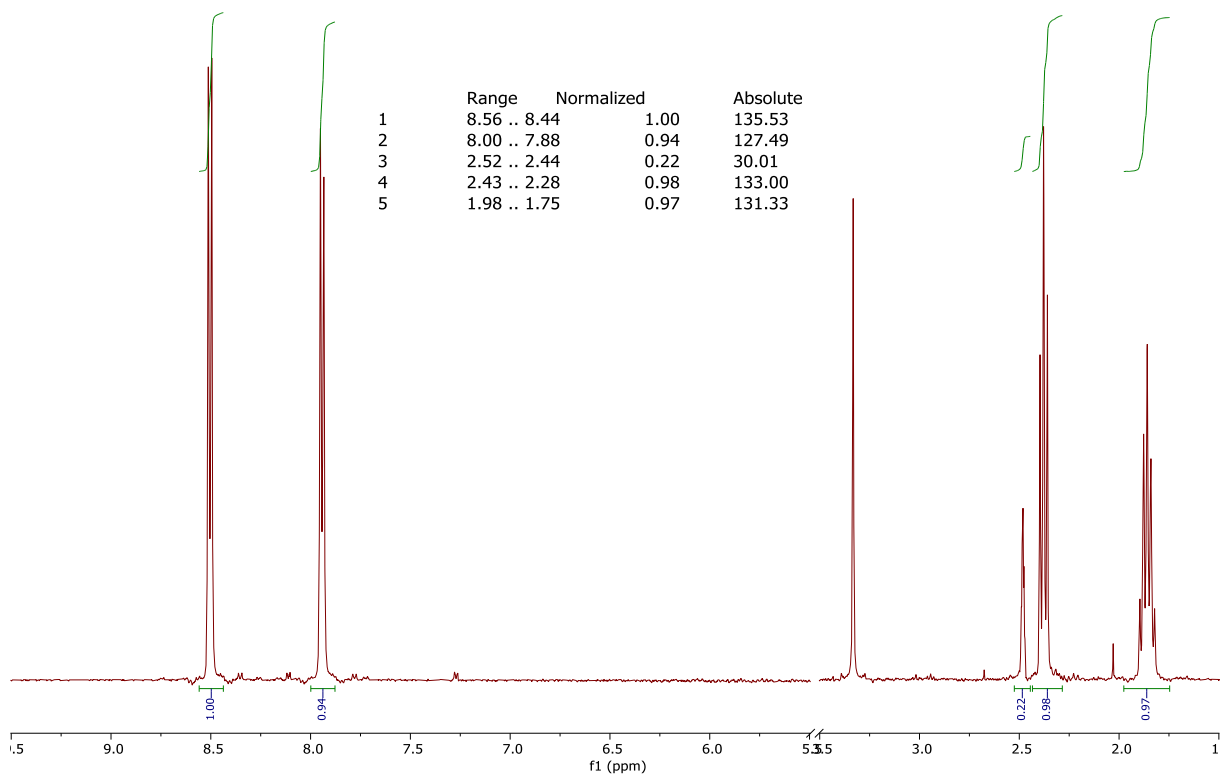


Figure S60 – $^1\text{H-NMR}$ post mortem analysis of the electrolyte containing **1a** in $1\text{M H}_2\text{SO}_4$ before (A) and after galvanostatic cycling for 1^{st} redox step (B).

A)



B)



C)

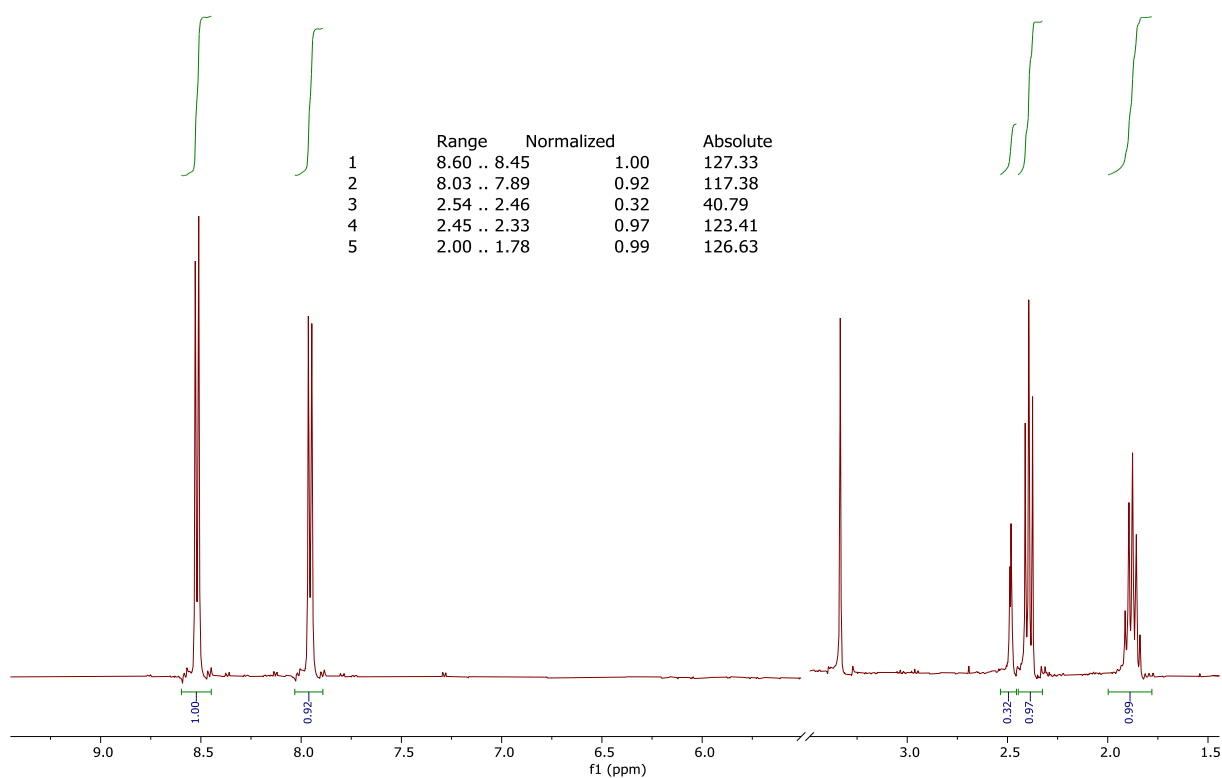
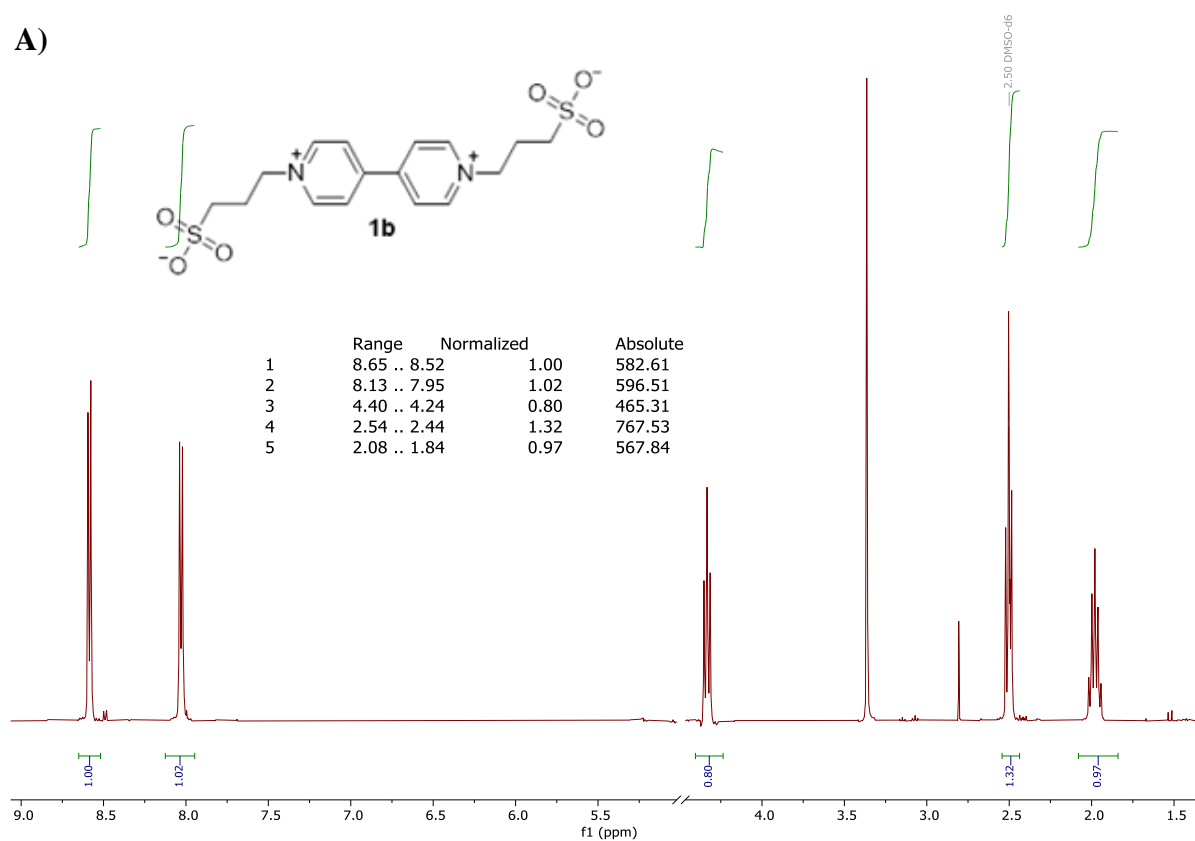


Figure S61 – $^1\text{H-NMR}$ post mortem analysis of the electrolyte containing **1b** in $1\text{M Na}_2\text{SO}_4$ before (A), after galvanostatic cycling for 1st redox step (B), after galvanostatic cycling for both redox steps (C).

A)



B)

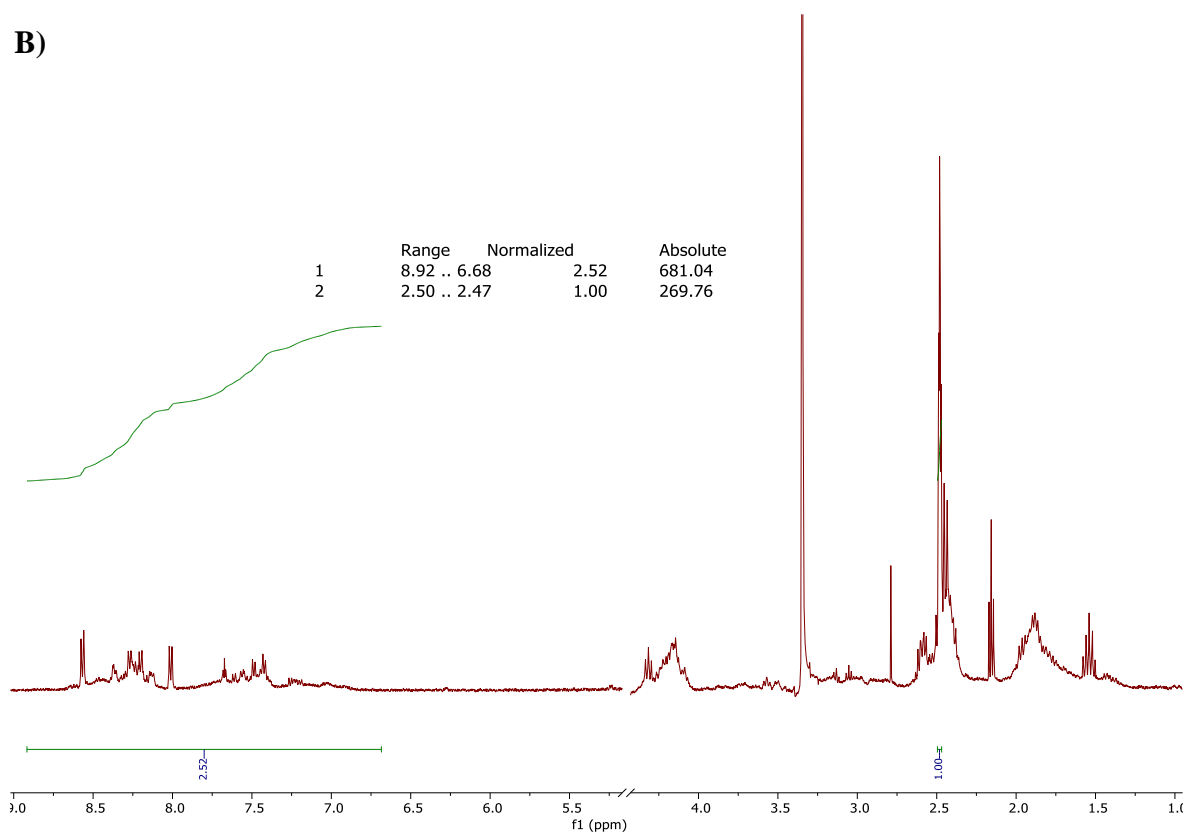


Figure S62 – $^1\text{H-NMR}$ post mortem analysis of the electrolyte containing **1b** in $1\text{M H}_2\text{SO}_4$ before (A) and after galvanostatic cycling for 1^{st} redox step (B).

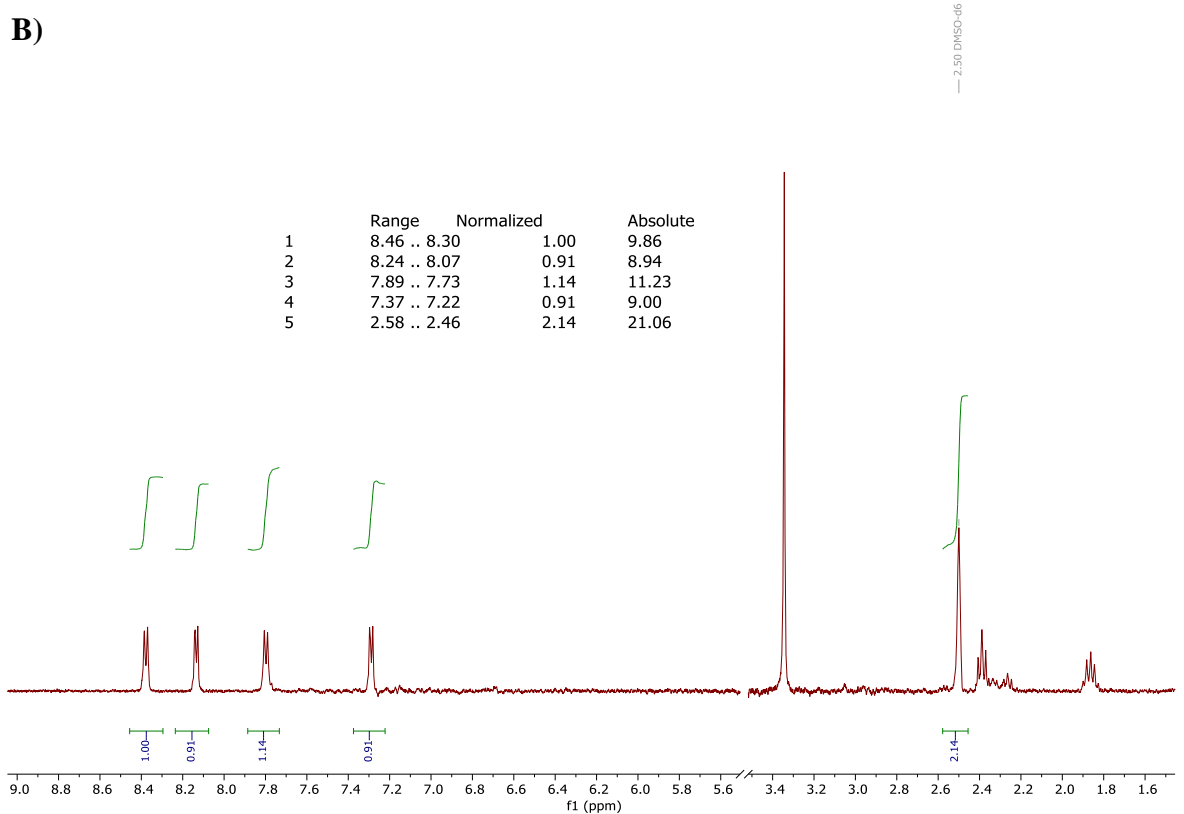
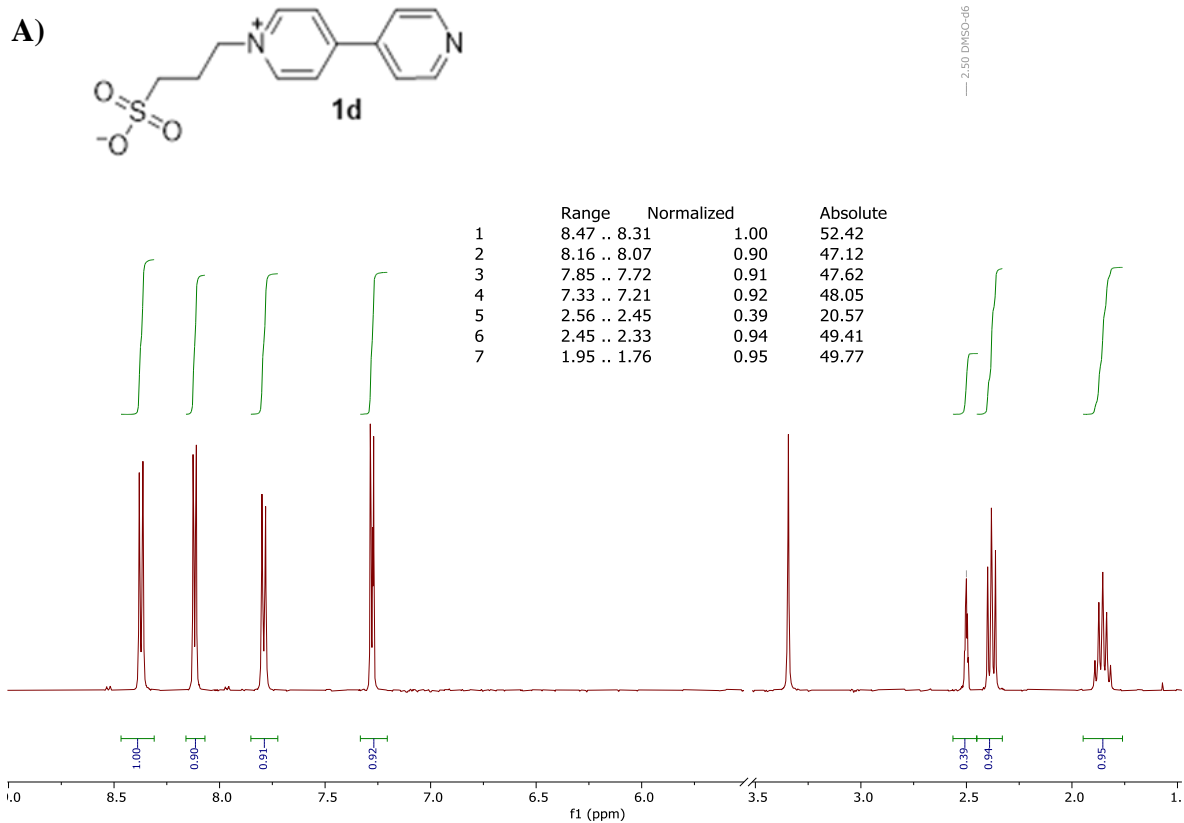
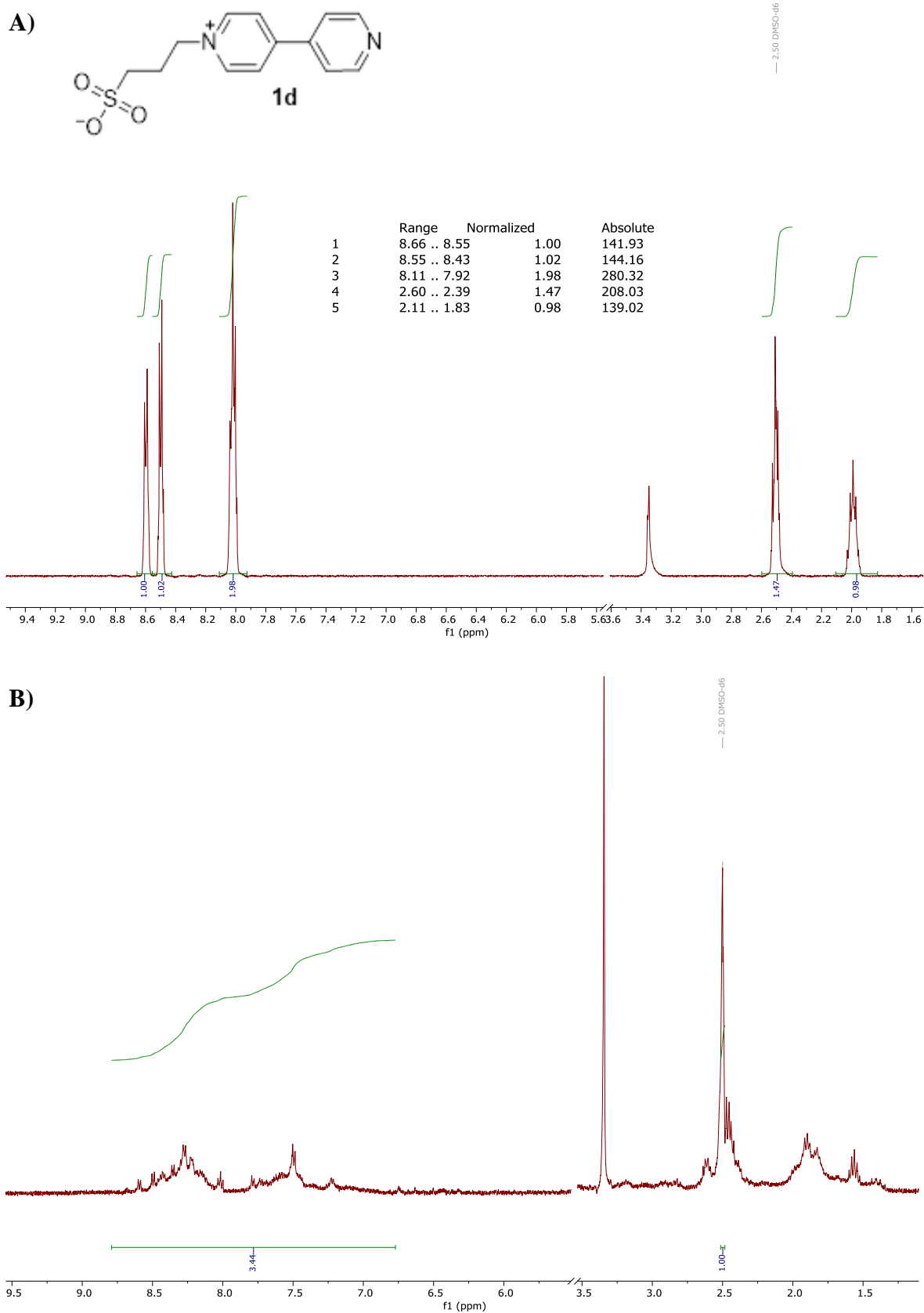


Figure S63 – $^1\text{H-NMR}$ post mortem analysis of the electrolyte containing **1d** in $1\text{M Na}_2\text{SO}_4$ before (A) and after galvanostatic cycling for 1^{st} redox step (B).



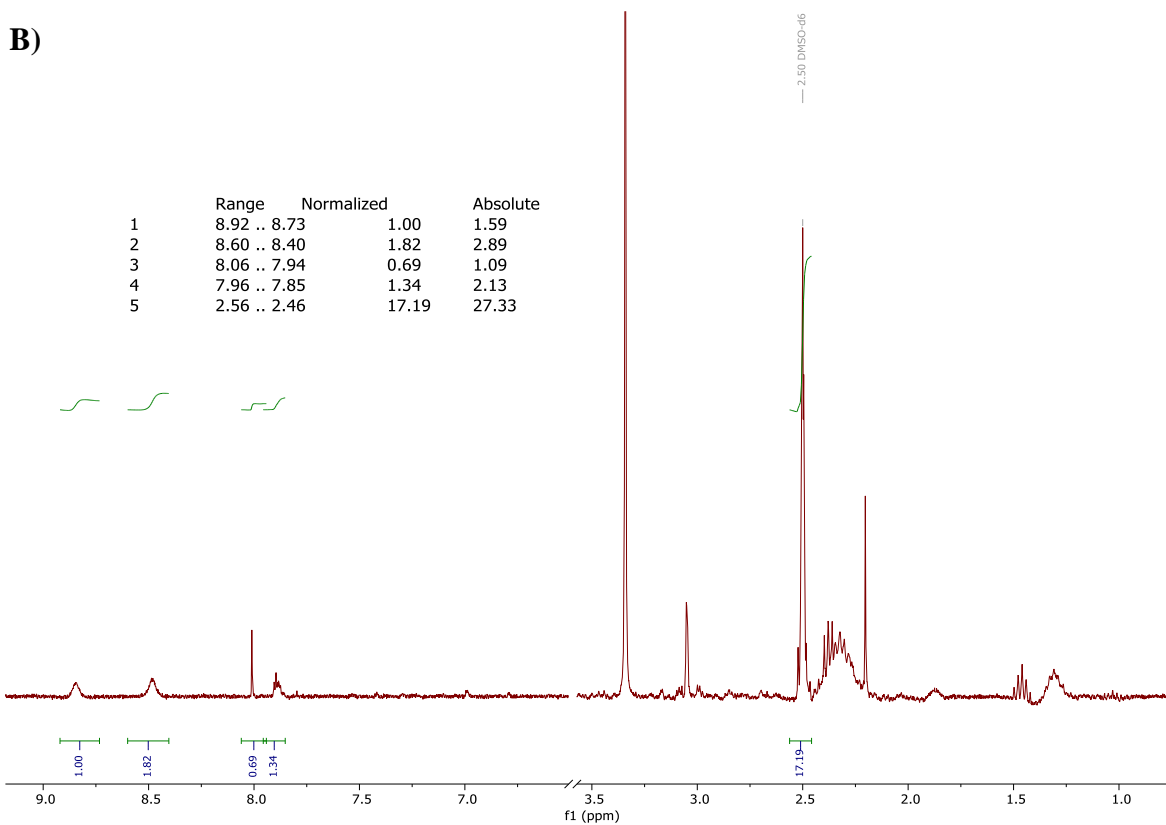
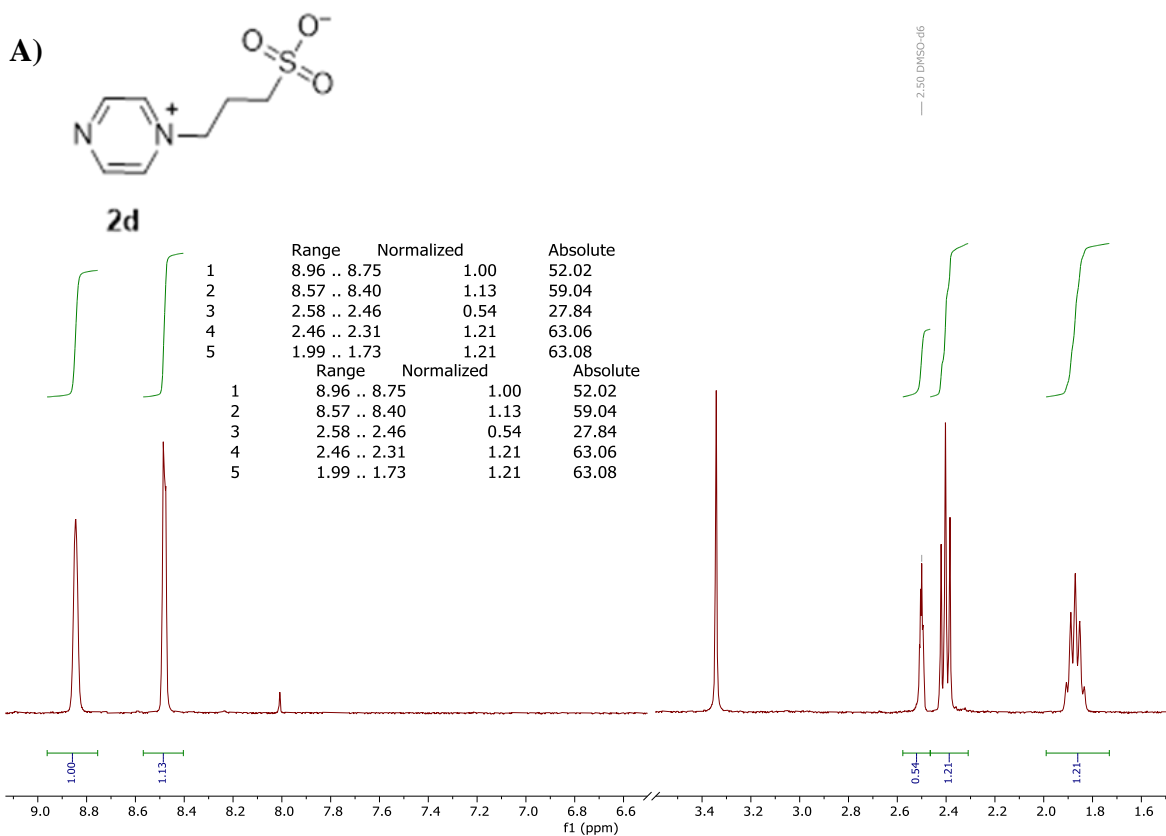
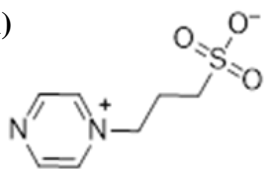


Figure S65 – ^1H -NMR post mortem analysis of the electrolyte containing **2d** in 1M Na_2SO_4 before (A) and after galvanostatic cycling for 1st redox step (B).

A)**2d**

	Range	Normalized	Absolute
1	9.03 .. 8.83	1.00	126.63
2	8.64 .. 8.44	1.05	132.33
3	2.60 .. 2.43	1.68	212.72
4	2.08 .. 1.86	1.07	135.92

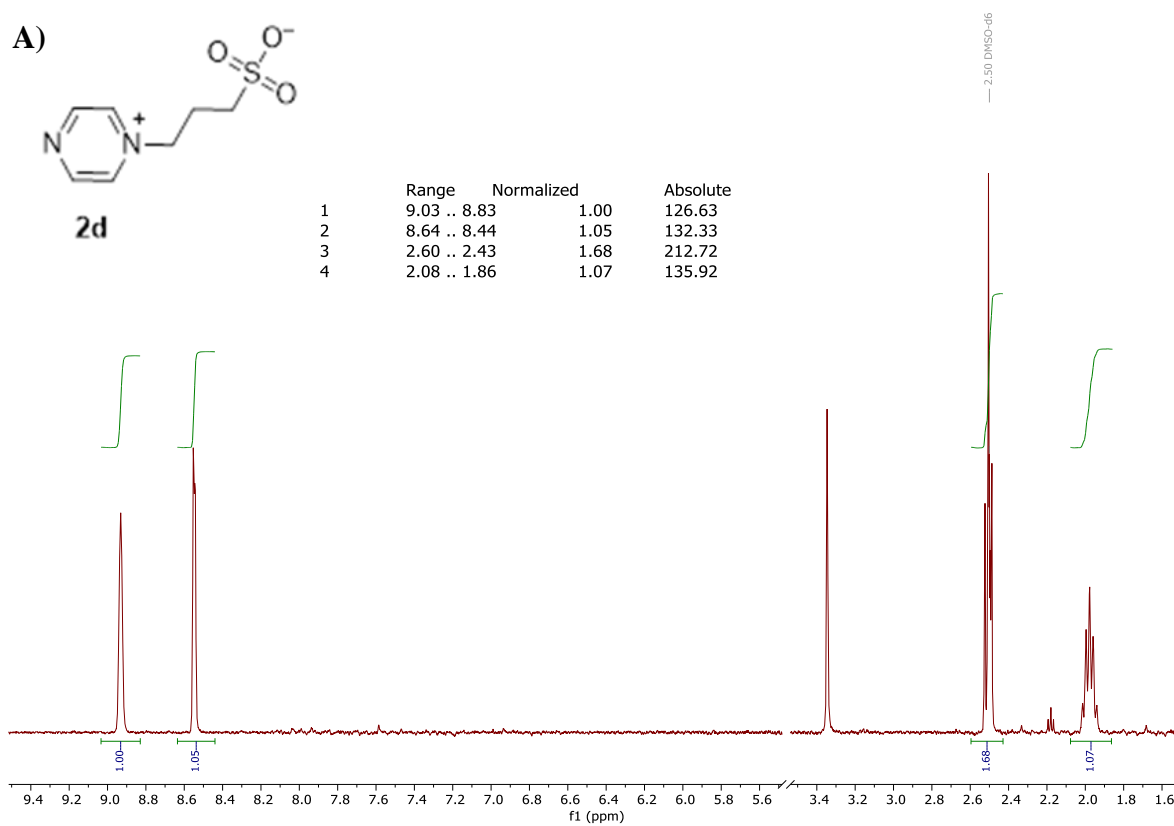
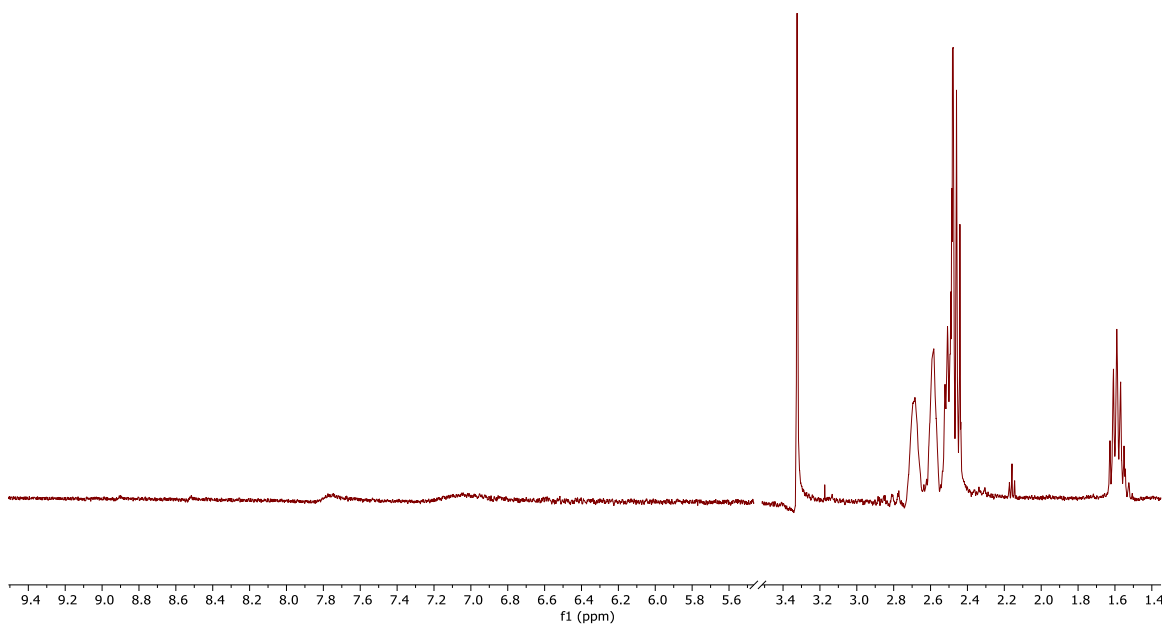
**B)**

Figure S66 —¹H-NMR post mortem analysis of the electrolyte containing **2d** in 1M H₂SO₄ before (A) and after galvanostatic cycling for 1st redox step (B).

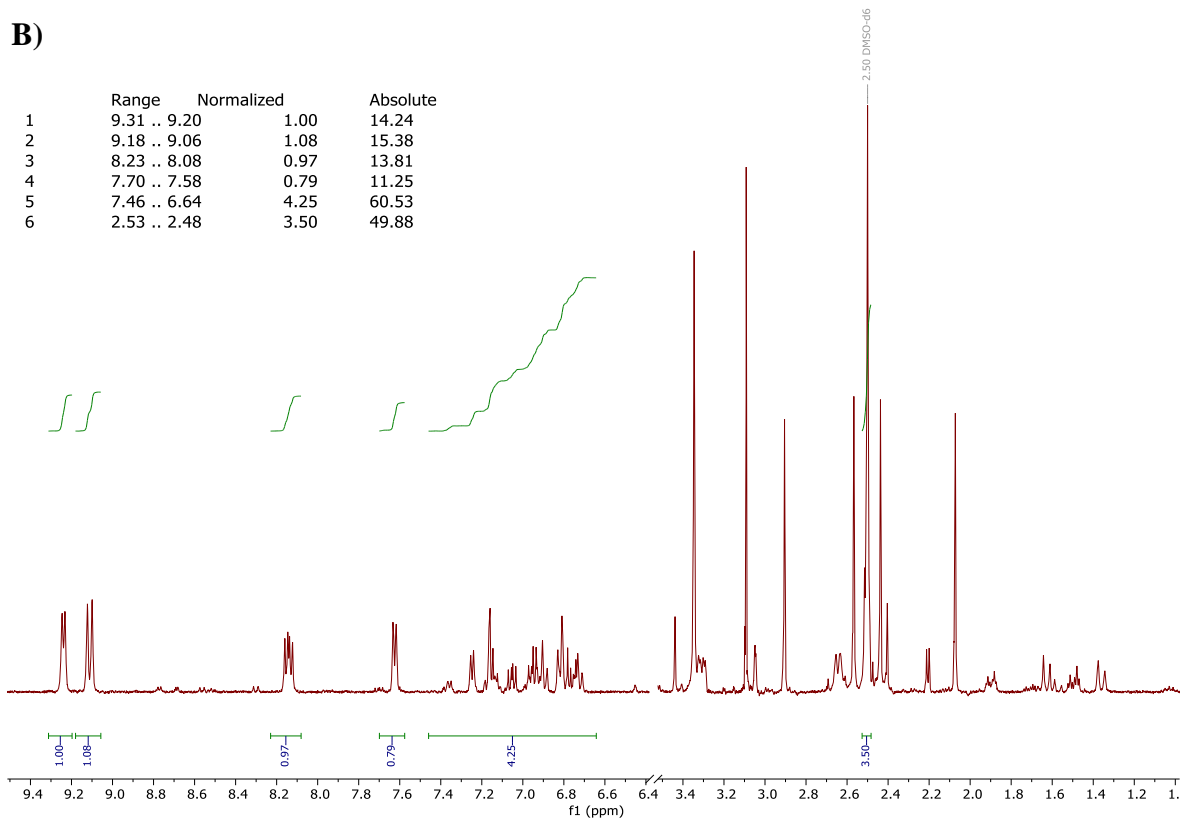
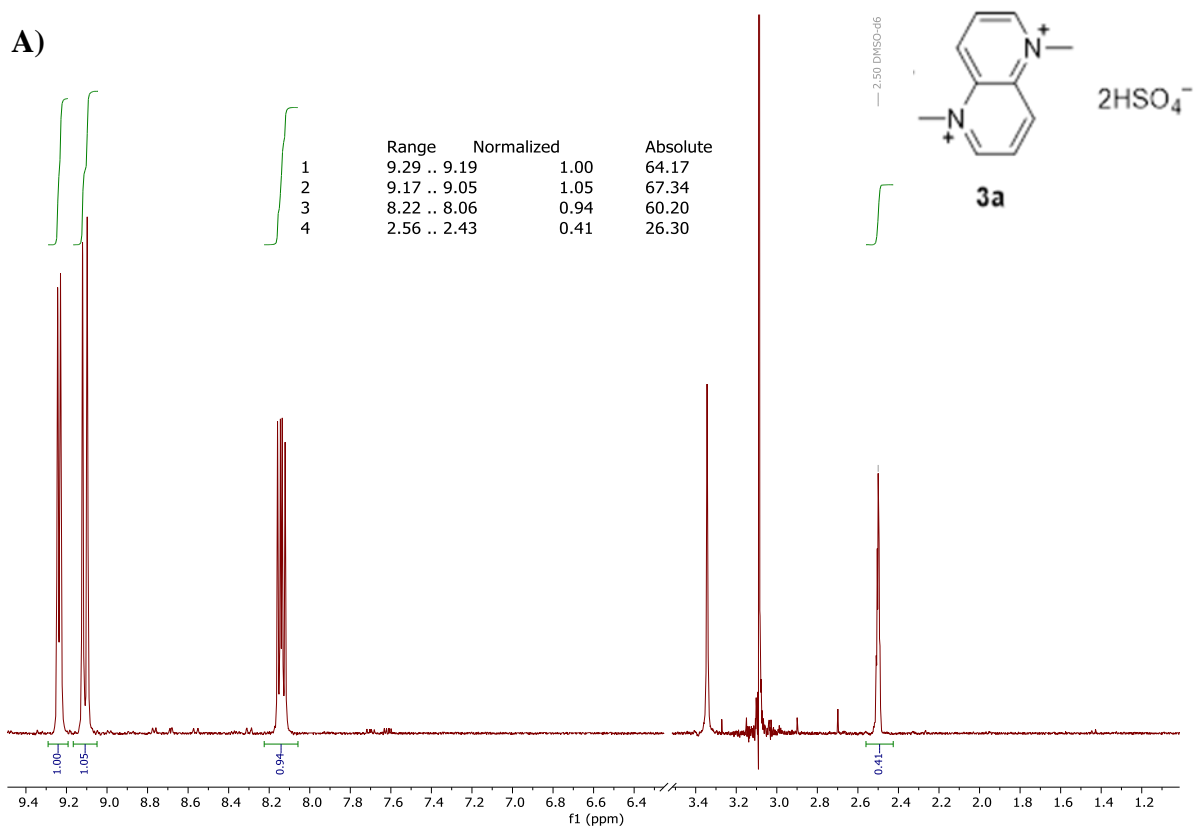


Figure S67 – ¹H-NMR post mortem analysis of the electrolyte containing **3a** in 1M Na₂SO₄ before (A) and after galvanostatic cycling for 1st redox step (B).

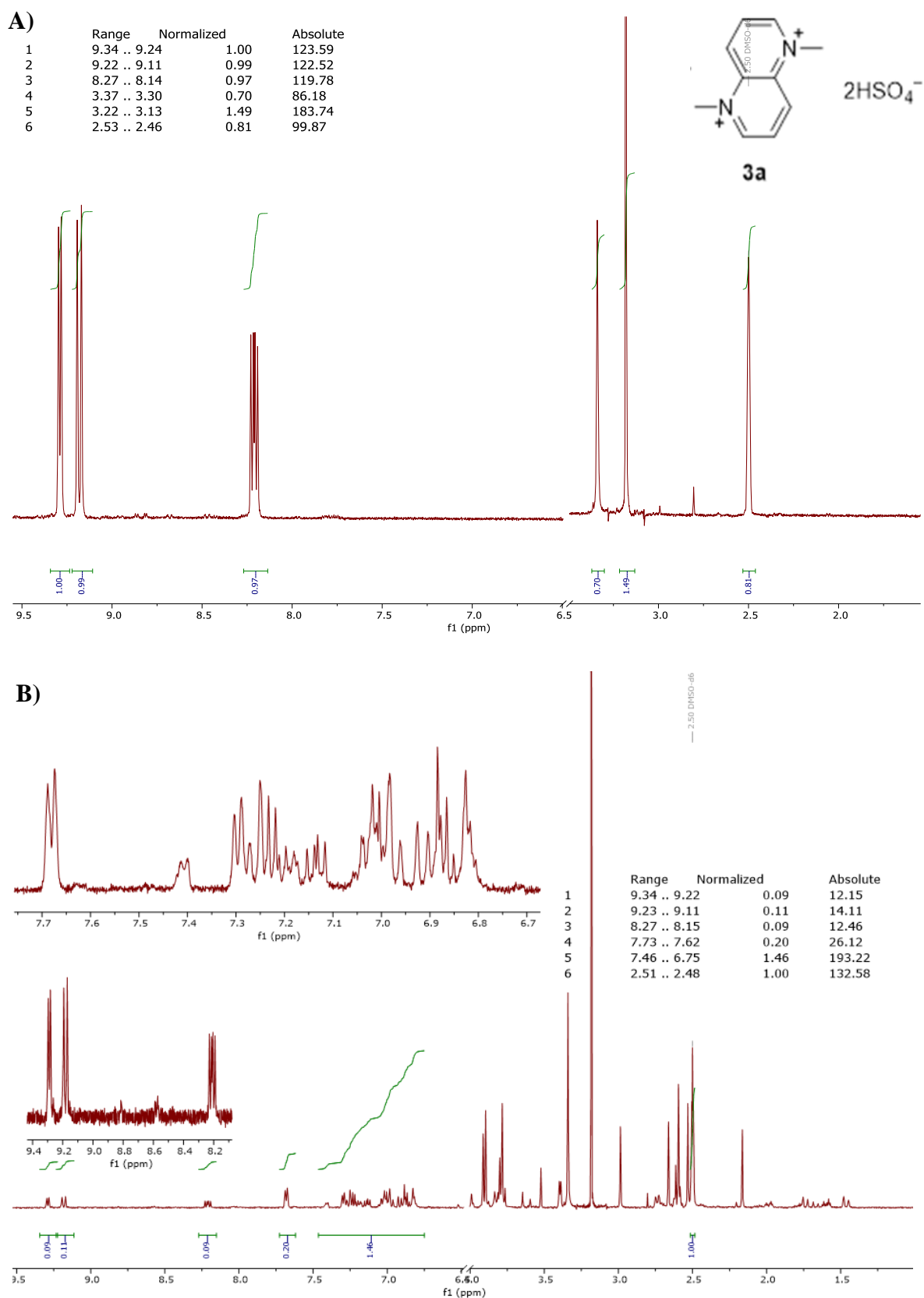


Figure S68 – $^1\text{H-NMR}$ post mortem analysis of the electrolyte containing **3a** in $1\text{M H}_2\text{SO}_4$ before (A) and after galvanostatic cycling for 1^{st} redox step (B).

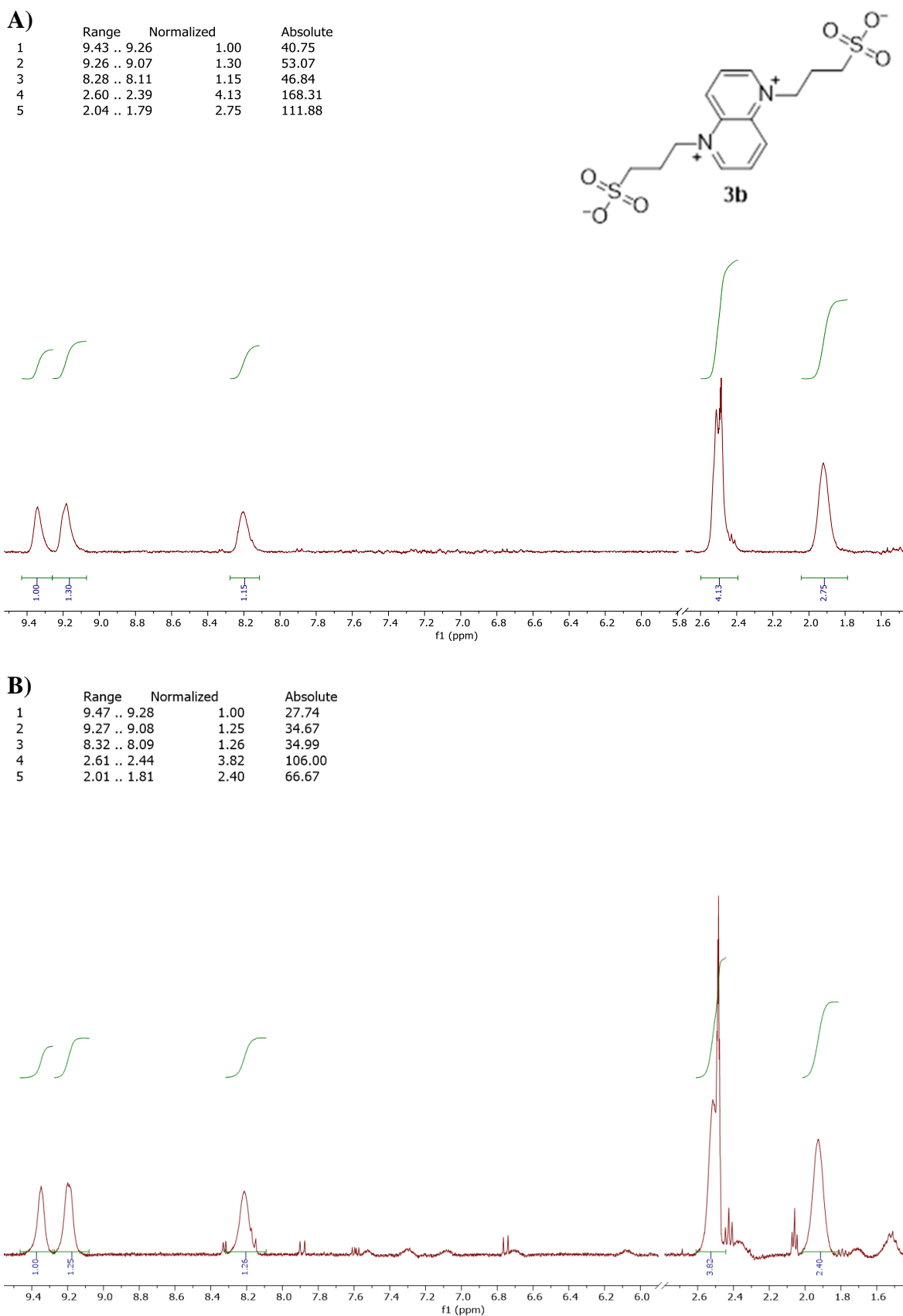
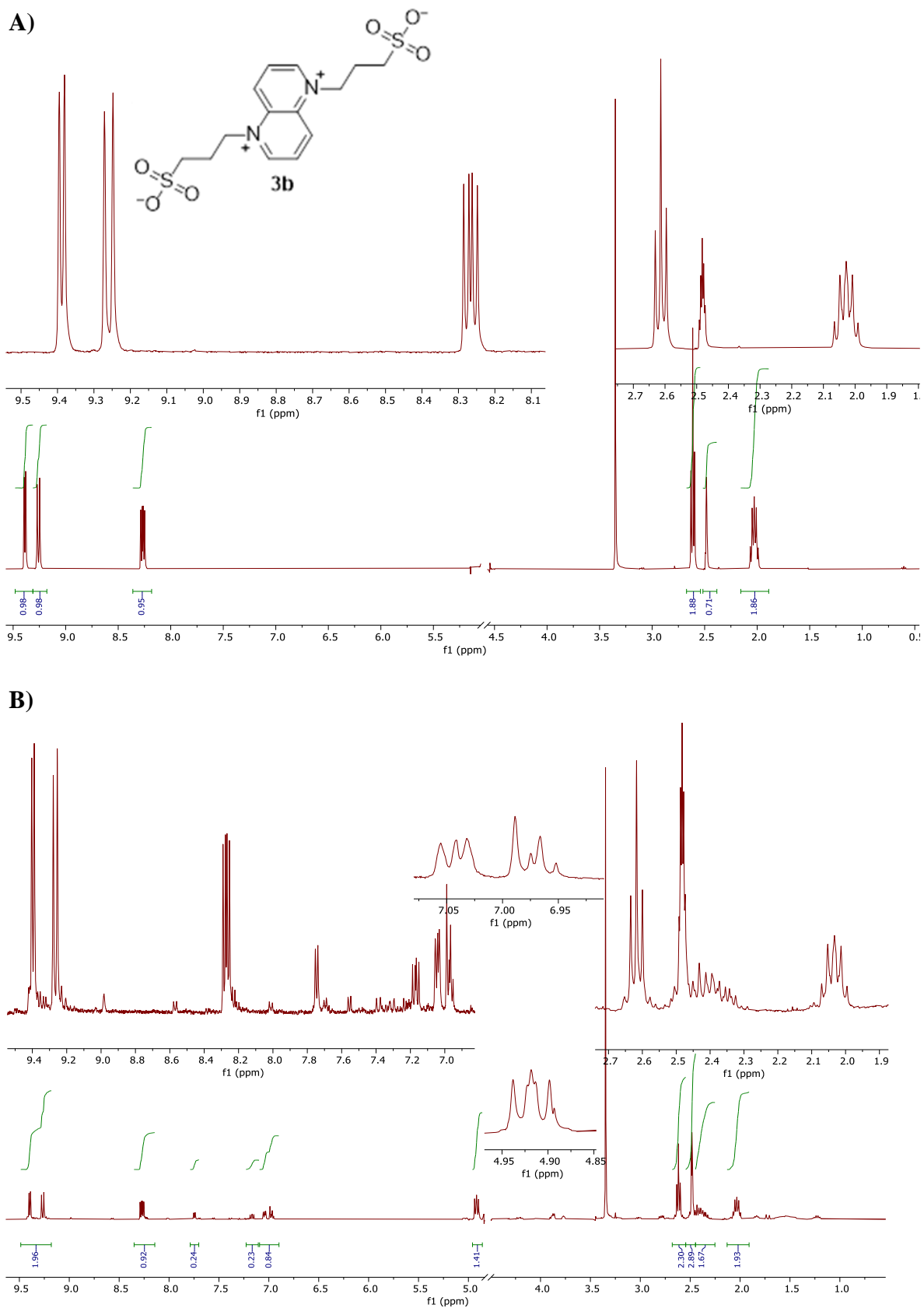


Figure S69 – ¹H-NMR post mortem analysis of the electrolyte containing **3b** in 1M Na₂SO₄ before (A) and after galvanostatic cycling for 1st redox step (B).



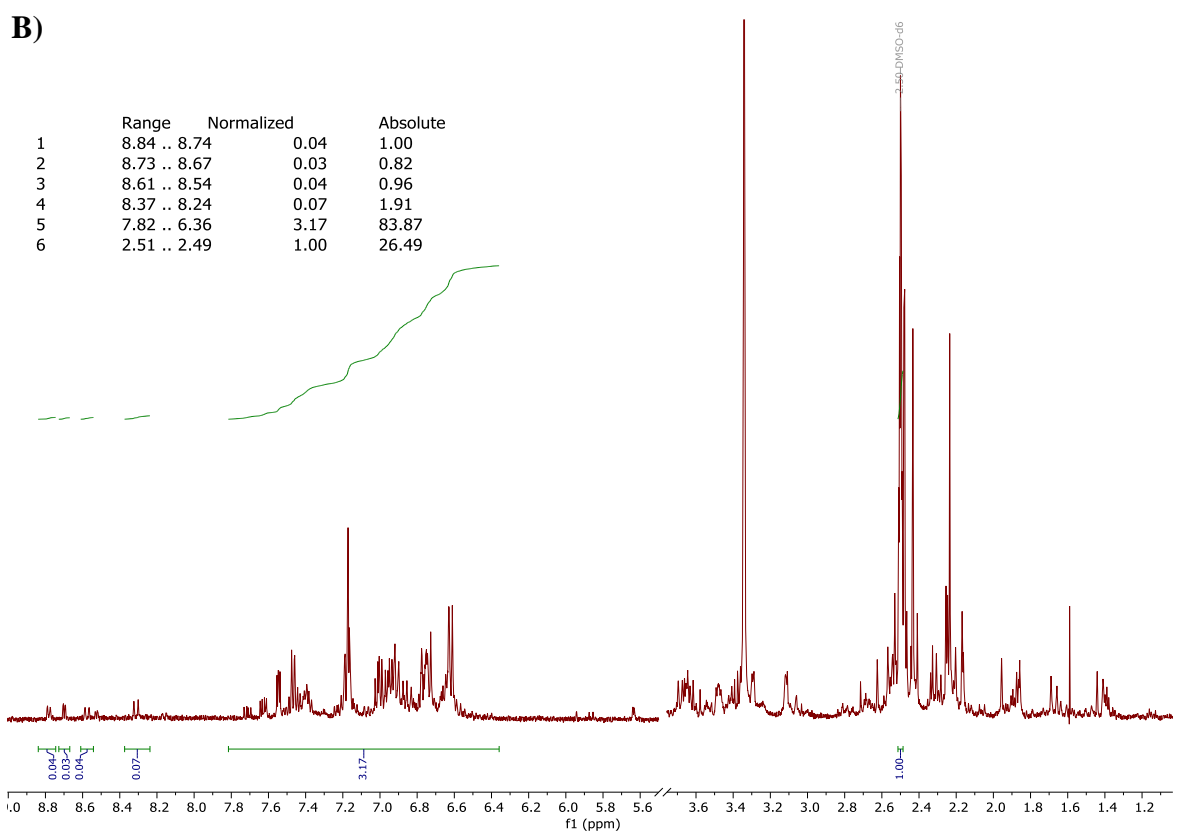
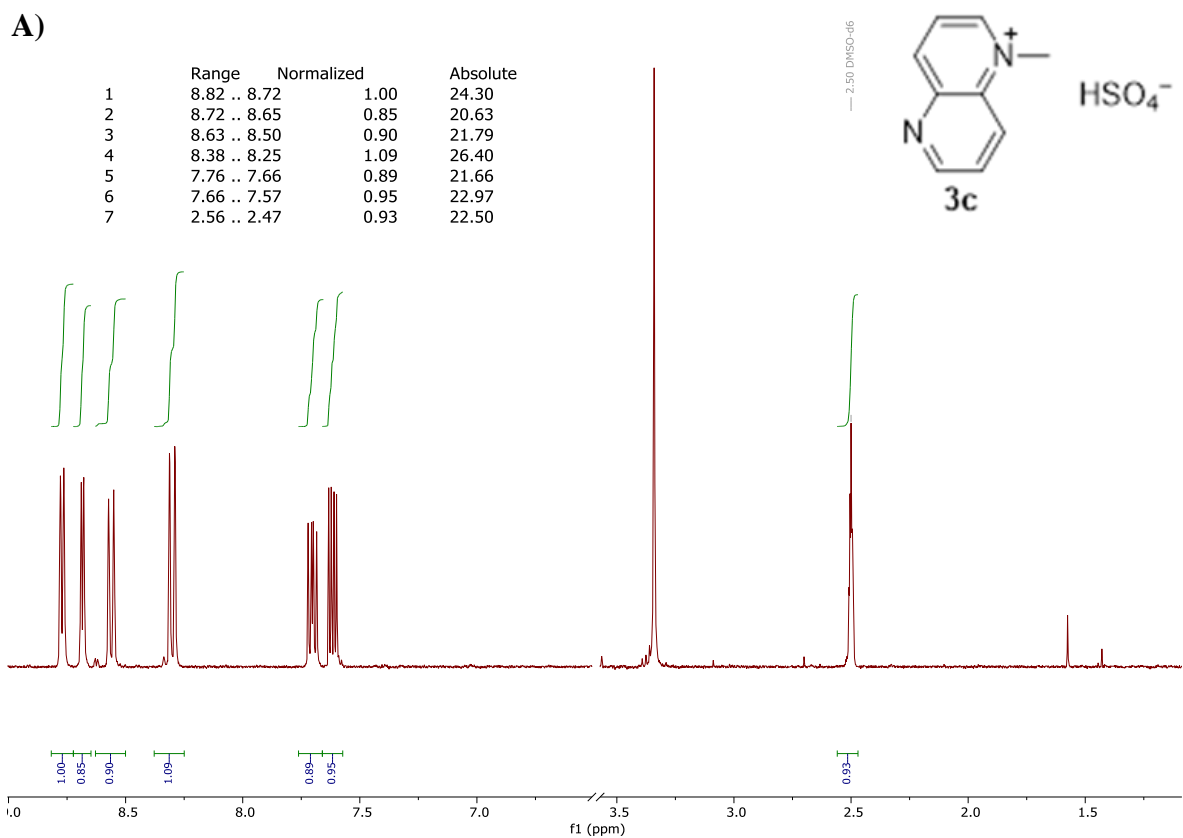


Figure S71 – $^1\text{H-NMR}$ post mortem analysis of the electrolyte containing **3c** in $1\text{M Na}_2\text{SO}_4$ before (A) and after galvanostatic cycling for 1^{st} redox step (B).

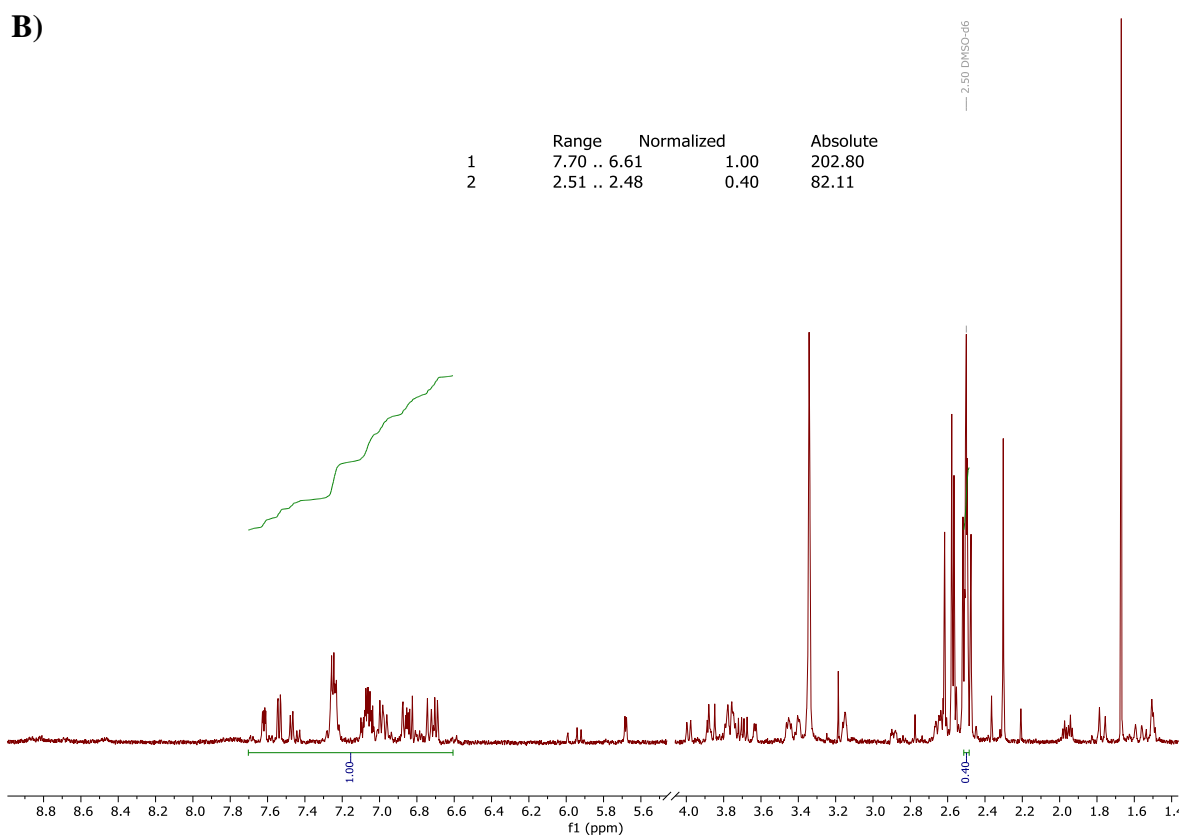
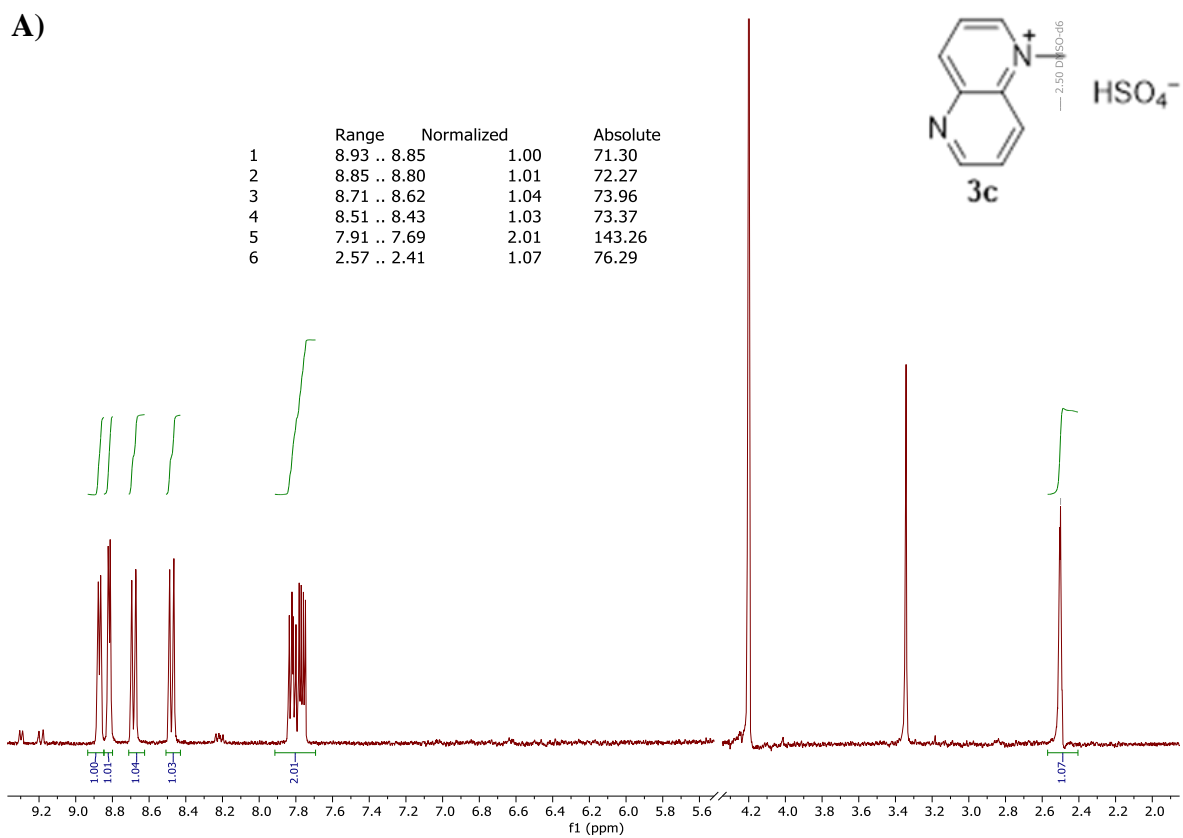


Figure S72 – $^1\text{H-NMR}$ post mortem analysis of the electrolyte containing **3c** in 1M H_2SO_4 before (A) and after galvanostatic cycling for 1st redox step (B).

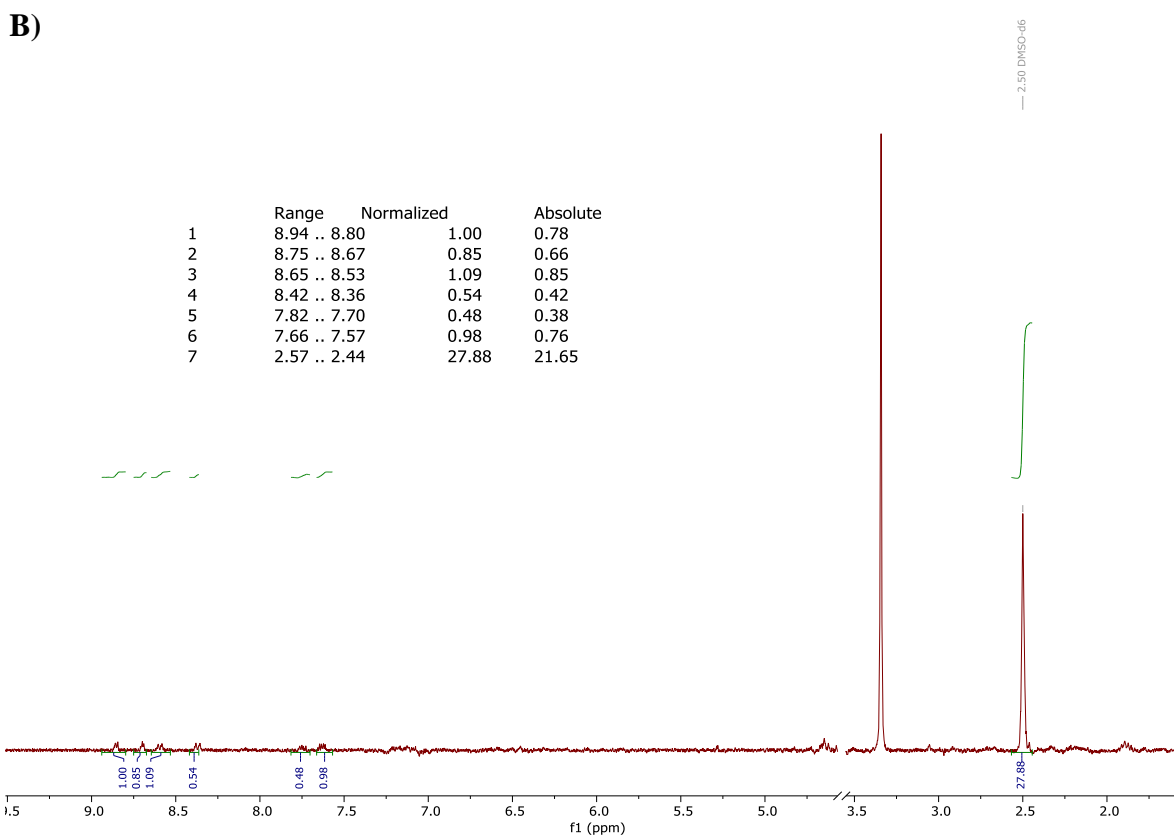
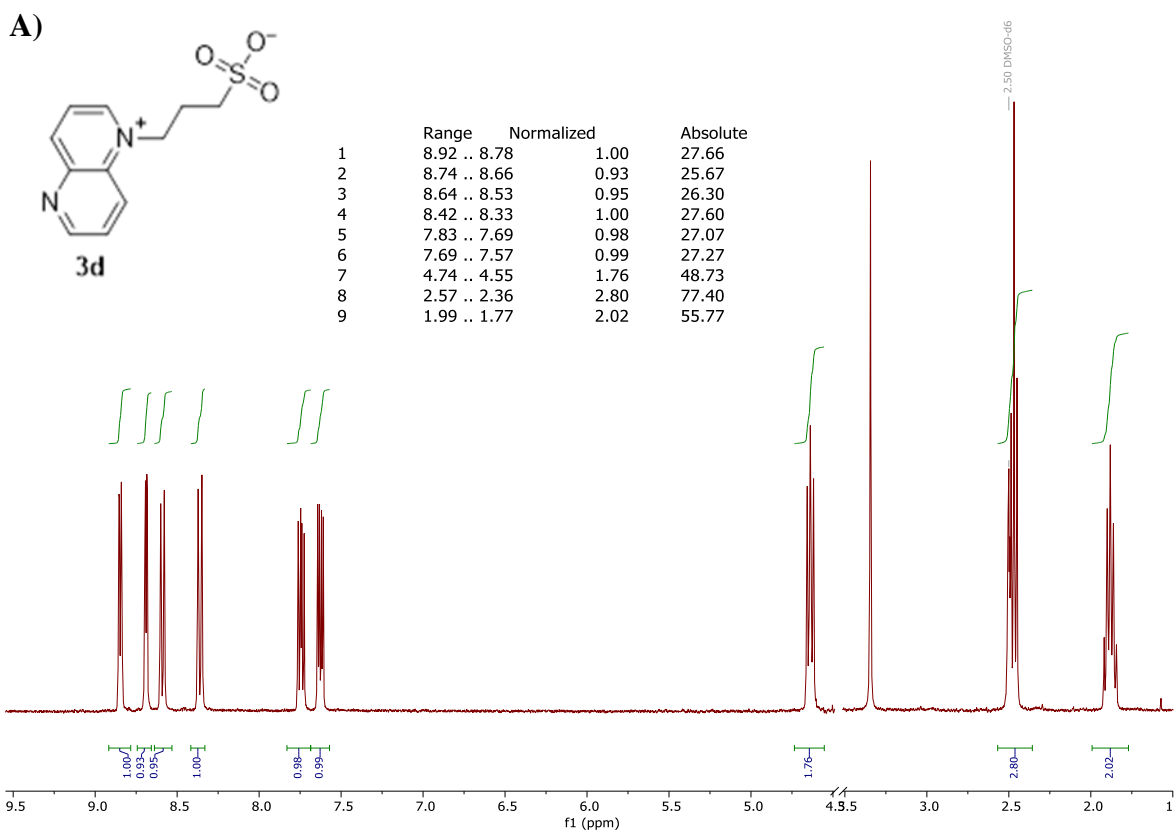


Figure S73 – $^1\text{H-NMR}$ post mortem analysis of the electrolyte containing **3d** in $1\text{M Na}_2\text{SO}_4$ before (A) and after galvanostatic cycling for 1^{st} redox step (B).

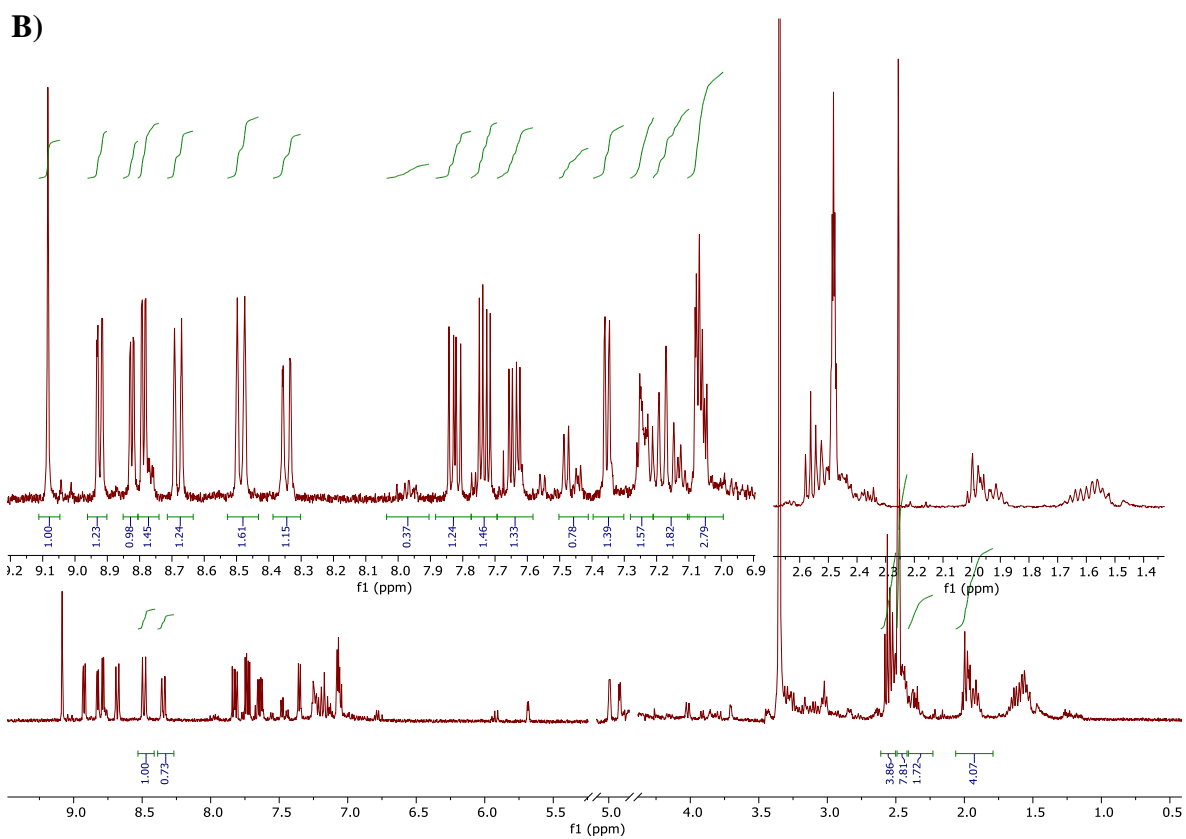
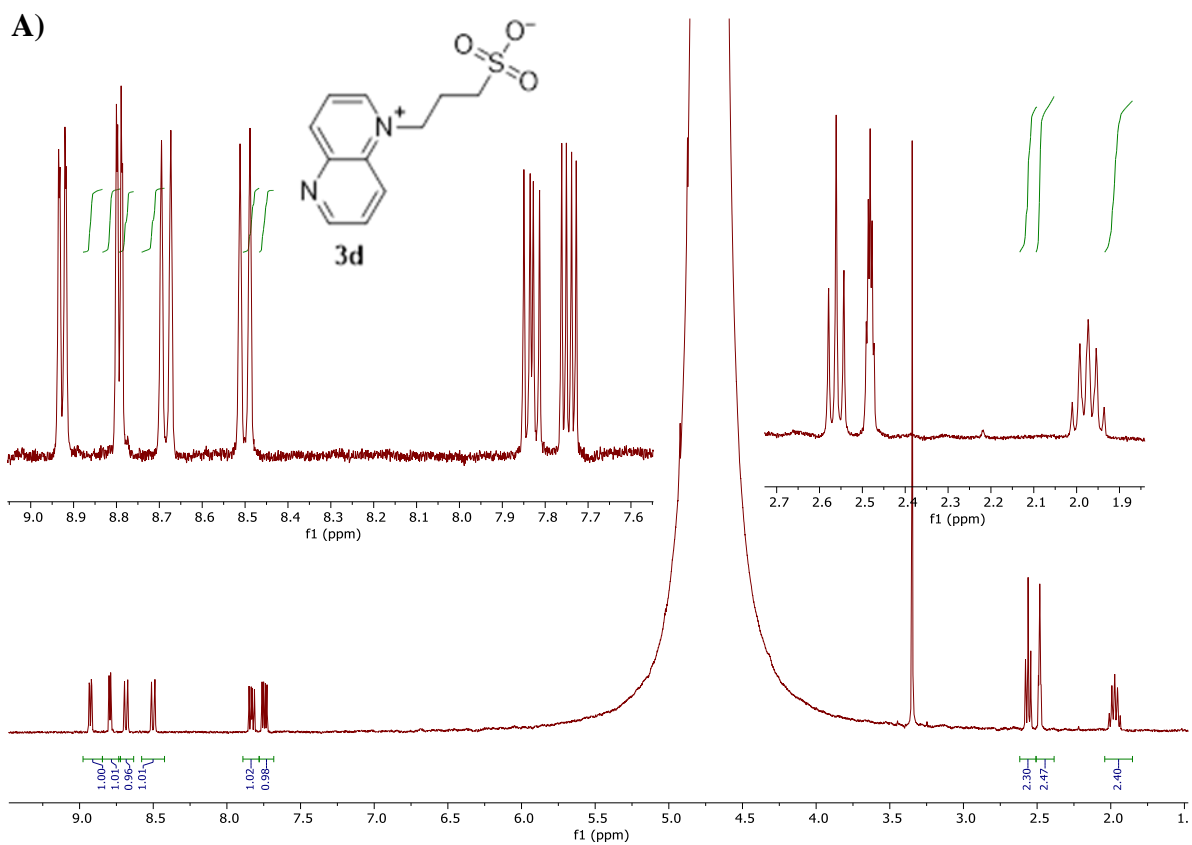


Figure S74 – $^1\text{H-NMR}$ post mortem analysis of the electrolyte containing **3d** in $1\text{M H}_2\text{SO}_4$ before (A) and after galvanostatic cycling for 1^{st} redox step (B).

7 NMR spectra of target compounds

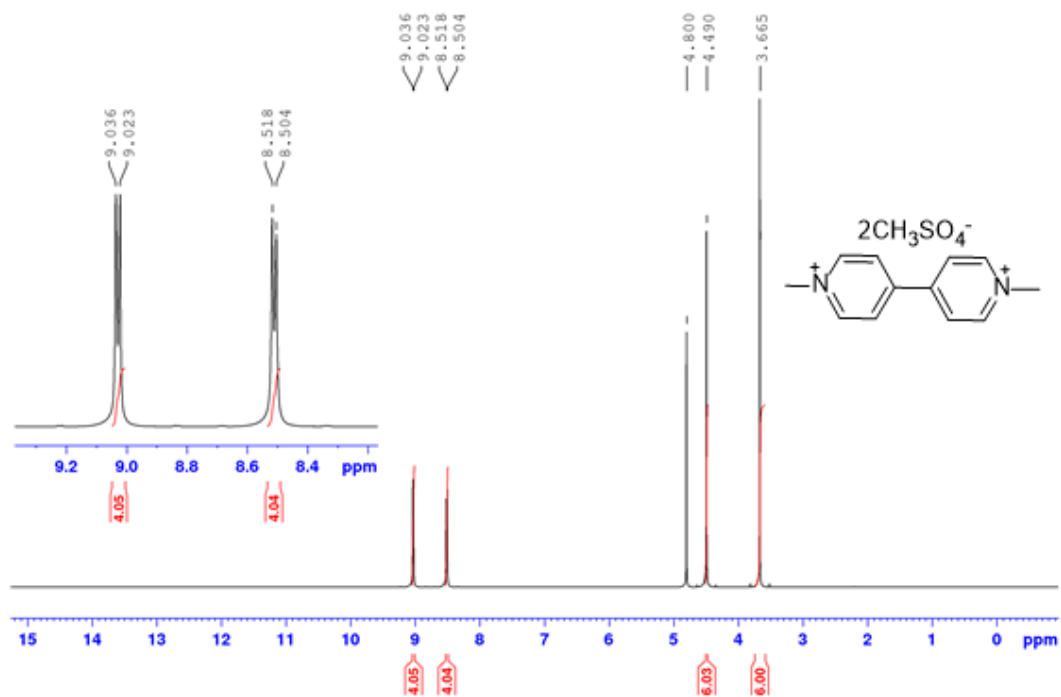


Figure S75 – ^1H -NMR (500 MHz, D_2O , 25 °C) spectrum of **1a**.

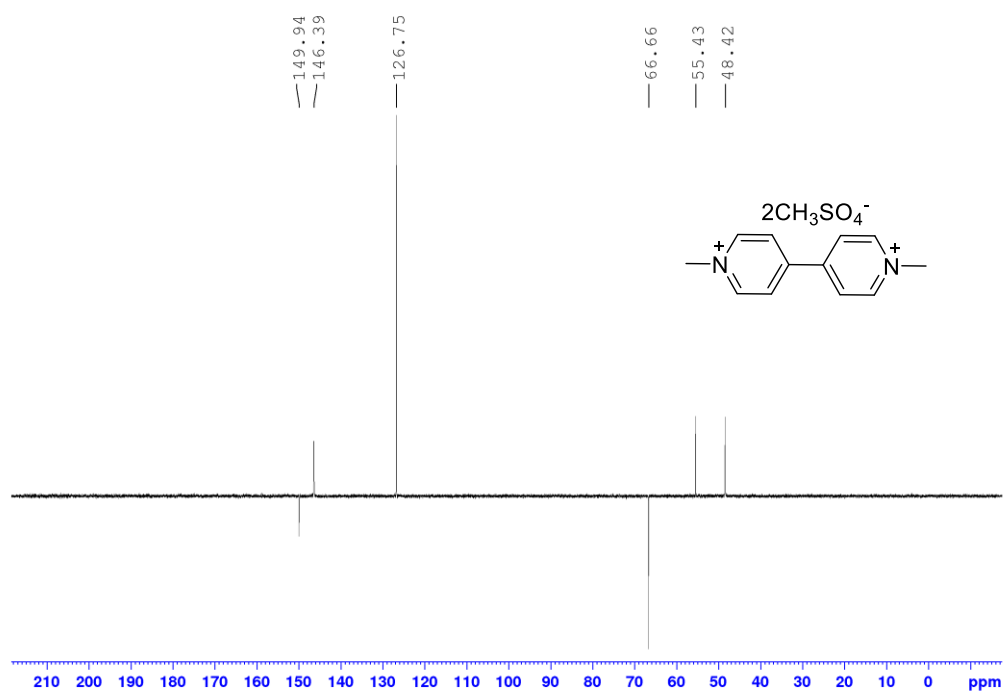


Figure S76 – ^{13}C -NMR APT (125 MHz, $\text{D}_2\text{O}/1,4\text{-dioxane}$ – $\delta = 66.7$ ppm, 25 °C) spectrum of **1a**.

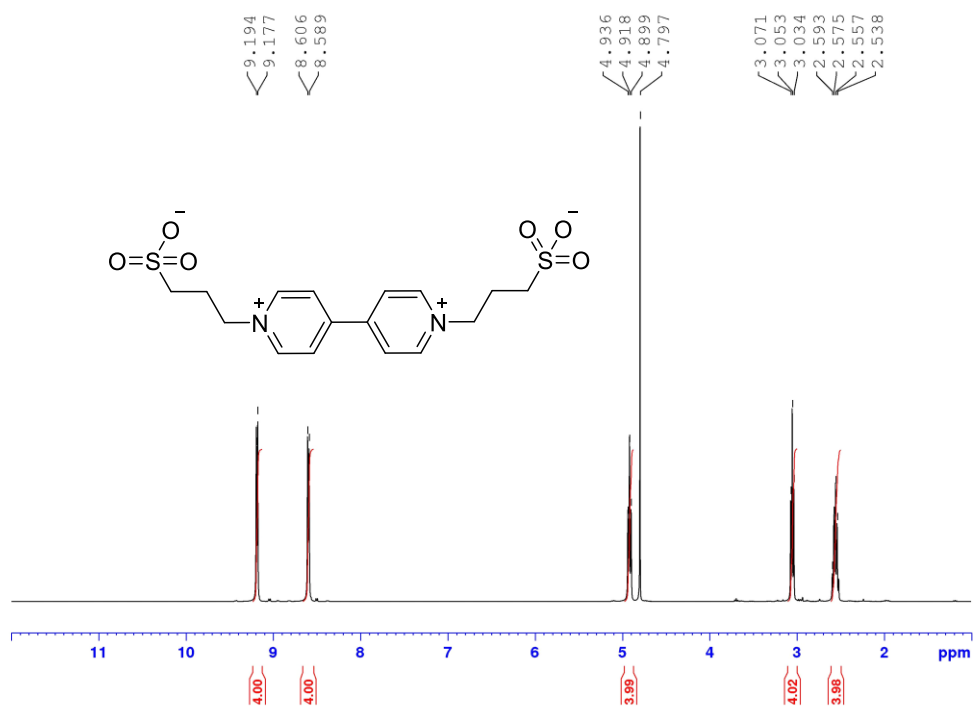


Figure S77 – $^1\text{H-NMR}$ (400 MHz, D_2O , 25 °C) spectrum of **1b**.

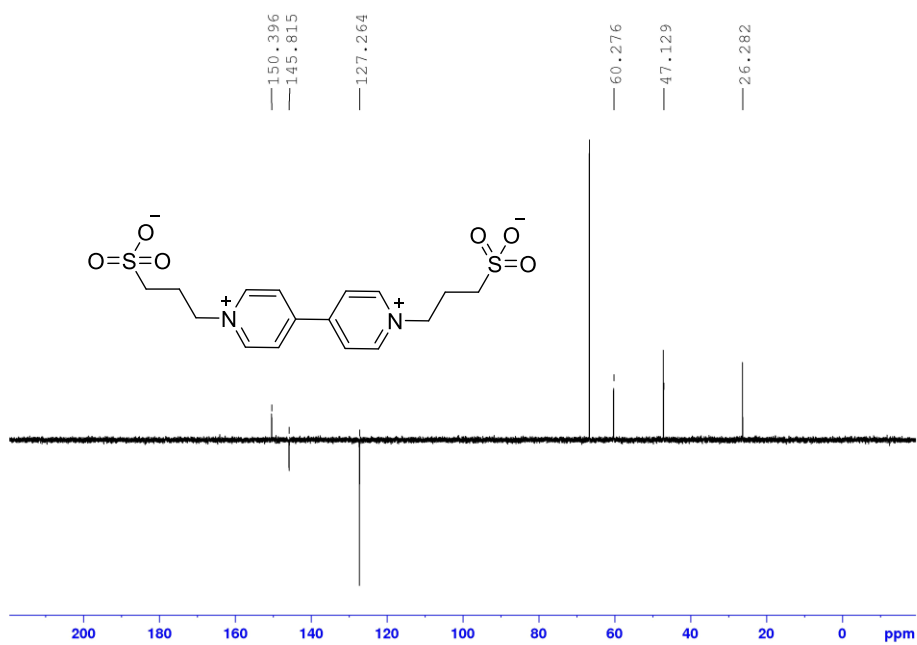


Figure S78 – $^{13}\text{C-NMR}$ APT (100 MHz, $\text{D}_2\text{O}/1,4\text{-dioxane}$ – $\delta = 66.7$ ppm, 25 °C) spectrum of **1b**.

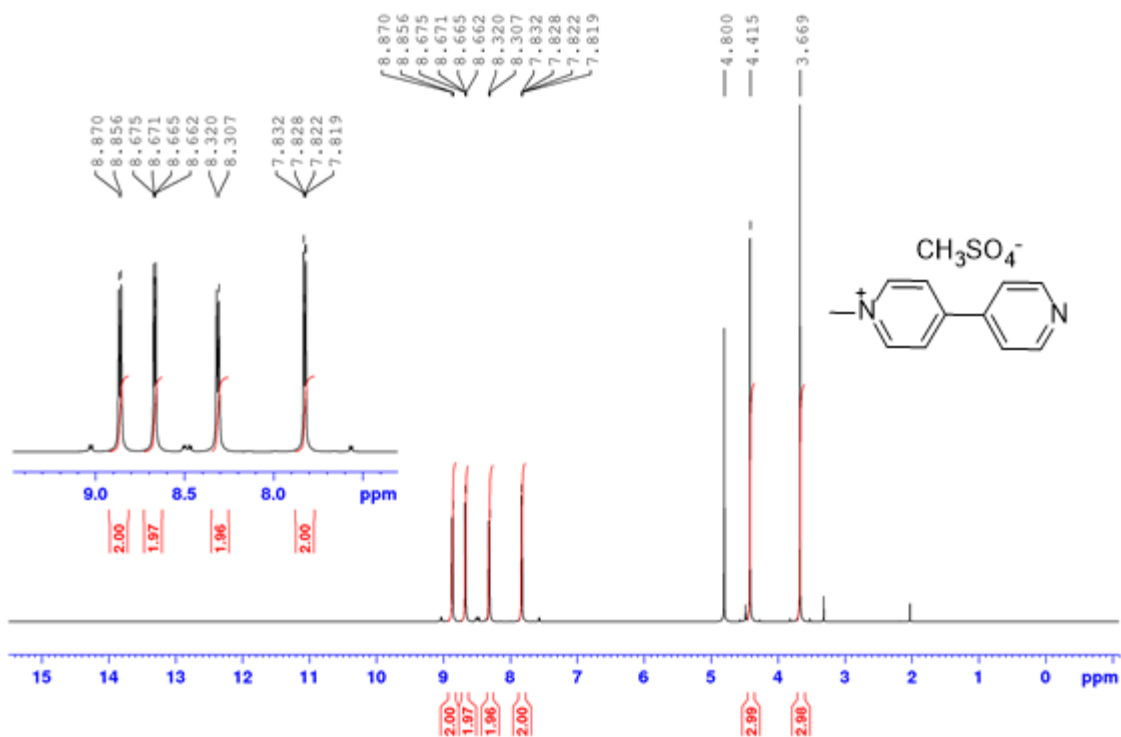


Figure S79 – $^1\text{H-NMR}$ (500 MHz, D_2O , 25 °C) spectrum of **1c**.

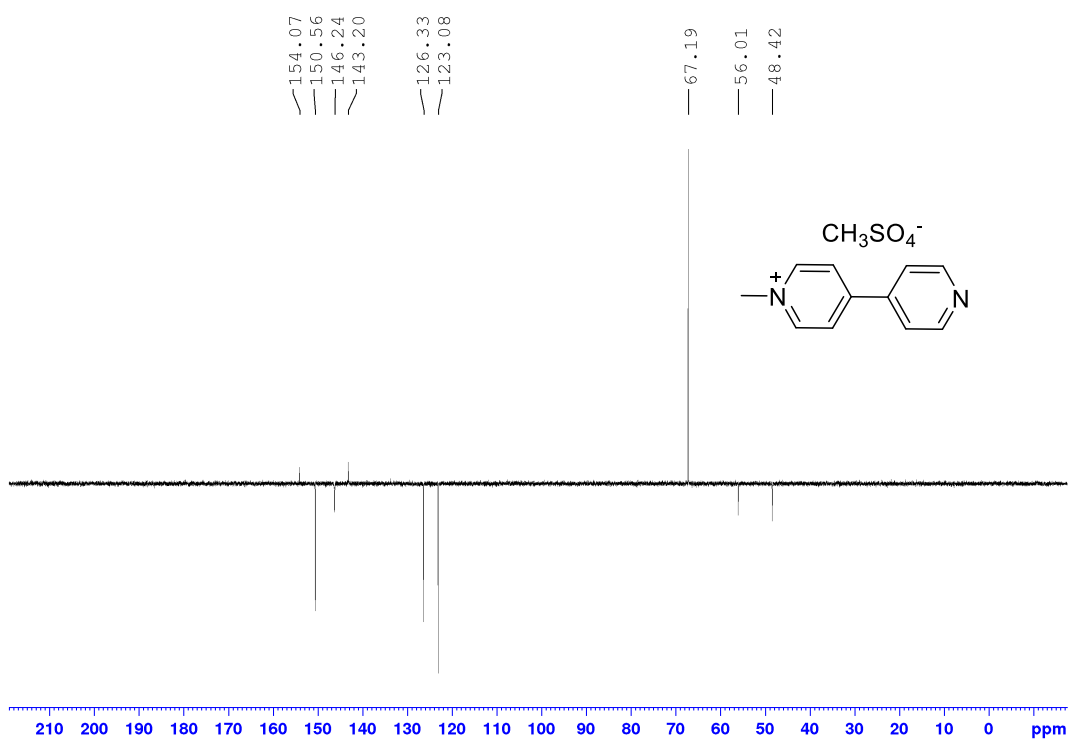


Figure S80 – $^{13}\text{C-NMR}$ APT (125 MHz, $\text{D}_2\text{O}/1,4\text{-dioxane}$ – $\delta = 67.2$ ppm, 25 °C) spectrum of **1c**.

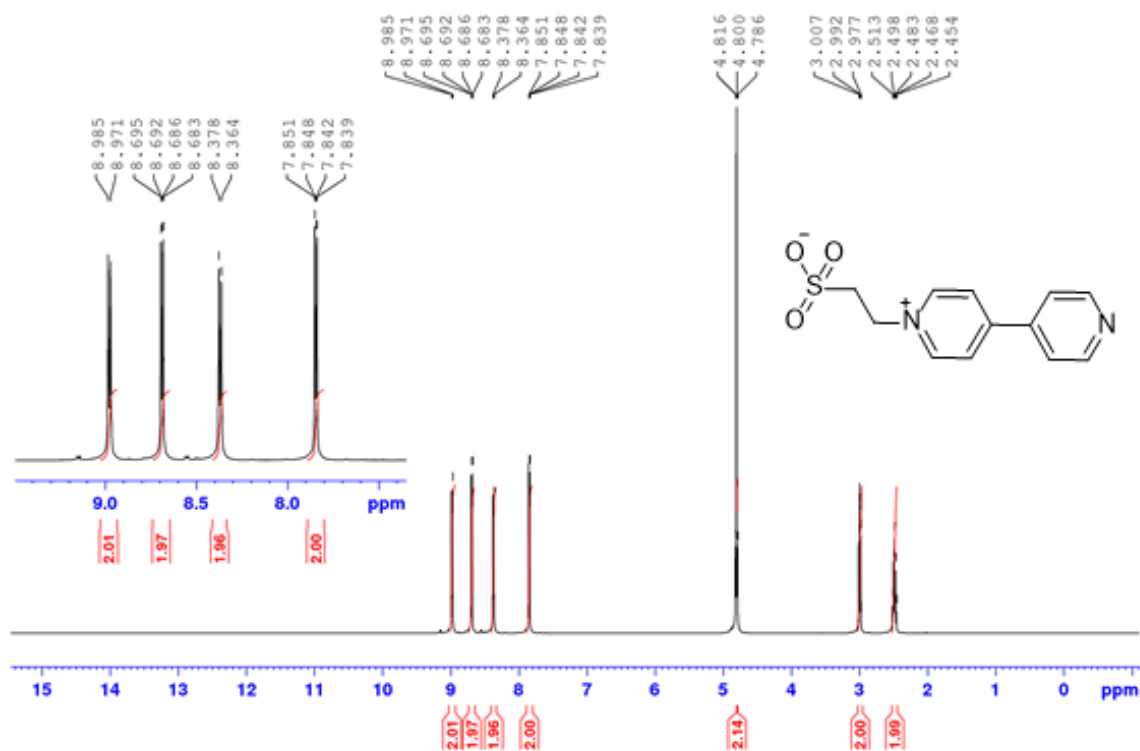


Figure S81 – $^1\text{H-NMR}$ (500 MHz, D_2O , 25 °C) spectrum of **1d**.

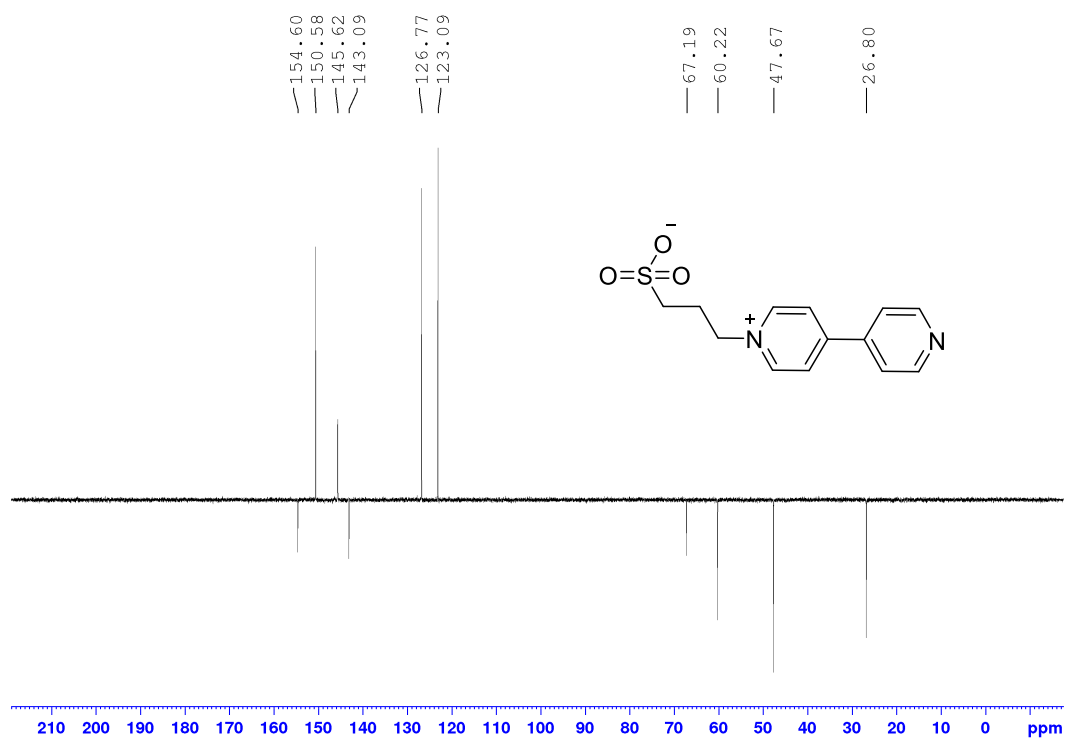


Figure S82 – $^{13}\text{C-NMR}$ APT (125 MHz, $\text{D}_2\text{O}/1,4\text{-dioxane}$ – $\delta = 67.2$ ppm, 25 °C) spectrum of **1d**.

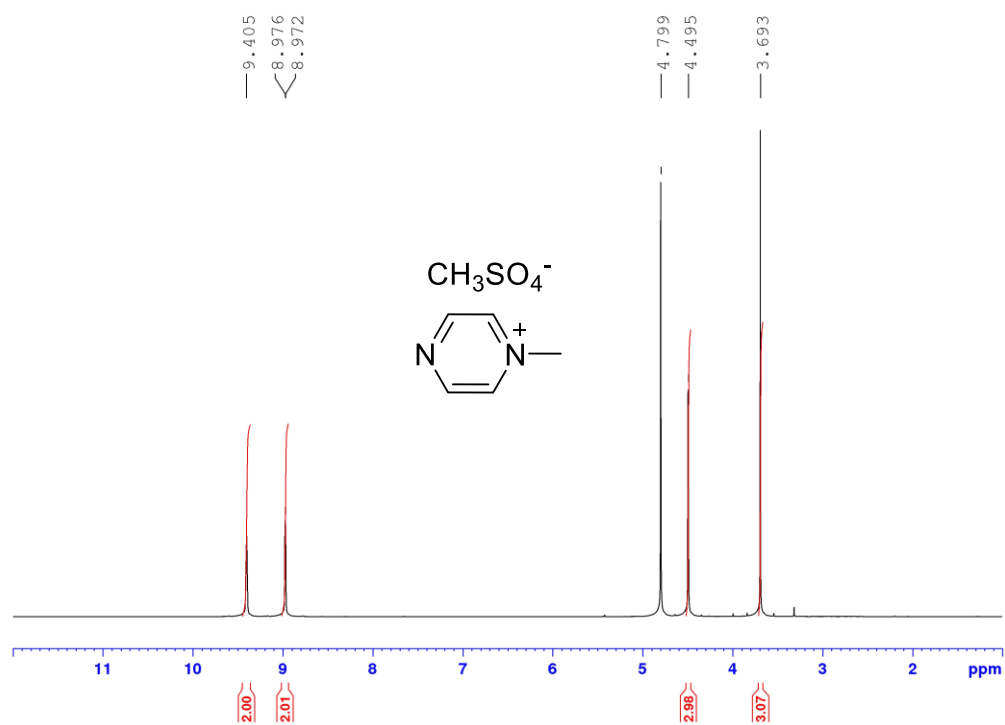


Figure S83 – $^1\text{H-NMR}$ (400 MHz, D_2O , 25 °C) spectrum of **2c**.

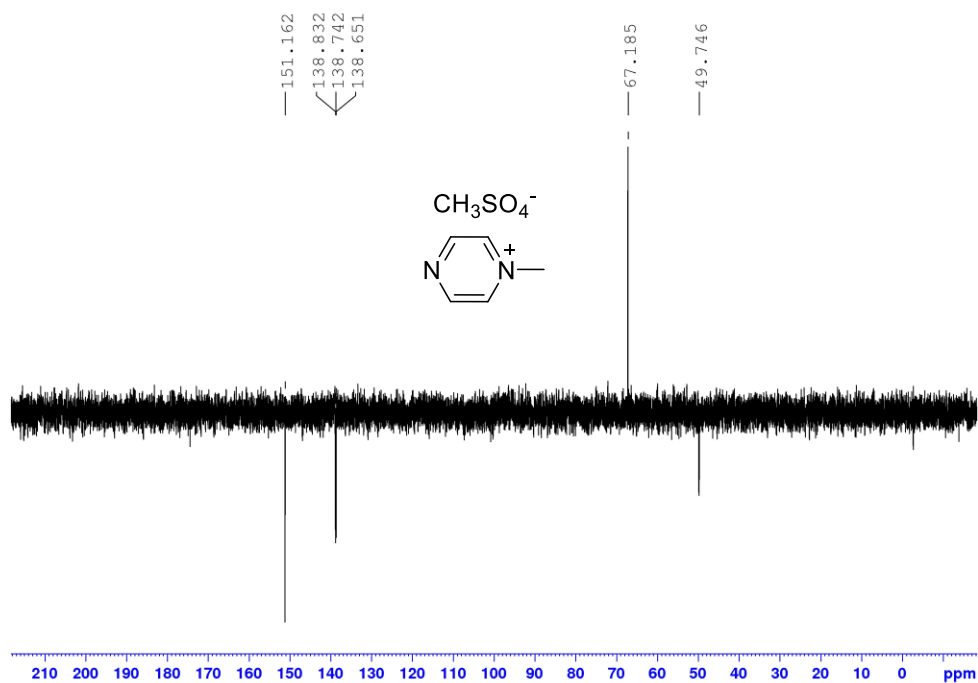


Figure S84 – $^{13}\text{C-NMR}$ APT (100 MHz, $\text{D}_2\text{O}/1,4\text{-dioxane}$ – $\delta = 67.2$ ppm, 25 °C) spectrum of **2c**.

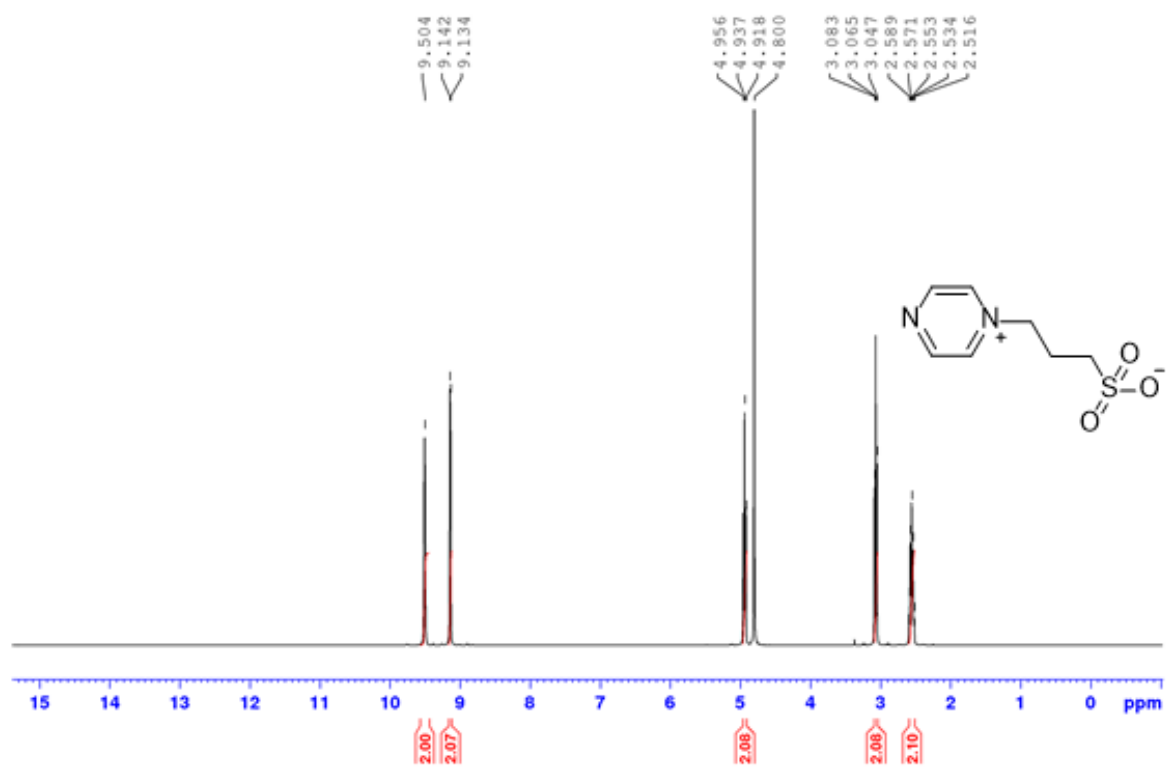


Figure S85 – $^1\text{H-NMR}$ (400 MHz, D_2O , 25 °C) spectrum of **2d**.

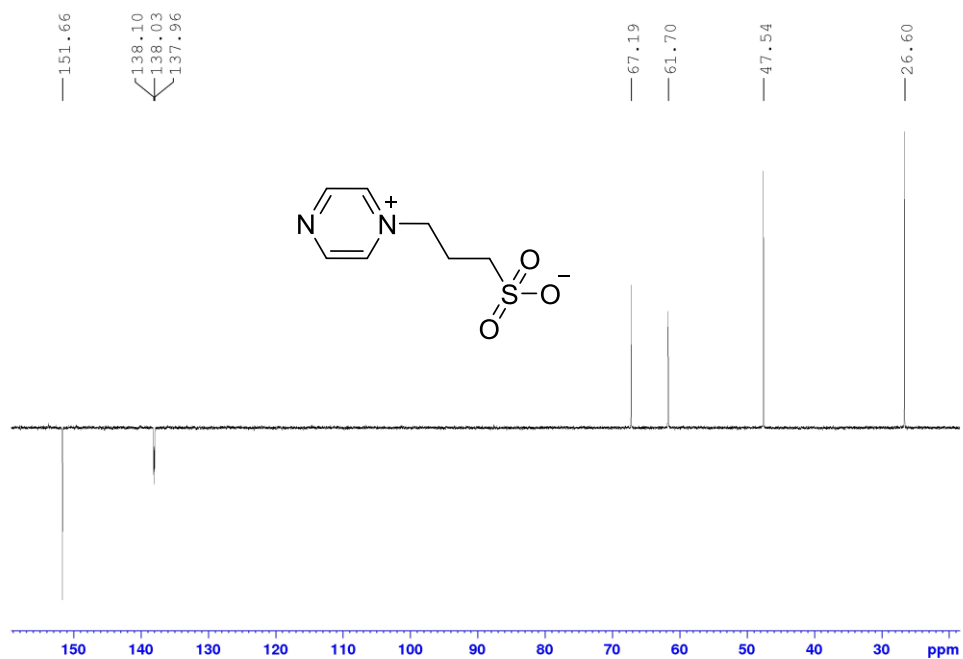


Figure S86 – $^{13}\text{C-NMR}$ APT (125 MHz, $\text{D}_2\text{O}/1,4\text{-dioxane}$ – $\delta = 67.2$ ppm, 25 °C) spectrum of **2d**.

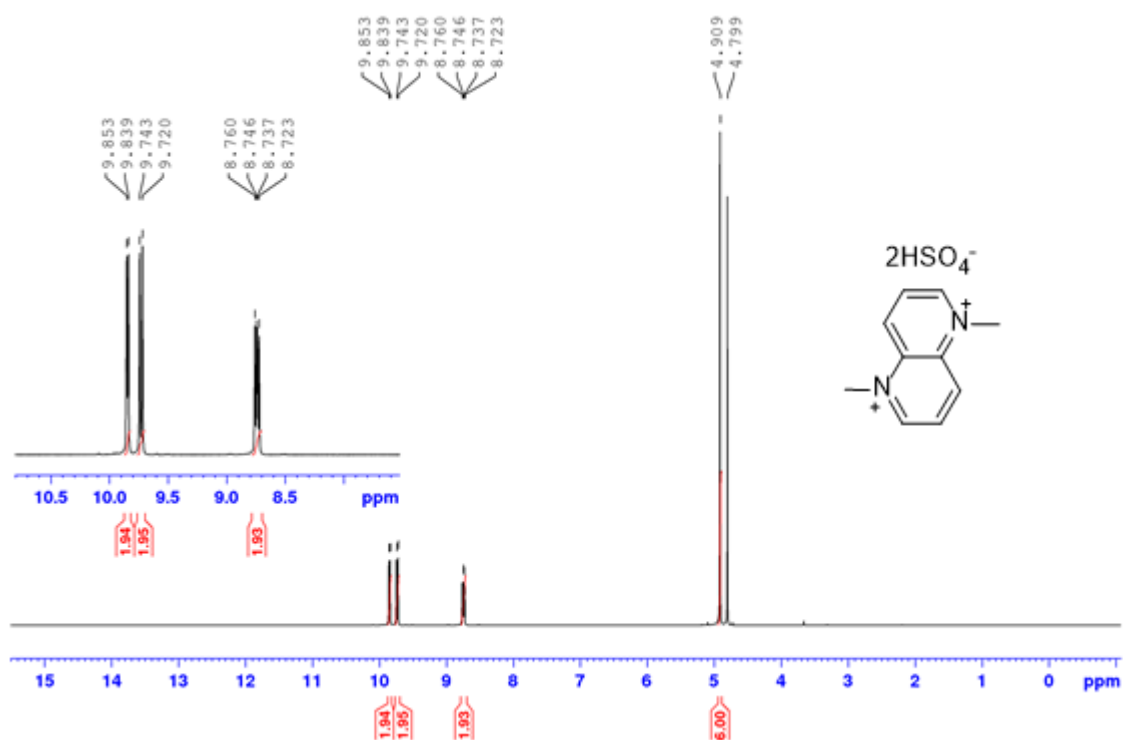


Figure S87 – $^1\text{H-NMR}$ (400 MHz, D_2O , 25 °C) spectrum of **3a**.

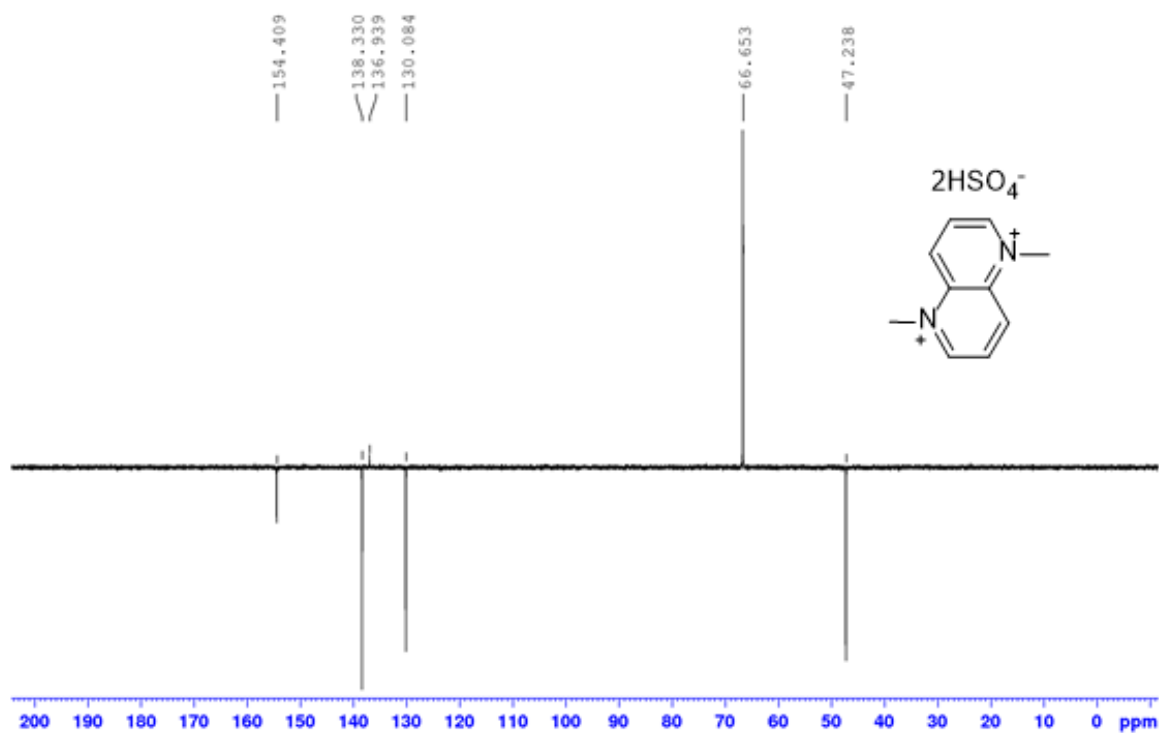


Figure S88 – $^{13}\text{C-NMR}$ APT (100 MHz, $\text{D}_2\text{O}/1,4\text{-dioxane}$ – $\delta = 66.7$ ppm, 25 °C) spectrum of **3a**.

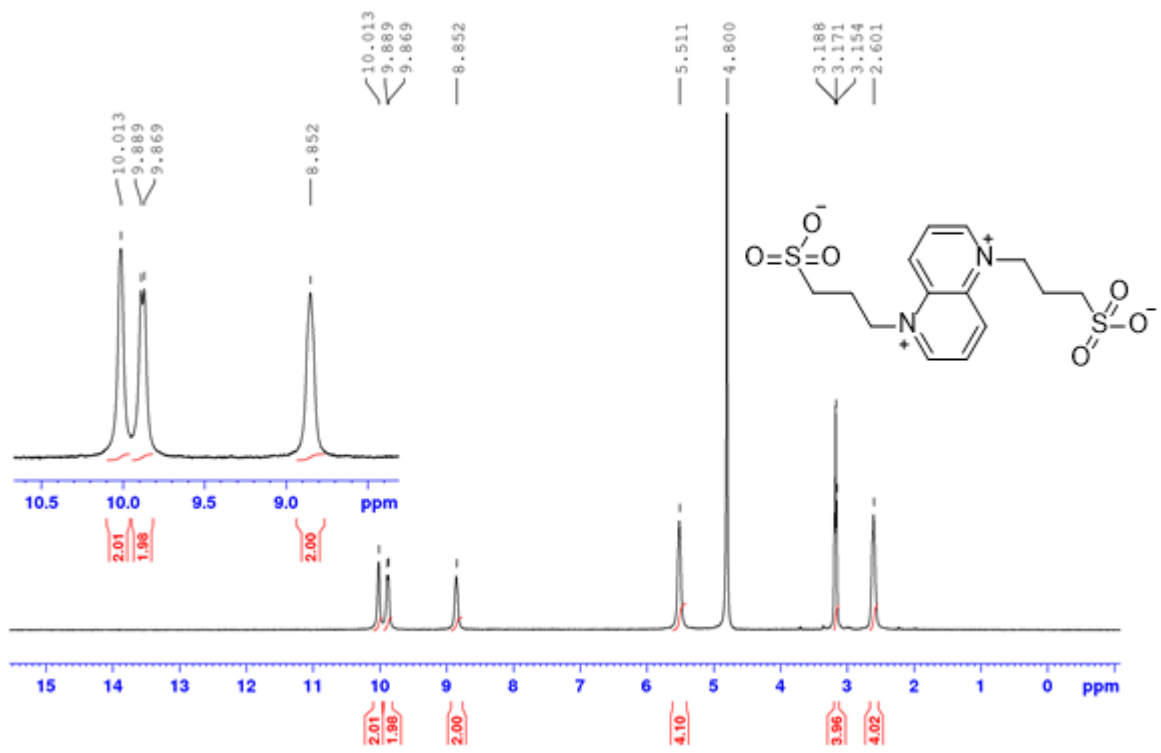


Figure S89 – $^1\text{H-NMR}$ (400 MHz, D_2O , 25 °C) spectrum of **3b**.

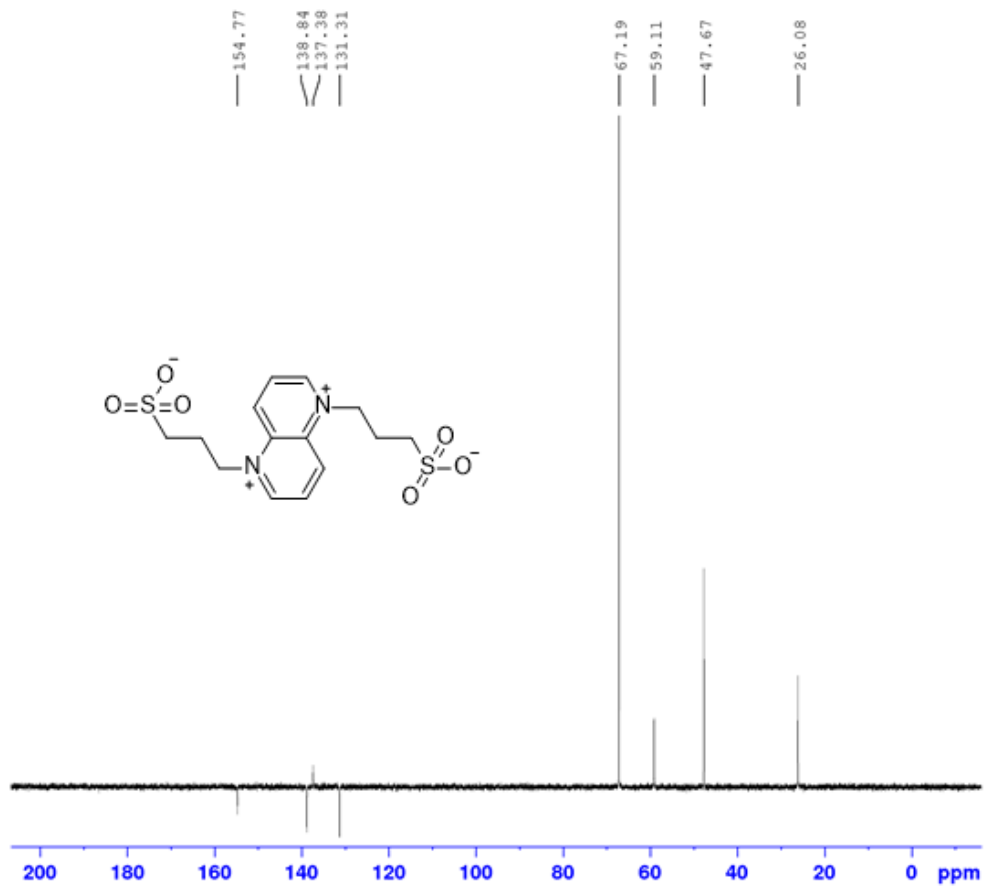


Figure S90 – $^{13}\text{C-NMR APT}$ (125 MHz, $\text{D}_2\text{O}/1,4\text{-dioxane}$ – $\delta = 67.2$ ppm, 25 °C) spectrum of **3b**.

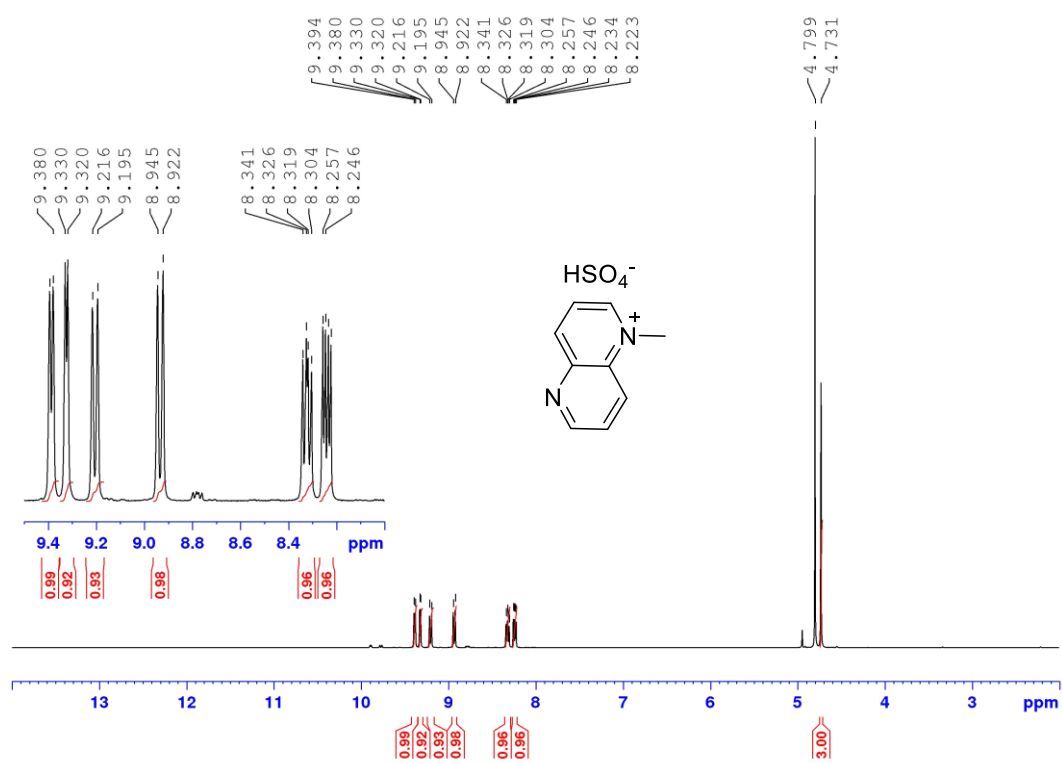


Figure S91 – $^1\text{H-NMR}$ (400 MHz, D_2O , 25 °C) spectrum of **3c**.

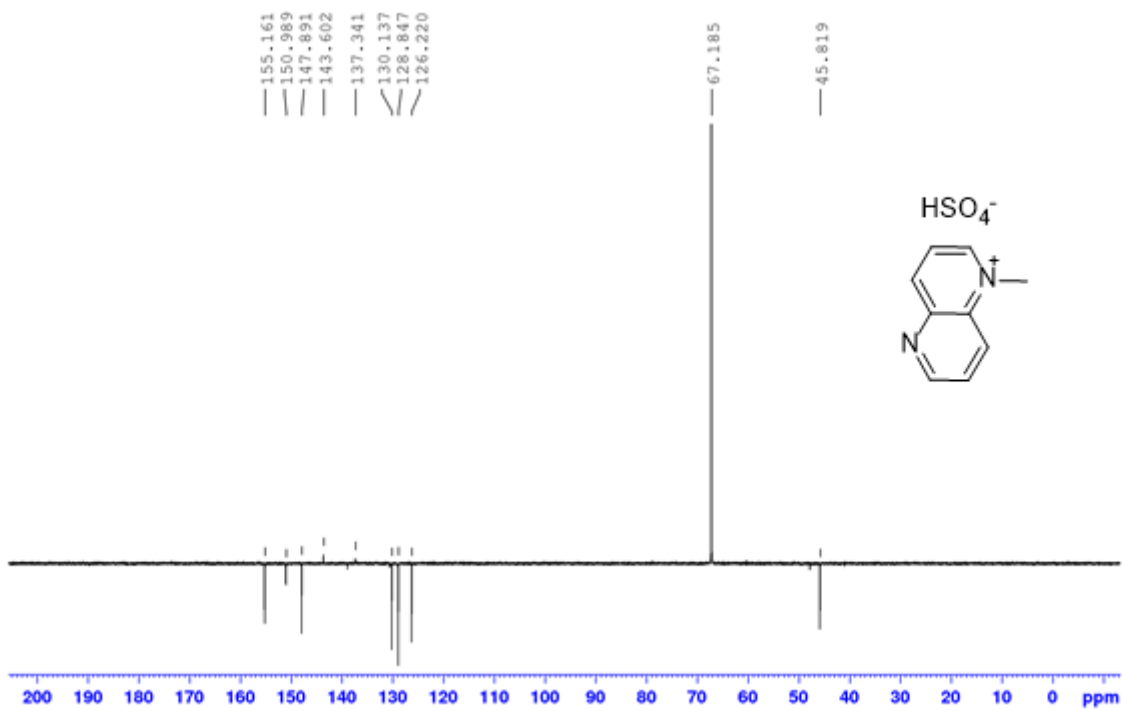


Figure S92 – $^{13}\text{C-NMR}$ APT (100 MHz, $\text{D}_2\text{O}/1,4\text{-dioxane}$ – $\delta = 67.2$ ppm, 25 °C) spectrum of **3b**.

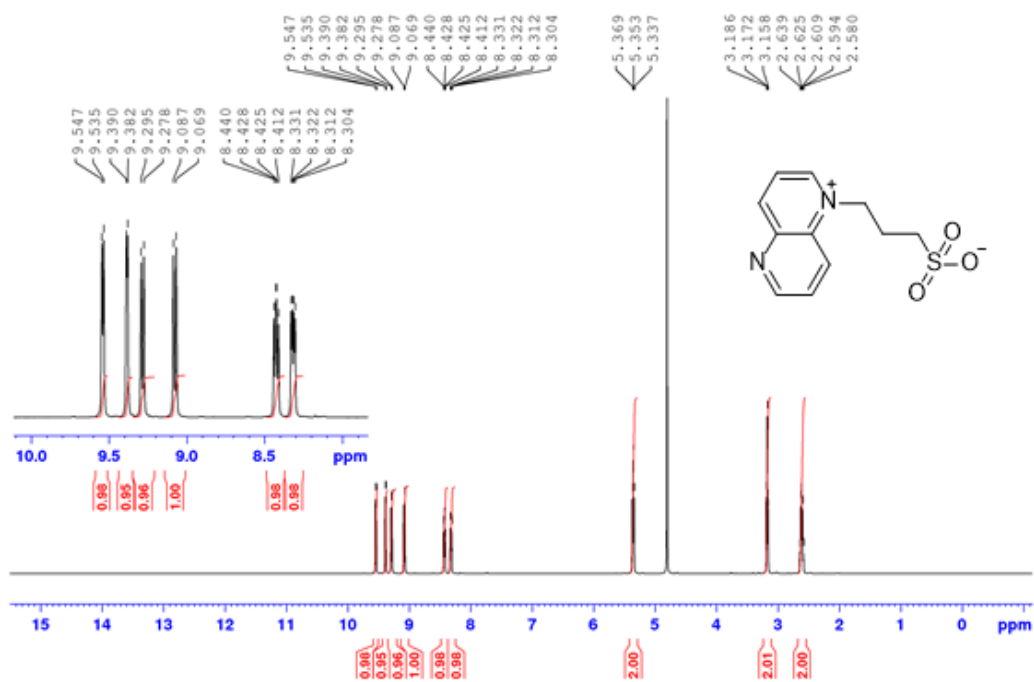


Figure S93 – $^1\text{H-NMR}$ (500 MHz, D_2O , 25 °C) spectrum of 3d.

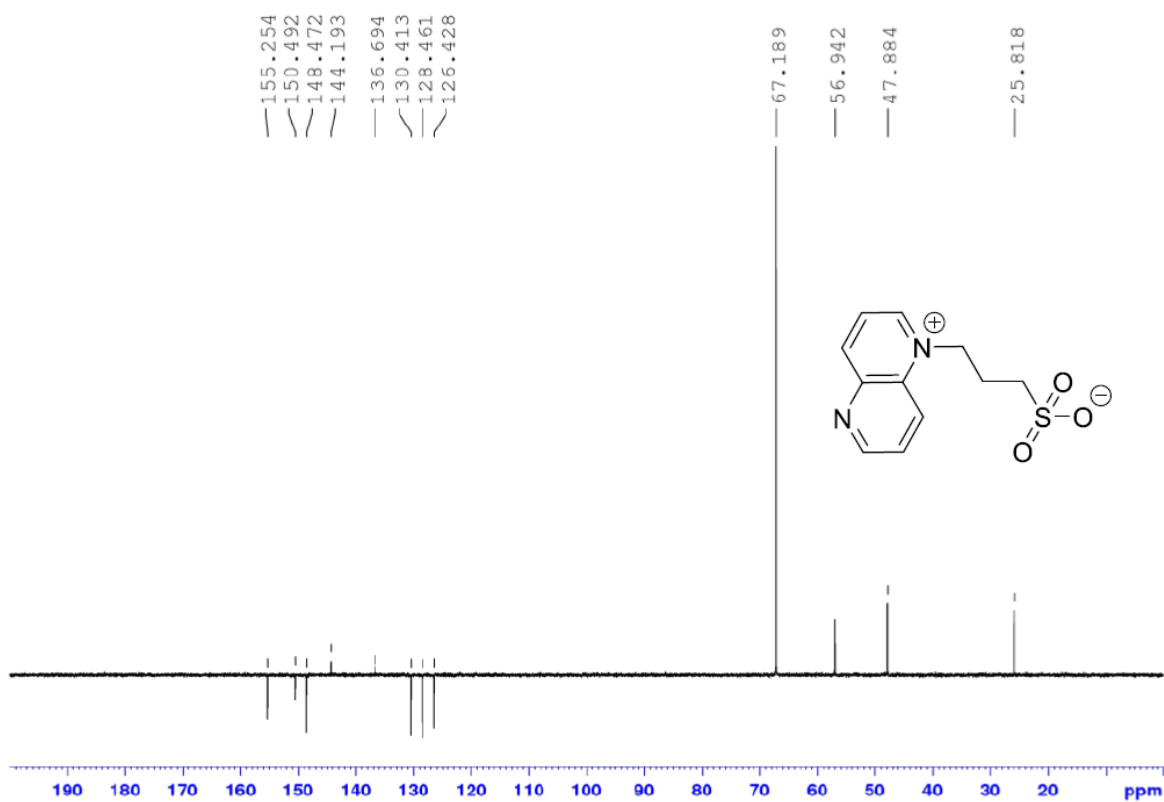


Figure S94 – $^{13}\text{C-NMR APT}$ (100 MHz, $\text{D}_2\text{O}/1,4\text{-dioxane}$ – $\delta = 67.2$ ppm, 25 °C) spectrum of 3d.

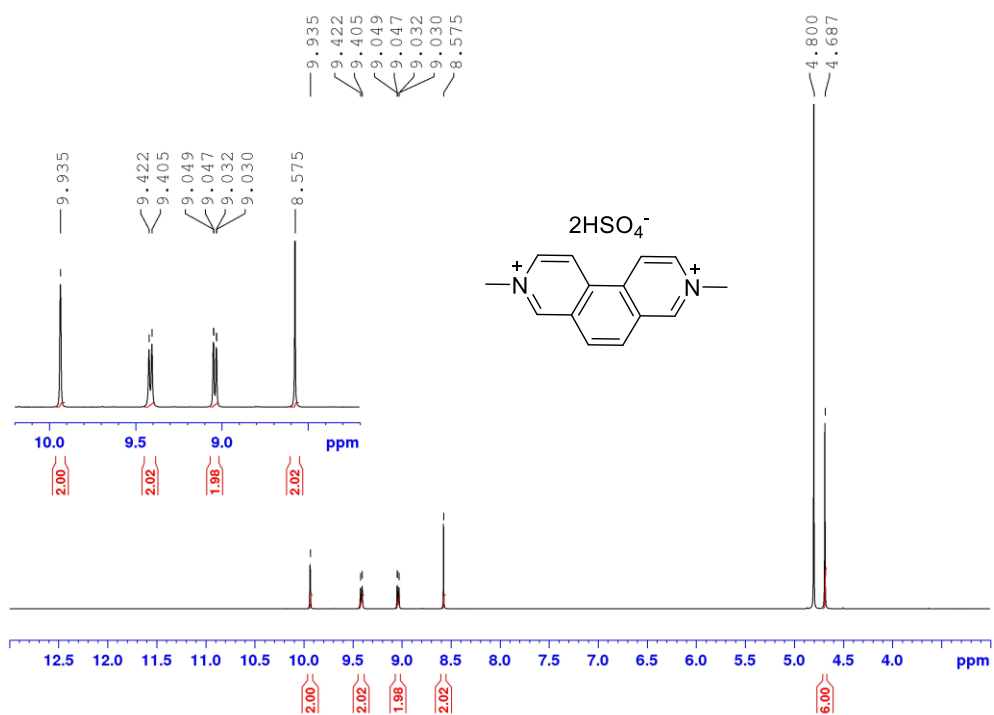


Figure S95 – ¹H-NMR (400 MHz, D₂O, 25 °C) spectrum of **4a**.

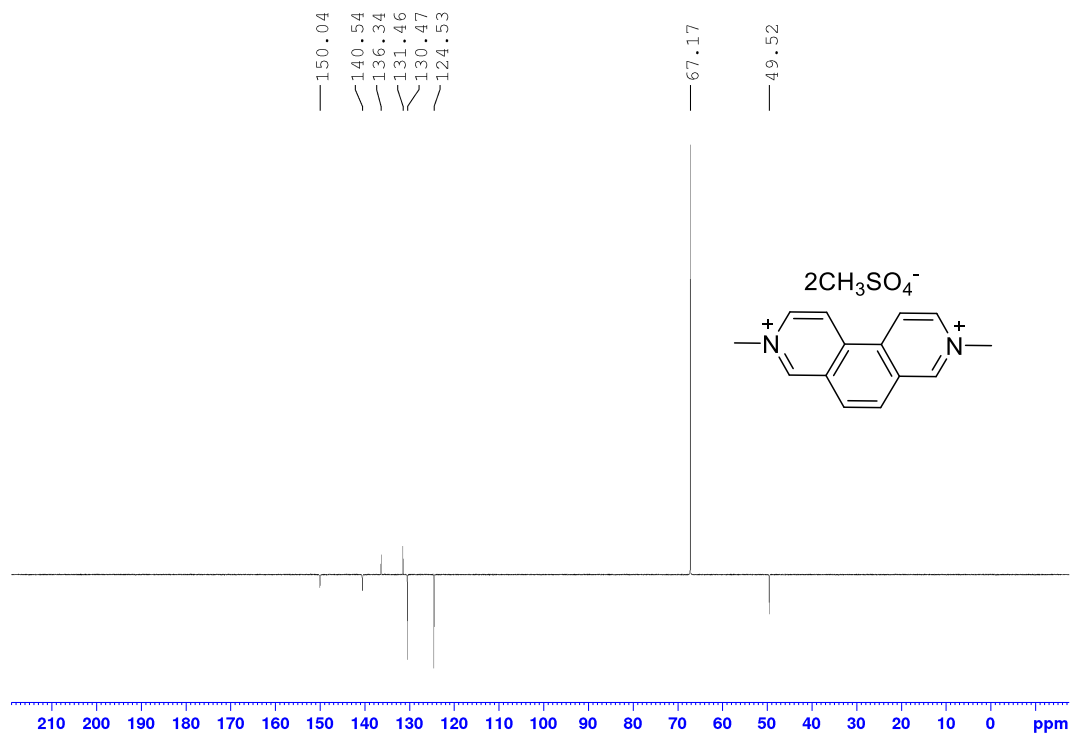


Figure S96 – ¹³C-NMR APT (125 MHz, D₂O/1,4-dioxane – $\delta = 67.2$ ppm, 25 °C) spectrum of **4a**.

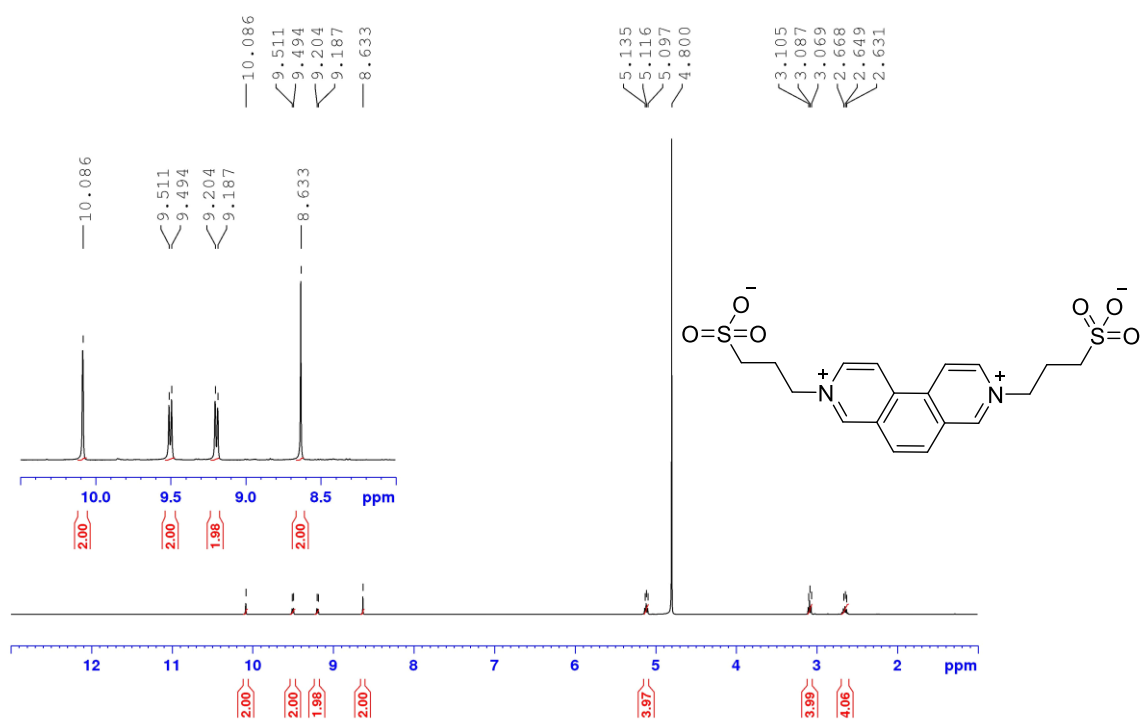


Figure S97 – $^1\text{H-NMR}$ (400 MHz, D_2O , 25 °C) spectrum of **4b**.

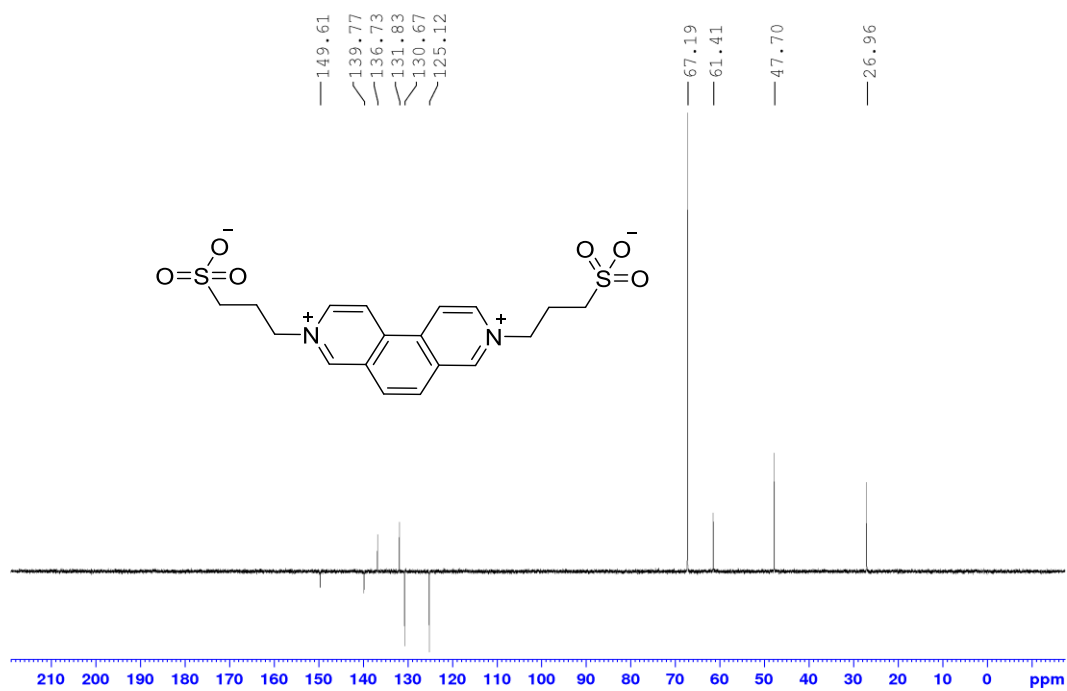


Figure S98 – $^{13}\text{C-NMR APT}$ (125 MHz, $\text{D}_2\text{O}/1,4\text{-dioxane}$ – $\delta = 67.2$ ppm, 25 °C) spectrum of **4b**.

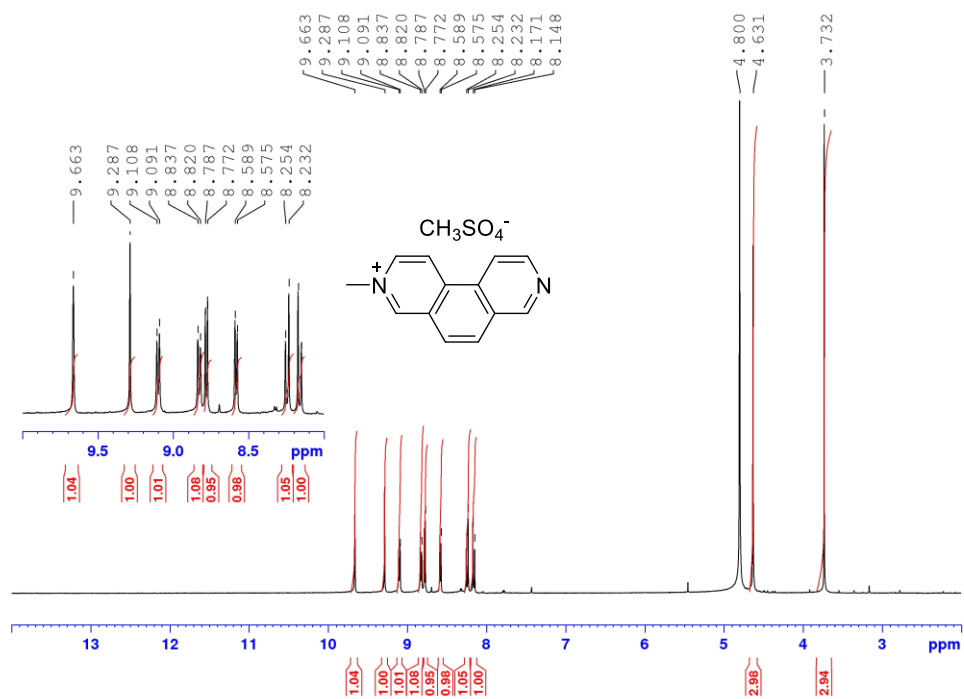


Figure S99 – $^1\text{H-NMR}$ (400 MHz, D_2O , 25 °C) spectrum of **4c**.

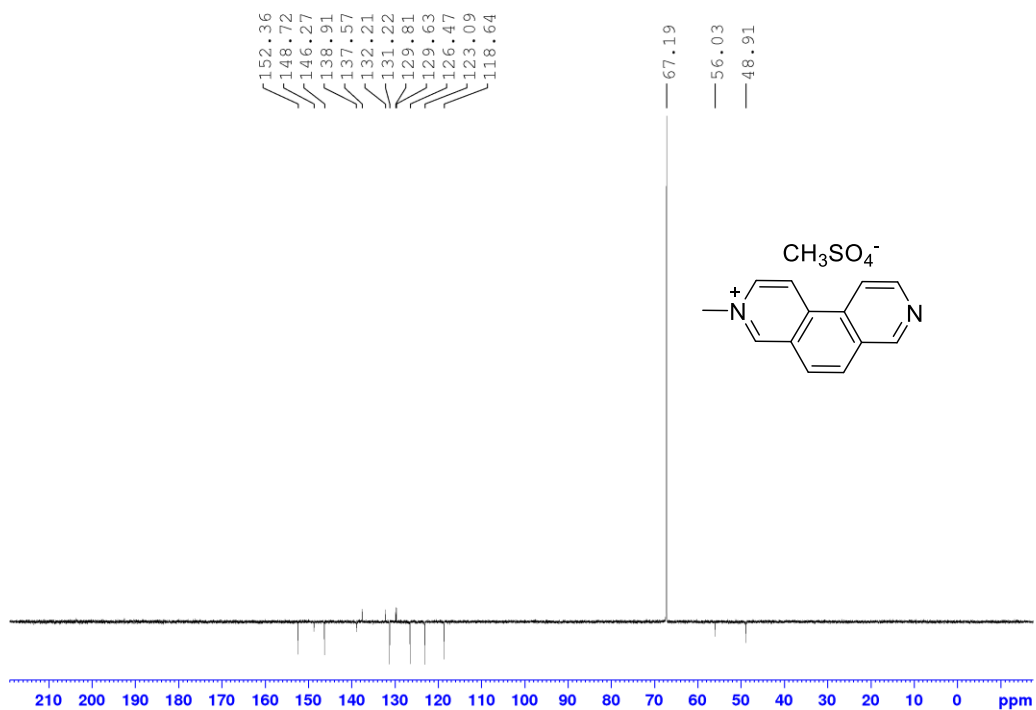


Figure S100 – $^{13}\text{C-NMR}$ APT (125 MHz, $\text{D}_2\text{O}/1,4\text{-dioxane}$ – $\delta = 67.2$ ppm, 25 °C) spectrum of **4c**.

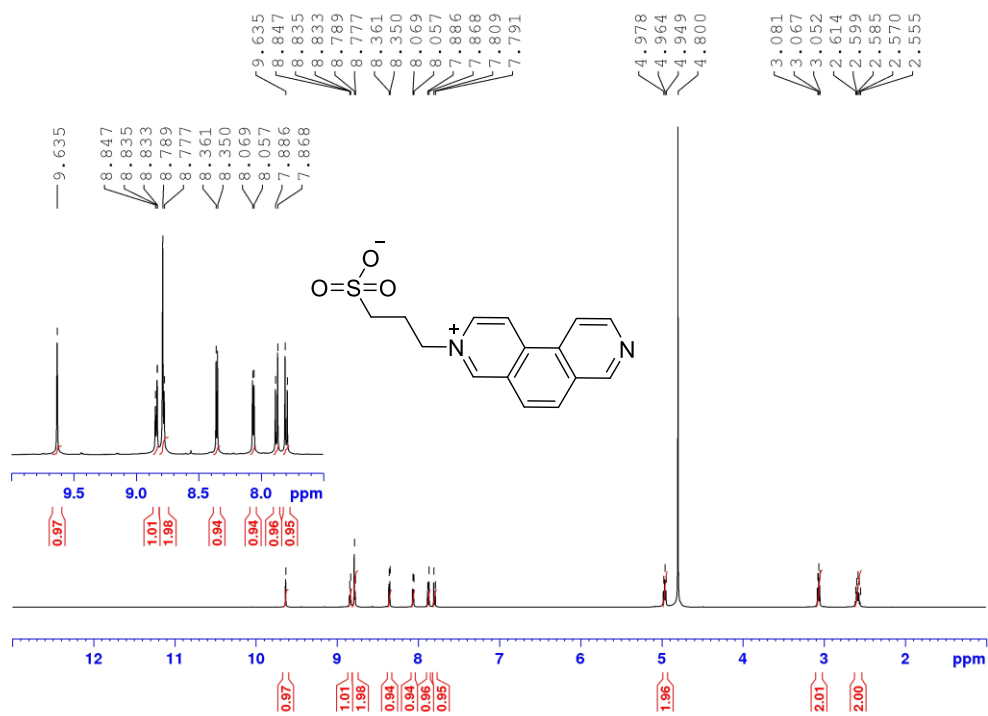


Figure S101 – $^1\text{H-NMR}$ (500 MHz, D_2O , 25 °C) spectrum of **4d**.

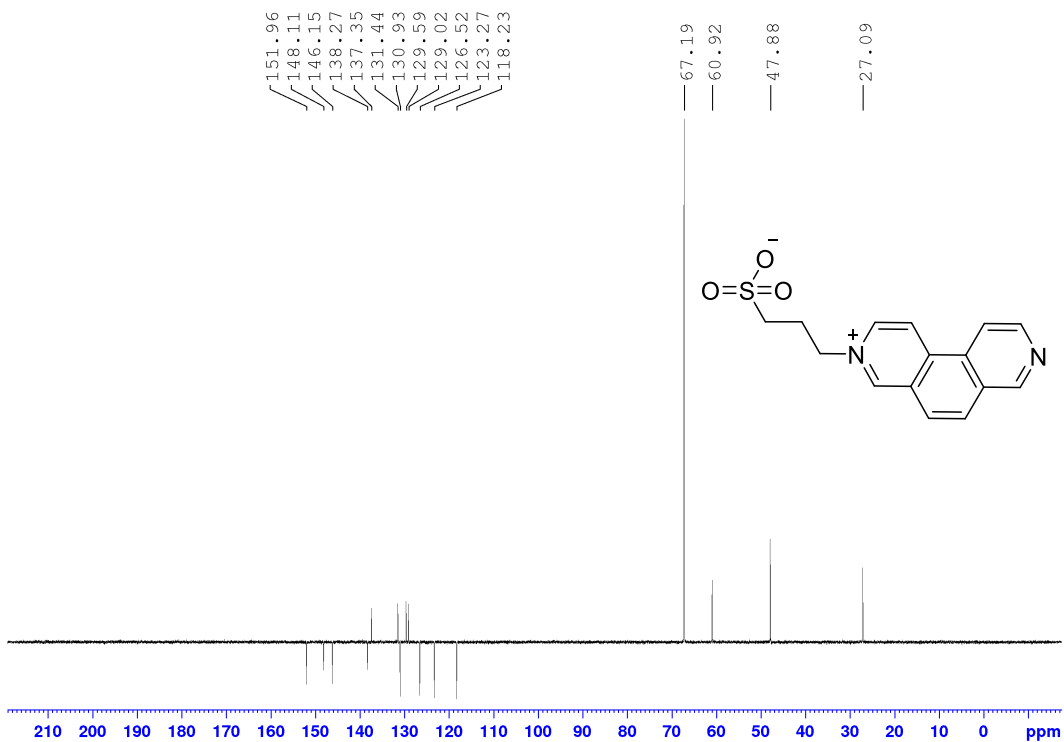


Figure S102 – $^{13}\text{C-NMR APT}$ (125 MHz, $\text{D}_2\text{O}/1,4\text{-dioxane}$ – $\delta = 67.2$ ppm, 25 °C) spectrum of **4d**.

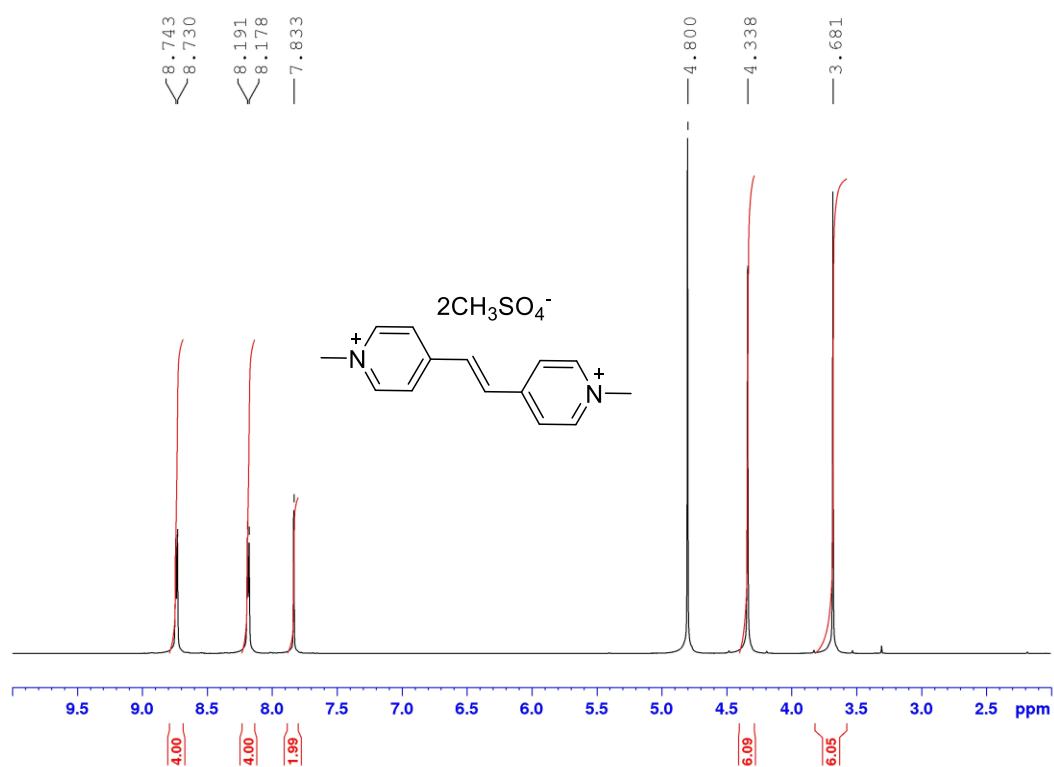


Figure S103 – $^1\text{H-NMR}$ (500 MHz, D_2O , 25 °C) spectrum of **5a**.

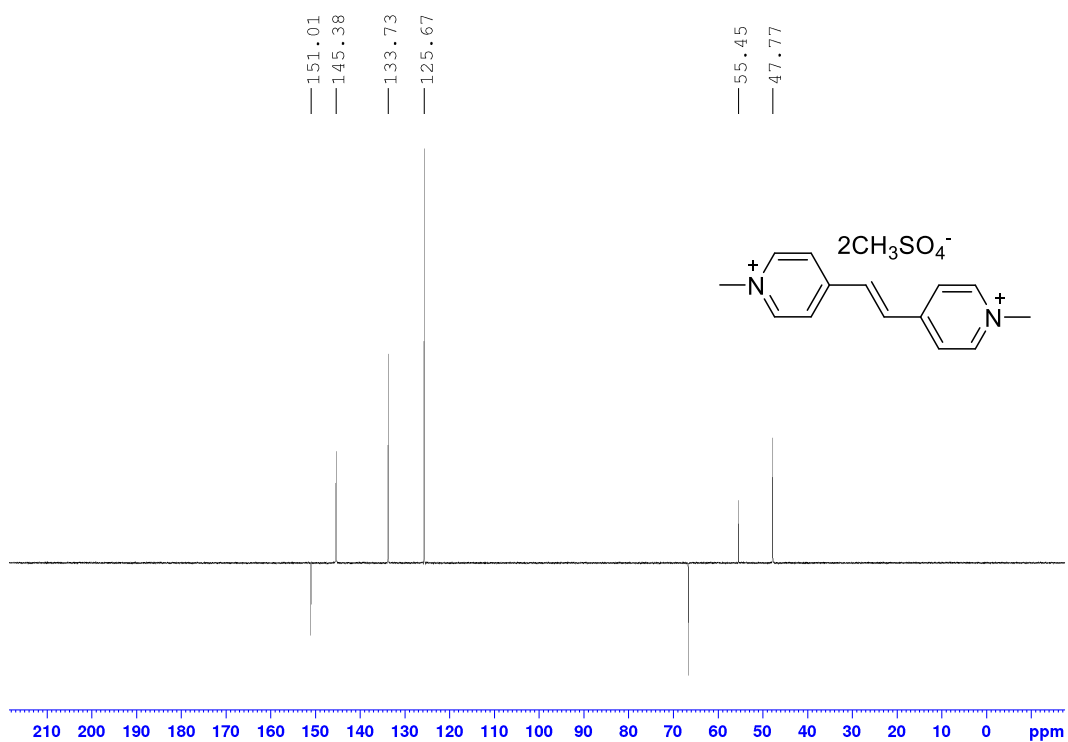


Figure S104 – $^{13}\text{C-NMR APT}$ (125 MHz, $\text{D}_2\text{O}/1,4\text{-dioxane}$ – $\delta = 67.2$ ppm, 25 °C) spectrum of **5a**.

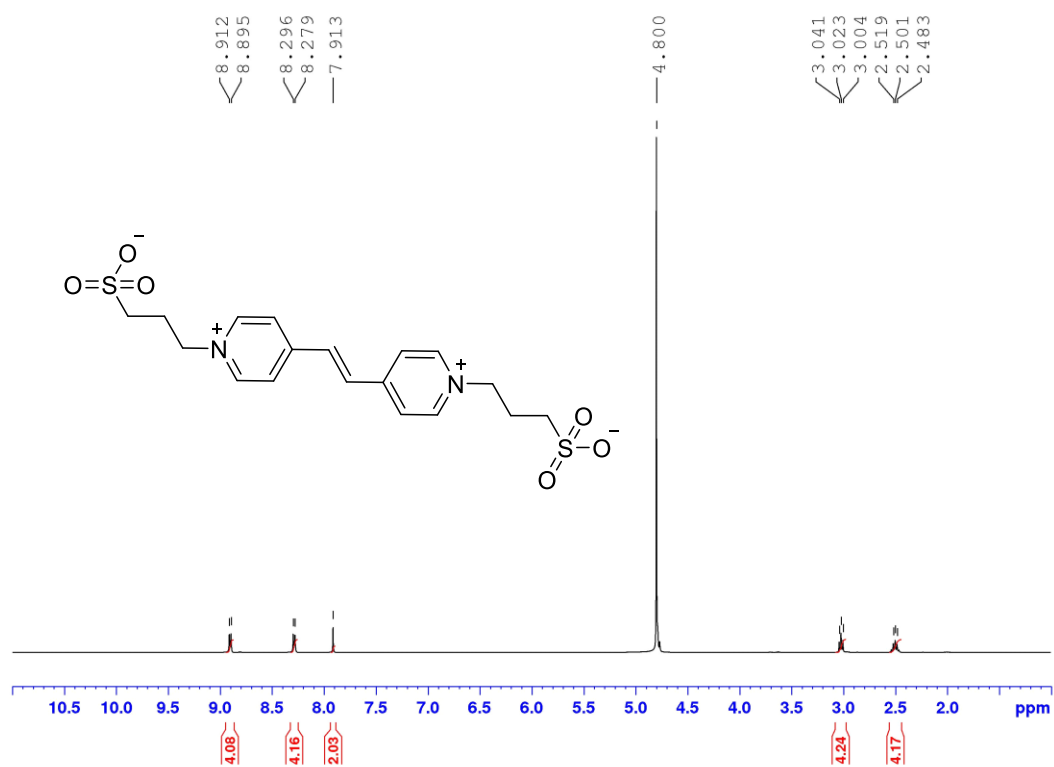


Figure S105 – $^1\text{H-NMR}$ (400 MHz, D_2O , 25 °C) spectrum of **5b**.

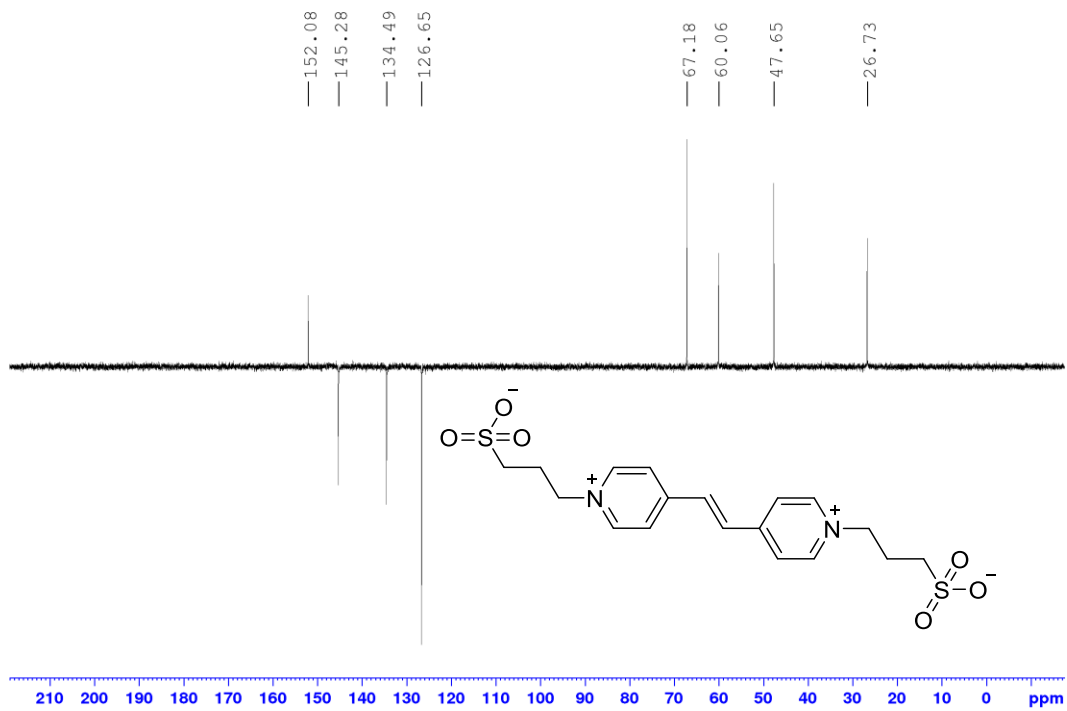


Figure S106 – $^{13}\text{C-NMR APT}$ (100 MHz, $\text{D}_2\text{O}/1,4\text{-dioxane}$ – $\delta = 67.2$ ppm, 25 °C) spectrum of **5b**.

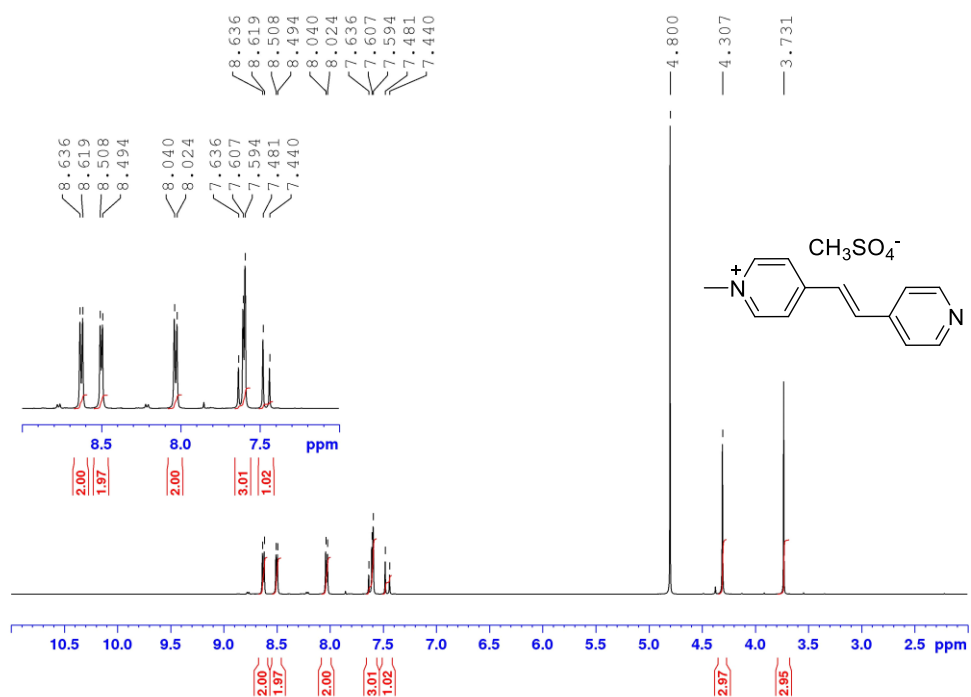


Figure S107 – $^1\text{H-NMR}$ (400 MHz, D_2O , 25 °C) spectrum of 5c.

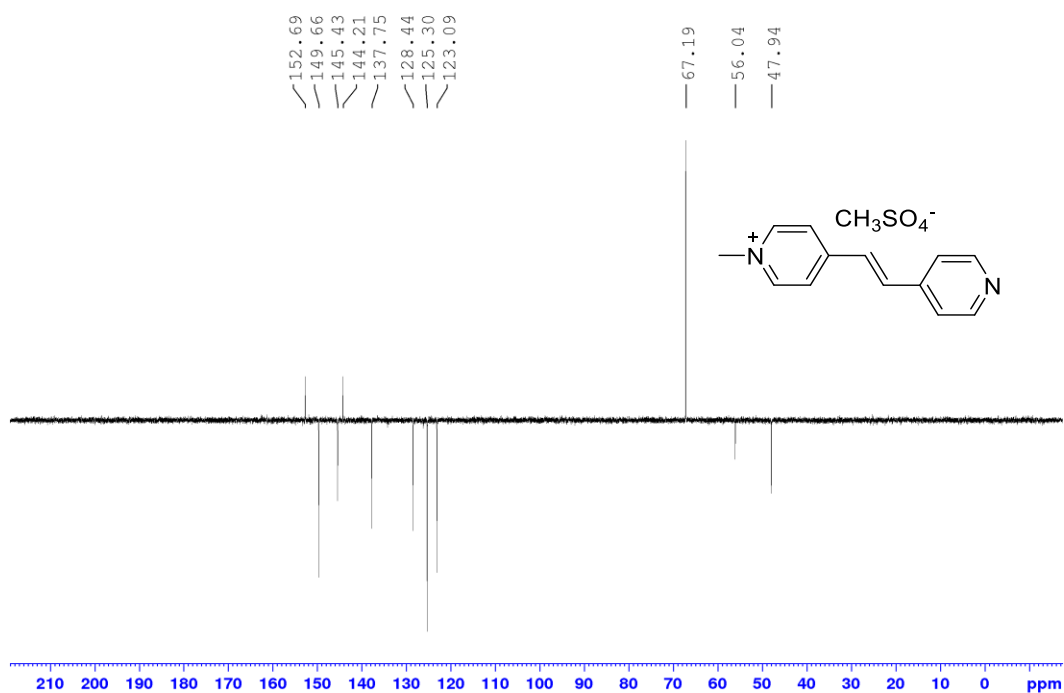


Figure S108 – $^{13}\text{C-NMR APT}$ (125 MHz, $\text{D}_2\text{O}/1,4\text{-dioxane}$ – $\delta = 67.2$ ppm, 25 °C) spectrum of 5c.

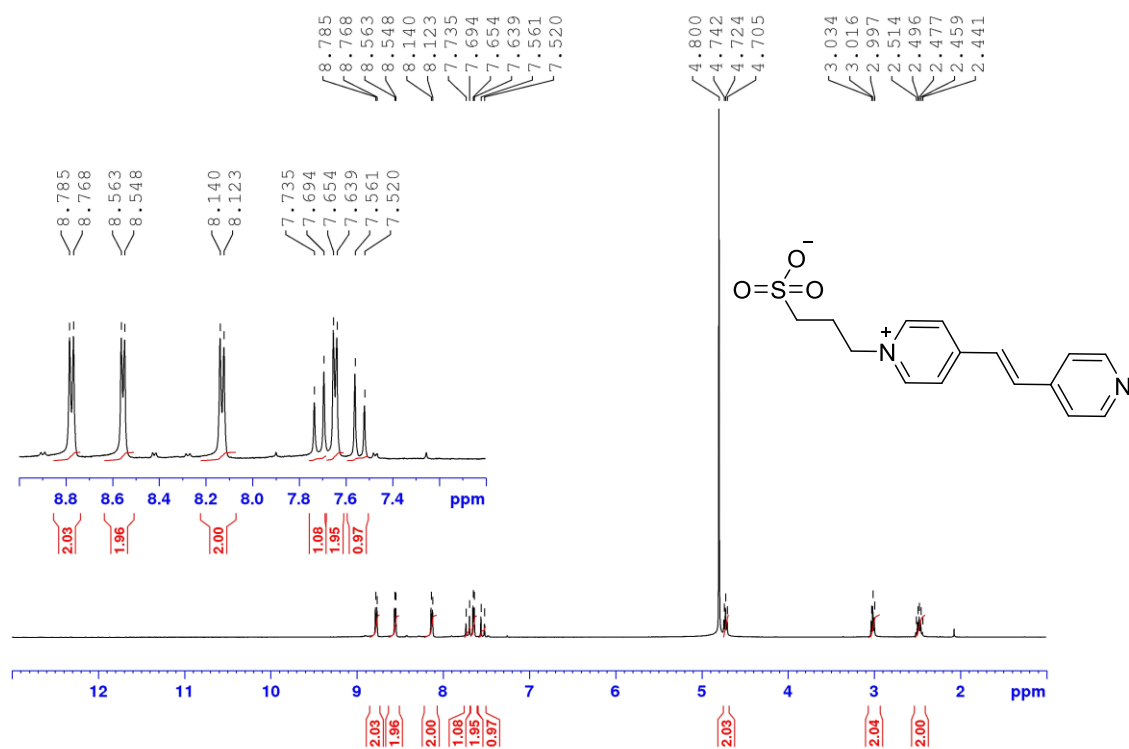


Figure S109 – ¹H-NMR (400 MHz, D₂O, 25 °C) spectrum of 5d.

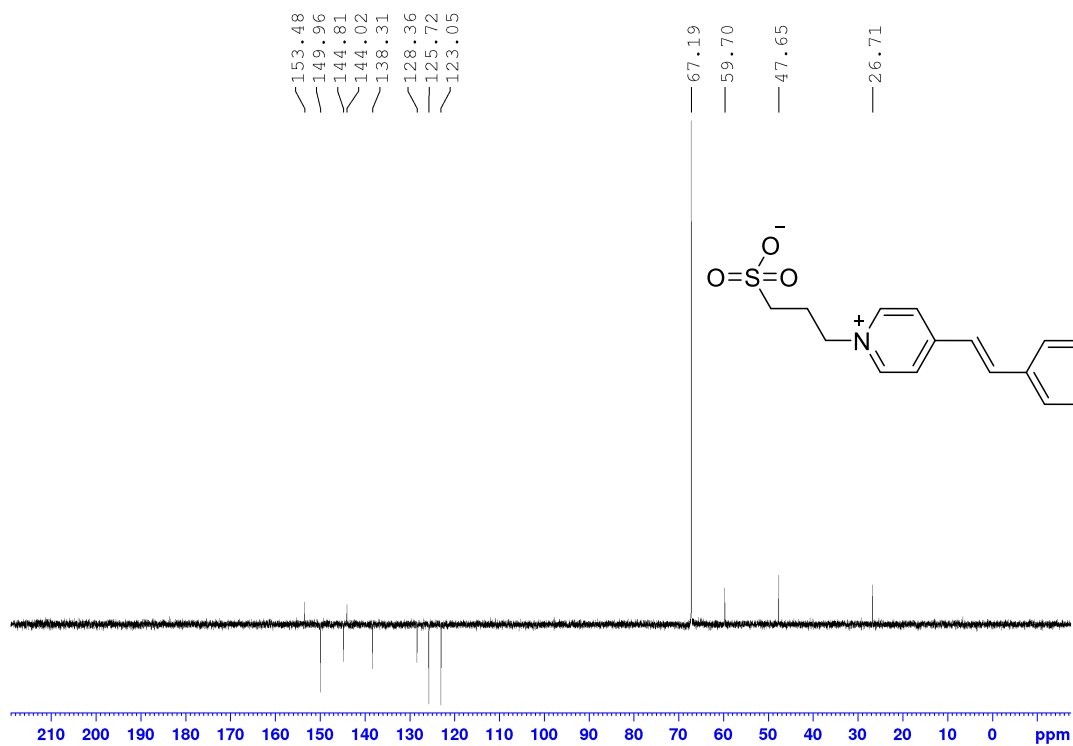


Figure S110 – ¹³C-NMR APT (125 MHz, D₂O/1,4-dioxane – δ = 67.2 ppm, 25 °C) spectrum of 5d.

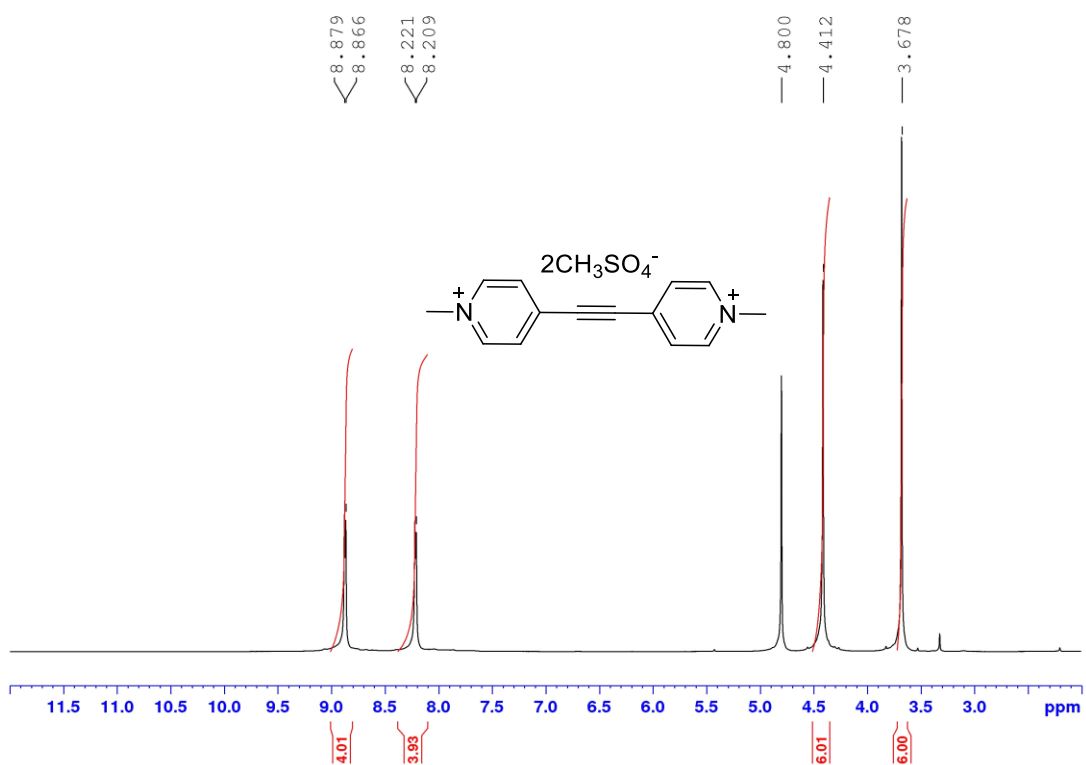


Figure S111 – $^1\text{H-NMR}$ (500 MHz, D_2O , 25 °C) spectrum of **6a**.

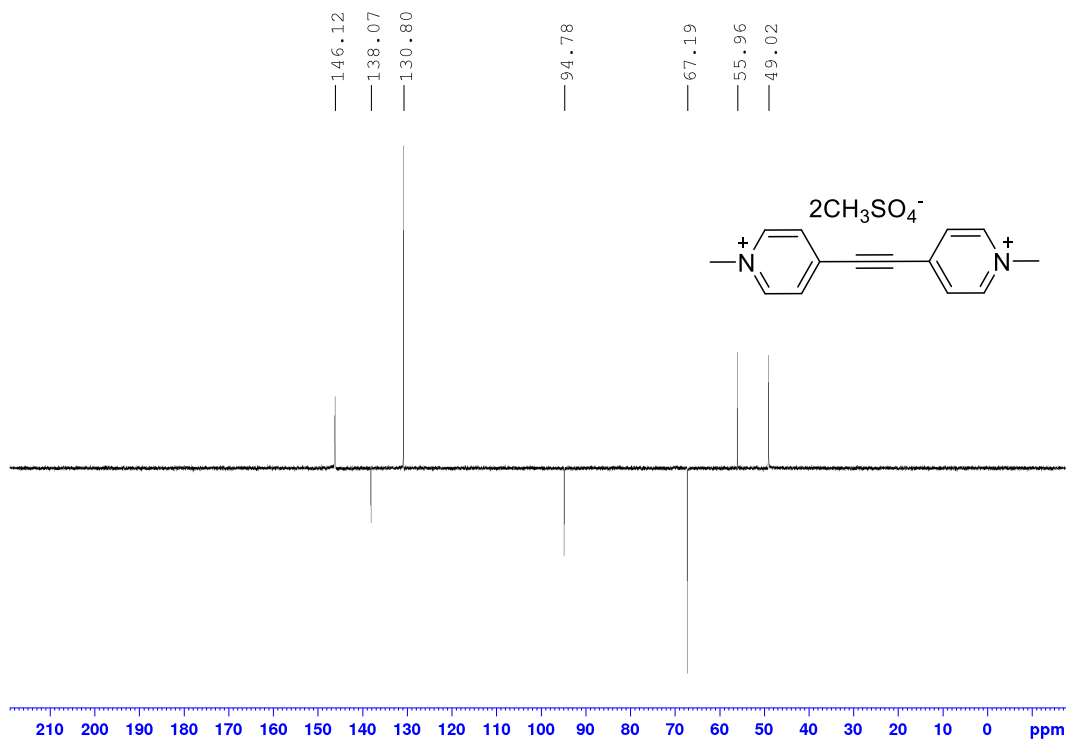


Figure S112 – $^{13}\text{C-NMR APT}$ (125 MHz, $\text{D}_2\text{O}/1,4\text{-dioxane}$ – $\delta = 67.2$ ppm, 25 °C) spectrum of **6a**.

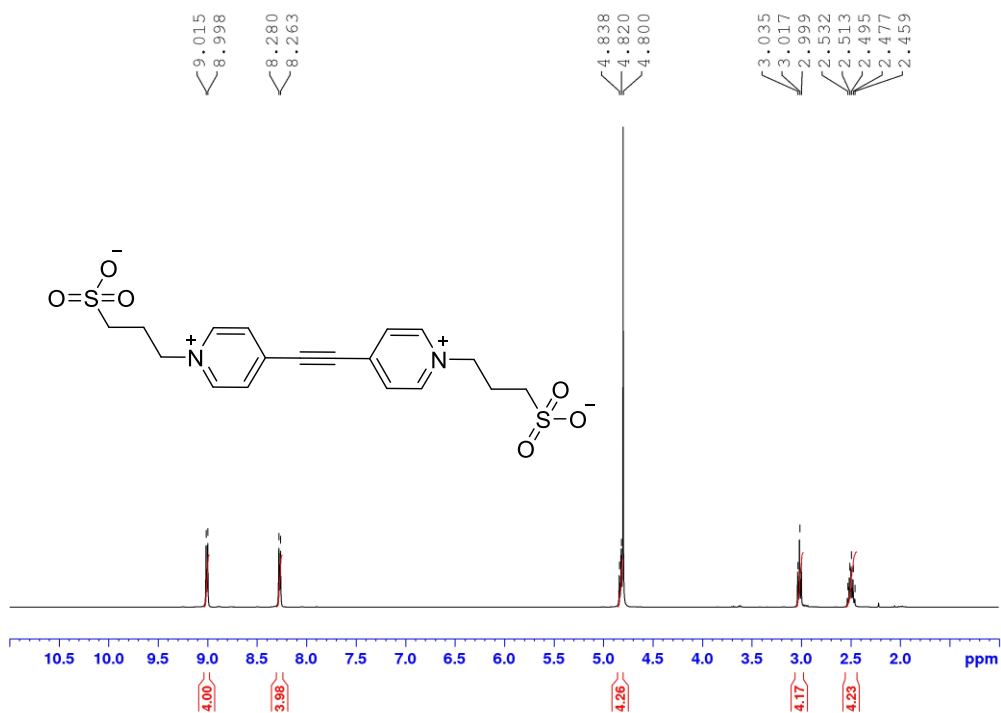


Figure S113 – ¹H-NMR (400 MHz, D₂O, 25 °C) spectrum of **6b**.

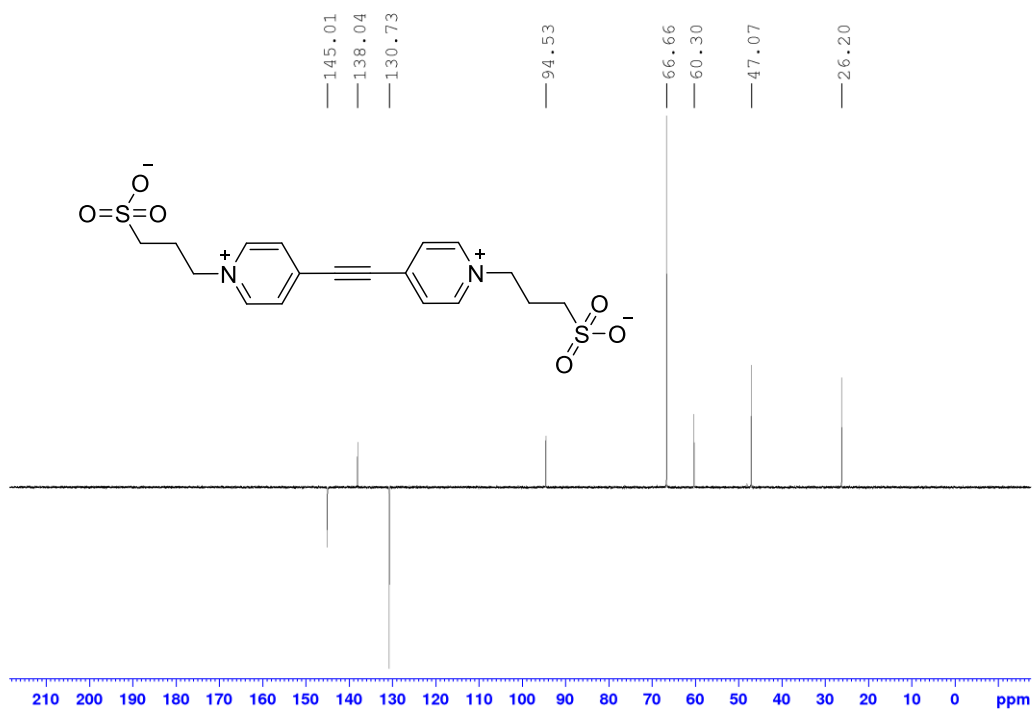


Figure S114 – ¹³C-NMR APT (125 MHz, D₂O/1,4-dioxane – δ = 66.7 ppm, 25 °C) spectrum of **6b**.

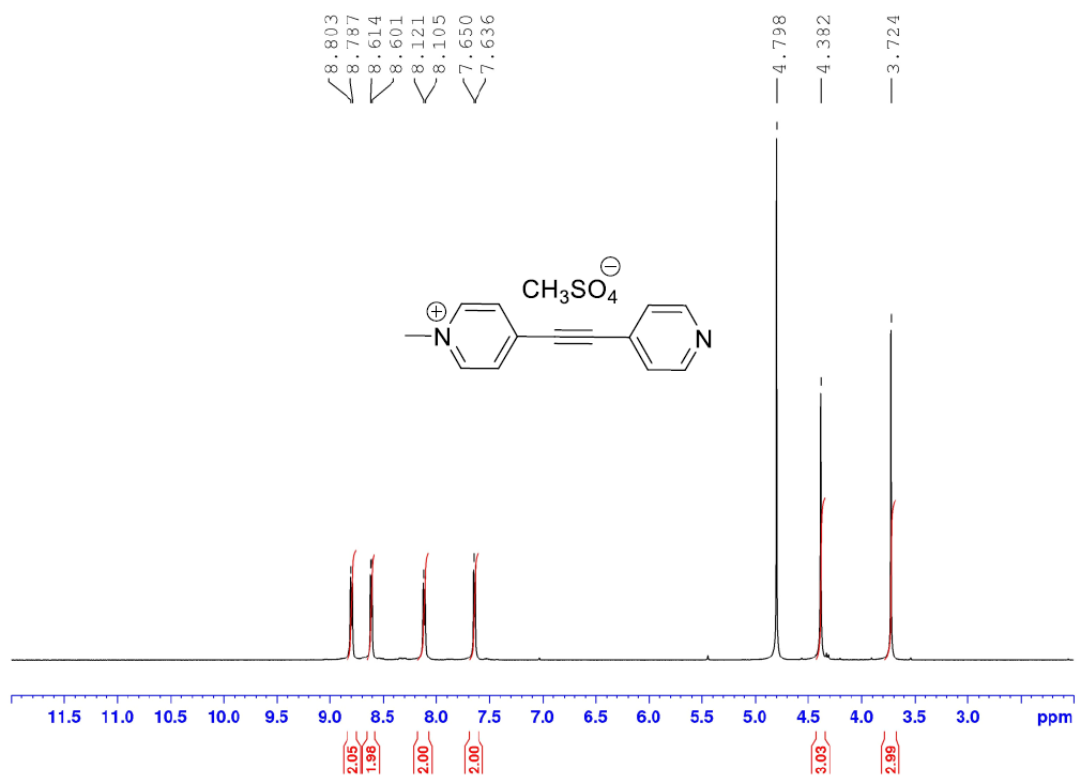


Figure S115 – ¹H-NMR (400 MHz D₂O, 25 °C) spectrum of **6c**.

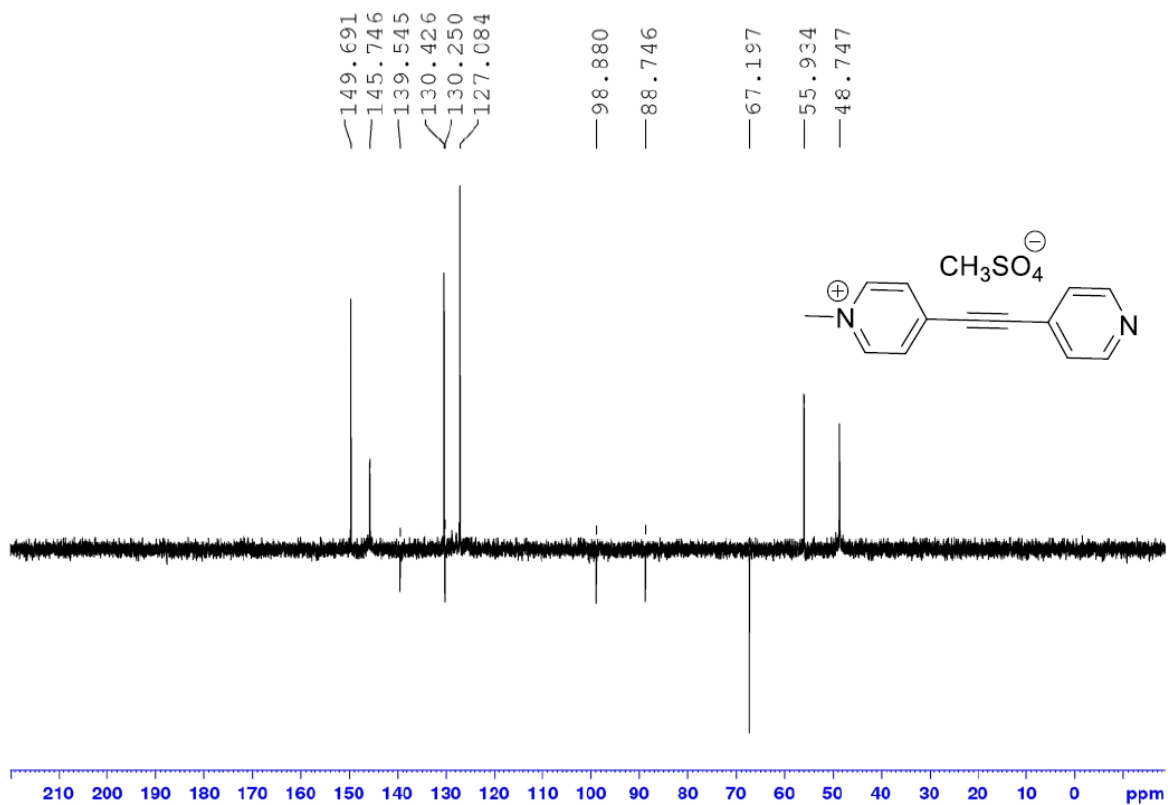


Figure S116 – ¹³C-NMR APT (100 MHz, D₂O/1,4-dioxane – δ = 67.2 ppm, 25 °C) spectrum of **6c**.

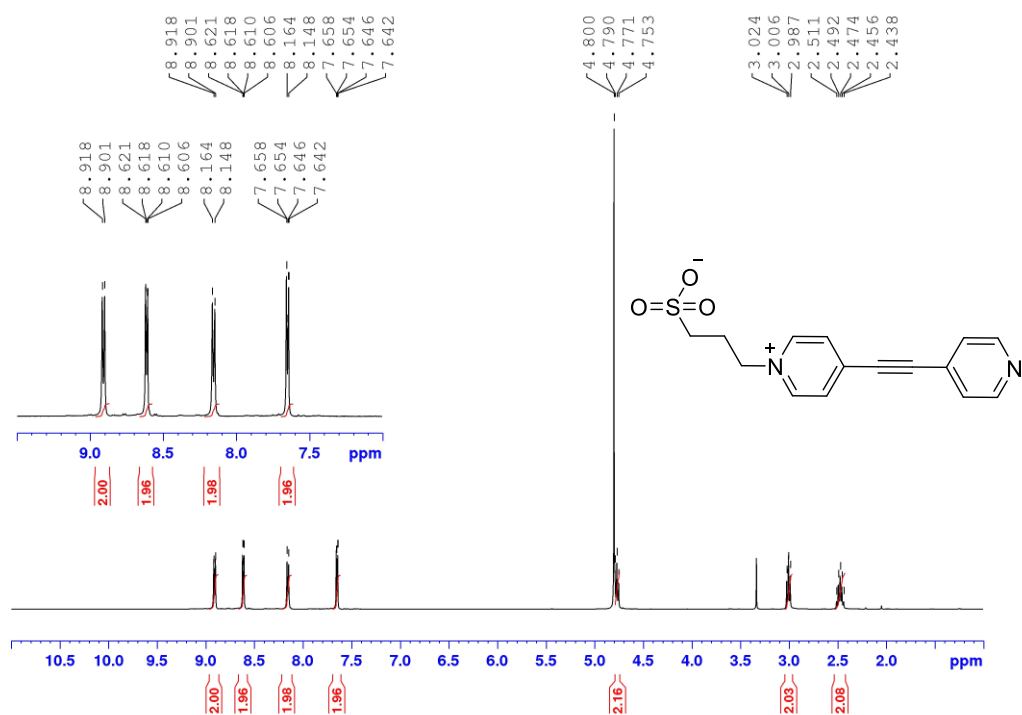


Figure S117 – ¹H-NMR (400 MHz, D₂O, 25 °C) spectrum of 6d.

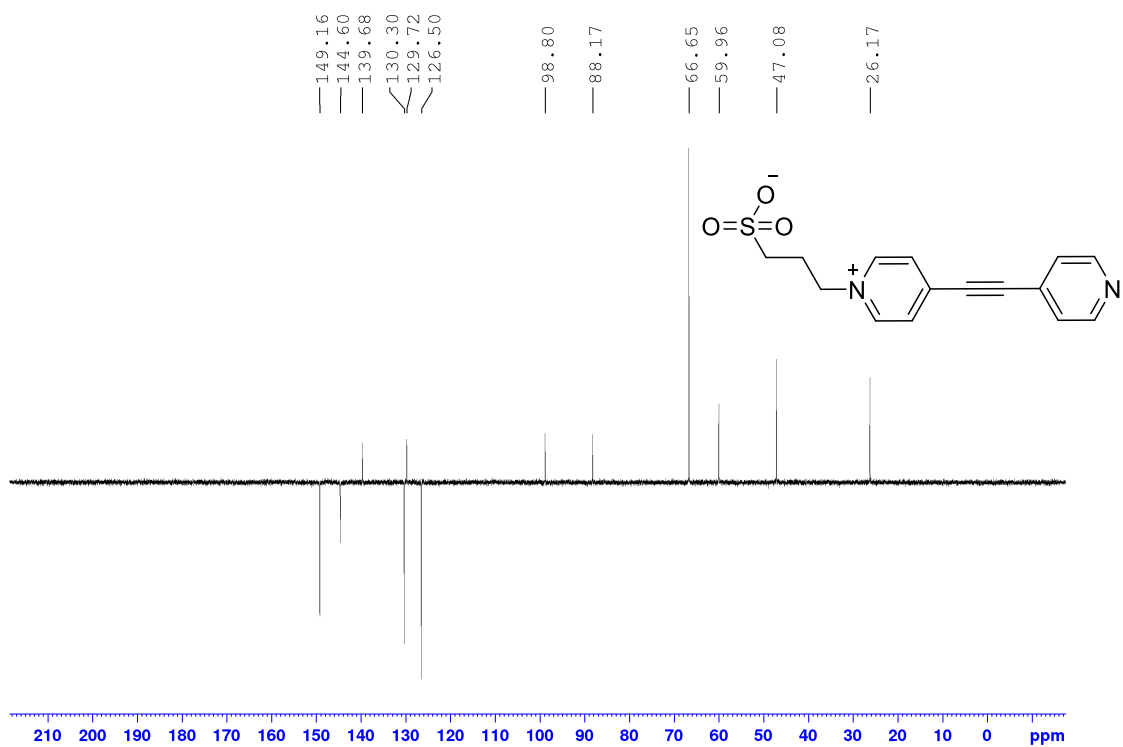


Figure S118 – ¹³C-NMR APT (125 MHz, D₂O/1,4-dioxane – δ = 66.7 ppm, 25 °C) spectrum of 6d.

8 References

- [1] S. Soni, R. L. Vekariya, and V. K. Aswal, *RSC Adv.*, 2013, **3**, 8398–8406.
- [2] H. Kamogawa, and T. Suzuki, *Bull. Chem. Soc. Jpn.*, 1987, **60**, 794–796.
- [3] M. Balkenhohl, R. Greiner, I. S. Makarov, B. Heinz, K. Karaghiosoff, H. Zipse, and P. Knochel, *Chem.-Eur. J.*, 2017, **23**, 13046–13050.
- [4] E. Botana, E. da Silva, J. Benet-Buchholz, P. Ballester, and J. de Mendoza, *Angew. Chem. Int. Ed.*, 2007, **46**, 198–201.
- [5] B. J. Coe, J. L. Harries, J. A. Harris, B. S. Brunshwig, S. J. Coles, M. E. Light, and M. B. Hursthouse, *Dalton Trans.*, 2004, **18**, 2935–2942.
- [6] V. K. Srirambhatla, A. Kraft, A. V. Powel, and S. Watt. *Cryst. Growth Des.*, 2012, **12**, 4870–4879.
- [7] J. T. Culp, C. Madden, K. Kauffman, F. Shi, and C. Matranga, *Inorg. Chem.* 2013, **52**, 4205–4216.
- [8] Z. Burešová, M. Klikar, P. Mazúr, M. Mikešová, J. Kvičala, T. Bystron, and F. Bureš, *Front. Chem.*, 2021, **8**, 631477.
- [9] T. Bystron, E. Sramkova, F. Dvorak and K. Bouzek, K., *Electrochimica Acta*, 2019, **299**, 963–970.